SSCL-N-798
GD M4A-100013

# Second Workshop on the Testing of SSC Magnet Cryogenic Performance

Edited by
Quan-Shen Shu

Magnet System Division
Superconducting Super Collider Laboratory*
2550 Beckleymeade Ave.
Dallas, TX 75237

August 1992

*Operated by the Universities Research Association, Inc., for the U.S. Department of Energy under Contract No. DE-AC35-89ER40486.

# CONTENTS

Summary Report of the Second Workshop on Testing of SSC Magnet Cryogenic Performance ..... 1

Workshop Agenda ..... 9

Cryostat Performance Assurance Plan and Review of Relevant Development Plans, S. Peck ..... 13

Cryogenic Performance of MLI in ASST, D. Franks ..... 57

Cool Down Simulation and Experimental Results of SSC Superconducting Magnets with Difference Cryogenic Systems, Q.S. Shu, D. Orris, A. Prodell, I. Syromyatnikov, and A. Yucel ..... 85

ASST Progress, J. G. Weisend II ..... 113

Design of GD Cold Test Stand Instrumentation, R. Churchill ..... 127

Review of Relevant Portions of Master Test Plan, R. Churchill and D. Gaughen ..... 147

Thermal Performance of 20 K MLI Systems, Bill Borosky ..... 163

MTL Cold Test Stand Cryogenic Instrumentation, Q.S. Shu and I. Syromyatnikov ..... 177

Status of Cross Flow Cooling Calculations, S. Peck ..... 193

Analysis of Cross Flow Cooling for CDM with Orificed Channels, A. Yucel ..... 207

Cross Flow Cooling, R. P. Shutt and M. L. Rahak ..... 229

Special Sttachments: (a) Beam Tube Support, (b) AC Performance of SSC Magnets, and (c) Completion of Thermal Contraction Measurements of Some Materials Used in Magnet Fabrication and Assembly ..... 281

AC Performance of SSC Magnets, R. Schermer, G. Snitchler, and B. Askel ..... 291

List of Attendees ..... 327

# Summary Report of the Second Workshop on Testing of SSC Magnet Cryogenic Performance

Quan Sheng Shu, Scott Peck, and Donald Franks

# Report of the "Second Workshop on Testing of SSC Magnet Cryogenic Performance"

Quan Sheng Shu, Scott Peck, and Donald Franks

Held at GD/San Diego, June 29, 1992

A second workshop on testing of the SSC CDM cryogenic performance was held at General Dynamics in San Diego on 6/29/92. There were 12 participants from SSCL, FNAL, GD, and BNL. Attendees included Bill Boroski, Moises Kuchnir, and Peter Mazur (FNAL), Margareta Rehak (BNL), and Quan-Sheng Shu, Adnan Yucel, Igor Syromyatnikov, John Weisend, Bob Smellie, Jon Simmons, Phil Kraushaar and Don Franks (all from SSCL). Nine presentations were made to review relevant development plans and calculations related to the thermal performance of the CDM cryostats. Three other presentations on cross-flow cooling calculations were made. An open discussion of issues related to a string test of GD prototype magnets was held, followed by a working group meeting. The working group proposed that a string test be pursued, with a parallel effort to define a heat leak test facility that might emulate a string test. We also recommend that Accelerator cryogenics develop tolerance bands on magnet heat leaks as a first step towards quantifying an acceptable sample size of magnets tested for heat leak.

## Review of the Purpose of the Workshop meeting

(1) Review the progress in plans, calculations and R&D test results of the magnet cryogenic performance and the cryogenic test instrumentation since the first workshop in Feb '92. (Our discussion all dealt with testing of the GD CDM Production design. We have not addressed any plan for CQM testing. This CQM testing may turn out to be quite different from that for the CDMs.)

(2) Discuss the status of ASST at SSCL and the GD Master Test Plan

(3) Discuss the work on magnet cross-flow cooling calculations and experiments and the issues related to possible String Tests of GD prototype magnets.

## Brief Summary of the Workshop Presentations

Scott Peck of General Dynamics opened the meeting with a presentation of the GD approach to assuring the thermal performance of the CDM cryostats. The approach consists of a combination of analysis, test, and process control at the individual component level and at the cryostat assembly level. The point was made that thermal performance assurance consists both of design verification and "as built" performance verification.

Ted Hardy of GD then followed with a review of the development plans for the helium adsorber module, support post, and thermal shields. These components are key players in the thermal performance of the cryostat. The key point here was that testing will verify the thermal performance of these components at the component level.

Next was Don Franks of SSCL, who summarized the testing that will be done on the MLI in the cryostats installed in the ASST. Temperature profiles through the blankets will provide insight into how the blankets perform installed in a string compared to the sample tests done at FNAL.

Quan-Sheng Shu of SSCL then presented results of an analysis of cooldown of a single magnet on the MTL test stand with variaties of cooling procedures using the MTL cryogenic system. Peter Mazur made a comment concerning the history of the cooldown rate, mentioning that actual testing has alleviated early concerns over cryostat warpage and adverse affects on quench behavior and recommends that future cooldowns be done as fast as possible.

A status of the ASST test was then presented by John Weisend of SSCL. There appeared to be no problems with the test and it was proceeding as planned.

Bill Isaacs of GD (substituting for Bob Churchill) followed with a review of the GD test stand instrumentation and relevant portions of the master test plan. There were questions related to aspects of the magnet interface that differ on magnets that are cold tested.

The final presentation related to the thermal performance of the cryostats was made by Igor Syromyatnikov of SSCL, on the MTL Cold Test Stand Cryogenic instrumentation.

Three presentations on cross-flow cooling calculations were then made by Scott Peck (GDSS), Adnan Yucel (SSCL), and Margareta Rehak (BNL). All three presented similar models with similar results which indicate that cross flow cooling is effective in removing heat introduced at the beam tube before it raises the conductor temperature and reduces margin.

## Key Thoughts Developed During the Meeting About Magnet Testing

### Magnet Cryogenic Testing

(1) Are we going the right way to be sure the cryostats are doing what they should - as regards heat leak ?

(2) The need for testing is driven by the Collider Ring requirement that magnet heat leak to the 4 K Helium does not greatly exceed the budget allocation. This allocation is based on the refrigeration system limit which, in turn, is largely driven by the Synchrotron heating - which is a big heat load in comparison to that of the magnet by itself.

Thermal testing needs to be done of the GD Prototype magnets. This is to ensure the thermal design is acceptable. Such testing also needs to be done of an "on going" sample of the Production design magnets. This is to assure they are being built in keeping with the Prototype design.

Concern is that if thermal design / assembly problems develop in the Production magnets, that without sample testing, these magnets might very well get all the way

into Collider Ring installation First indication of heat leak problems would then be from measurements of the cryogen flows through them. This is a long way down stream on the process. Furthermore, a lot of magnets could have been built by then with inherent problems.

It was agreed that unless all magnet are tested then there will be some risk of thermal problem magnets slipping through and getting installed. Since this is not feasible, some risk must be expected on magnets with thermal problems getting installed in the Collider Ring. Possibly some visual inspection may catch the worst of these.

(3) A related question, then, is how bad does magnet heat leak have to be before it would have to be removed from the Collider Ring? This appears an Accelerator Cryogenics determination.

(4) Consensus on magnet thermal acceptance testing was that the Production magnets need to be tested for heat leak in either a String or something that "emulates" a String. This is for reasons of "end effects" heat leak.

The problem here is that the 4 K heat leak to be verified is very small. In comparison, in a test fixture, such as FNAL MTF or even the planned SSCL MTF, the end effects heating can be formidable. At the First Workshop (Feb '92), Tom Peterson reported that he measured some "3+" watts heating into the 4 K Helium through the CDMs at FNAL MTF. In comparison, their budget value is 0.36 watts.

(5) About using the ASST String for such magnet testing, John Weisend said it was his experience that it took a long time to install magnets into such a String, and is no easy thing. Also, there is a mechanical fit problem, too. The ASST magnets are 600 mm longer than the standard CDMs.

(6) What got discussed as an alternative to ASST was to develop a test fixture that "emulated" - for the test magnet - the adjacent magnets and their temperatures. This would eliminate end effects heating.

This fixture could be in a separate, "Heat Leak Test Facility". Desirability perceived for this is that incoming magnets could be tested in this facility for meeting the heat leak requirements. After passing this testing they would go to the magnetic testing.

Rationale here is that the requisite thermal testing can be done much faster and simpler than the magnetic testing. Also, no electrical connections would be involved here; these are a possible source of heat leak. Ideally, the thermal test could be structured to supply specified cryogenic flow rates and inlet temperatures to the test fixture. If so, the thermal test could then become a "Go / No Go " test, depending on heat leak measured from the test magnet.

Unresolved issues seen on the above measurement include:

A) How precisely can the heat leak into the test magnet be measured ?
It was reported (? by Peter Mazur) that FNAL MTF had problems on measuring the 3 watt heat load that went into the test magnet 4 K Helium, there. Also related to this are concerns about "stratification" in the single-phase he at low flow rates.

B) What is an allowable tolerance on the test magnet heat leak acceptability ? We need to develop a "tolerance band" - how much "over" the limit can the magnet go and still be OK ?

(7) About the test magnets, unresolved issues include :

A) How many magnets do we want to sample test ? GD said the production rate is 10 / day.

B) What amount of time is needed for test magnet thermal acceptance testing ? About this, GD (Bill Isaacs) said they had planned "60 hours" for the time for the magnet thermal testing. It seemed this time is roughly in keeping with what Peter Mazur cited for getting magnets into test at FNAL MTF, too. We need further sure whether the thermal equilibrium is reached in such a period of time.

C) Are special instrumentation / sensors needed on those magnets planned for testing?

(8) About the thermal testing (5.A), above, discussion developed on the possibility of trading the cost of the accuracy on the test magnet heat leak for some increase in the Collider Ring cryogen refrigeration system.

What is the cost for measurement accuracy ? Do we want to spend a lot of money and get the best possible accuracy ? or do we want to investigate the cost (and problems / control issues) involved in increasing the refrigeration capacity of the Collider Ring refrigeration system to accept the possibly somewhat higher heat associated with this magnet testing uncertainty ? Where is the money better spent ?

(9) An Interface Issue that got brought up, but not resolved, was that of the flanges to be used on the GD magnets. These flanges need to mate with SSC hardware for test purposes. It was agreed to defer this issue to Rich Bailey to work out with SSCL, separately. Maybe use flanges that remove for magnet installation into the Collider Ring.

## ASST Status at SSCL and the GD Master Test Plan

In this part of the meeting John Weisend and Don Franks presented on their respective involvements with ASST. GD presented a little on their test schedule.

On ASST, John showed pictures of the String magnets and the building. Don presented on plans for RGA measurements of the Half Cell vacuum and also thermal test data reduction.

On the GD testing, they said they had contracted to build two more test stands at Hammond. This would increase their capacity to four stands. Don Franks told GD of his concerns for conducting thermal tests at these stands. The concerns being that they would experience "end effects" heating such as at FNAL MTF and the resulting impact would overwhelm whatever heating flowed through the magnet thermal insulation. Upshot being they would not get any detailed thermal data - just as there are none from the FNAL MTF tests.

## Magnet Cross-Flow Cooling Calculations

Three people presented on this. Adnan Yucel presented on his recent modeling work. Also, Scott Peck and Margarita Rehak.

Models involved were all theoretical. There were no test data, yet, to substantiate anyone's models. GD had used some limited test data, though, to show, apparently, there was some change ( Reynolds Number effect ?) to be expected on cross-flow 4 K Helium pressure drop versus flow rate through the magnet. Previously, they had not been sure such an effect existed - flow rates though the magnet being in the "turbulent" flow regime where friction factor depends primarily on surface roughness.

Margarita Rehak said BNL had been working on cross-flow cooling for several years, now. Ron Schutt had started the effort. She had now taken it over. She said they saw "mole heating" as the "driving need" for such. Said they saw problems on this cooling arrangement if there was internal leakage in the 1/4-inch laminations.

## Management Decisions Required

The following are seen to be management decisions, per the above discussion;

(1) Whether to build a test fixture ("heat leak test facility" ) that emulates a String.
(2) If a test fixture is to be built, where? It needs to be in close proximity to the magnetic test area.
(3) Who's to build (pay for) and operate (people) such a test fixture ? Is this a GD task since they are responsible for guaranteeing performance ? If GD, only test GD magnets ?
(4) If it is decided to pursue such a facility, a realistic budget cost of such is needed. Who's to do this? Associated questions include : refrigeration system needed and its controls, vacuum pumps and controls, the fixture that the test magnet will mount into, flow system instrumentation, etc.
(5) Getting Accelerator Cryogenics to identify what the cost / problems are in increasing the Collider Ring 4 K Helium refrigeration system capacity.

## Recommendations

Recommendations regarding magnet testing per the above include:

(1) Conduct "reduced flow rate" tests of 4 K Helium in ASST. See how low flow rates can go before an indication of stratification. This should give good data on magnet system level heating. This is a String. Consequently, no " end effects" heating.

(2) Make a decision to determine if a Thermal Test Facility is needed. If so, what testing is needed there and with what accuracy ? If a decision against such a facility is made, determine what the alternatives are.

Issues associated with such a facility include: Where do the cryogens come from, what controls and sensors are needed for the cryogen system, vacuum pumps and their controls, thermal sensors needed, etc.

(3) If a separate test facility (Thermal Test Facility) is to be built, where? Is this to be at the subcontractors or is it to be at SSCL. If at SSCL it could be used for testing magnets from the various magnet subcontractors. Also, it would permit testing magnets after they had been shipped.

(4) If a decision is made to build the test facility, a conceptual design needs to be developed. From this an assessment needs to be made of how much time is to be allotted to magnet testing, there. This would determine how many magnets can be tested during Production.

(5) Accelerator Cryogenics should determine heat leak limits on the Collider Ring refrigeration system. Also, assess of cost / work to increase system capacity (4 K Helium, in particular).

# Workshop Agenda

***Superconducting Super Collider Laboratory***
*2550 Beckleymeade Avenue, MDL, MS-1002*
*Dallas, TX 75237-3946*

*Magnet Systems Division*
*Test and Data Management Department*

**MEMORANDUM**

**To:** **Distribution**

**From:** **Quan Sheng Shu (SSCL), Scott Peck (GD)** **MT04**

**Date:** **6/23/92** **92 5830 R M ******

**Subject:** **The Second Workshop on Test of SSC Magnet Cryogenic Performance**

You and your representatives are invited to attend "The Second Workshop on Testing of SSC Magnets Cryogenic Performance". The Workshop will be held at San Diego, California, on June 29, 1992, and be hosted by General Dynamics.

The Workshop will review the progress in plans, calculations and R&D test results of the magnet cryogenic performance and the cryogenic test instrumentation since the first workshop at SSCL in February 1992. The status of ASST at SSCL and the GD Master Test Plan will be discussed. Also, calculations and magnet cross-flow cooling experiments and the issues related to possible string test of GD prototype magnets will be discussed at the Workshop. The titles of these presentations are listed in the preliminary agenda (attachment 1). The Workshop will be held at General Dynamics, from 8:00 am to 5:30 pm, in the Century Park Building 1, X-Ray Conference Room. There will be a working group meeting after the presentations.

One hard copy of each presentation sheet should be submitted to Scott Peck or Quan-Sheng Shu by Monday noon, June 29, 1992.

Attachments:

Preliminary agenda of the Workshop.

Distribution:

| | |
|---|---|
| Aksel, B. | MS 1001 |
| Boroski, W. | Fermilab |
| Bush, T. | MS 1000 |
| Coombes, R. | MS 1000 |
| Devred, A | MS1002 |
| Franciscovich, J. | MS 1005 |
| Franks, D. | MS 1005 |
| Jayakumar, J. | MS 1009 |
| Kuchnir, M. | Fermilab |
| LaBarge, A | MS 1001 |
| Martin, D. | MS 1005 |
| Mazur, P. | Fermilab |
| McAshan, M. | MS 4003 |
| Meinke, R. | MS 1040 |
| Nicol, T. | Fermilab |
| Peterson, T. | Fermilab |
| Pletzer, R. | MS 1005 |
| Prodell, A. | BNL |
| Sanger, P. | MS 1001 |
| Rehak, M. | BNL |
| Schermer, R. | MS 1000 |
| Snitchler, G. | MS 1001 |
| Syromyatnikov, I. | MS 1002 |
| Taylor, C. | LBL |
| Tompkins, J. | MS 1002 |
| Weisend, J. | MS 6000 |
| Yucel, A. | MS 4003 |
| Zbasnik, J | MS 1001 |

FYI: A separate memo is being sent to all magnet product managers.

# PROPOSED AGENDA
# FOR
# SECOND WORKSHOP
# ON
# SSC MAGNET CRYOGENIC TEST

**General Dynamics, San Diego, CA**

**June 29, 1992**

| | | | |
|---|---|---|---|
| 08:00 am - 08:10 am | Remarks | S. Peck | 10 min. |
| 08:10 am - 08:50 am | Presentation of Cryostat Performance Assurance Plan | S. Peck | 40 min. |
| 08:50 am - 09:10 am | Review Relevant Development Plans: Helium Adsorber Module, Post, Thermal Shield | T. Hardy | 20 min. |
| 09:10 am - 09:40 am | Cryogenic Performance of CDM MLI in ASST | D. Franks, et al | 30 min. |
| 09:40 am - 10:10 am | Cooldown Simulation of Single SSC Magnet with MTL Cryogenic System | Q.S. Shu, et al | 30 min. |
| 10:10 am - 10:20 am | **BREAK** | | 10 min. |
| 10:20 am - 10:50 am | Status of ASST at SSCL | J. Weisend | 30 min. |
| 10:50 am - 11:20 am | Design of GD Cold Test Stand Instrumentation | R. Churchill | 30 min. |
| 11:20 am - 11:40 am | Review Relevant Portions of Master Test Plan | R. Churchill, D. Gaughen | 20 min. |
| 11:40 am - 12:00 pm | MTL Cold Test Stand Cryogenic Instrumentation | Q.S. Shu, I. Syromyatnikov | 20 min. |
| 12:00 pm - 12:50 pm | **WORKING LUNCH** | | 50 min. |
| 01:00 pm - 01:20 pm | Status of GD Cross Flow Cooling Calculations | S. Peck | 20 min. |
| 01:20 pm - 01:50 pm | SSCL Cross Flow Cooling Calculations | A. Yucel | 30 min. |
| 01:50 pm - 02:10 pm | Cross Flow Experimental Results | M. Rehak | 20 min. |
| 02:10 pm - 02:40 pm | Open Discussion of Issues Related to Proposed String Test of GD Prototypes | All | 30 min. |
| 02:40 pm - 02:50 pm | **BREAK** | | 10 min. |
| 02:50 pm - 05:30 pm | Working Group Meeting | Working Group | 140 min. |

Total time for presentations plus working group meeting: 9.5 hours (including Working Lunch of 50 minutes)

# Cryostat Performance Assurance Plan and Review of Relevant Development Plans

S. Peck

# Cryostat Performance Assurance Plan

or

# How Do We Assure Ourselves the Production Cryostats Meet Heat Leak Requirements?

Scott Peck

2nd Workshop on Testing of SSC Magnet Cryogenic Performance
General Dynamics Space Systems Division, San Diego, Ca
June 29, 1992

# CRYOSTAT PERFORMANCE ASSURANCE PLAN Objectives

- Design Verification
  - — Demonstrate that the design itself meets the heat leak requirements
    - – (Do we have a good design?)
- "As Built" Verification (Acceptance Test)
  - — Demonstrate that production CDM cryostats meet heat leak requirements when delivered
    - – (Are we building to our design?)

# CRYOSTAT PERFORMANCE ASSURANCE PLAN
## Philosophy

If the cryostat design works, and it is well understood why the design works , then if the cryostat is built to the design, it will have good, repeatable performance.

- Verify the design
- Demonstrate that the design is understood
- Demonstrate that the design is being built

# CRYOSTAT PERFORMANCE ASSURANCE PLAN
## Design Verification Approach

- Analysis
  - — Component models provide insight into behavior of design
    - – support post, MLI blankets, infrared radiation, gas conduction, thermal straps, voltage tap
  - — Integrated models provide additional insight on behavior
    - – boundary conditions, gas pressure, internal interfaces
- Test
  - — Component testing verifies analytical models
    - – support post, MLI blanket, absorber capacity, thermal straps
  - — Testing at assembly level verifies design
    - – single magnet on test stand
      - - 20K, 80K heat leaks
      - - benchmark temperatures (post, shield, strap, voltage tap)
    - – string test
      - - 4K, 20K, 80K heat leaks
      - - benchmark temperatures (post, shield, strap, voltage tap)
      - - gas pressure

# CRYOSTAT PERFORMANCE ASSURANCE PLAN "As Built" Verification Approach

- Test
  - Component testing to assure design fidelity
    - property verification (emissivities, conductivities)
    - performance verification (post heat leak, absorber capacity)
  - Assembly level testing to demonstate repetitive performance
    - in-process checks (shield:shield resistance, removable shroud, clear line of sight)
    - single magnet cold testing (20K, 80K heat leak, benchmark temperatures, gas pressure)
- Process Control / Inspection
  - Component properties
    - dimensions, cleanliness
  - Assembly procedures
    - integrity (strap connections, post intercepts, absorber mounting, voltage tap heat sink, no holes / cuts in MLI blanket)
    - fit (shield sections, MLI blankets)
    - no FOD (loose straps, tools, fasteners, rags / cleaners, chips, solder slag, MLI remnants, solvents / lubricants)

# CRYOSTAT PERFORMANCE ASSURANCE PLAN
## Component Analysis

- Support post
  - conduction
    - key parameters are tube conductivity, length, cross-sectional area
- MLI blankets
  - radiation, gas conduction, solid conduction
    - key parameters are reflector emissivity, layer density, internal gas pressure, gaps at seams, spacer conductivity
- Shields
  - infrared radiation
    - key parameters are shield emissivity, view factors
- Residual gas pressure
  - gas conduction
    - key parameters are gas pressure, gas temperature, gas species, accommodation coefficients, shape factor
- Thermal straps
  - conduction
    - key parameters are strap conductivity, length, cross-sectional area, contact conductance at joints
- Voltage tap
  - conduction
    - key parameters are tube conductivity, length, cross-sectional area, effectiveness of heat sink connection to shield

# CRYOSTAT PERFORMANCE ASSURANCE PLAN
## Integrated Analysis

- Simultaneous solution of component models
  - Boundary conditions
    - vacuum vessel, cryoline, cold mass temperatures
  - Gas pressure
    - helium absorber module effectiveness
    - residual pressure in MLI blankets
  - Internal interfaces
    - support post intercepts
    - thermal strap connections to shields and cryolines
    - voltage tap heat sinking to thermal shields
- Sensitivity of heat leak to key parameters
- Reference values for benchmark temperatures

# CRYOSTAT PERFORMANCE ASSURANCE PLAN
## Component Design Verification Testing

- Component Development
  - Support post
    - post development plan
    - measure heat leak, validate mat'l conductivity data
  - MLI blankets
    - FNAL development program
    - blanket heat leak, seam heat leak
  - Helium adsorber module
    - HAM development plan
    - measure adsorber capacity, pumping speed
  - Thermal straps
    - thermal shield development plan
    - measure contact conductance, strength of joints to piping, shields

# CRYOSTAT PERFORMANCE ASSURANCE PLAN
## Cryostat Design Verification Testing

- Single Magnet on Test Stand (Prototypes)
  - 20K, 80K heat leaks
    - measured at reduced flow rate to get $\Delta T$ sensitivity from end to end
  - gas pressure
    - introduce calibrated leak to verify absorber performance in cryostat
  - benchmark temperatures
    - effectiveness of straps, intercepts on posts & voltage tap,
    - abnormal shield temperatures indicative of thermal shorts (FNAL)
- String test
  - 4K, 20K, 80K heat leaks
    - 4K heat leak requires multiple magnets to get enough $\Delta T$ sensitivity, even at reduced flow rate
    - results not colored by end can effects
  - gas pressure
  - benchmark temperatures

# CRYOSTAT PERFORMANCE ASSURANCE PLAN
## Component Acceptance Testing

- In-process acceptance testing, source inspection, material certification
  - Critical property verification
    - shield emissivity (300 K)
    - MLI reflector emissivity (300 K)
    - post tube thermal conductivity (300 K, 80 K, 20 K, 4K)
  - Component performance verification / acceptance testing
    - post heat leak (4K with intercepts at 20K, 80K)
    - adsorber capacity
    - MLI blanket heat flux (small calorimeter)

# CRYOSTAT PERFORMANCE ASSURANCE PLAN
## Assembly Level Verification Testing

- In-process checks to demonstrate SPC
  - Electrical continuity
    - between shields (thermal shorts)
    - across strap connections (bad contact)
    - at post intercepts, voltage tap heat sink locations (bad contact)
  - Visual inspections
    - end to end line of sight (thermal shorts, blanket compression)
    - shield alignment
    - MLI blanket integrity
  - Removable shroud
    - pulled out from cryostat after insertion into vacuum vessel (thermal shorts, blanket compression)
- Single magnet cold testing (Production sample)
  - 20K, 80K heat leaks
  - benchmark temperatures
  - gas pressure

# CRYOSTAT PERFORMANCE ASSURANCE PLAN
## Component Process Control / Inspection

- Component properties
  - Cleanliness
    - radiating surfaces
    - adsorber contamination
  - Dimensional fidelity
    - post tube wall thickness
    - MLI blanket layer density, seam gaps
    - thermal strap cross-section, joint area
    - voltage tap cross-section, heat sink area

# CRYOSTAT PERFORMANCE ASSURANCE PLAN
## Cryostat Assembly Process Control / Inspection

- Assembly Procedures
  - Inspect for mechanical integrity
    - thermal strap connections
    - post intercept connections
    - adsorber mounting
    - voltage tap heat sink
    - blanket (no shine through)
  - Fit
    - thermal shield sections (no shine through)
    - MLI blanket gaps at seams, post cutouts (no shine through)
  - Eliminate FOD (foreign object damage)
    - loose straps
    - MLI remnants
    - tools
    - fasteners
    - solder slag
    - rags / cleaners
    - solvents / lubricants

# CRYOSTAT PERFORMANCE ASSURANCE PLAN

## Conclusion

- Performance Assurance of SSC CDM Cryostats Depends On
  - Design verification at component and assembly levels
  - Valid component and integrated thermal models to understand effect of key parameters
  - Rigorous control of materials, components, and assembly processes to ensure predicted performance

# REVIEW OF RELEVANT DEVELOPMENT PLANS

- HELIUM ADSORBER
- SUPPORT POST
- THERMAL SHIELD

# HELIUM ADSORBER MODULE DEVELOPMENT PLAN

# HELIUM ADSORBER MODULE SCOPE AND OBJECTIVES

- The helium adsorber module (HAM) will be designed to maintain the vacuum level in the cryostat at the nominal operating condition of $1 \times 10^{-6}$ torr.
- The HAM will consist of an activated charcoal either in cloth or granule form.
- The charcoal will be mounted so that it is thermally coupled to a 4.2K sink yet isolated from uncontrolled temperature fluctuations (i.e. quench).
- The HAM will need to be isolated from any heat sources including radiation from higher temperature sources such as the 20K thermal shield.
- The HAM will be designed so that it can be regenerated coincident with the 20 thermal cycles during the life of the collider. This regeneration will consist of heating the HAM to a temperature high enough to desorb the helium. The helium gas will then be pumped out using mechanical pumps.
- The HAM will need to be sized in order to handle any other gas constituents that may be present in the cryostat due to outgassing from the MLI blankets or other cryostat surfaces. This is in addition to the helium leak rate defined in the PIDS.

# HELIUM ADSORBER MODULE SCOPE AND OBJECTIVES

From M8A-1000004

**3.2.1.5 Thermal Performance**

The cryostat shall be designed to accomodate the following :

e. The maximum heat load to the single phase helium is not to exceed 10 W under degraded vacuum conditions (ref 6.2).

**6.2.11 Degraded Vacuum Condition**

Degraded vacuum is defined as that condition occuring with a helium leak rate of 10-6 std cm3/s that extends over period of time of 1 year (with subcontractor-defined pumping or getters). This is a leakage into the normal operation environment.

# HELIUM ADSORBER MODULE CONCEPTUAL DESIGN

- Helium adsorber module concept shown mounted to GHe return line.

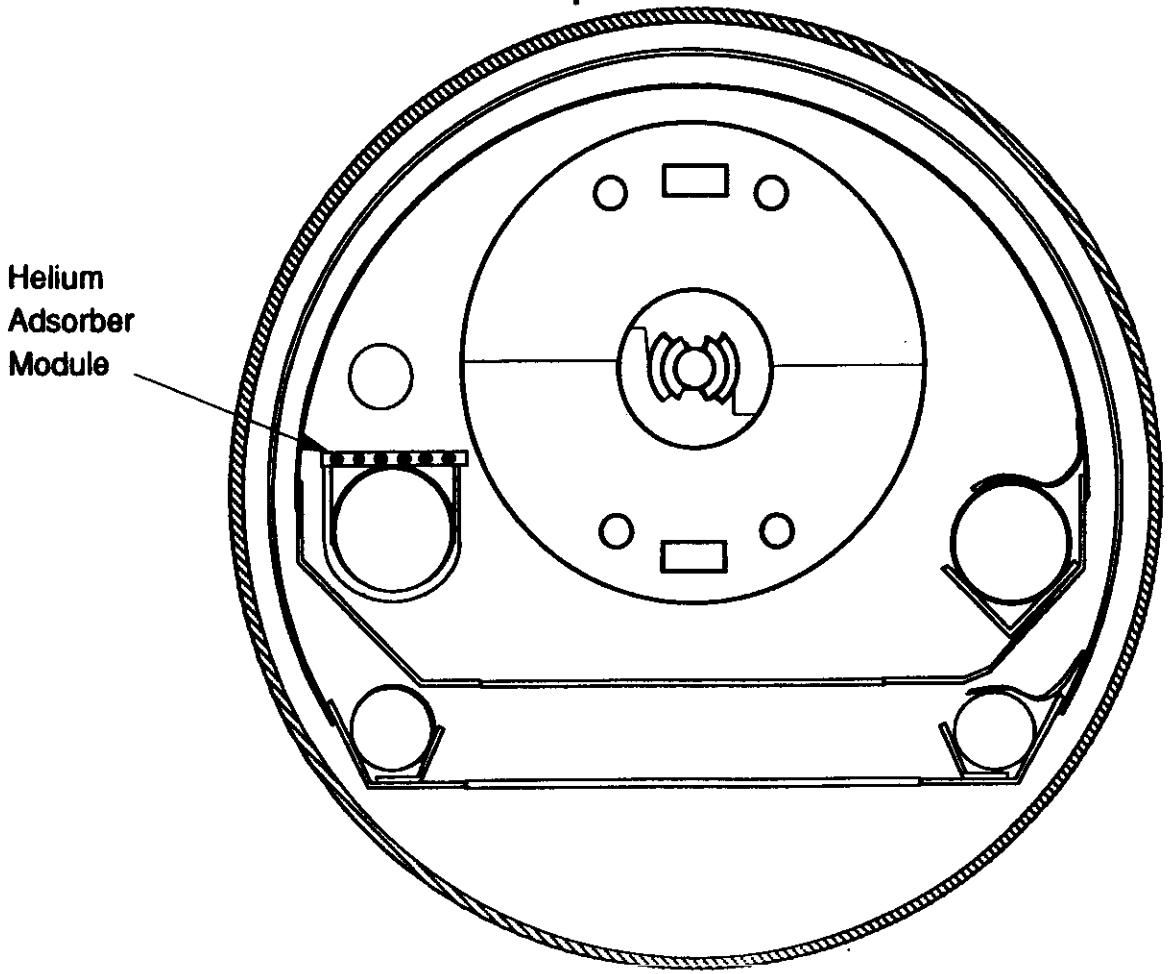

# HELIUM ADSORBER DEVELPOMENT PLAN
## Baseline and Alternatives

The design alternatives investigated for handling the helium leak rate were

- 1) a mechanical pumping device to continually pump out vacuum space.
- 2) use of Multi-layer Insulation (MLI) to impede gaseous conduction.
- 3) sorption pumping where gas molecules are removed by adsorbing to an activated charcoal surface.

# HELIUM ADSORBER DEVELPOMENT PLAN
## Verification

Component level test. (Vendor)

- Verify the ability of the charcoal (granular or cloth) to adsorb a calibrated amount of helium under the nominal operating conditions (4.2K $1X10^{-6}$ torr).
- Demonstrate the dependency of the helium adsorption capacity on charcoal area and helium leak rate.
- Demonstrate the abilty of the adsorbers to adsorb helium after exposure to "other" gases. "Other" gases will be defined as those gases which would be present in the cryostat during normal operation such as water vapor , hydrocarbons etc.
- Validate bond performance (charcoal to substrate) over long term exposure.

# HELIUM ADSORBER DEVELPOMENT PLAN
## Verification

Magnet level testing.

- The magnet level testing will consist of mounting the HAM in a completed cryostat, possibly a magnet on a test stand at Hammond.
- The test could be included in a thermal cycle on the test stand. The pressure level in the cryostat will be monitored and a calibrated amount of helium will be introduced into the magnet.
- This test will be a pass/fail test which will demonstrate the ability of the adsorber to operate in a functional cryostat.
- This test will demonstrate the ability of the HAM to adsorb not only the calibrated helium leak but also any other gas constituents introduced due to outgasssing from the MLI or other cryostat components.

# HELIUM ADSORBER DEVELOPMENT PLAN
## Verification

Analysis

- Leak rate introduces 24 torr-l into the cryostat in one year
- Adsorption capacity of up to 8 torr-l/cm$^2$ (Reference 1)
- Design adsorption capacity .1 torr-l/cm$^2$ to maintain 1.33 X 10$^{-4}$ Pa (1X10$^{-6}$ torr)
- 240 cm$^2$ (37 in$^2$)of charcoal required per dipole
- Need to verify adsorption capacity as a function of pressure and temperature
- Need to verify relationship between mass and surface area of charcoal

1) H. C. Hseuh, H. J. Halama , Isabelle Project Technical Note No. 139, Insulating Vacuum in Magnet System, October 15, 1979.

# HELIUM ADSORBER MODULE
## Verification

Analysis

- Degraded vacuum allowable heat leak to 4K is met when operating vacuum maintained below $1.8X10^{-2}$ Pa ($1.5X10^{-4}$ Torr).

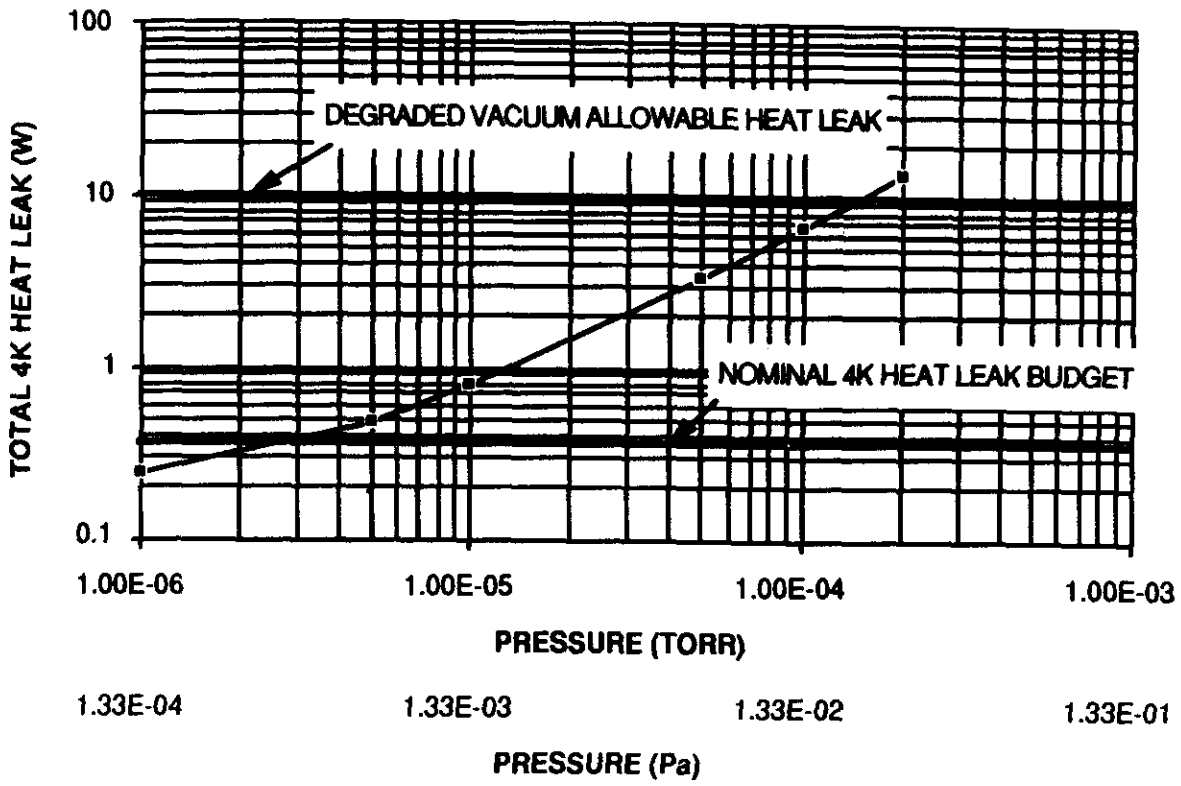

# HELIUM ADSORBER DEVELPOMENT PLAN
## Production implementation

- Performance specification will be put out for competitive bid to vendors of granular bonded charcoal and charcoal cloth.
- The specification will define all of the performance requirements for the HAM including the physical envelope available.
- The specification will also include definition of component verification tests to be performed by the vendor .
- Vendors have been receptive to this procedure in discussions held to date.

# HELIUM ADSORBER MODULE SCHEDULE

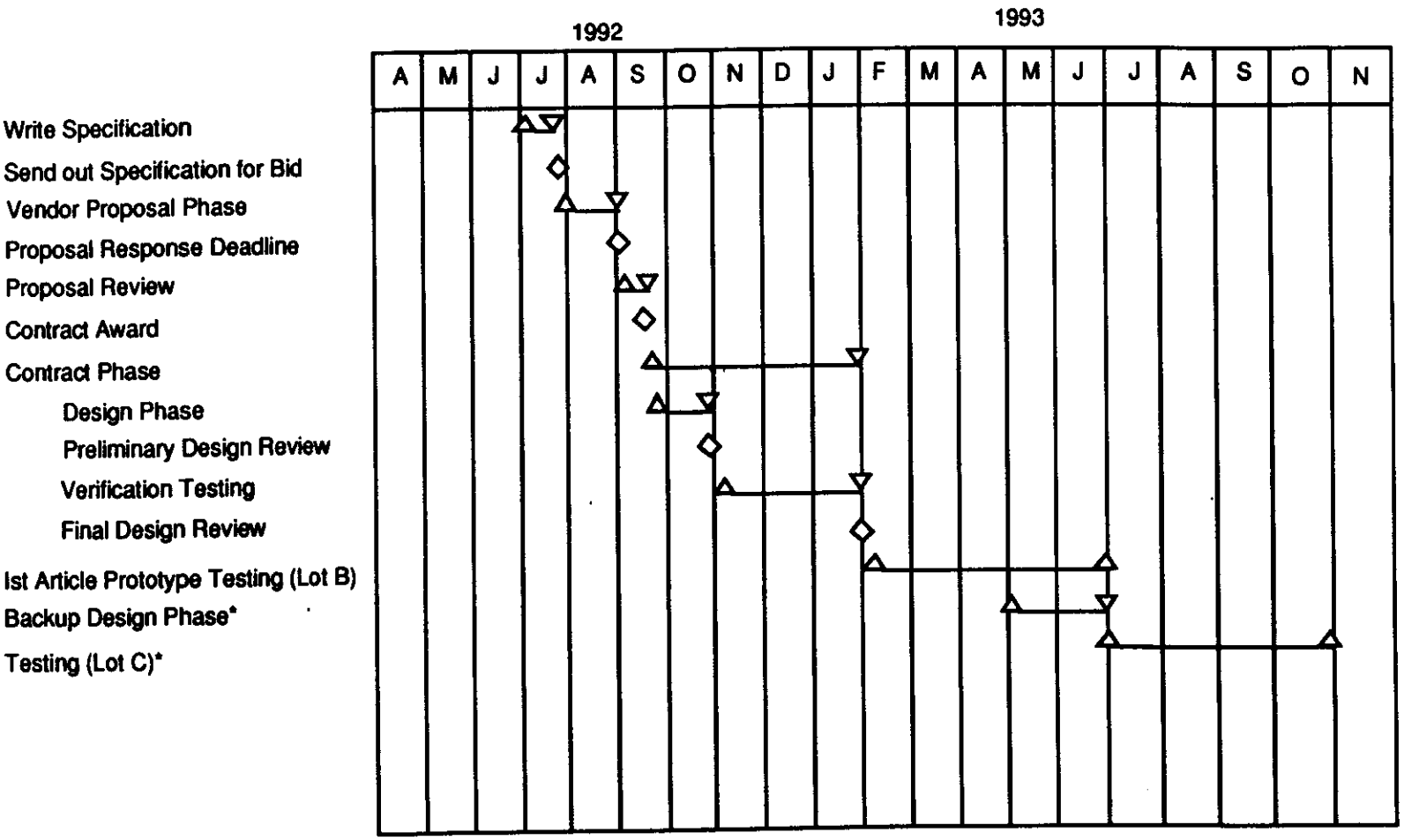


* - If necessary

# SUPPORT POST DEVELOPMENT PLAN

# Support Post Development Plan Review
# Initial Screening Testing

- Initial Screening Test Program Tasks
  - Vendor/GDSS Producibility Evaluation/Assessment
  - Vendor/GDSS Preliminary draft of Manufacturing Specification
  - Fabrication of Coupon Test Cylinders
  - Coupons Instrumented and Tested to Failure in Compression
  - Measure Thermal Conductivity of each material
    - Glass Micro-Balloon Filled Epoxy Syntactic Film
    - Graphite/Epoxy (T300/977-2)
    - Glass/Epoxy (S-Glass/977-2)
  - Evaluation/Selection of Design Configuration

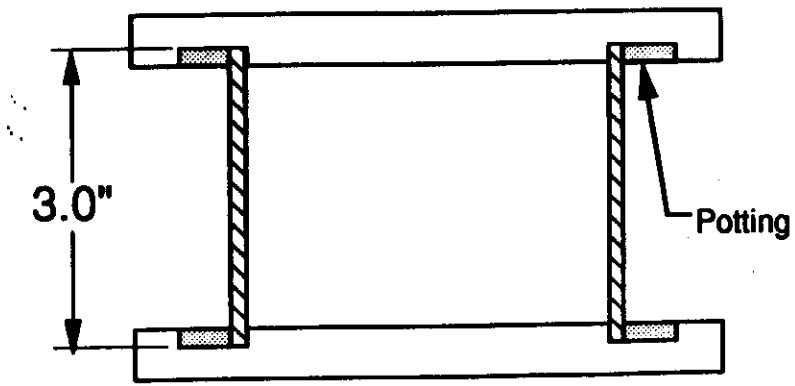

# Support Post Development Plan Review
# Initial Screening Testing

- Evaluate Optional Support Post Options
  - Syntactic Core Sandwich Design
  - Hybrid Composite Joint Design
  - Two Piece Config. (Butt Joint/ Lap Joint)

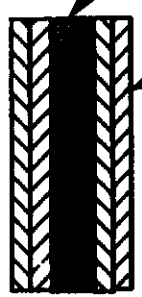


Graphite/Epoxy, Syntactic core Sandwich Composite Tube Concept

Graphite/Epoxy, Glass/Epoxy Hybrid Composite Tube Concept

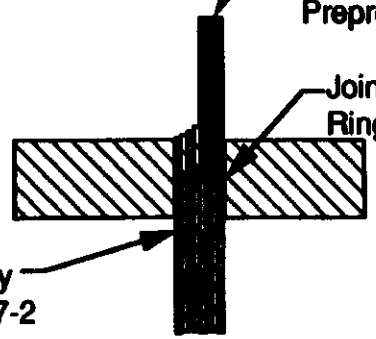


Graphite/Epoxy, Glass/Epoxy Butt Joint Composite Tube Concept

# Support Post Development Plan Review
# Component Test Program

- Component Test Program Tasks
  - Final draft of Manufacturing Specification
  - Structural Testing of Post Assemblies
  - Thermal Testing of Post Assemblies
  - Support Post Slide Testing
  - Long Term Creep Testing

- Structural Testing
  - Validate Design and establish cridical failure mode
  - Establish "A" Allowables for the Support Post Design (F.S. of 2.5)

- Thermal Testing
  - Validate thermal performance of Support Post Design
  - Establish Post Design's contribution to the thermal budget

- Support Post Slide Testing
  - Using two support posts, Measure Friction as a Function of Sliding Cycles
  - Validate Assy does not bind-up and evaluate wear characteristics

- Long Term Creep Testing
  - Load Post to Proof Load and measure axial creep over Six (6) months
  - Validate long term dimensional stability of post design

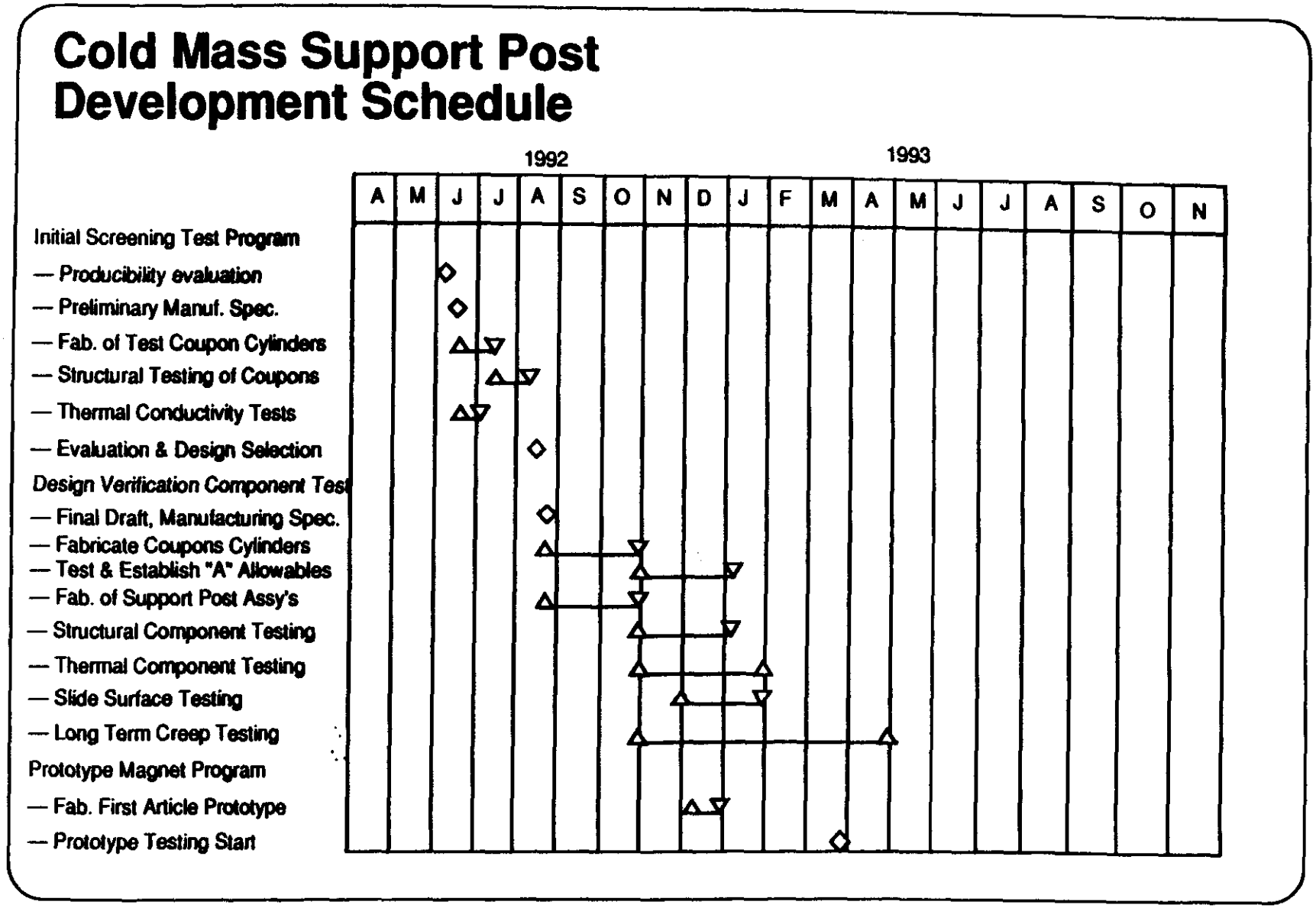


Figure 6. Cold Mass Support Post Development Plan Schedule

# Support Post Development Plan Review
# Current Baseline Approach

- Select Baseline Design
  - FNAL Concept of Straight Post with Press-Fit Thermal Intercepts
  - Comp. Tube: Syntactic Core Sandwich with Carbon/Epoxy face sheets
  - Use existing typical material property & thermal property data
  - Use a Safety Factor of 5 (vs. 2.5) on typical material properties
  - Thermal Analysis ( Design meets Thermal Budget based on extrapolation of existing typical data)

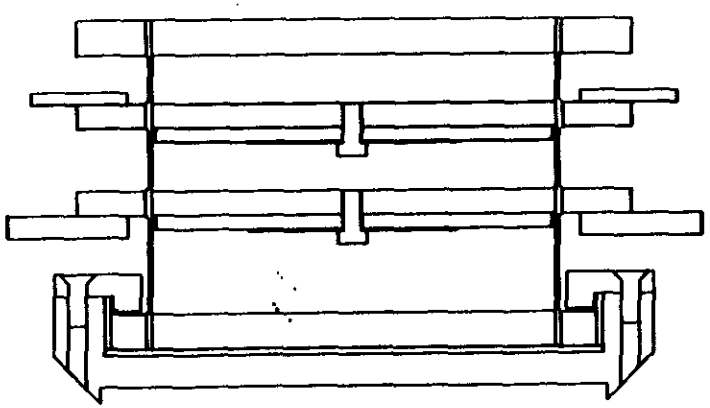

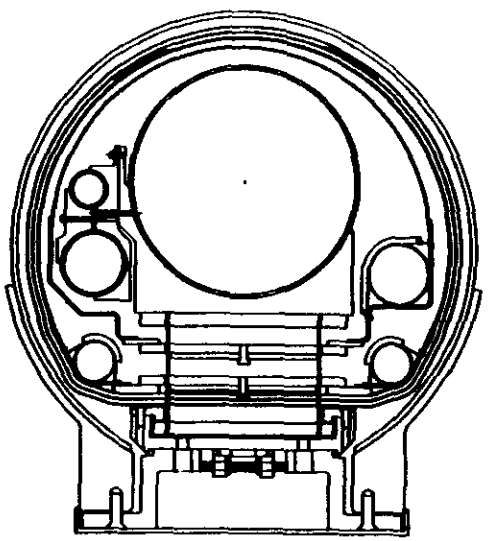

Syntactic Core Sandwich (T300/epoxy cloth face sheets)

# T300/SYNCORE POST HEAT LEAK PREDICTIONS

Heat leak calculation based on :

- $Q = A/L \int K \, dT$
- Syntactic core K extrapolated from room temp. value
- Perfect thermal intercept performance
- T300 fiber orientation 50% warp 50% fill

| CRYOGENIC STATION | HEAT LEAK IN W PER POST * | | |
|---|---|---|---|
| | 4 PLYS | 5 PLYS | GOAL |
| 80K | 2.61 | 3.24 | 3.16 |
| 20K | 0.21 | 0.25 | 0.48 |
| 4K | 0.028 | 0.034 | 0.032 |

# THERMAL SHIELDS DEVELOPMENT PLAN

- THERMAL STRAPS
- THERMAL SHIELD EMISSIVITY

# THERMAL SHIELD DEVELOPMENT PLAN
# THERMAL STRAPS

## TRADE STUDY ISSUES

- Brazing the strap directly to the stainless steel cryogenic line and thermal shield.
- Swaging the strap into a stainless lug on one end, and an aluminum lug on the other, and fusion welding the lugs to the stainless pipe or aluminum shield.
- Clamping copper sleeve around cryoline, and soldering strap to the sleeve.
- Swaging an aluminum lug to the strap, and bolting the lug to the thermal shield with or without a soft interstitial material to improve thermal contact.
- Magneforming a copper sleeve around the cryogenic line, and soldering the strap to the sleeve.
- Partially or entirely copper plating the outer surface of the cryogenic line and soldering the strap to the line.
- Locally brush plating of copper to the aluminum shield at one end, and to the cryogenic line at the other , and soldering the thermal strap to the shield and the cryogenic line at the local copper pads.

# THERMAL SHIELD DEVELOPMENT PLAN
# THERMAL STRAPS

Verification

1. Each plating vendor is send 1 piece of 304 sheet stock 1000mm x 200mm x 3mm, and 1 piece of 1220mm x 305mm x 2.5 mm 6061-T6 aluminum sheet stock.

2. Each vendor plates 10 patches of approx. 25 by 25 mm on each material and returns the plated pieces to GDSS for evaluation.

3. GDSS cryoshocks each plated sample in LN2 to locate any unsound plating areas.

4.GDSS solders one end of a thermal strap to each patch on the aluminum sheets, and the other end to each patch on the stainless sheets. The soldered assemblies are cut into test articles for cryogenic testing.

5. All test articles are subjected to a cryoshock test which will show poor adhesion conditions. For this test, the test articles are submerged in LN2 until boiling stops, followed by warming to ambient temperature.This cycle is repeated 5 times.

# THERMAL SHIELD DEVELOPMENT PLAN
# THERMAL STRAPS

Verification continued.

6. Two samples from each vendor are used to test the quality of adhesion between the thermal straps and the soldering patches. The test will be conducted in liquid hydrogen and consists of laterally moving one of the two metal sheets which are interconnected by a thermal strap, a total of one inch with respect to the other, and returning it to its original position. This action will be repeated 200 times. A test will be considered successful, if no debonding of the thermal straps from the sheet metal parts is visually observed.

7. Should the results of these tests indicate a problem with these thermal strap attachment methods, we will repeat them using alternate attachment concepts. If the problem is with the attachment of the straps to the cryogenic lines, we will test magneformed copper sleeves around the cryogenic lines. If the other strap end does not meet our requirements, the strap attachment will then be accomplished by swaging an aluminum sleeve onto the strap and welding it onto the aluminum sheet. The schedule in section 1.6 shows that on May 22 it will be determined whether the adhesion of the plating to the substrate is adequate. If not, there is sufficient time to the start of production of the first prototype magnet to repeat the test program.

# THERMAL SHIELD DEVELOPMENT PLAN
# THERMAL STRAPS

## Verification

Prototype CDM's temperature sensor locations.

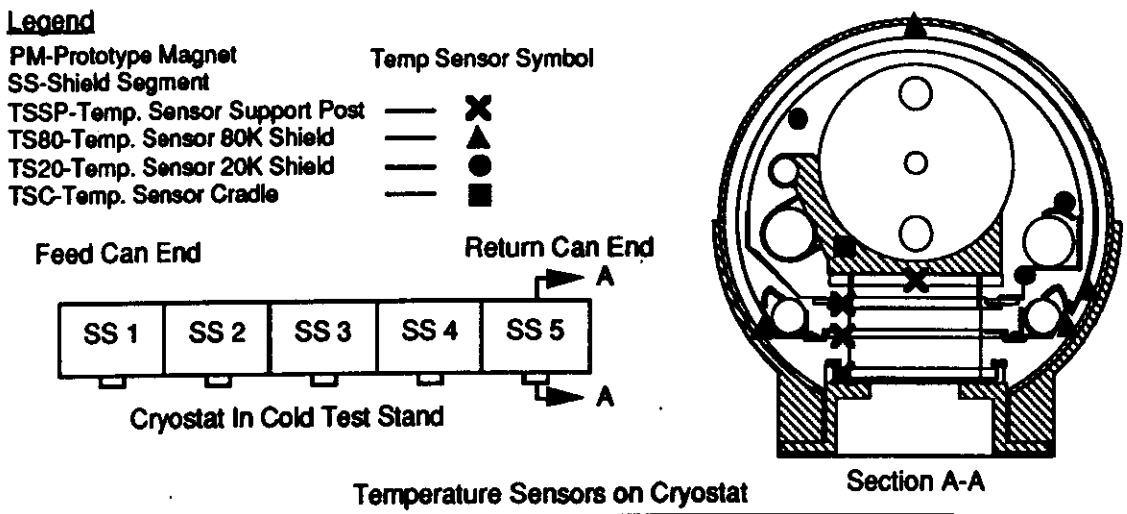


Temperature Sensors on Cryostat

| Cryostat Shield Element | SS 1 | SS 2 | SS 3 | SS 4 | SS 5 | Total On PM Num. | |
|---|---|---|---|---|---|---|---|
| | | | | | | 2,9 & 12 | 4,6 & 11 |
| 80 K Shield | 4 | 0 | 0 | 4 | 4 | 12 | 12 |
| 20 K Shield | 0 | 3 | 3 | 0 | 3 | 9 | 9 |
| Cradle | 1/0 | 1/0 | 1/1 | 1/0 | 1/0 | 5 | 1 |
| Support Post | 4/0 | 4/0 | 4/4 | 4/0 | 4/0 | 20 | 4 |

# THERMAL SHIELD DEVELOPMENT PLAN
# THERMAL STRAPS

## Schedule

| Task | Start Date | Complete Date |
|---|---|---|
| Procure CRES and Al; | Completed | Completed |
| Send Mat'l to 5 vendors | Completed | Completed |
| Obtain Thermal Straps | 5/11/92 | 6/26/92 |
| Vendors Plate Samples | ongoing | 5/15/92 |
| Receipt & Inspect samples | 5/20/92 | 5/22/92 |
| LN2 Shock samples | 5/22/92 | 5/22/92 |
| Solder Straps to samples | 6/29/92 | 6/30/92 |
| LN2 shock soldered samples | 6/29/92 | 6/30/92 |
| Send samples to thermal Test | 6/29/92 | 6/29/92 |
| LH2 cycle samples | 6/29/92 | 7/6/92 |
| Compile Data & Publish | 7/6/92 | 7/20/92 |

# THERMAL SHIELD DEVELOPMENT PLAN
# THERMAL SHIELD EMISSIVITY

## Summary of Trade Study Issues

No trade study was performed or nessessary other than the selection of the following surface treatments which should be evaluated:

1.As received, cold rolled sheet with no surface treatment or coating. If this material meets the emissivity requirements even after the samples have been exposed to the ambient environment for an ewxtended period of time, this would clearly be the material of choice.

2. Mechanically polished surface protected with plastic film until used. This material is less desirable since it requires an additional operation prior to installation.

3. Electropolished + 0.0025 mm Sulfuric Acid Anodize

4. Alodine 1500, a clear chemical film covering the surface.

# THERMAL SHIELD DEVELOPMENT PLAN
# THERMAL SHIELD EMISSIVITY

## Tests

Several samples of 6061-T6 sheet stock were obtained from General Dynamics Convair Division Materials & Processes Laboratories. The samples were quality control specimens for several MD-11 surface finishing processes. The following values of absorbance and emittance for 4 of these surface tratments were obtained at room temperature:

| Surface Condition | Absorbance | Emittance |
|---|---|---|
| 1.Off the shelf, as received with no coating | 0.455 | 0.07 |
| 2. Polished surface w/plastic sheet (bare) | 0.260 | 0.05 |
| 3. Electropolished +0.0025mm Sulfuric Acid Anodize | 0.260 | 0.69 |
| 4. Alodine 1500 (Clear Chem Film) | 0.141 | 0.05 |

# Cryogenic Performance of MLI in ASST

D. Franks

# CRYOGENIC PERFORMANCE OF MLI IN ASST

Don Franks

MSD / Cryostat Design

Monday June 29, 1992

Figure 1

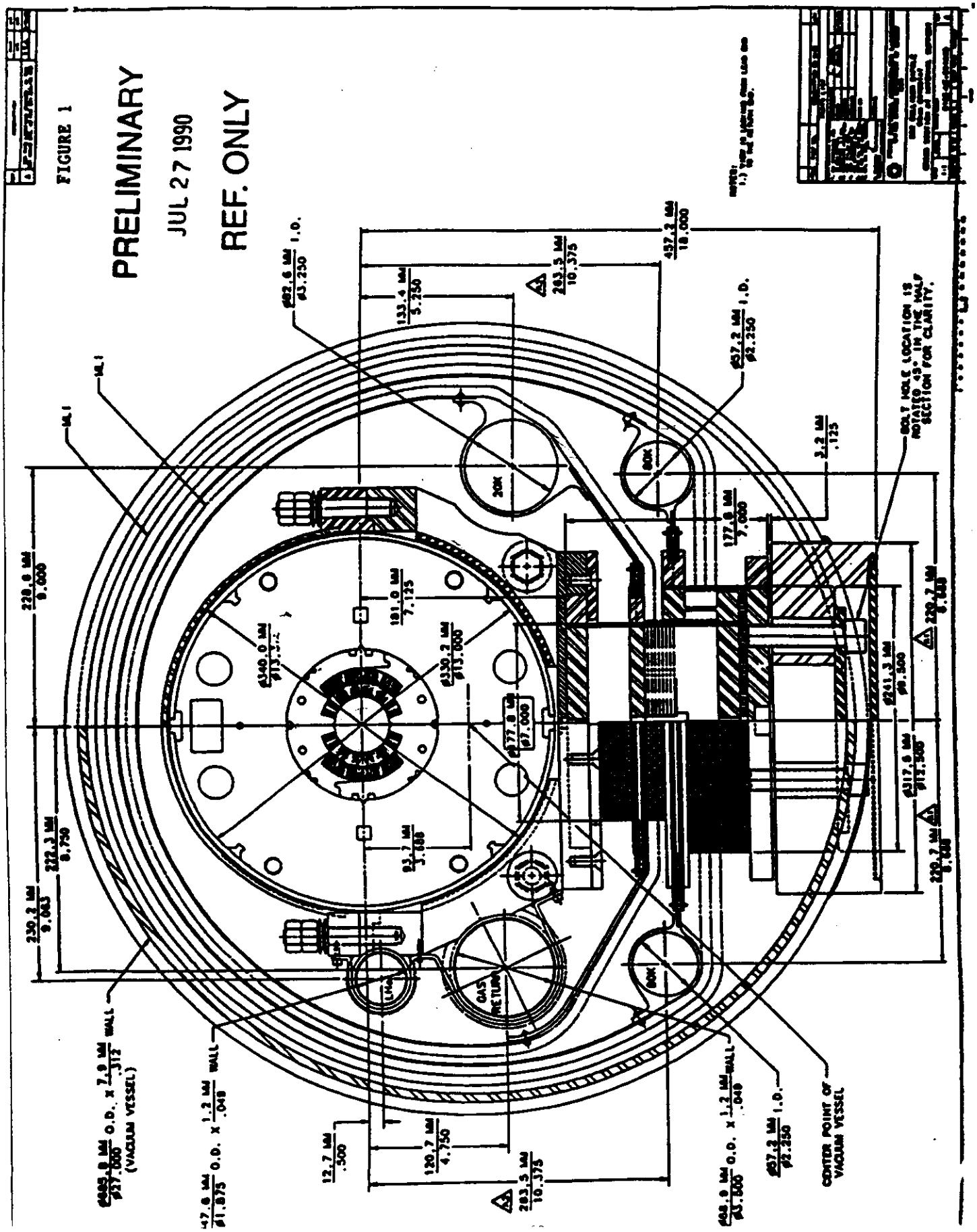
FIGURE 1
PRELIMINARY
JUL 27 1990
REF. ONLY
20K
80K
GAS RETURN
CENTER POINT OF VACUUM VESSEL
BOLT HOLE LOCATION IS ROTATED 45° IN THE HALF SECTION FOR CLARITY.

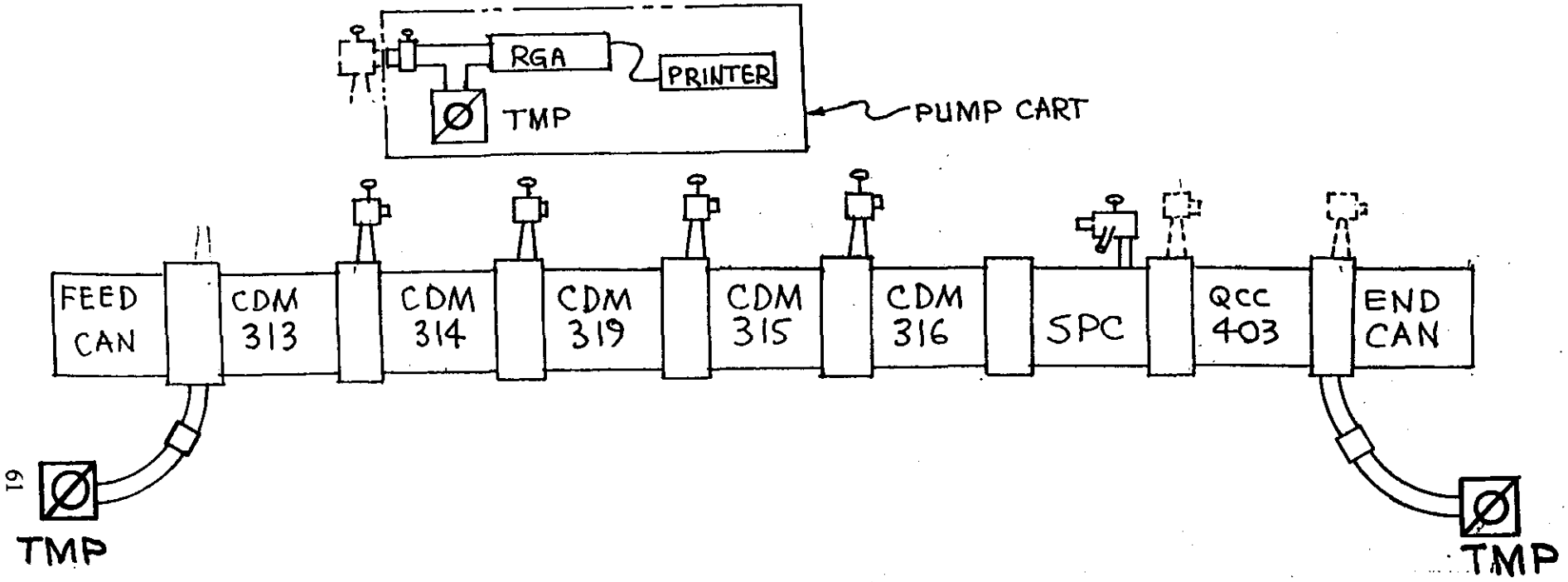


# ASST Magnets and RGA Sensing Locations

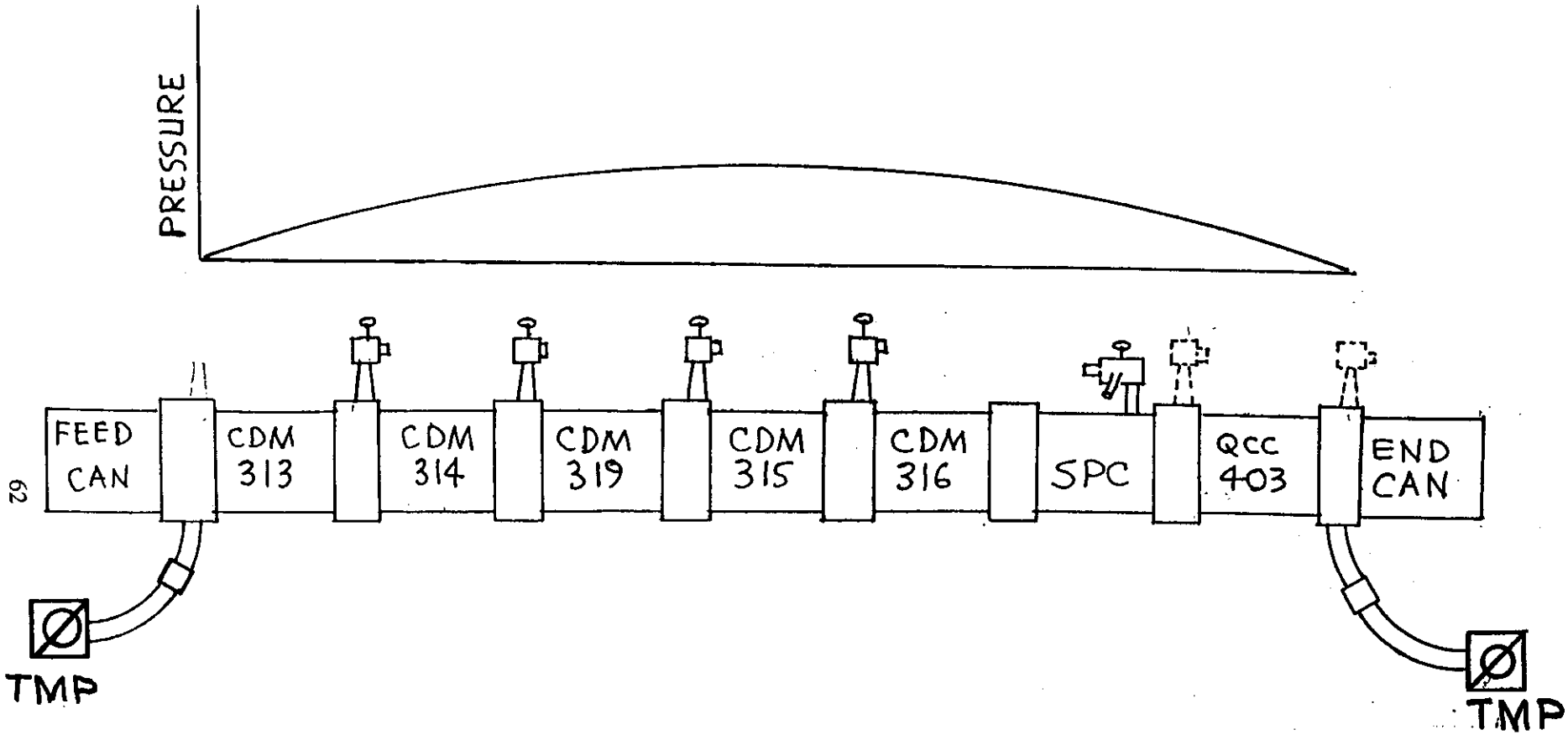


# ASST Magnet Cryostat Vacuum Outgassing Expected Pressure Distribution

SMS BAR GRAPH
STORING BACKGROUND

PRINT MODE--SINGLE
PRECISION---4
GAIN--------E-11
MASS IDENT--18
PART PRESS--E.E

MULTIPLIER--ON
FIL #1------ON
RESET-------OFF
DISP SPAN---100
FULL SPAN---OFF

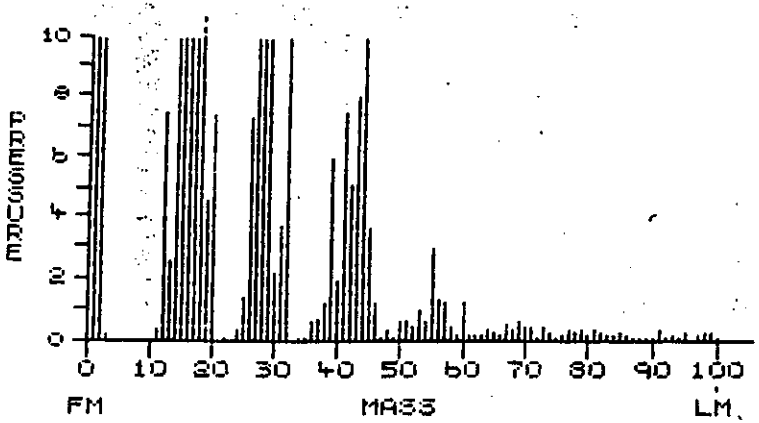


4.0° K

Background test
ER Sept 2 91
9-6-91

Before quench

SMS PEAK SELECT ON LINE

PRINT MODE--SINGLE
PRECISION---5
GAIN

FIL #1------ON
RESET-------OFF

| CHANNEL | MASS | ALARM | TORR | M/F |
|---|---|---|---|---|
| 1 ON | 0 | OFF | 3.3xE-08A | F |
| 2 ON | 1 | OFF | .7xE-10A | F |
| 3 ON | 2 | OFF | .xE-10A | F |
| 4 ON | | OFF | .5xE-11A | F |
| 5 ON | 17 | OFF | .2xE-09A | F |
| 6 ON | 18 | OFF | .1xE-08A | F |
| 7 ON | 20 | OFF | .1xE-10A | F |
| 8 ON | 28 | OFF | .0xE-09A | F |
| 9 ON | 32 | OFF | .7xE-10A | F |
| 10 ON | | OFF | .xE-11A | F |
| 11 ON | | OFF | .xE-10A | F |
| 12 OFF | 17 | OFF | .-xE-05A | F |
| 13 OFF | 20 | OFF | .-xE-05A | F |
| 14 OFF | | OFF | .-xE-05A | F |
| 15 OFF | 50 | OFF | .-xE-11A | F |
| 16 OFF | 0 | OFF | .-xE-11A | F |

# RGA Measurement from FNAL 40 mm Dipole String Test at ER Sept 6, 1991



5

FNAL ER RGA DATA 7/6/91

(LAST DISTRIBUTION BEFORE QUENCH)

9-10-91

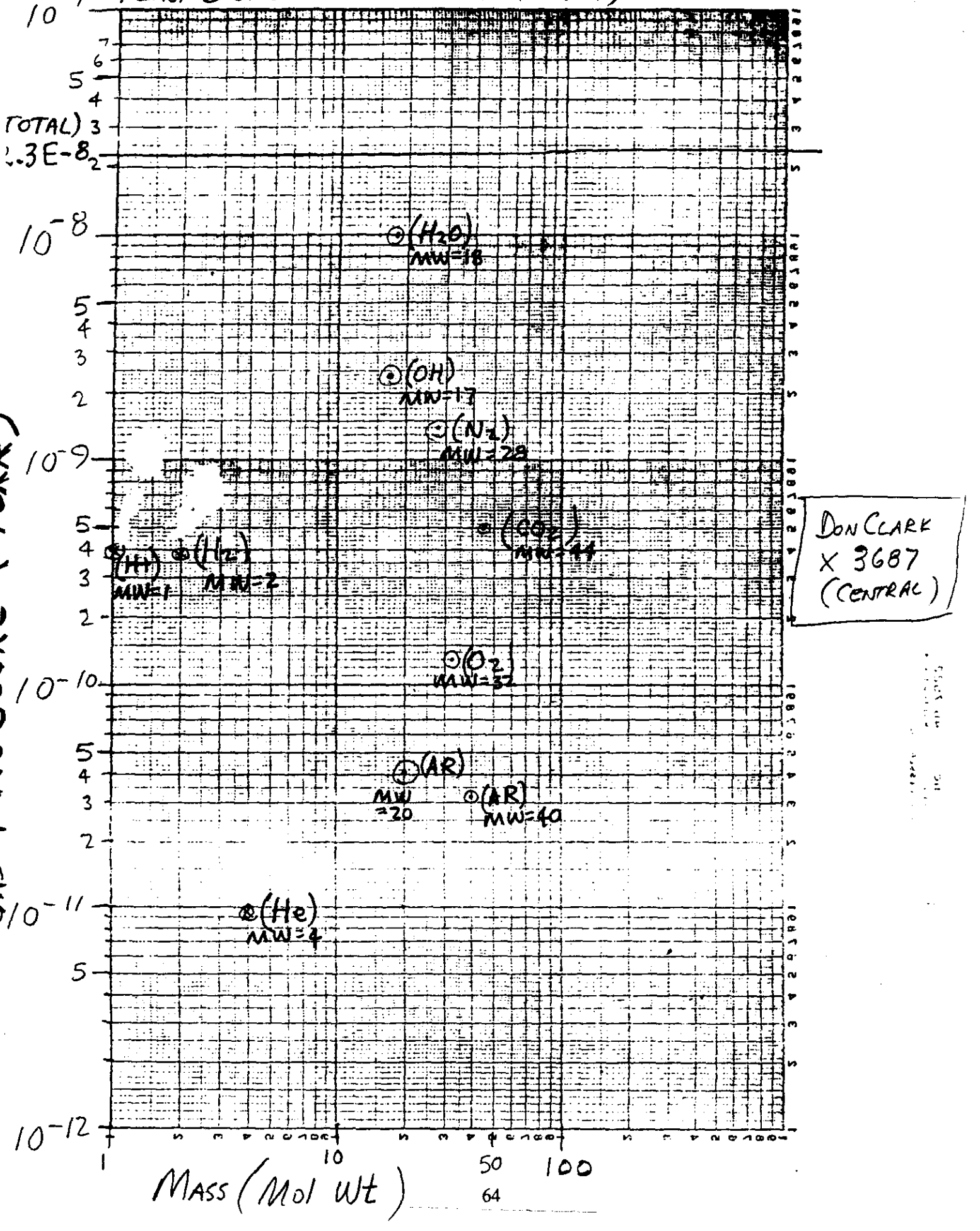

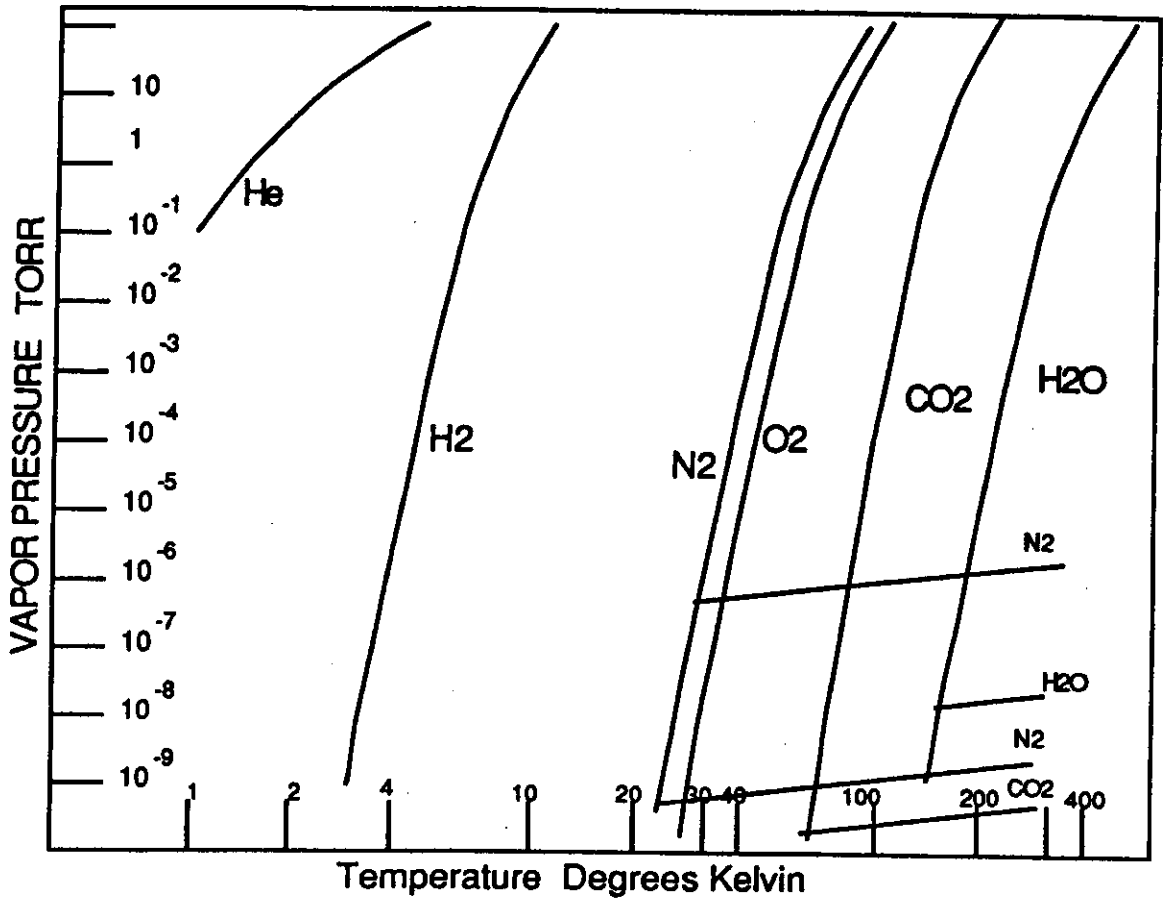


**Vapor Pressure Versus Temperature for Several Gases and Their Expected Cryocondensation Temperatures**

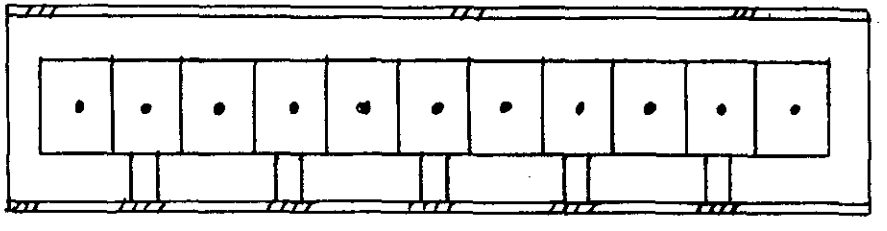

# THERMAL MODEL CONCEPT

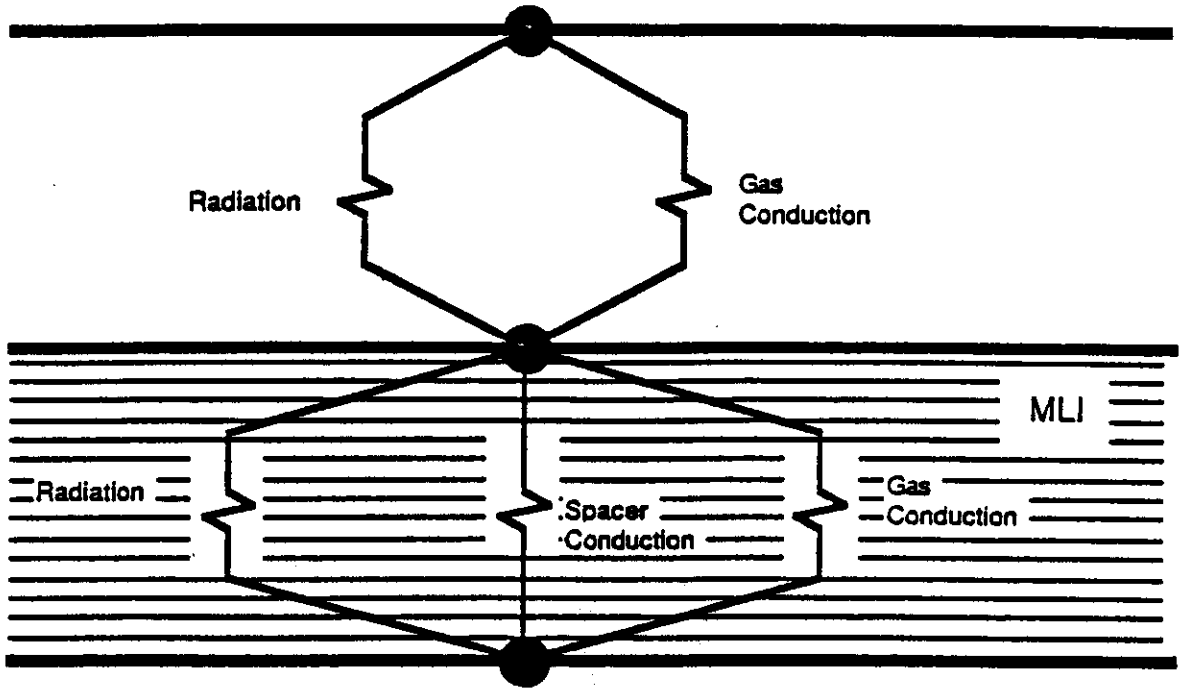


# Modeling of Radiation, Gas Conduction and Spacer Conduction in MLI and Spaces Between Shields

| | 4.5K | 20K | 80K |
|---|---|---|---|
| **Static Heat Loads** | | | |
| Infrared | 0.053 W | 2.335 W | 19.1 W |
| Support conduction | 0.160 W | 2.400 W | 15.8 W |
| Interconnect | 0.150 W | 0.320 W | 2.1 W |
| Total static | 0.363 W | 5.055 W | 37.0 W |
| **Dynamic Heat Loads** | | | |
| Synchrotron radiation | 2.169 W | | |
| Splice IR heating | 0.140 W | | |
| Beam microwave | 0.195 W | | |
| Beam gas | 0.136 W | | |
| Total dynamic | 2.640 W | | |
| Total Dipole | 3.003 W | 5.055 W | 37.0 W |

# Dipole Magnet Heat Leak Budget

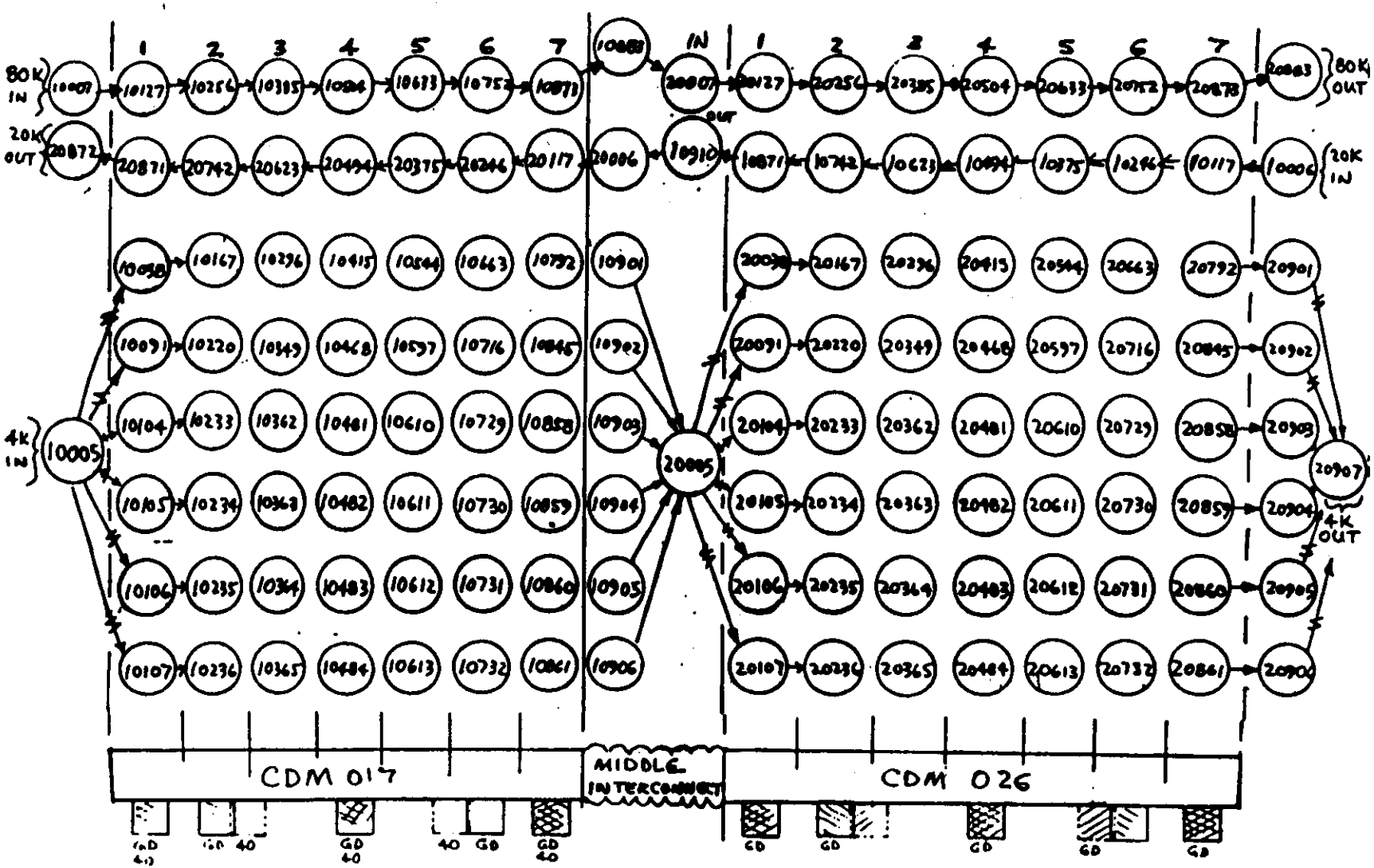


ER ST FLOW MODEL NETWORK

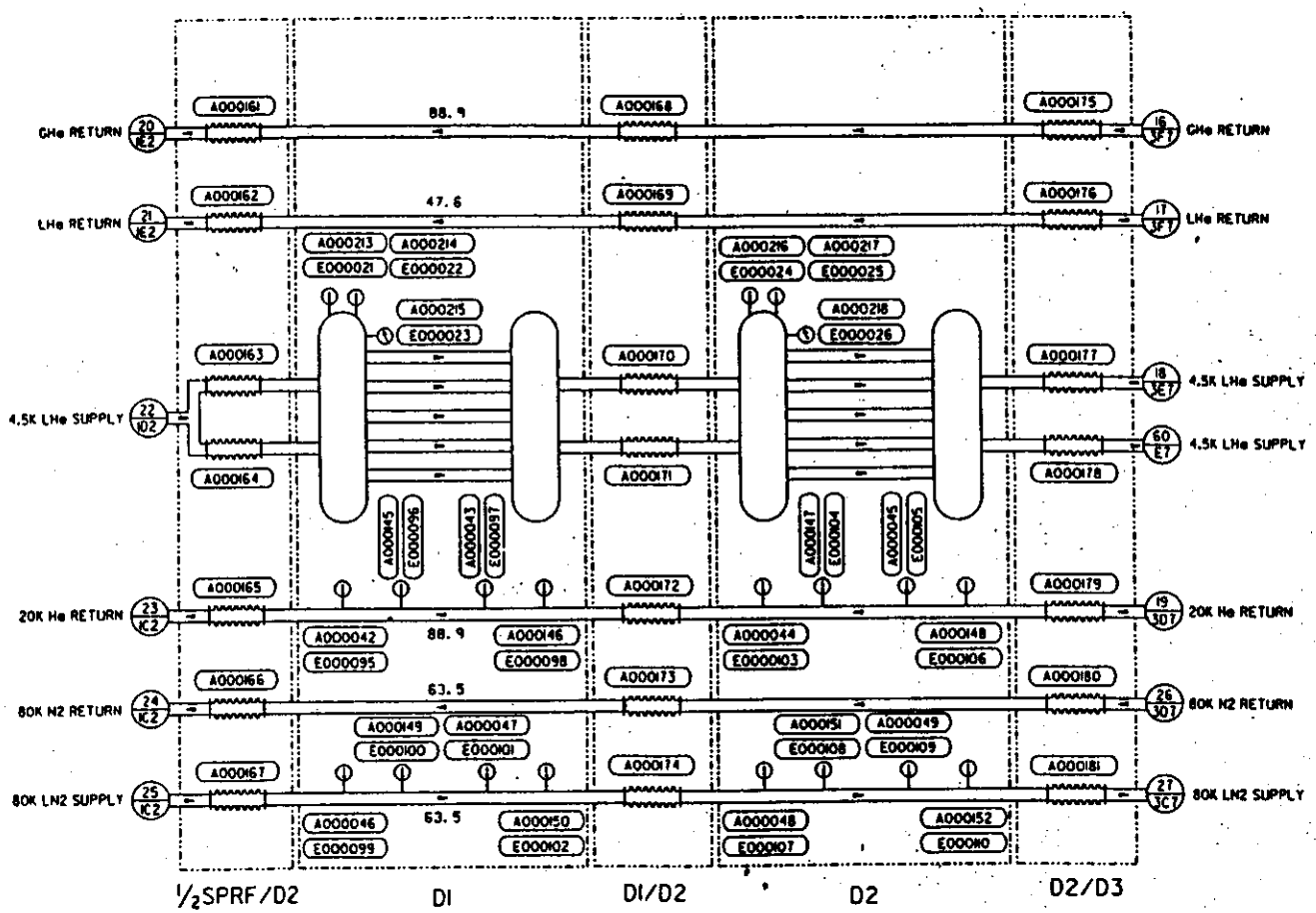


# ASST Ph 1 Flow Schematic and Instrumentation for Dipole Magnets 1 (#313) and 2 (#314) and Associated Interconnect Regions

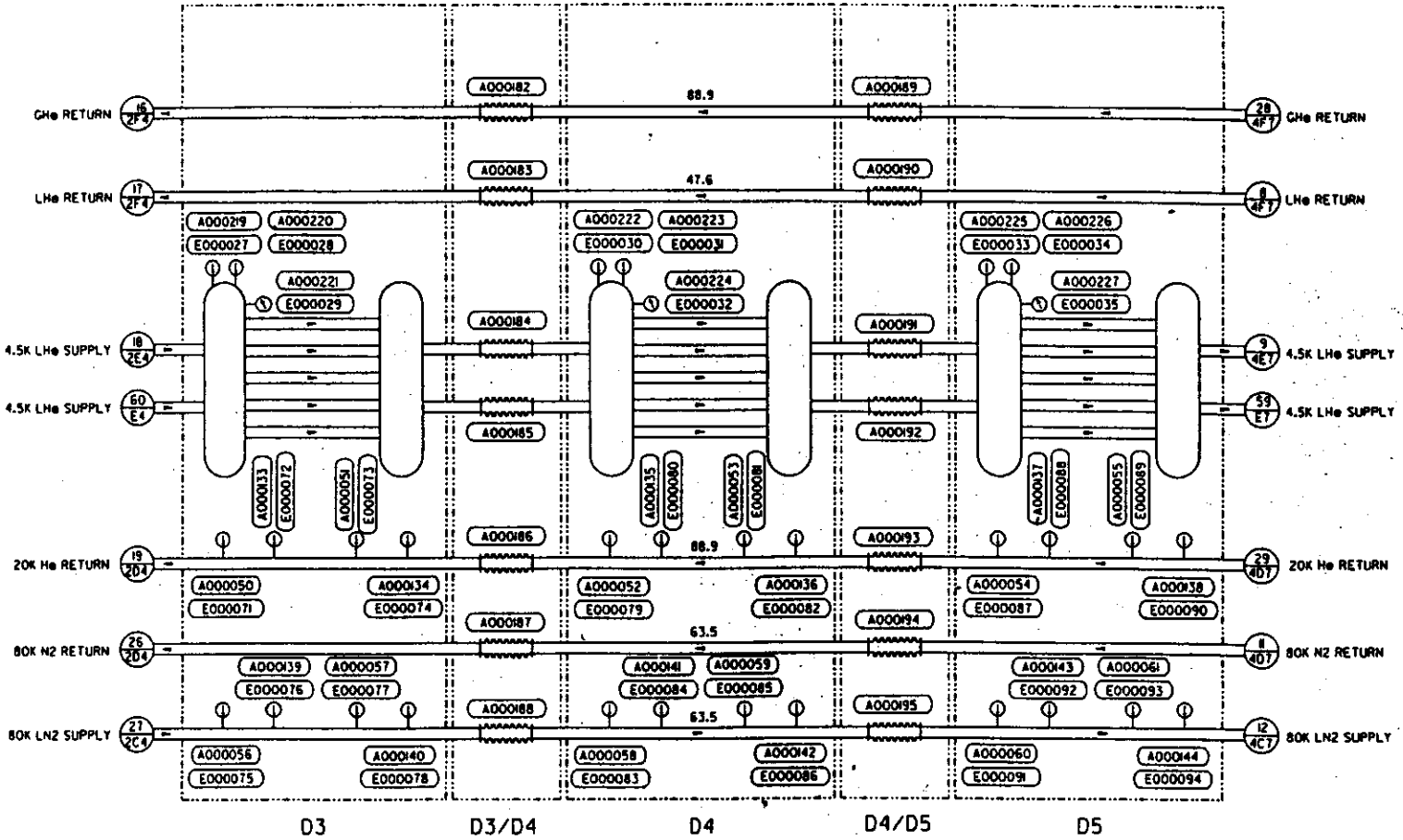


# ASST Ph 1 Flow Schematic and Instrumentation for Dipole Magnets 3 (#319), 4 (#315) and 5 (#316) and Associated Interconnect Regions

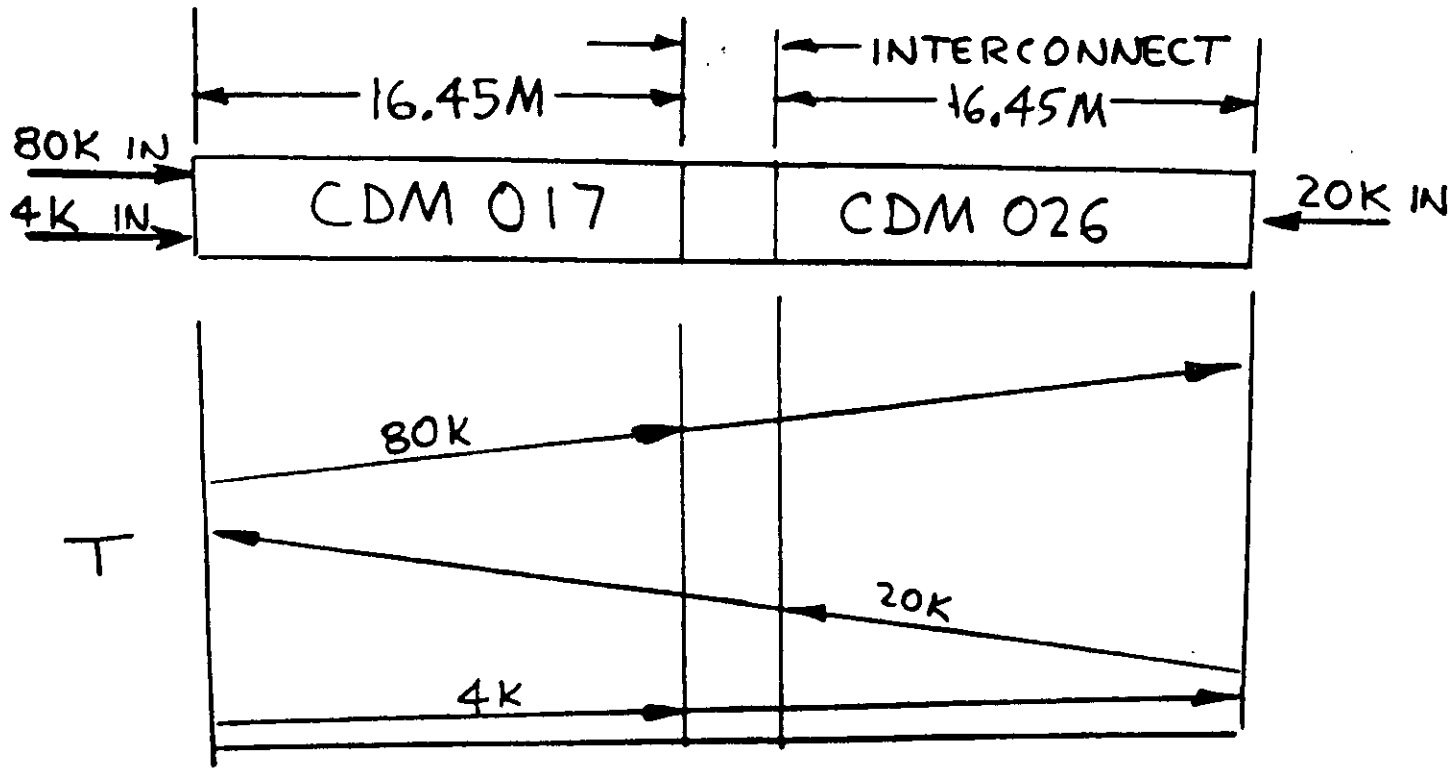


# ER String Test Flow Arrangement

PROB#1 (12/17/90)

D&F 10/17/91

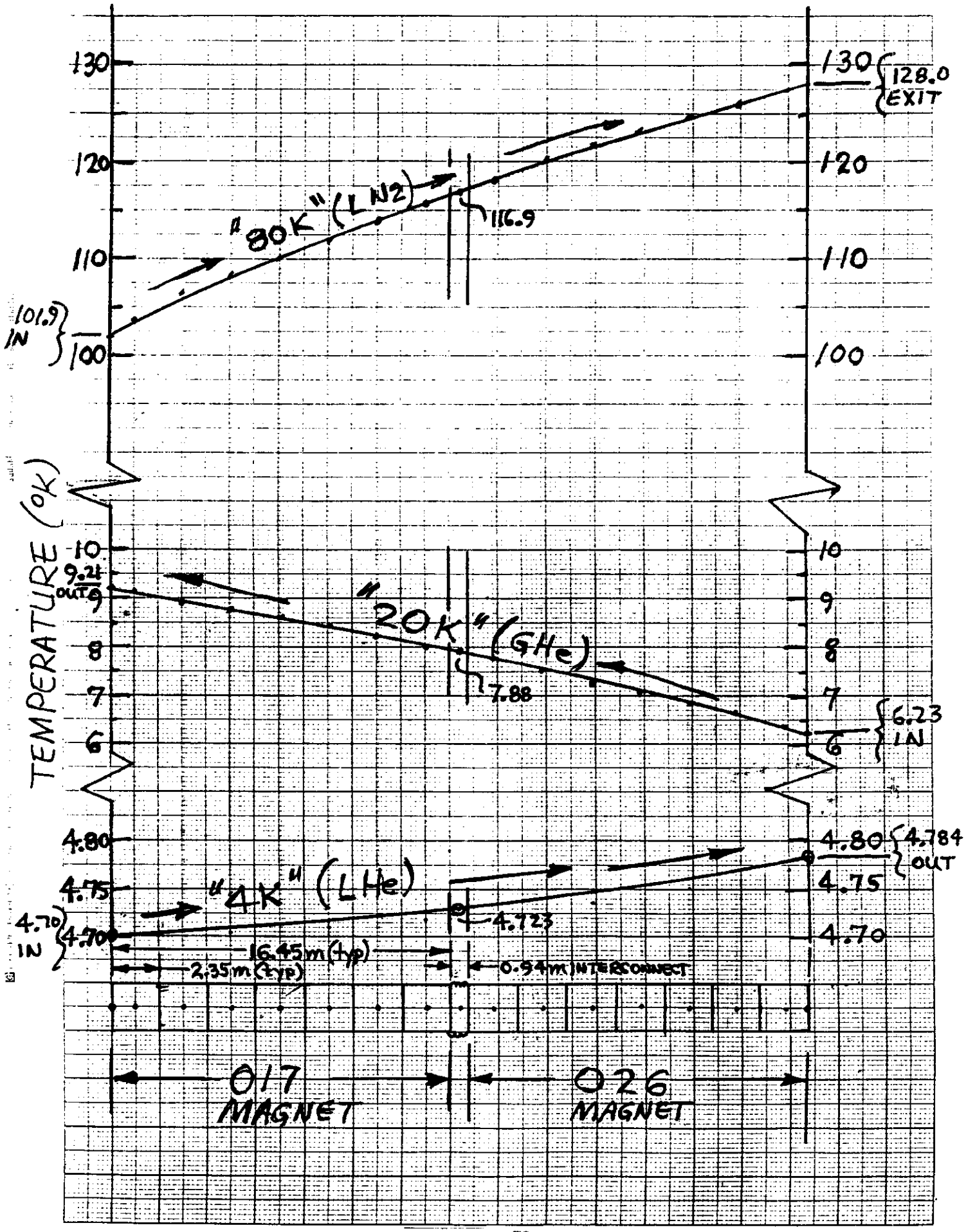

PROBLEM #2 (12/18/90)

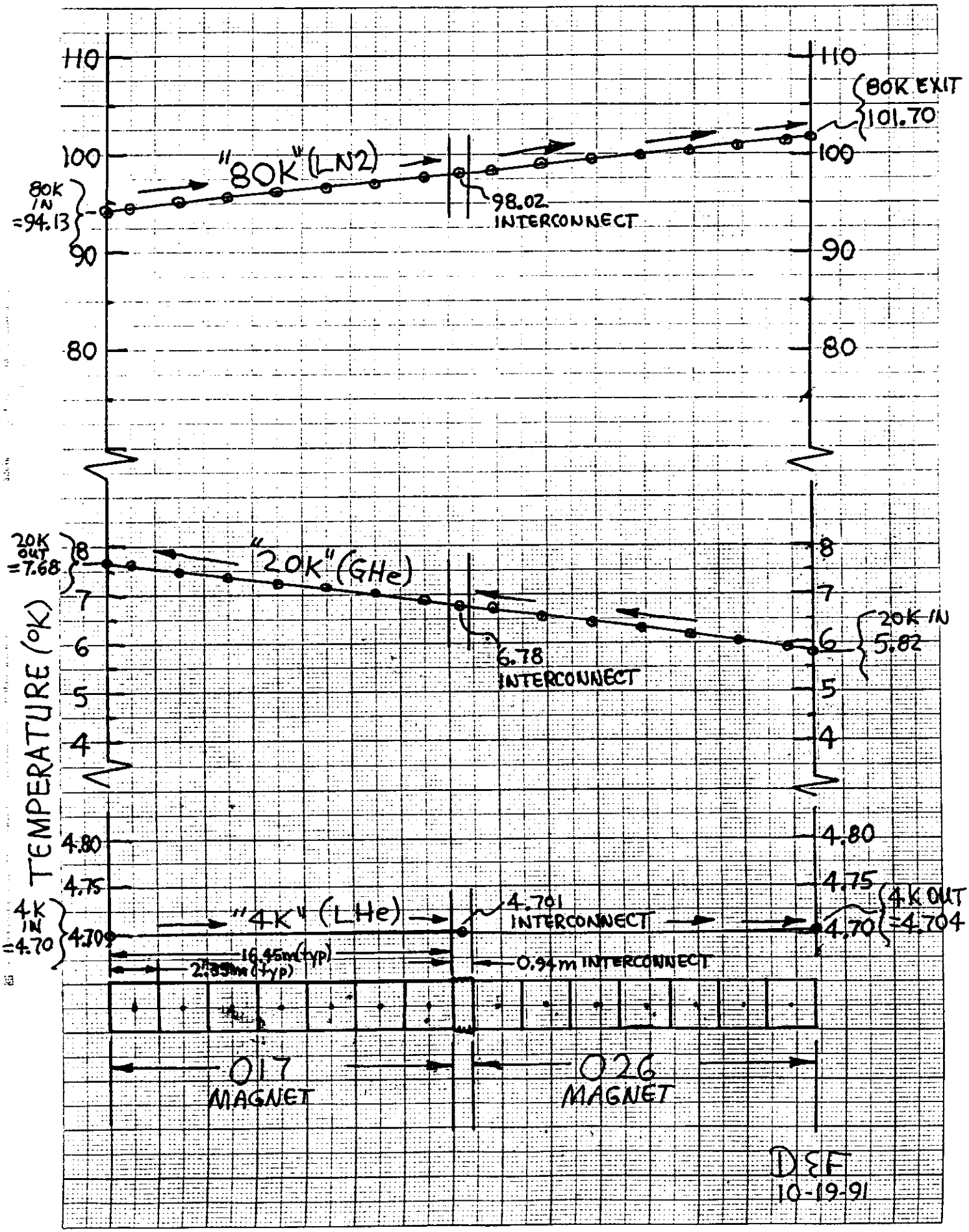

## Areas of Some Magnet Thermal Uncertainty - As Seen by MSD / Cryostat Design

o Thermal radiation emittances of cryostat materials at cryogenic temperatures

(A) MLI reflector (DAM) in 80 K and 20 K MLI
and
(B) 80 K and 20 K thermal shields

o No component testing on any of above at cryogenic temperatures

0 Randy Pletzer has "bracketed" e, some, for 80 K MLI. This is per the Stan Augustynowicz MLI Heat Transfer ER-FNAL, 5 Dipole String Test data, dated 5 Dec, '91. However, we need more data, here (80 K MLI). Especially with instrumented layers of MLI and 80 K shields below.

## PLANS FOR ASST THERMAL SUPPORT

- o Make some additions - unique to ASST - to Randy Pletzer's 50 mm CDM Interconnect thermal model (e.g., Interconnect wiring, voltage tap, etc).
- o Link this Interconnect thermal model to that for the CDM to form a "comprehensive" single magnet ASST thermal model.
- o Use this ASST CDM model with the cryogen supply flow conditions to predict thermal performance for "perfect design" ASST Dipole magnets.
- o We can use Randy's Quadrupole magnet thermal model to assess QCC-401 thermal performance. We are unable to evaluate the Spool Piece.
- o We will also take a series of RGA readings over some period of time of the outgassing in the ASST magnets insulating vacuum.

## ASST BENEFICIAL THERMAL RESULTS ( HOPED FOR )

- o "Effective" (implied) e values for MLI and shields - if the test results are not overshadowed by extra heat leak through "thermal shorts" ( 80K MLI with vacuum vessel wall and 20 K MLI with 80 K shield).

- o More thermal performance data on 80 K MLI. This will carry over to the GD CDM as well as other subcontractor efforts.

- o RGA measurements of outgassing in the cryostat ( Half Cell) insulating vacuum.

  These data will be useful for residual gas conduction analysis and for developing cryostat material handling and cleaning procedures.

  By virtue of the various RGA connection ports we should be able to measure outgassing from each magnet. This will all us to see if there are any differences.

## WHAT WILL AFFECT ASST THERMAL TEST RESULTS

Several Things -

- o Supply cryogen flow conditions. The ASST conditions will not be those of the Collider Ring cooling. Instead, they will be at some "reduced" rates and, probably, something other than "design" inlet conditions, 80K, 20 K and 4.3 K.

- o The "20 K" ( GHe) flow will be in a "counterflow" arrangement to the 80 K and 4.3 K flows. This is different from the Collider Ring.

## ABOUT THE ASST THERMAL RESULTS -

- **What we will get for ASST thermal data measurements will be system level heating ( temperature rises of the 3 cryogen flows through each magnet ) as opposed to component level heating, e.g., through support posts.**

## ABOUT THE ASST MAGNET HEAT LEAK MEASUREMENTS -

- o Collider Ring magnet "budget" heat leak values are those occurring for Collider Ring cooling conditions.

- o Heat transfer is "proportional" to the temperature differences involved. It is also affected by flow rates, too.

- o For ASST, magnet cooling will be different from Collider Ring conditions. Also, the 20 K flow will be "counterflow".

- o Consequently, we can expect heat leaks into the various cryogen flows to be something other than "budget" values. Conceivably, this could be acceptable.

- o However, the only way to know for sure what to expect for heat leaks with ASST flow conditons is through use of thermal math models. This is the same situation for thermal acceptance testing of subcontractor magnets, too.

# THERMAL TESTING TO DETERMINE MLI CRYOGENIC PERFORMANCE

- o Instrumented MLI blanket and shield testing is needed for this.

- o Some such data were taken on the 5 CDM FNAL ER String Test. However, we, MSD / Cryostat Design, need more extensive data.

- o The plan to obtain such data is to instrument a magnet and test it. This is to be done on DCA 323.
  FNAL is installing various thermal sensors throughout the magnet. There will be sensors in both the 80 K and 20 K MLI blankets and on the thermal shields below.

- o Our plan is to test this magnet in ASST Phase 2. We are scheduled into this testing. Tentative date is November '92. We may be the # 2 or # 3 magnet in the extension of the present Half Cell into a Full Cell.

- o If we test this November we may have some results to share by December. DCA 323 will be a "permanent" magnet in this String. Consequently, we should be able to get more data, if needed, later on.

# Quantity and Description of DCA 323 Sensor Instrumentation

| Location | Sensor Quantity | Total # of Sensors |
|---|---|---|
| o Heat intercepts on one support post (300K, 80K, 20K, 4K) | 4 Primary + 4 Backup | (4 + 4) = 8 |
| o One strain gage on each of the five support posts | 5 | 5 |
| o 20K Shields | 8 Primary + 8 Backup | (8 + 8) = 16 |
| o 80K Shields | 8 Primary + 8 Backup | (8 + 8) = 16 |
| o Vacuum vessel - two locations | 1 Primary + 1 Backup at ea location | (2 + 2) = 4 |

Additionally, FNAL plans already call for the DCA323 magnet to use 80K and 20K MLI blankets with temperature sensors at various locations inside. Installation of these sensors was done at FNAL expense. These instrumented blankets are already on hand there. There are in the

o 80K MLI Blanket 18 layers with 3 sensors on ea layer = 54

and

o 20K MLI Blanket 6 layers with 3 sensors on ea layer = 18

Cost for the magnet structure sensors above is about $ 30K. Again, FNAL is supplying the instrumented MLI blankets at their own expense.

# DCA 323 20K MLI Blanket Temperature Sensor Locations

1. THERMOMETER LOCATION IN THE CRYOSTAT

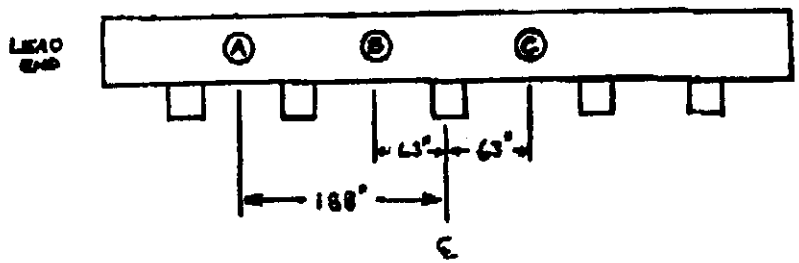


3. THERMOMETER LAYOUT IN THE 20K MLI BLANKET

| LAYER # | SERIAL # |
|---|---|
| 1 | |
| 3 | |
| 5 | |
| 7 | |
| 9 | |
| 10 | |

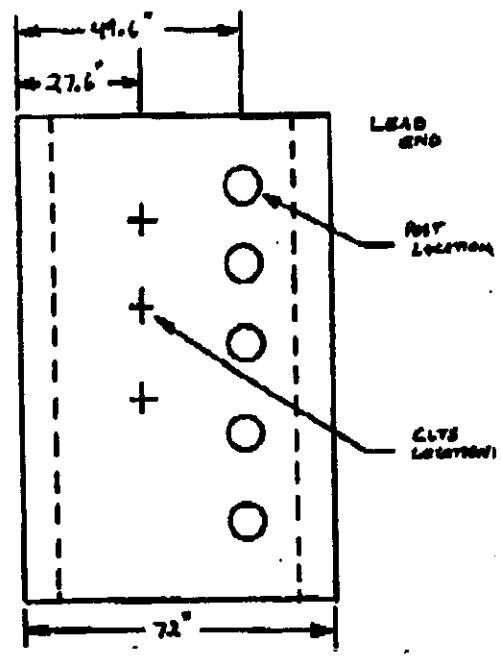

# DCA 323 80 K MLI Blanket Temperature Sensor Locations

1. THERMOMETER LOCATION IN THE CRYOSTAT

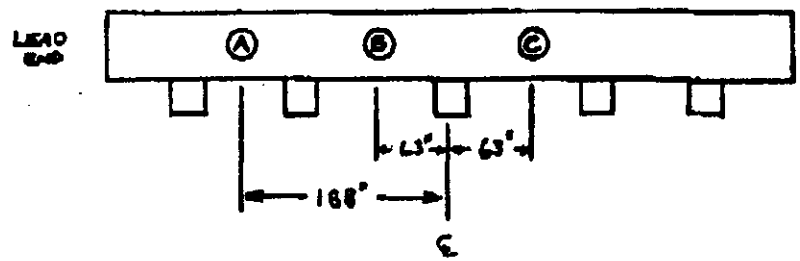


2. THERMOMETER LAYOUT IN THE 80K MLI BLANKETS

. INNER 80K BLANKET

| LAYER # | SERIAL # |
|---|---|
| 1 | |
| 4 | |
| 8 | |
| 12 | |
| 16 | |
| 20 | |
| 24 | |
| 28 | |
| 32 | |

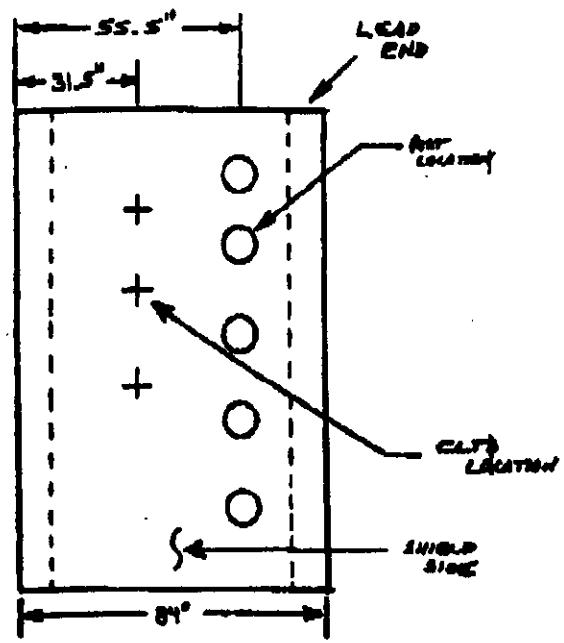

# Cool Down Simulation and Experimental Results of SSC Superconducting Magnets with Difference Cryogenic Systems

Q.S. Shu, D. Orris, A. Prodell, I. Syromyatnikov, and A. Yucel

Presented at the Second Workshop on Testing
of SSC Magnet Cryogenic Performance,
San Diego, Ca. June 29, 1992

# Cool Down Simulation and Experimental Results of SSC Superconducting Magnets with Different Cryogenic Systems

Q. S. Shu, D. Orris*. A. Prodell**,
I. Syromyatnikov and A. Yucel

*Superconducting Super Collider Laboratory*
*Magnet System Division*

# CONTENTS

1. The Math. and Code for Cooldown and Warmup Analyses

2. Comparison of Simulation Results with Fermilab Tests

3. Comparison of Simulation Results with BNL Tests

4. Simulation Results with Different Cooling Procedures

5. Simulation Results with SSCL MTL Cryogenic System

6. A Method to Quickly Estimate The Magnet Cooldown Time

* Fermi National Accelerator Laboratory

** Brookhaven National Laboratory

# COOLWARM CODE

Finite-difference code

Spatial and temporal distributions of iron temperature, helium temperature, helium mass flow rate and helium pressure

Single magnet
Magnet strings with detailed cell structure

Helium and Iron properties incorporated

Input:

- Magnet length, channel diameter, other geometrical information
- Iron mass per unit length
- Entrance helium pressure and temperature
- Entrance helium mass flow rate
- Initial ramping period
- Total simulation time
- Time and distance steps
- Control information for output

Output:

- Files for post-processing
- TOPDRAWER files: iron and helium temperature profiles, and mass flow rate profiles at selected times; exit iron, helium, mass flow rate and pressure vs time, etc.

# COOLDOWN AND WARMUP ANALYSIS

One-dimensional channel flow of single-phase helium
Lumped model for iron; distributed model also available.

Helium mass conservation:

$$A\frac{\partial \rho_g}{\partial t} + \frac{\partial w_g}{\partial x} = 0$$

Helium energy:

$$\tau_g \frac{\partial T_g}{\partial t} + \lambda_g \frac{\partial T_g}{\partial x} = T_i - T_g$$

Helium pressure:

$$-\frac{\partial p}{\partial x} = 2\frac{f}{D}\left(\frac{w_g}{A}\right)^2 \frac{1}{\rho_g}$$

*Iron Temperature:*

$$\tau_i \frac{\partial T_i}{\partial t} = T_g - T_i$$

Parameters:

$$\tau_g = \frac{C_{pg} A \rho_g}{h P} \quad \text{and} \quad \lambda_g = \frac{C_{pg} w_g}{h P}$$

$$\tau_i = \frac{C_{pi} m'_i}{h P}$$

# Temperature profile along the magnet.

( 10 atm, 25 g/s;....- He., ___- Iron.)

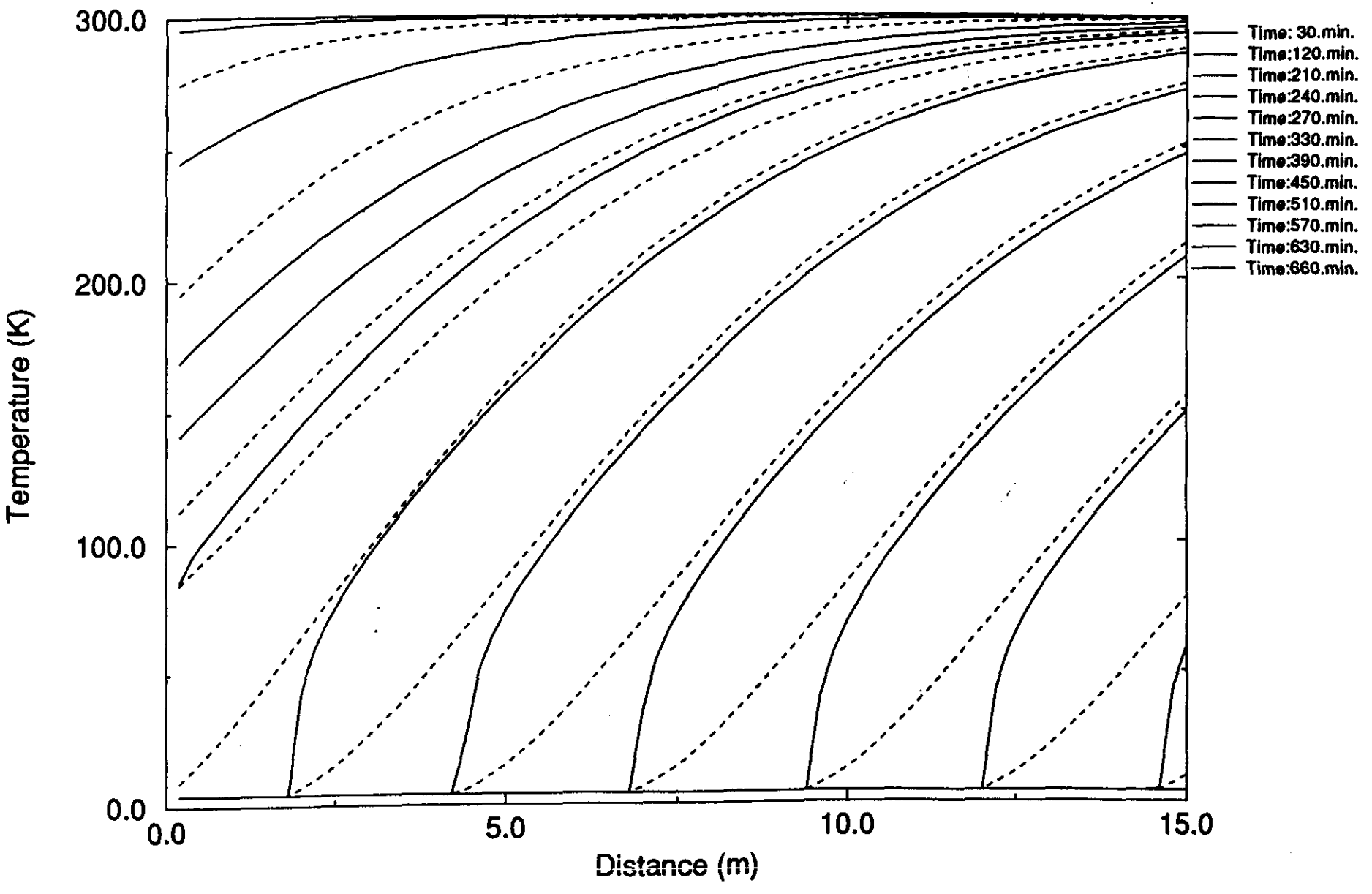

# Temperature gradient along the magnet.

( 10 atm, 25 g/s)

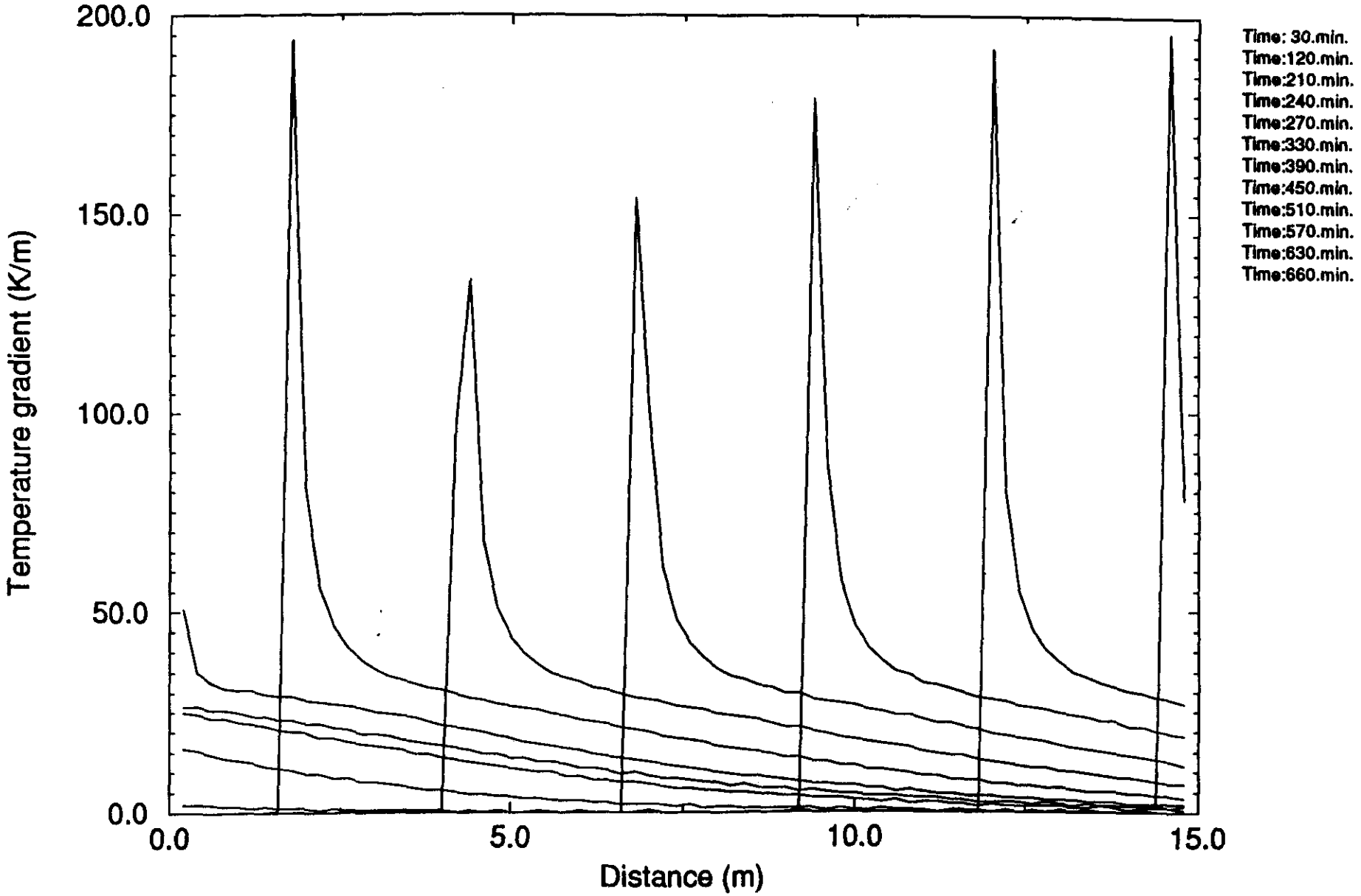

# Temperature difference between the magnet ends.

(10 atm, 25 g/s)

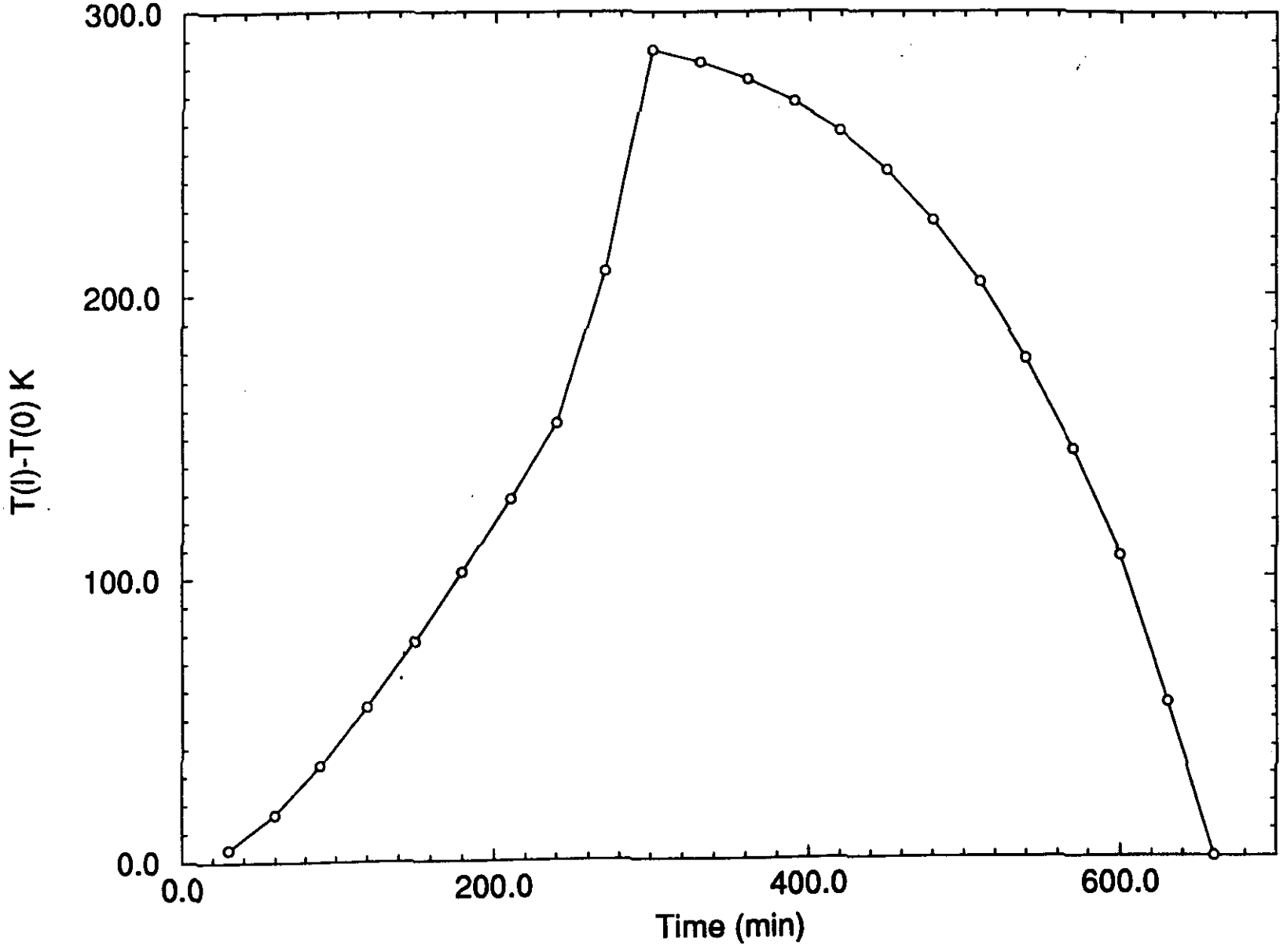

# Comparison of Simulation Results with Fermilab MTF Test Results

# LEAD END OF MAGNET

## TEST STAND #5 THERMOMETRY

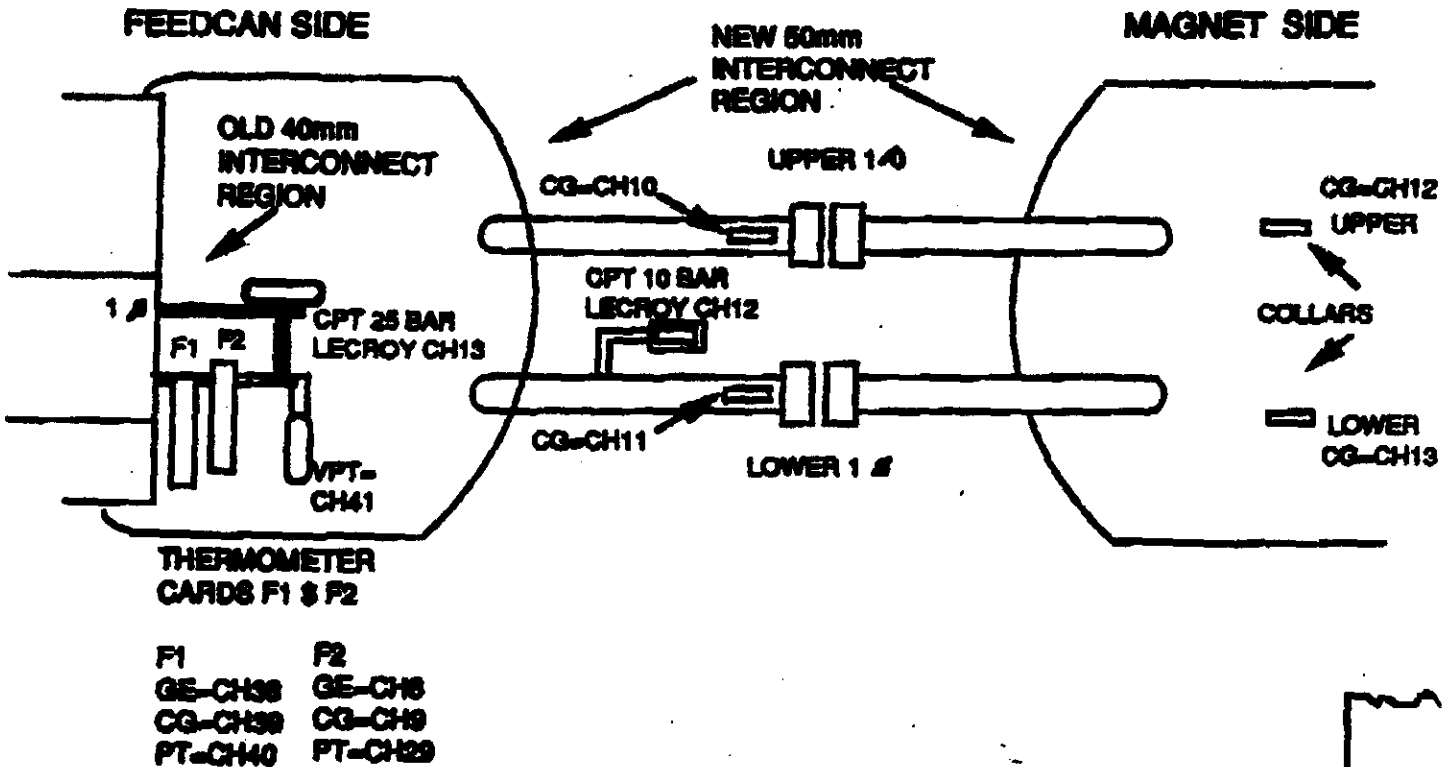


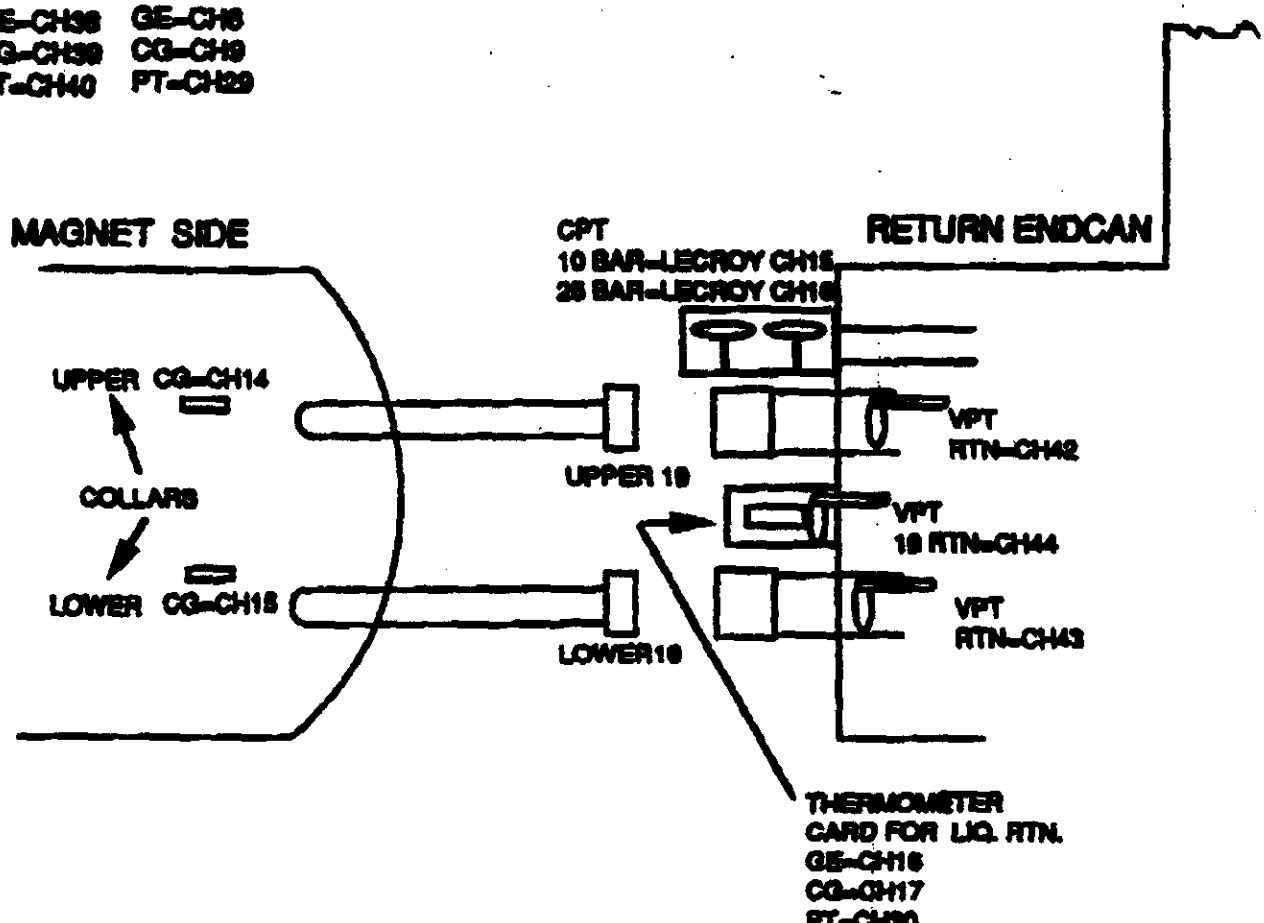


# RETURN END OF MAGNET



JUN-12-'92 FRI 17:16 ID:TECHNICAL SUPPORT HW TEL NO: P096 P02

# Exit gas temperature.

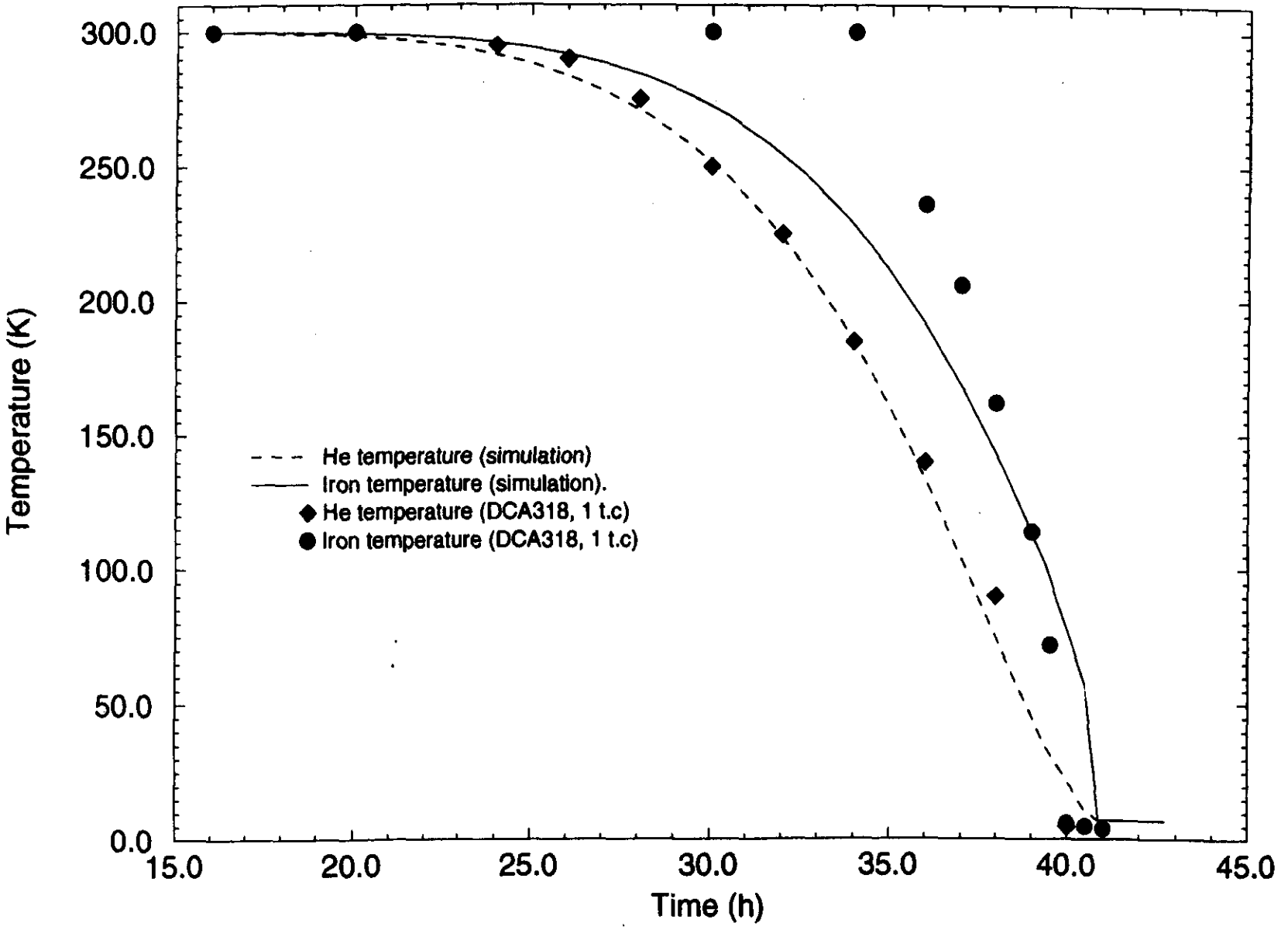

# Temperature difference between magnet ends.

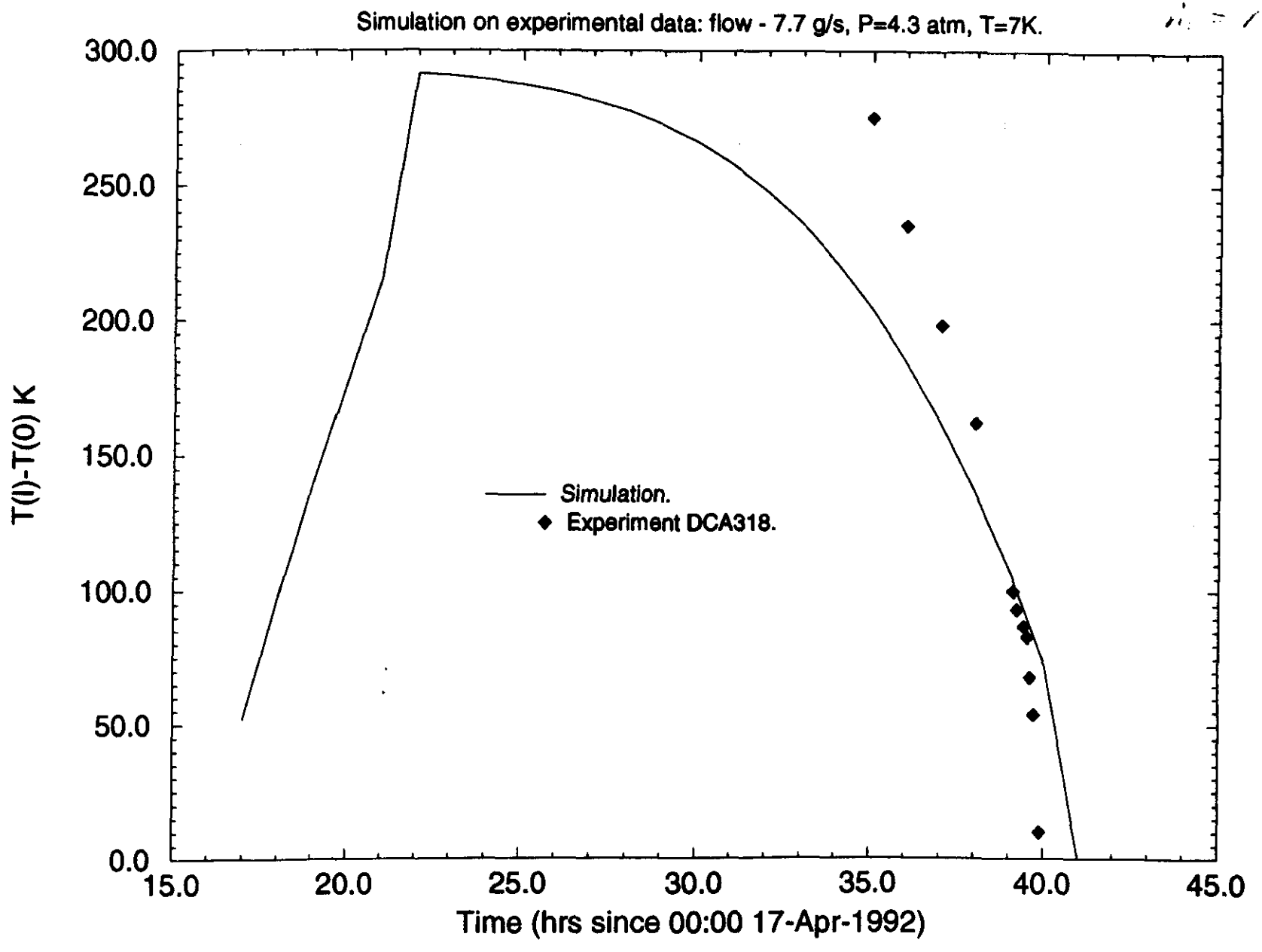

# Comparison of Simulation Results with Brookhaven National Laboratory MTF Test Results

# 4. Simulation Results with Different Cooling Procedures

# Cooldown procedure

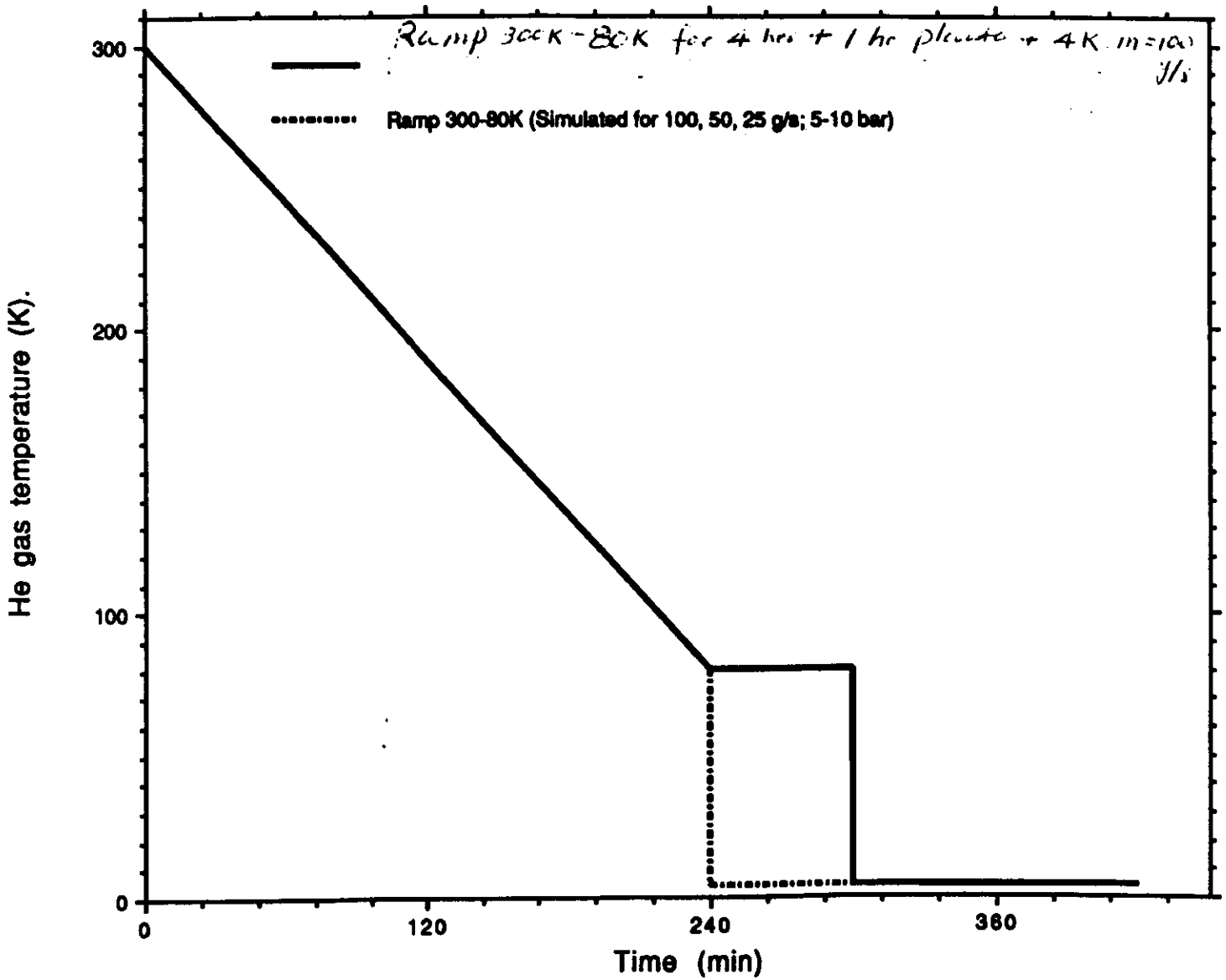

# Temperature difference between the magnet ends.

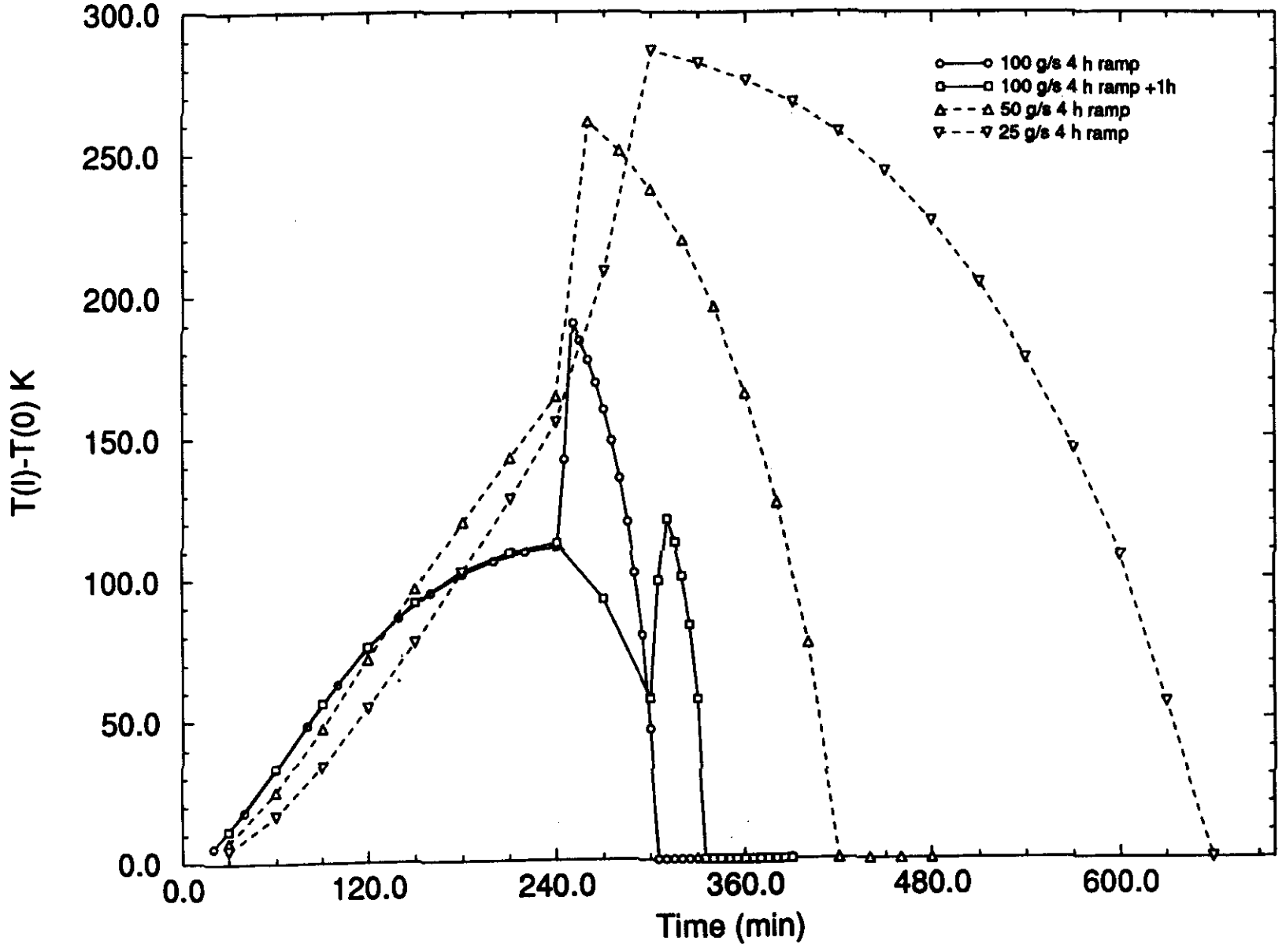

# Temepereture difference between the magnet ends

Different ramping time.

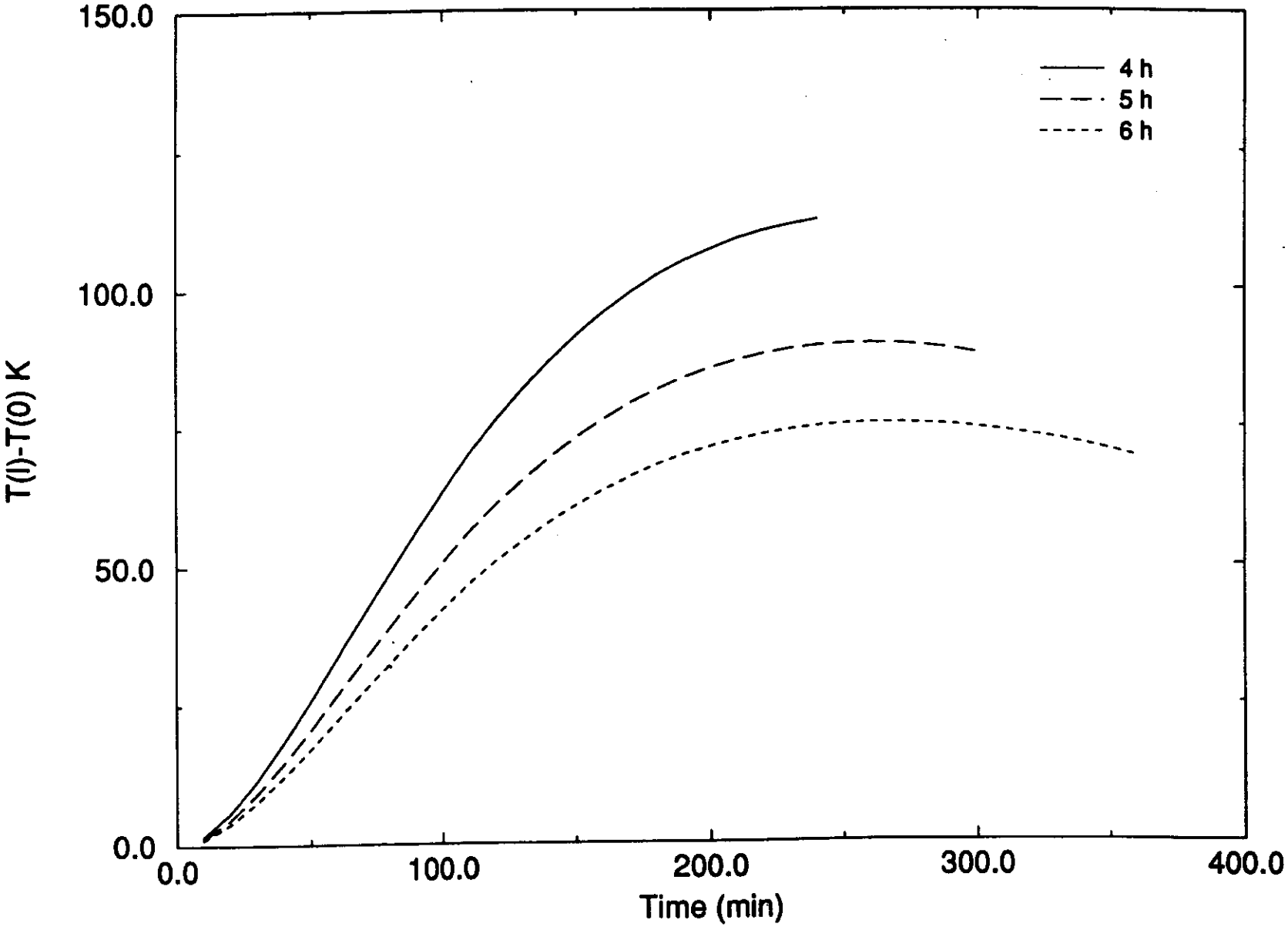

# 5. Simulation Results with SSCL MTL Cryogenic System

# Cooldown procedure

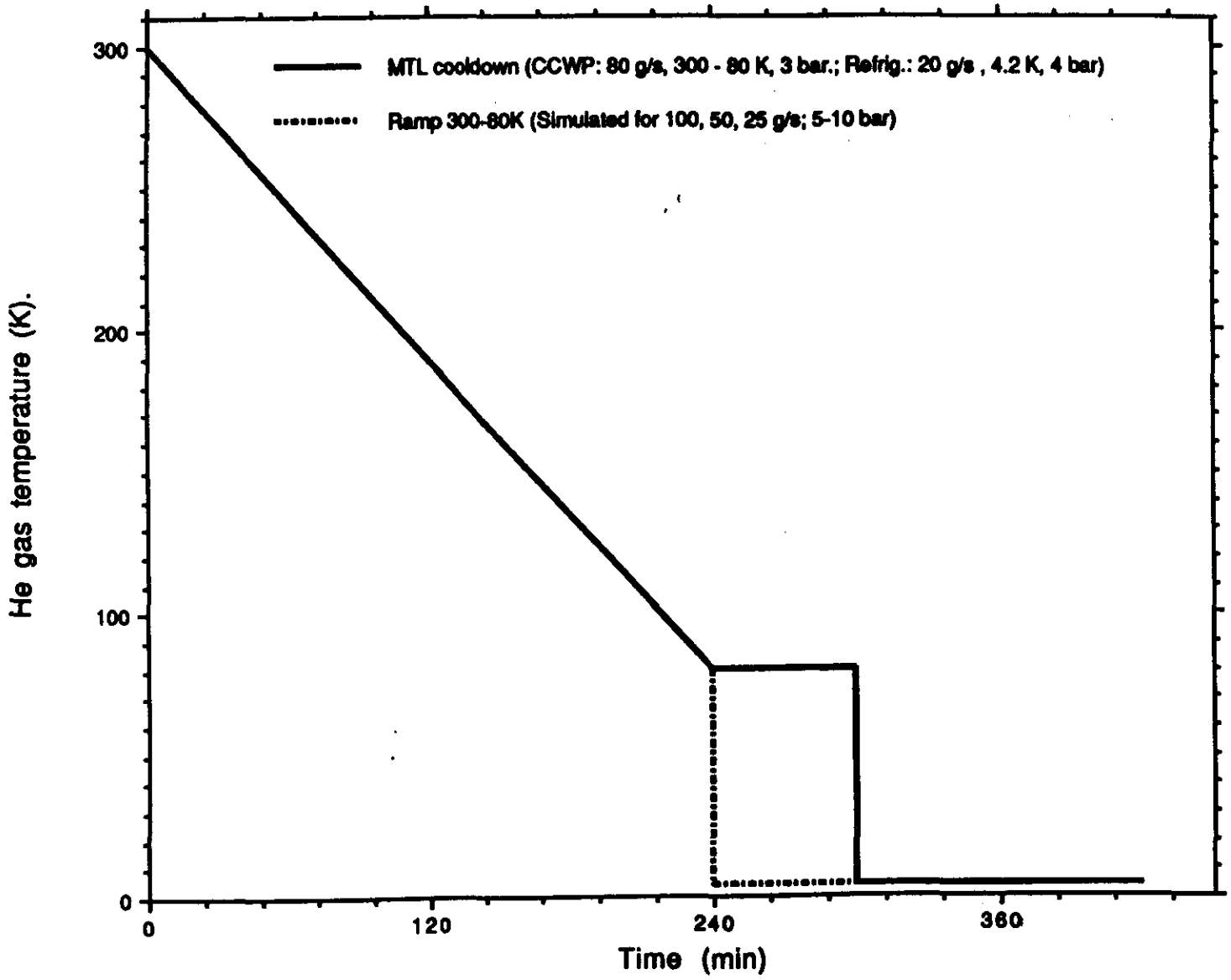

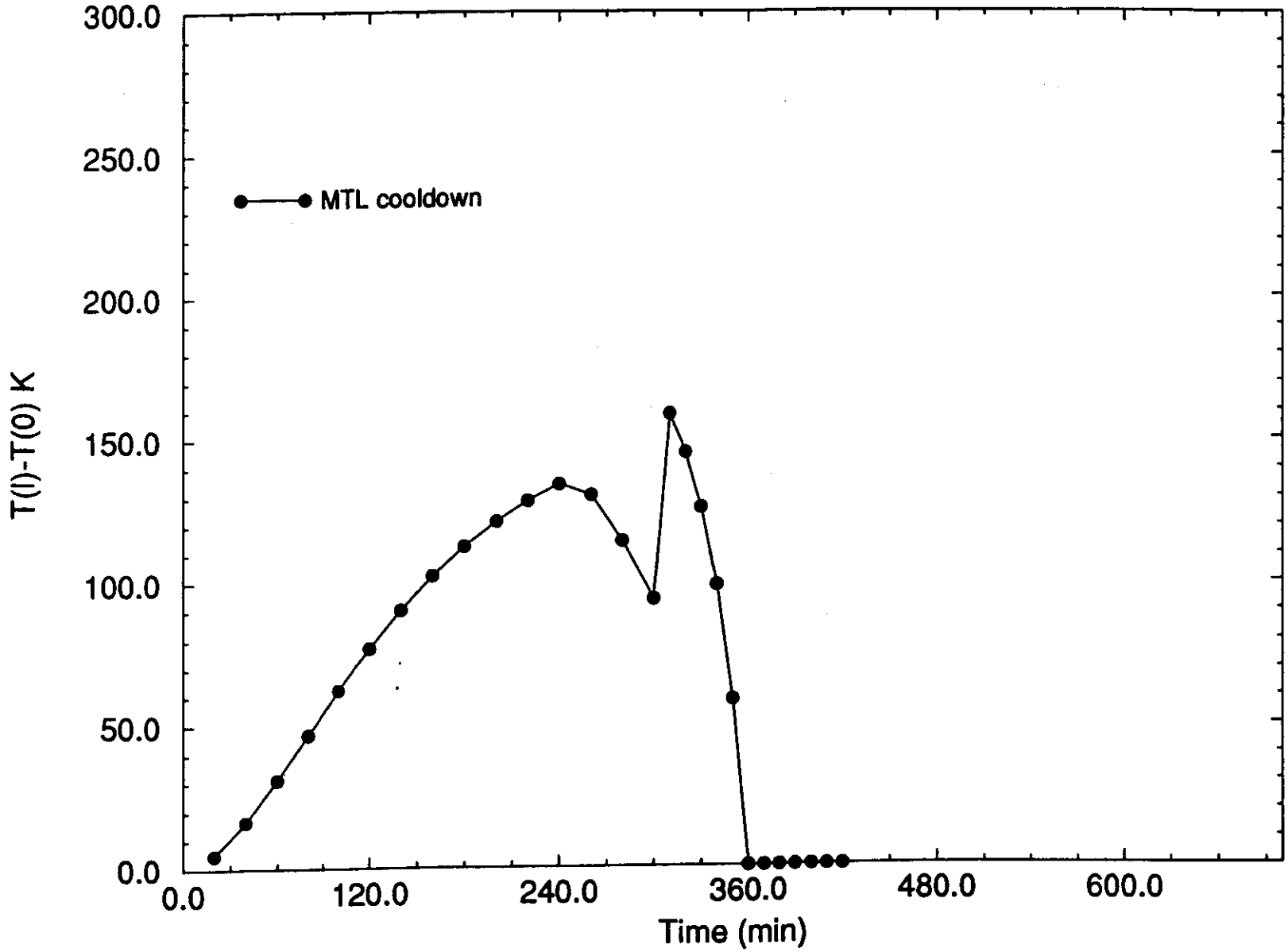
MTL cooldown
T(l)-T(0) K
300.0
250.0
200.0
150.0
100.0
50.0
0.0
0.0
120.0
240.0
360.0
480.0
600.0
Time (min)

# Temperature gradient along the magnet.

( MTL cooldown : ..... - He., _____ - Iron.)

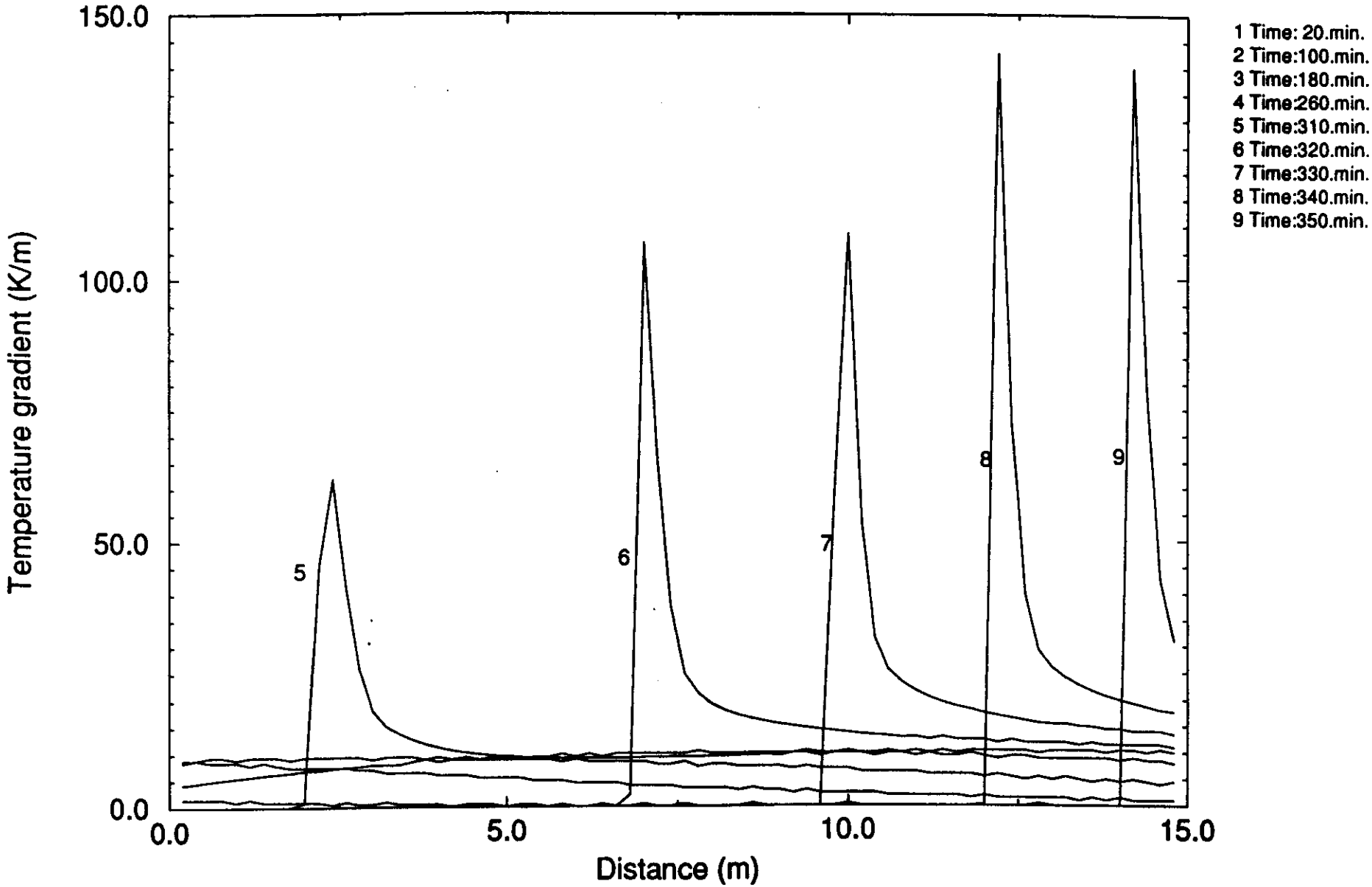

# Temperature profile along the magnet.

( MTL cooldown : ..... - He., _____ - Iron.)

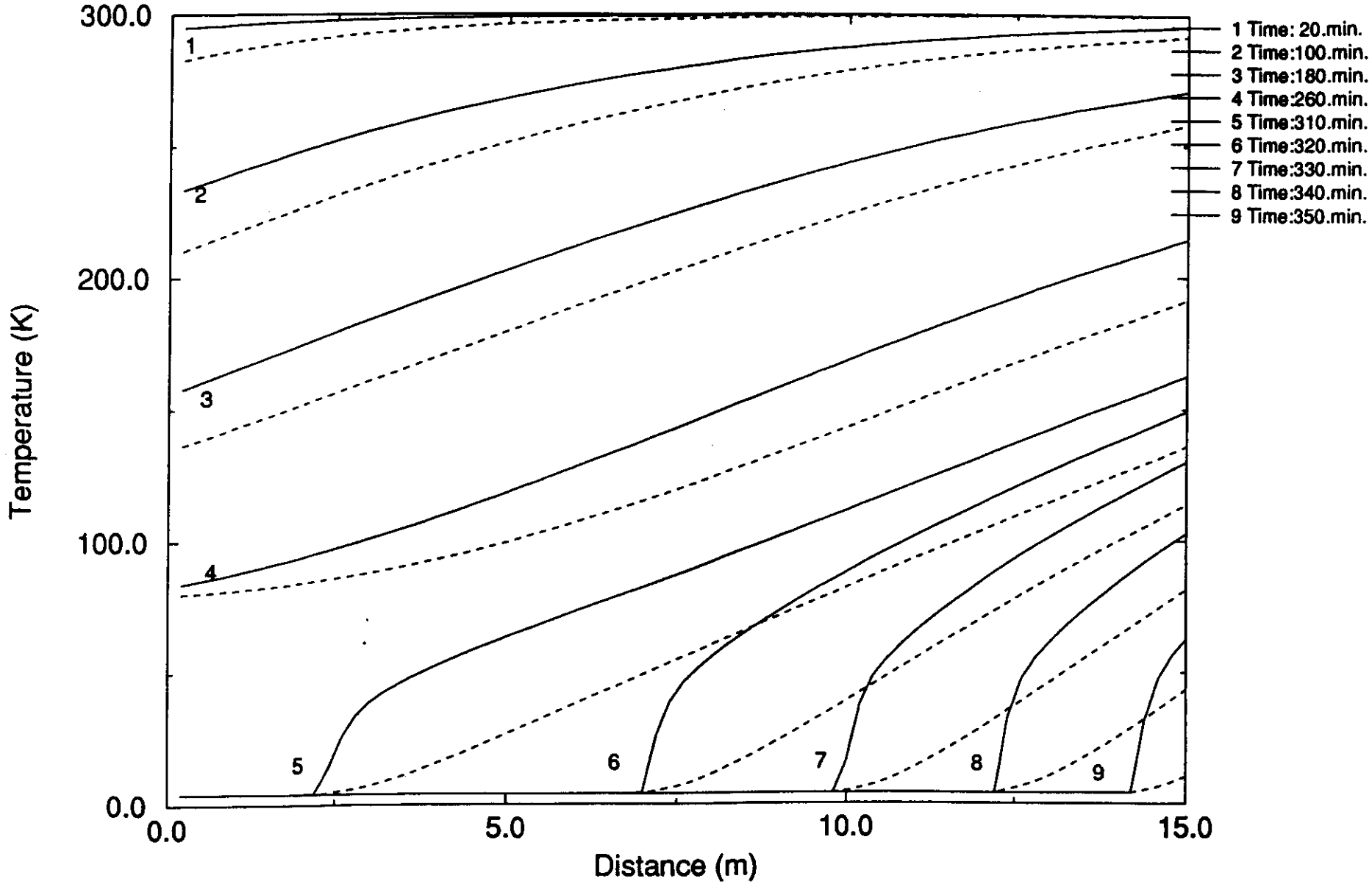

# 6. A Method to Quickly Estimate The Magnet Cooldown Time

# A Method to Quickly Estimate The Cool Down Time of a Single SSC Magnet

Q. S. Shu (Magnet Test Department)

8/14/91


## ABSTRACT

The author developed an approximate method to quickly estimate the cool down time of an SSC single magnet with relatively simple calculations. As examples, the cool down times for an SSC single dipole were calculated following a proposed cooling procedure close to the collider ring operating condition, but with cryogen (He) flow rates respectively of 8, 25, 50 and 100 g/s, which cover the region of the flow rates used at Fermilab, BNL, LBL and the future MTL at SSC. The results are in good agreement with Fermilab's test results as well as the results from a numerical method. In principle, this method can be used for other magnets having similar geometrical design to the SSC magnets. The other issues about the effects of cooling procedures and cryogen flow rates on the magnets will be discussed later.


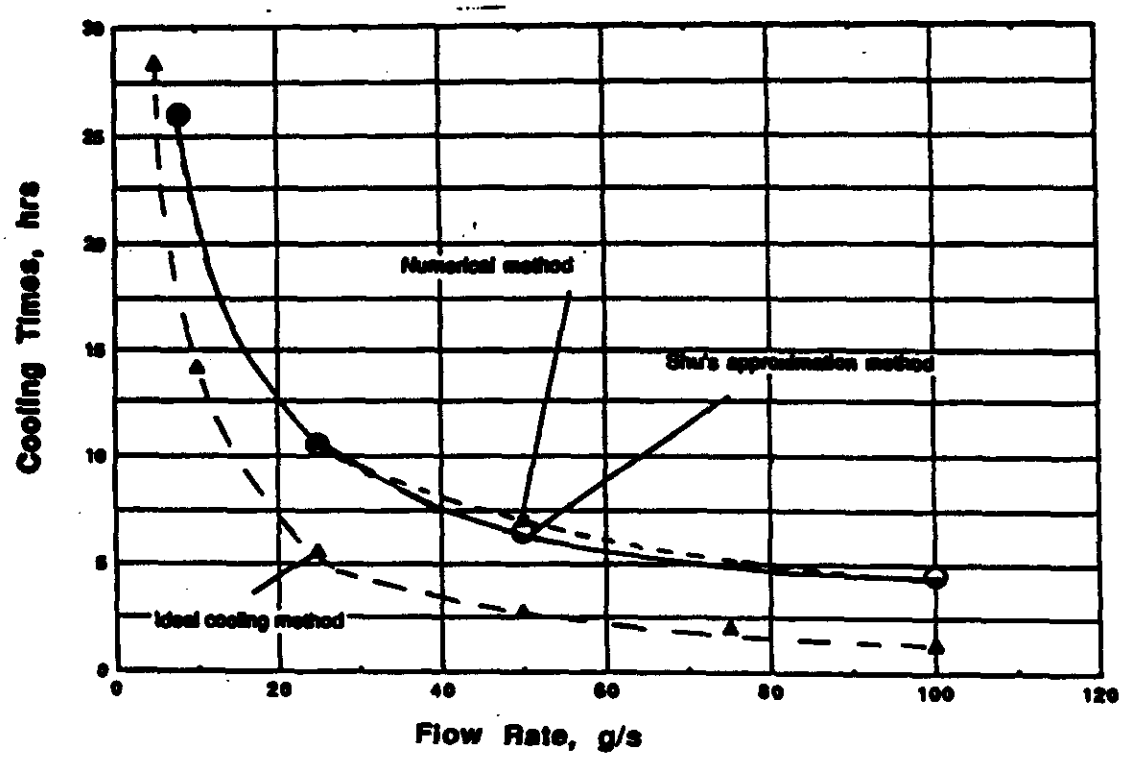


Fig. 7. A comparison of the cooling times predicted by the three different discussed methods, for different cryogen flow rate.

## THE APPROXIMATION METHOD

### I. Basic Ideas of The Method

The SSC magnet consists of the coil, collars, yokes, shells bonnet/end plates and interconnect region. Since the collars, yoke and shells contribute the largest fraction of the cold mass [3], one can use the enthalpy of stainless steel to represent the cold mass during the calculation of cool down and warm up. The cold mass of the SSC dipole magnet is about 9910 kg (652 kg/m). The enthalpy of the cold mass is calculated as a function of temperature from 300 K to 3 K, shown in Fig. 1.

*In order to approximate the situation of a magnet cool down with a fixed temperature* difference across the magnet, one cooling procedure is proposed as an example for the calculation, shown as Fig. 2. Initially, the temperature of the He gas entering the cold mass is linearly decreased from 300 K to 80 K within 4 hrs. Then, the 4.2 K single phase He is introduced through the cold mass cooling passage until the temperature of the cold mass at the outlet reaches 4.2 K. The magnet thermal insulation is designed to be so efficient that the heat leak from the outside to the iron yoke is negligible during the time interval of the magnet cool down.

Fig. 3 shows the cross section of the SSC dipole magnet. The ratio of the diameter of the cooling passage to the length of the magnet is << 1. Also, the cold mass is much larger than the mass of the He inside the cooling passage. So the heat exchange is very good between the cold mass and the He flow.

In my approximate method, I ignore the details of the space-time variation of magnet temperature and treat the cold mass as a lumped thermal element with equivalent temperature $T_{eq}$. The temperature of the liquid helium that contacts this element is allowed to vary with time; Fig 2 shows the variation that will be assumed in the numerical examples. The ideal cooling model assumes that complete temperature equilibrium occurs between the entering helium and the cold mass, so that the temperature at any time may be calculated simply from an energy balance. This is not true at the flow rates of interest; all the cooling enthalpy in the helium is not used before the helium exits the magnet. By comparison with numerical calculations, however, I find that this inefficiency can be represented to sufficient accuracy by a simple correction factor.

To carry out the computations I make the following detailed assumptions:

1. During the initial ramp period, and only during this period, all the cooling enthalpy of the He is totally absorbed by the cold mass. This approximation becomes less satisfactory as the length of the ramp period is increased beyond 4 hours, and as the flow rate increases beyond 100 g/s.

2. For a linear ramp, the entering He has an enthalpy corresponding an average temperature $T_{av} = (300 + 80)/2 = 190K$.

3. At the end of the initial ramp the magnet has an equivalent temperature $T_{eq}$ that can be computed from the H-T plot of Fig. 1. This occurs at time $t_1$, which is always set equal to 4 hours in this note.

4. After the initial ramp, even with ideal cooling, only the cooling enthalpy of the LHe between 4.2K and $T_{eq}$ is available to cool the cold mass. an ideal cooling time $t_2$ can be calculated for this part of the process.

5. Because of inefficiency in heat transfer, only a part of the ideal cooling in (4) is utilized, and the process takes an additional time $\gamma t_2$. By comparison with numerical calculations and the measured cool down time at FANL, $\gamma = 0.36$.

6. The total time t for magnet cool down is given by $t = (t_1 + t_2 + \gamma t_2)$

## II. An Example of the Calculation of Cool Down Time

In the case of a constant flow rate of 25 g/s:

The cooling enthalpy of He at 5 atm [4] with its temperature linearly ramping down to 80 k from 300 k in 4 hrs at a flow rate m = 25 g/s can be calculated.

$$H_{(He)1} = [\,H(\text{at } 300\text{ K}) - H(\text{at } T_{av} = 190\text{ K.})] \times \text{flow rate} \times \text{time}$$
$$= 571\text{ J/g} \times 25\text{ g/s} \times 3600\text{ s} \times 4$$
$$= 2.06 \times 10^8\text{ J}$$

The total enthalpy of the dipole cold mass at 300 K is,

$$H_{(mass)} = 8.04 \times 10^8\text{ J}$$

and the total enthalpy of the dipole after ramp equals,

$$H_{(mass)1} = H_{(mass)} - H_{(He)1}$$
$$= 5.98 \times 10^8\text{ J.}$$

The temperature across the dipole is not uniform and rather complicated. However, we can find an equivalent temperature Teq for the cold mass from the H - T graph of the cold mass.

$$T_{(mass)eq} = 244\text{ K}$$

The cooling enthalpy $H_{(He)2}$ of He from 4.2K to 244 K is 1281 J/g.

The enthalpy change $\Delta H_{(mass)}$ of the magnet from 244 K to 4.2 K is about $5.98 \times 10^8$ J

The nominal time needed to cool down the magnet from 244 K to 4.2 K is,

$$t_2 = \Delta H_{(mass)} / H_{(He)2} \times \text{flow rate}$$
$$= 5.98 \times 10^8 / (1281 \times 25 \times 3600) = 5.2\text{ hrs}$$

The total time t needed to cool down the dipole from 300 K to 4.2 K is,

$$t = t_1 + t_2 + (\gamma t_2) = 4 + 5.2 + (5.2 \times 0.36)$$
$$= 11.07\text{ hrs}$$

Following the same procedure, I calculated the cool down times also respectively with the cryogen flow rates of 5, 25, 50 and 100 g/s. The calculated cool down times are 26,11, 6.5 and 4.5 hrs. Figure 4 shows the cool down time as a function of the cryogen flow rates.

# ASST PROGRESS

## J. G. WEISEND II

## 6 / 29 / 92

**THE ACCELERATOR SYSTEM STRING TEST (ASST ) CONSISTS OF :**

**5 GD / FNAL DIPOLES**

**1 LBL / SSC QUAD**

**3 PROTOTYPE SPOOL PIECES**

**THE TEST WILL INCLUDE POWER AND CRYOGENIC TESTS.**

**HEAT LEAK MEASUREMENTS WILL BE MADE ON THE 20 K AND 80 K SHIELD AND ON THE COLD MASS. HEAT LEAKS DUE TO INTERCONNECTS MAY ALSO BE MEASURED.**

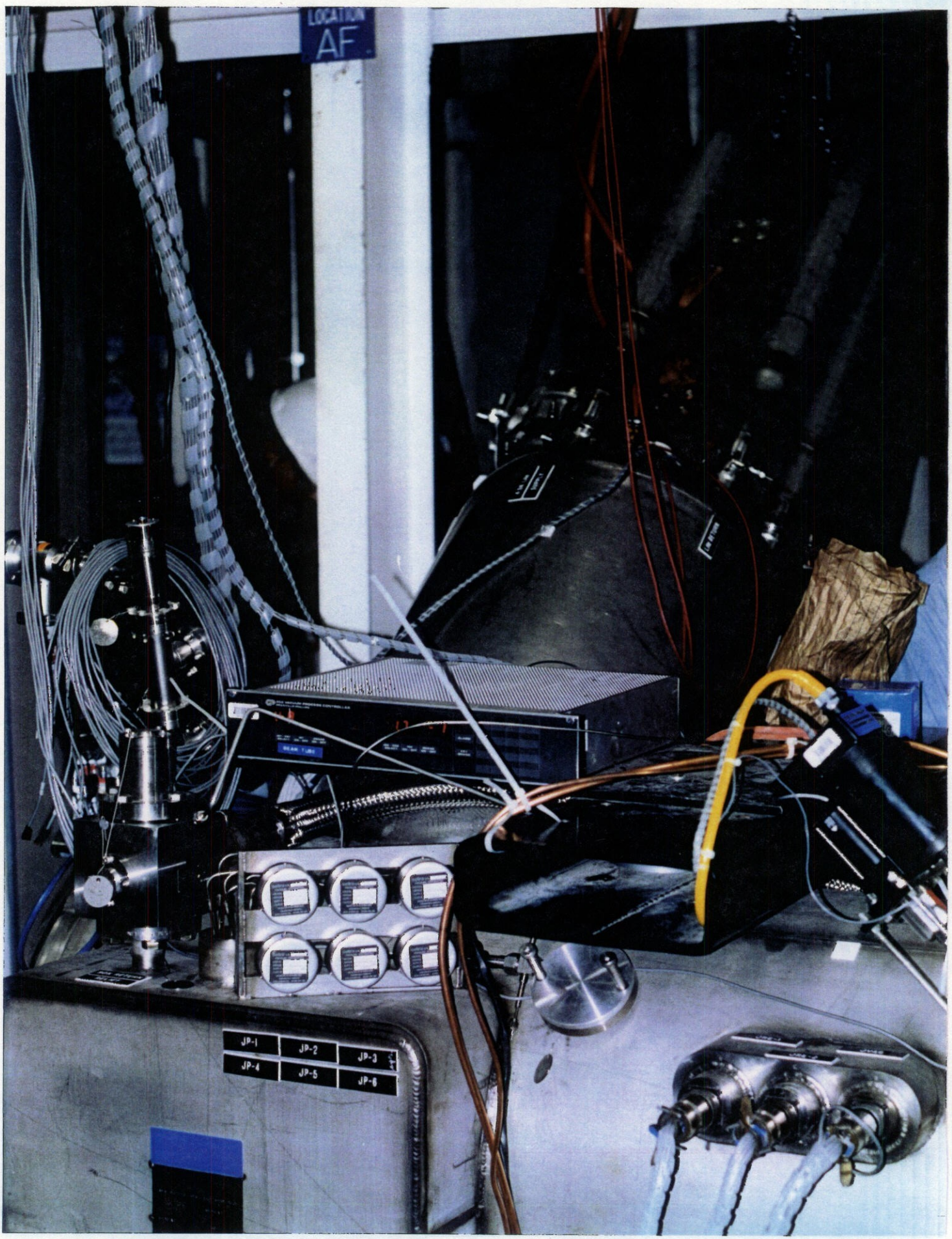
LOCATION
AF
JP-1
JP-2
JP-3
JP-4
JP-5
JP-6

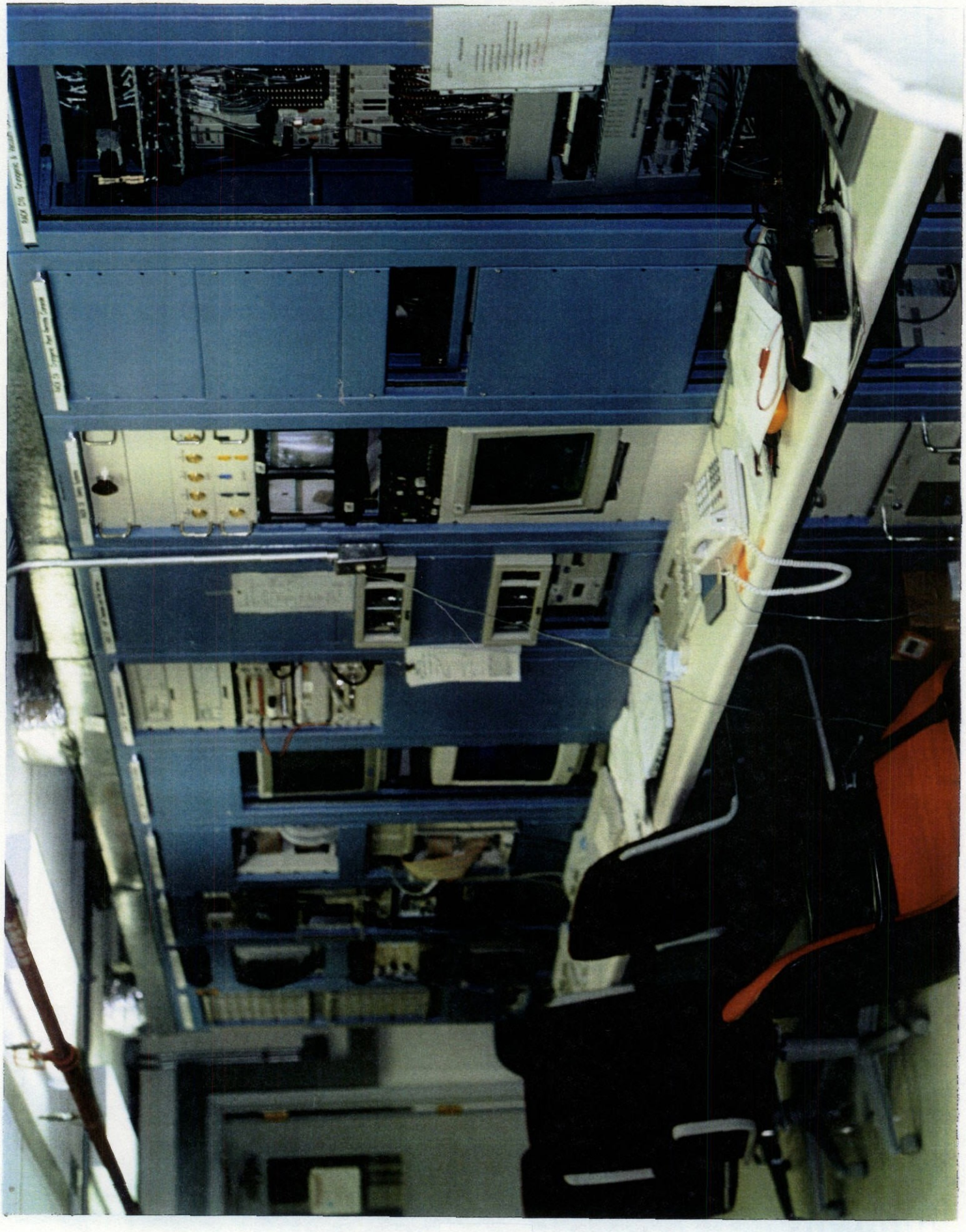

## Current Status

## ( 7 / 19 / 92 )

- All String Components Installed.
- All Leak and Pressure Tests Completed.
- Refrigeration Plant has been commissioned.
- All Instrumentation has been checked and is functioning.
- String Insulation Vacuum has been established.
- String Cool Down began 6 / 28 / 92. String at Operating Temperatures by 7 / 6 / 92.

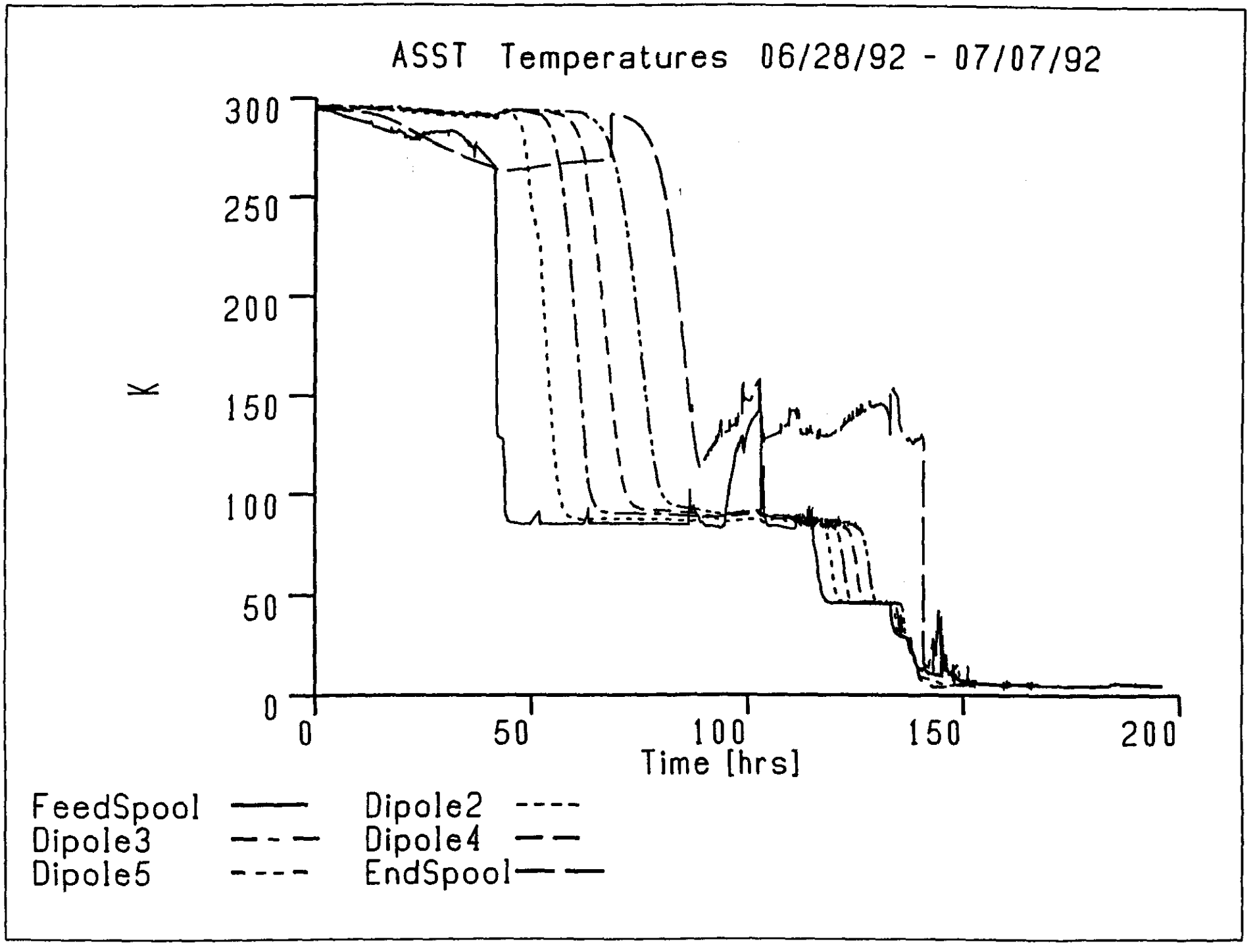
ASST Temperatures 06/28/92 - 07/07/92
K
300
250
200
150
100
50
0
0
50
100
150
200
Time [hrs]
FeedSpool
Dipole2
Dipole3
Dipole4
Dipole5
EndSpool

## SCHEDULE

- POWER TESTS WILL BEGIN IN JULY.
- HEAT LEAK MEASUREMENTS WILL TAKE PLACE IN LATE JULY / EARLY AUGUST.

R. Churchill

General dynamics San Diego Div.

# Design of GD Cold Test Stand Instrumentation.

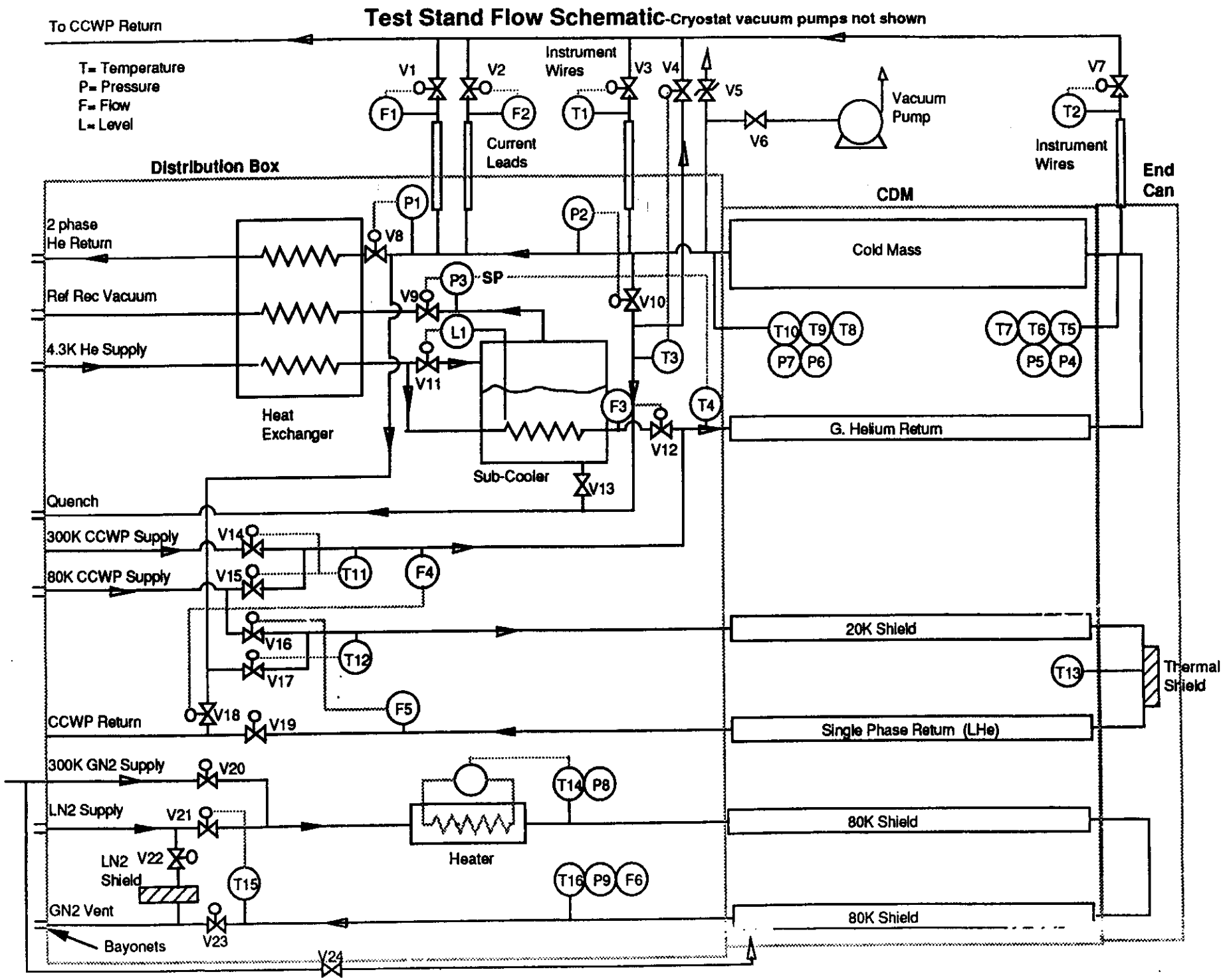
Test Stand Flow Schematic-Cryostat vacuum pumps not shown
To CCWP Return
T= Temperature
P= Pressure
F= Flow
L= Level
V1
V2
Instrument Wires
V3
V4
V5
V6
V7
F1
F2
T1
T2
Current Leads
Vacuum Pump
Instrument Wires
End Can
Distribution Box
CDM
P1
P2
P3
SP
V8
V9
V10
V11
V12
V13
L1
T3
T4
F3
2 phase He Return
Ref Rec Vacuum
4.3K He Supply
Heat Exchanger
Sub-Cooler
Cold Mass
T10
T9
T8
P7
P6
T7
T6
T5
P5
P4
G. Helium Return
Quench
300K CCWP Supply
80K CCWP Supply
V14
V15
V16
V17
V18
V19
T11
F4
T12
F5
20K Shield
T13
Thermal Shield
CCWP Return
Single Phase Return (LHe)
300K GN2 Supply
V20
LN2 Supply
V21
LN2 Shield
V22
T15
Heater
T14
P8
T16
P9
F6
80K Shield
GN2 Vent
V23
Bayonets
V24
80K Shield

## Cold Test Stand Cooling System Sensors

| Quantity | Location | Measurement | Sensor Type | Range | Accuracy |
|---|---|---|---|---|---|
| 6 | T6,9,11, 14-16 | Temperature | Platinum | 80-300K | .05K |
| 7 | T3-5,8,12, 13 | Temperature | Carbon Glass | 1-80 K | 5mK for T<10k |
| 2 | T7,10 | Temperature | Vapor Pressure | 3-10K | .05K |
| 2 | T1,2 | Temperature | Thrmocpl or Carbon Glass | 80-300K | 2k |
| 6 | P1,2,4,6,8, 9 | Pressure (warm) | Strain Gage | 0-20 atm | 0.05 atm |
| 2 | P5,7 | Pressure (cold) | Strain Gage* | 0-20 atm | 0.50% |
| 1 | P3 | Pressure (warm) | Strain Gage | 0-2 atm | 0.5% |
| 2 | F1,2 | Mass Flow | TBD | 0-1 g/s | 0.1 g/s |
| 2 | F3,4 | Mass Flow | TBD | 0-100 g/s | 0.5 g/s |
| 2 | F5,6 | Mass Flow | TBD | 0-10 g/s | 0.05 g/s |
| 1 | L1 | Liquid He Level | Supercond. | 0-1 m | 1cm |

* Keller PSI, semiconductor bridge

| Circuit | Grp. No. | Gage No. | Conductor Config. | Wire Form | Volt Rtg of Insul | Volt Rtg. to Gnd | Total No. of Devices | Wires Exiting Lead\Return |
|---|---|---|---|---|---|---|---|---|
| | | | **Table II** | **Prototype Magnet Wiring List** | | | | |
| Coil Protection V Taps | 1 | 28 | 19\40 | TM | 2.5kv | 5kv | 3 | 0\9 ^ |
| 1/4 Coil Taps | 2 | 22 | 19\34 | TM | 2.5kv | 5kv | 4 | 4\0 |
| Aux V Taps | 3 | 28 | 19\40 | TM | 2.5kv | 5kv | 52 | 28\24 |
| Expan Loop V Taps | 4 | 28 | 19\40 | TM | 2.5kv | 5kv | 4 | 0\4 |
| Spot Heater V Taps | 5 | 28 | 19\40 | TM | 2.5kv | 5kv | 2 | 2\2 |
| Quench Heater V Taps | 6 | 28 | 19\40 | TM | 2.5kv | 5kv | 4 | 4\4 |
| Collar Gages | 7 | 30 | 7\40 | TQ | 250v | 1kv | 28 | 56\56 |
| Bullet Gages | 8 | 30 | 7\40 | TQ | 250v | 1kv | 10 | 0\40 |
| Collar Hoop Str. Gages | 9 | 30 | 7\40 | TQ | 250v | 1kv | 2 | 4\4 |
| Thermometers (spare) | 10 | 30 | 7\40 | TQ | 250v | 1kv | 8 | 16\16 |
| Press. Transducer | 11 | 30 | 7\40 | TQ | 250v | 1kv | 2 | 4\4 |
| Spot Heater Power | 12 | 22 | 19\34 | TP | 1kv | 5kv | 2 | 0\2 |
| Quench Heater Power | 13 | 12 | 19\27 | TP | 1kv | 5kv | 4 | 0\4 ^ |
| Thermometers | 14 | 30 | 7\40 | TQ | 250v | 1kv | 6 | 12\12 |
| Support Post Gages | 15 | 30 | 7\40 | TQ | 250v | 1kv | 25 | 100\0 * |
| Shell Gages | 16 | 30 | 7\40 | TQ | 250v | 1kv | 38 | 0\152 * |
| Thermometers | 17 | 30 | 7\40 | TQ | 250v | 1kv | 46 | 100\84 * |
| Deflection Sensors | 18 | 28 | 7\40 | TQ | 250v | 1kv | 4 | 12\12* |
| | | | | T - Twisted | | | total | 331\416 |
| | | | | Q - Quad | | | single phase | 131\180 |
| | | | | P - Pair | | | vacuum spac | 200\236 |
| | | | | M - Multiple | | | | |
| **The following are not part of magnet instrumentation wiring, but are part of the test stand** | | | | | | | | |
| Vapor Cool Lead V Tap | 1 | | | | | | 4 | 0\8 Δ |
| Bus Protection V taps | 1 | | | | | | 2 | 0\4 Δ |

**NOTES**

1. All insulation ETFE Kapton
2. All wires exit through the lower single phase helium lines unless noted
3. Magnet return end connects to test stand distribution box.

* Exit through vacuum space, not single phase fluid line

Δ Exit through upper single phase fluid line

^ Quench heater power and coil protection voltage taps remain for production magnets

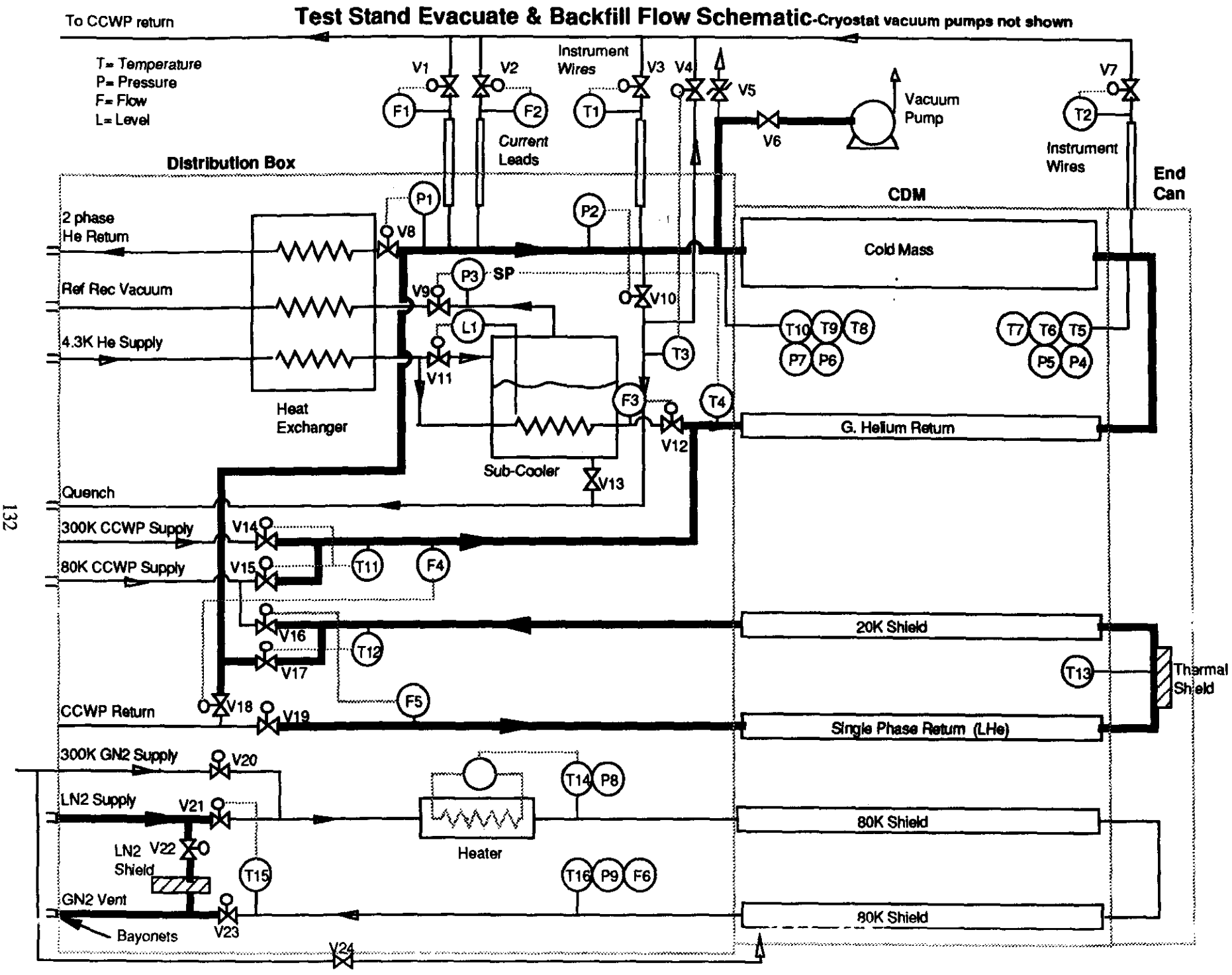
Test Stand Evacuate & Backfill Flow Schematic-Cryostat vacuum pumps not shown
To CCWP return
T= Temperature
P= Pressure
F= Flow
L= Level
Distribution Box
V1
V2
Instrument Wires
V3
V4
V5
V6
V7
F1
F2
T1
T2
Current Leads
Vacuum Pump
Instrument Wires
End Can
CDM
P1
P2
P3
SP
V8
V9
V10
V11
V12
V13
L1
T3
T4
F3
2 phase He Return
Ref Rec Vacuum
4.3K He Supply
Heat Exchanger
Sub-Cooler
Cold Mass
T10
T9
T8
P7
P6
T7
T6
T5
P5
P4
G. Helium Return
Quench
300K CCWP Supply
80K CCWP Supply
V14
V15
T11
F4
V16
V17
T12
20K Shield
T13
Thermal Shield
CCWP Return
V18
V19
F5
Single Phase Return (LHe)
300K GN2 Supply
V20
LN2 Supply
V21
T14
P8
Heater
80K Shield
LN2 Shield
V22
T15
T16
P9
F6
GN2 Vent
V23
Bayonets
80K Shield
V24

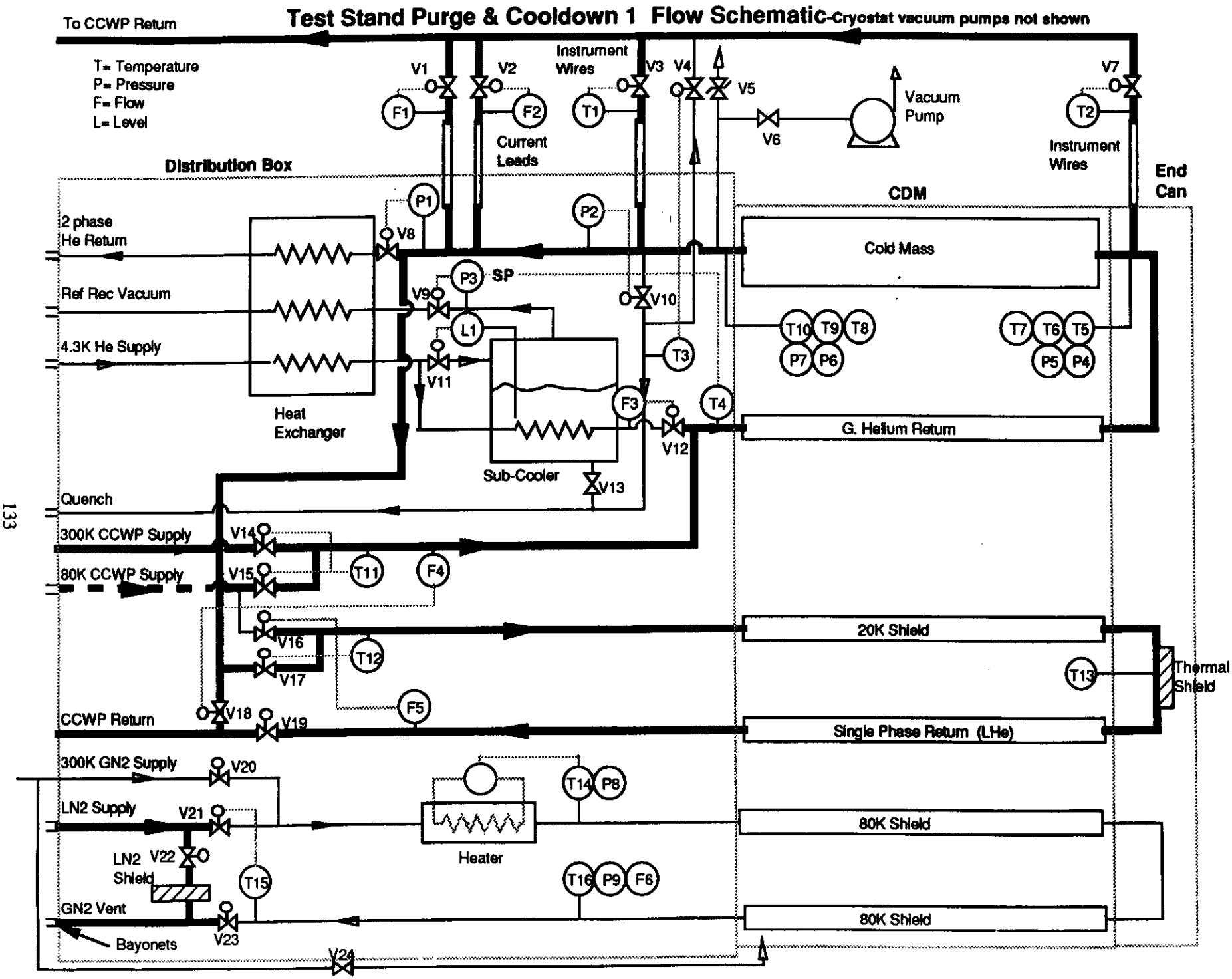
Test Stand Purge & Cooldown 1 Flow Schematic-Cryostat vacuum pumps not shown
To CCWP Return
T= Temperature
P= Pressure
F= Flow
L= Level
V1
V2
Instrument Wires
V3
V4
V5
V6
V7
F1
F2
T1
T2
Current Leads
Vacuum Pump
Instrument Wires
End Can
Distribution Box
CDM
P1
P2
P3
SP
V8
V9
V10
V11
V12
V13
L1
T3
T4
F3
2 phase He Return
Ref Rec Vacuum
4.3K He Supply
Heat Exchanger
Sub-Cooler
Cold Mass
T10
T9
T8
P7
P6
T7
T6
T5
P5
P4
G. Helium Return
Quench
300K CCWP Supply
80K CCWP Supply
V14
V15
T11
F4
V16
V17
T12
20K Shield
T13
Thermal Shield
F5
CCWP Return
V18
V19
Single Phase Return (LHe)
300K GN2 Supply
V20
LN2 Supply
V21
T14
P8
Heater
80K Shield
LN2 Shield
V22
T15
T16
P9
F6
GN2 Vent
V23
Bayonets
80K Shield
V24

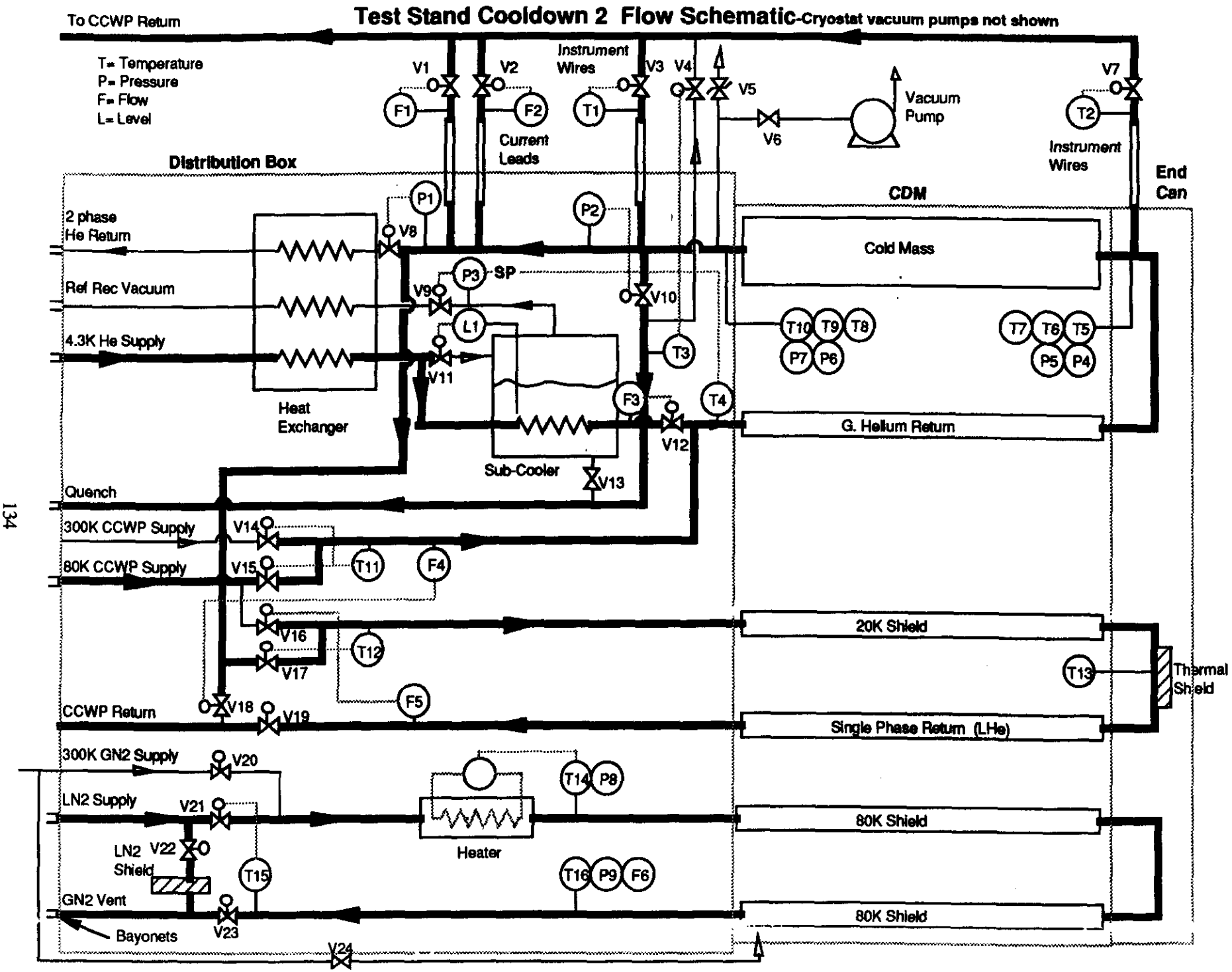
Test Stand Cooldown 2 Flow Schematic-Cryostat vacuum pumps not shown
To CCWP Return
T= Temperature
P= Pressure
F= Flow
L= Level
Distribution Box
V1
V2
Instrument Wires
V3
V4
V5
V6
V7
F1
F2
Current Leads
T1
Vacuum Pump
T2
Instrument Wires
End Can
CDM
P1
P2
2 phase He Return
V8
Cold Mass
P3
SP
Ref Rec Vacuum
V9
V10
L1
T10
T9
T8
T7
T6
T5
4.3K He Supply
V11
T3
P7
P6
P5
P4
Heat Exchanger
F3
T4
G. Helium Return
V12
Sub-Cooler
V13
Quench
300K CCWP Supply
V14
80K CCWP Supply
V15
T11
F4
V16
20K Shield
T12
V17
T13
Thermal Shield
F5
CCWP Return
V18
V19
Single Phase Return (LHe)
300K GN2 Supply
V20
T14
P8
LN2 Supply
V21
80K Shield
Heater
LN2 Shield
V22
T15
T16
P9
F6
GN2 Vent
V23
80K Shield
Bayonets
V24

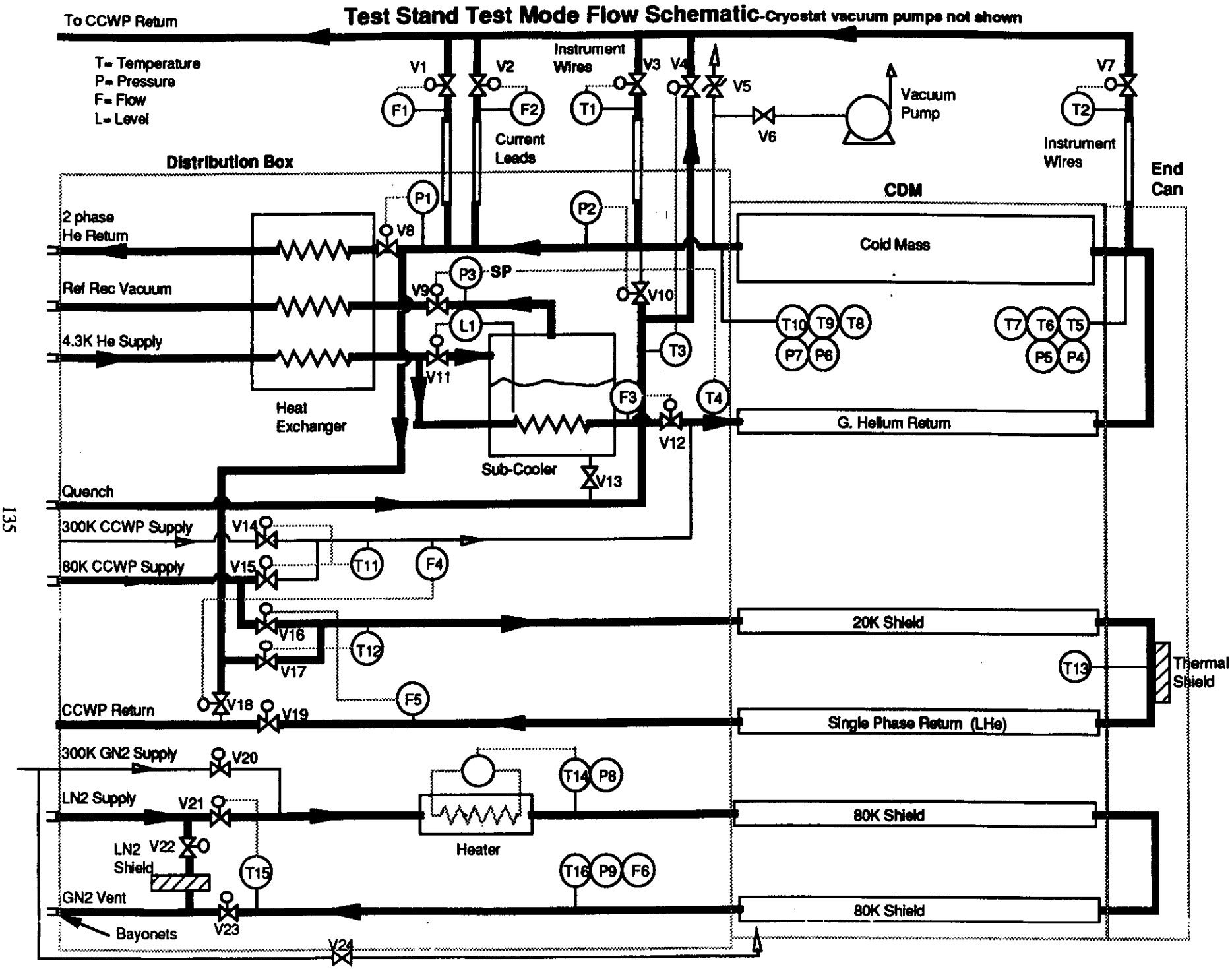
Test Stand Test Mode Flow Schematic-Cryostat vacuum pumps not shown
To CCWP Return
T= Temperature
P= Pressure
F= Flow
L= Level
Distribution Box
V1
V2
Instrument Wires
V3
V4
V5
V6
V7
Vacuum Pump
F1
F2
T1
T2
Current Leads
Instrument Wires
End Can
CDM
Cold Mass
P1
P2
P3
SP
V8
V9
V10
V11
V12
V13
L1
T3
T4
F3
T10
T9
T8
P7
P6
T7
T6
T5
P5
P4
2 phase He Return
Ref Rec Vacuum
4.3K He Supply
Heat Exchanger
Sub-Cooler
G. Helium Return
Quench
300K CCWP Supply
80K CCWP Supply
V14
V15
T11
F4
V16
V17
T12
20K Shield
T13
Thermal Shield
CCWP Return
V18
V19
F5
Single Phase Return (LHe)
300K GN2 Supply
V20
LN2 Supply
V21
T14
P8
80K Shield
Heater
LN2 Shield
V22
T15
T16
P9
F6
GN2 Vent
V23
Bayonets
80K Shield
V24

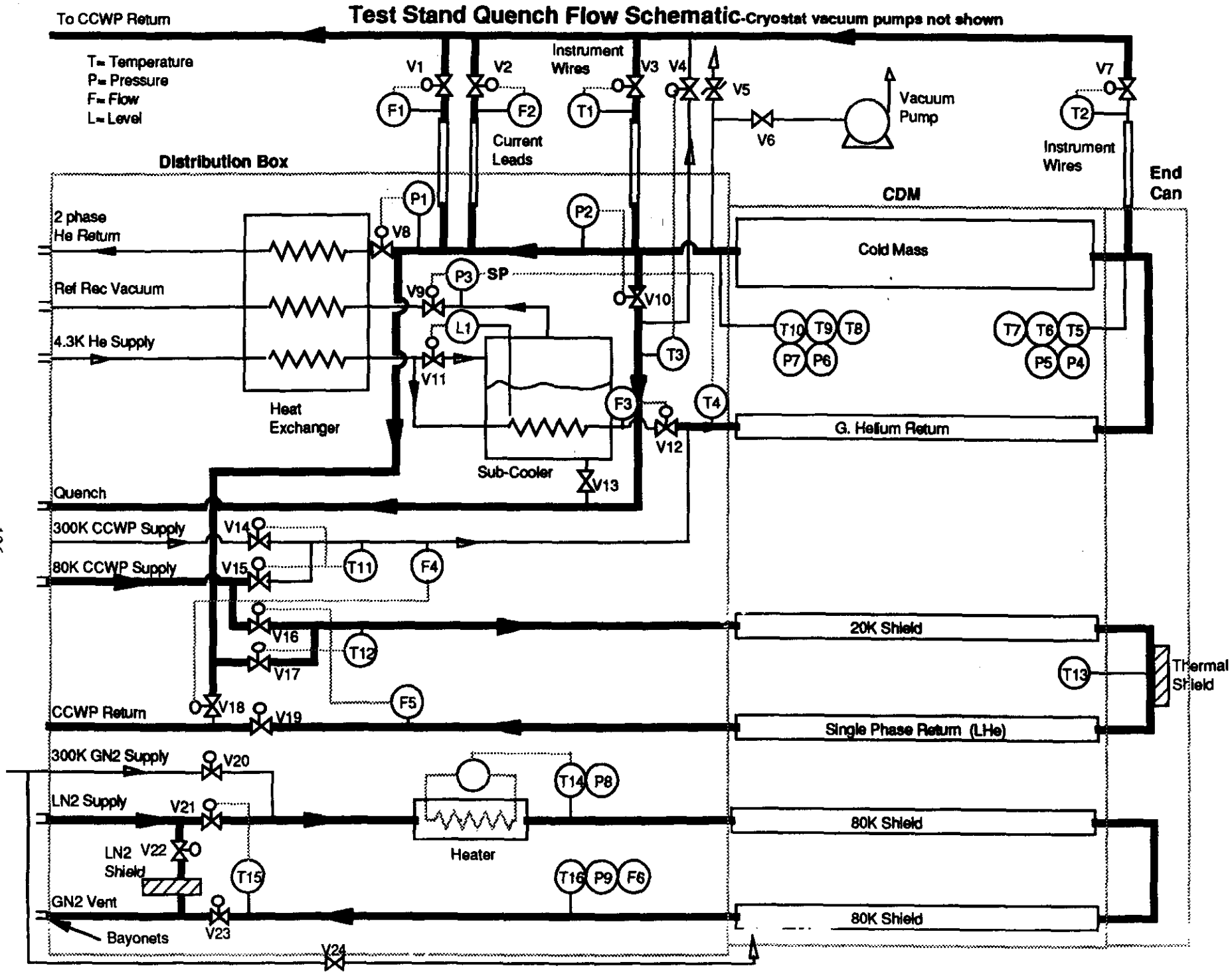
Test Stand Quench Flow Schematic-Cryostat vacuum pumps not shown
To CCWP Return
T= Temperature
P= Pressure
F= Flow
L= Level
Distribution Box
V1
V2
Instrument Wires
V3
V4
V5
V6
V7
F1
F2
T1
T2
Current Leads
Vacuum Pump
Instrument Wires
End Can
CDM
P1
P2
P3
SP
V8
V9
V10
V11
V12
V13
L1
T3
T4
F3
2 phase He Return
Ref Rec Vacuum
4.3K He Supply
Heat Exchanger
Sub-Cooler
Cold Mass
T10
T9
T8
P7
P6
T7
T6
T5
P5
P4
G. Helium Return
Quench
300K CCWP Supply
80K CCWP Supply
V14
V15
T11
F4
V16
V17
T12
20K Shield
T13
Thermal Shield
F5
CCWP Return
V18
V19
Single Phase Return (LHe)
300K GN2 Supply
V20
LN2 Supply
V21
T14
P8
80K Shield
Heater
LN2 Shield
V22
T15
T16
P9
F6
GN2 Vent
V23
Bayonets
80K Shield
V24

# CRYOGENIC PERF. WORKSHOP #2
## Thermal Performance (Mapping)

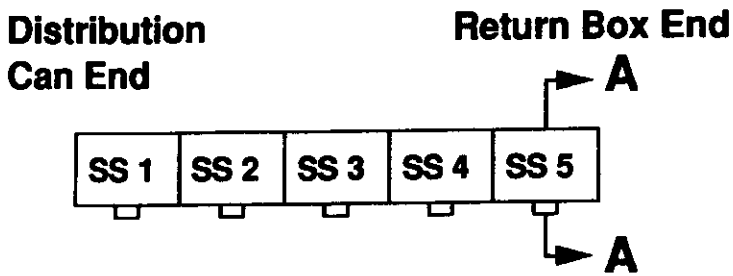


Cryostat In Cold Test Stand

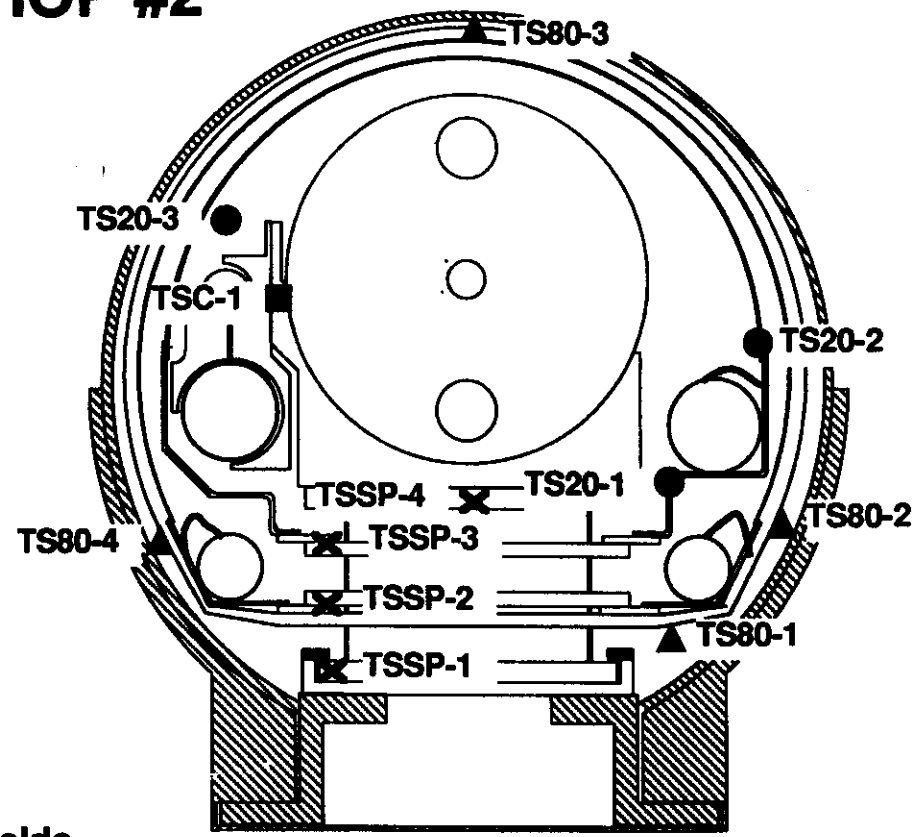


Section A-A

**Temperature Sensors on Cryostat Shields**

| Cryostat Element \ Shield | SS 1 | SS 2 | SS 3 | SS 4 | SS 5 | Total PM# | |
|---|---|---|---|---|---|---|---|
| | | | | | | 2,9 &12 | 4,6 &11 |
| 80 K Shield | 4 | 0 | 0 | 4 | 4 | 12 | 12 |
| 20 K Shield | 0 | 3 | 3 | 0 | 3 | 9 | 9 |
| Saddle | 1/0 | 1/0 | 1/1 | 1/0 | 1/0 | 5 | 1 |
| Support Post | 4/0 | 4/0 | 4/4 | 4/0 | 4/0 | 20 | 4 |

Legend
PM#-Prototype Magnet Number
SS-Shield Segment
TSSP-Temperature Sensor Support Post ✕
TS80-Temperature Sensor 80K Shield ▲
TS20-Temperature Sensor 20K Shield ●
TSC-Temperature Sensor Cradle ■

# CRYOGENIC PERFORMANCE WORKSHOP # 2
## Prototype Magnet Instrumentation

| | Vendor | Part Number |
|---|---|---|
| **Cold Mass Instrumentation** | | |
| End Dome Pressure Sensor | Carbon Glass CRG-1-1000-4B | Lake Shore |
| End Dome Temperature Sensor | 600187-25BAR | Keller |
| **Cryostat Instrumentation** | | |
| 4.35K Temperature Sensors | Carbon Glass CRG-1-1000-4B | Lake Shore |
| Cold Mass Saddle | | |
| Support Post | | |
| 20K Temperature Sensors | Platinum PT-103-14D | Lake Shore |
| Support Post 20K | | |
| 20K Shields | | |
| 80K & 300K Temperature Sensors | Platinum PT-103-77D | Lake Shore |
| Support Post 80K | | |
| 80K Shields | | |
| Support Post 300K | | |

# Series CGR Carbon-Glass Resistance Temperature Sensors*

## An excellent choice for accurate measurement at low temperature in the presence of a magnetic field

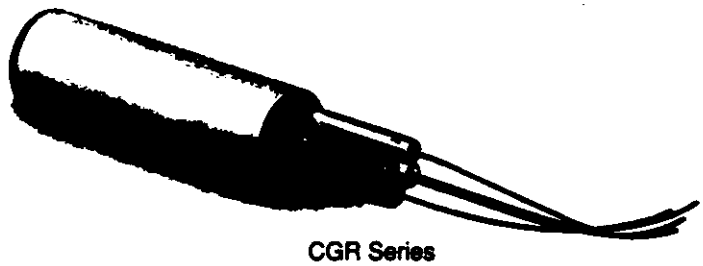

CGR Series

### Features

- *For use in magnetic fields to 19 tesla or higher*
- *Good reproducibility in the range from 1.4K to 100K*
- *Monotonic in R vs T and dR/dT*
- *With high sensitivity at helium temperature it is useful for sub-millikelvin control at 4.2K and below*
- *Usable sensitivity over the broad range 1.0K to 325K*
- *Good resistance to ionizing radiation*

The CGR series carbon-glass resistance temperature sensors are still the best choice for a highly reproducible sensor that can be used from 1.0K to 100K and above in magnetic fields up to 19 tesla or higher. Because of the sensor's extremely high sensor gain at helium temperatures, it is very useful for sub-millikelvin control at 4.2K and below. Carbon-glass sensors are monotonic in resistance temperature characteristics between 1.0K and 325K, but their reduced sensitivity above 100K makes their usage near room temperature somewhat limited. (See tables below)

**Resistance and Sensitivity (dR/dT) Values for Carbon-Glass Resistance Temperature Sensors**

| CGR-1-500, R, ohms | S.N.C4628 dR/dT,ohm/K | T(K) | CGR-1-1000, R,ohms | S.N.C4730 dR/dT, ohm/K |
|---|---|---|---|---|
| 70,392 | -312,319 | 1.40 | 120,805 | -485,568 |
| 468.76 | -267.11 | 4.20 | 1,011.5 | -706.6 |
| 68.483 | -10.681 | 10.0 | 148.09 | -23.55 |
| 16.235 | -0.268 | 40.0 | 32.889 | -0.590 |
| 11.167 | -0.069 | 77.35 | 21.765 | -0.151 |
| 9.9302 | -0.0429 | 100.0 | 19.092 | -0.092 |
| 7.6092 | -0.0132 | 200.0 | 14.175 | -0.027 |
| 6.6350 | -0.0073 | 300.0 | 12.181 | -0.015 |

Resistance and Sensitivity (dR/dT) Values for Sample 500 ohm and 1000 ohm CGR's.

| CGR-1-1500, R, ohms | S.N.C4741 dR/dT,ohm/K | T(K) | CGR-1-2000, R,ohms | S.N.C4649 dR/dT, ohm/K |
|---|---|---|---|---|
| 209,608 | -804,439 | 1.40 | 260,963 | -1,039,128 |
| 1,591.3 | -914.5 | 4.20 | 1,828.1 | -1,337.2 |
| 217.36 | -35.75 | 10.0 | 242.23 | -40.42 |
| 45.985 | -0.845 | 40.0 | 50.265 | -0.933 |
| 30.143 | -0.213 | 77.35 | 32.828 | -0.234 |
| 26.367 | -0.130 | 100.0 | 28.704 | -0.143 |
| 19.461 | -0.038 | 200.0 | 21.143 | -0.042 |
| 16.687 | -0.020 | 300.0 | 18.107 | -0.022 |

Resistance and Sensitivity (dR/dT) Values for Sample 1500 ohm and 2000 ohm CGR's.

**Note:** Specific sensor data is provided in the tables above to illustrate the effective range of use for each model. Actual dR/dT values will vary from sensor to sensor, but sensitivity characteristics within each model type will be similar. The graph on page 34 illustrates this point.

**Typical Response Curve for Carbon Glass Resistance Temperature Sensors**

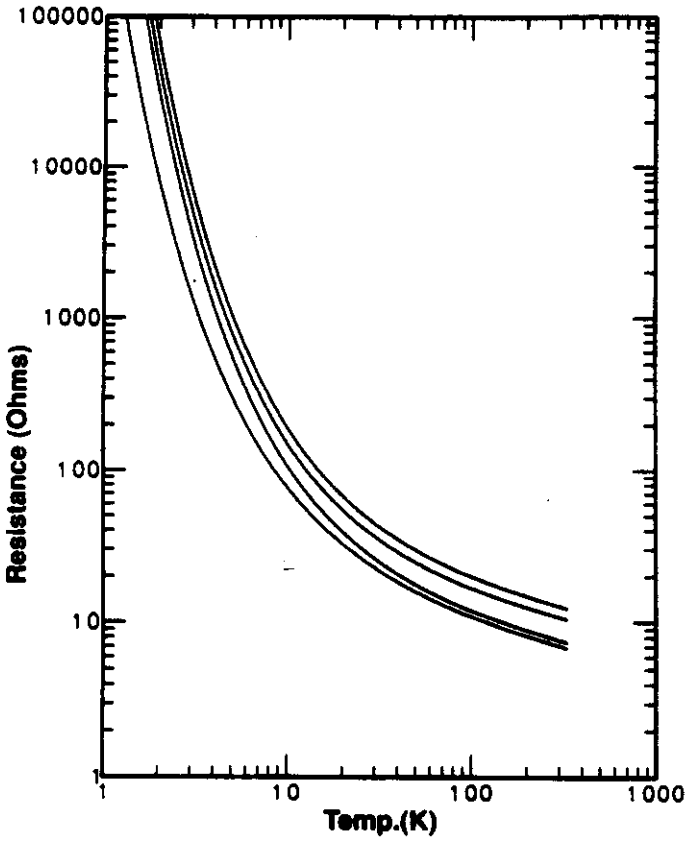


Illustration of the similarity of temperature versus resistance curve characteristics within each carbon-glass resistor model type. Shown are the plotted resistance-temperature curves for four Model CGR-1-1000 sensors.

**CGR-1 Series Construction Detail**

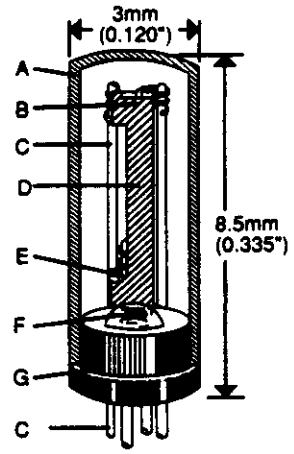


A. Gold-plated copper enclosure
B. Current contact zone
C. Phosphorus-bronze leads 0.20mm (0.008" dia.)
D. Sensing element
E. Gold leads 0.05mm (0.002" dia.)
F. Epoxy heat sink
G. Beryllium oxide base

## Ordering Information

| Model | Typical Resistance at 4.2K | Recommended Useful Range* | |
|---|---|---|---|
| CGR-1-500 | 350-750 ohms | 1.0K to 77K | (325) |
| CGR-1-1000 | 750-1300 ohms | 1.4K to 100K | (325) |
| CGR-1-1500 | 1300-1750 ohms | 2.0K to 200K | (325) |
| CGR-1-2000 | 1750-2400 ohms | 2.5K to 325K | |

* All carbon-glass resistors can be used up to 325K with reduced sensitivity.

**Carbon-Glass Resistor Calibration Options**

| Model | Type | Range(K) | Type | Range(K) |
|---|---|---|---|---|
| CGR-1, | 1.4B | 1.4 to 40 | 4B | 4 to 40 |
| -500, -1000 | 1.4D | 1.4 to 100 | 4D | 4 to 100 |
| -1500, -2000 | 1.4L | 1.4 to 325 | 4L | 4 to 325 |

**Robust package option available:**
CGR-1 series resistors can be mounted in a relatively large, rugged copper bobbin 14.3mm diameter by 5mm thick, with QUAD-LEAD (QL-36) 36 AWG, 4-wire leads.
Order model BOBBIN-CGR

For detailed information on Calibration Services, see pages 47-48.

# Temperature Sensor Calibration Service

Lake Shore provides calibration services for virtually all types of cryogenic temperature sensing elements. We maintain a low temperature calibration facility capable of performing calibrations from 0.05 kelvin (-273°C) to 473 kelvin (200°C).

All Lake Shore calibrations are based on the new temperature scale, the International Temperature Scale of 1990 (ITS-90). The ITS-90 scale became the official international temperature scale on January 1, 1990; it supersedes the International Practical Temperature Scale of 1968 (IPTS-68) and the 1976 Provisional Temperature Scale (EPT-76). ITS-90 covers the temperature range above 0.65K. For temperatures below 0.65K, a cerium magnesium nitrate magnetic thermometer is used in conjunction with NBS superconducting fixed points SRM768 to generate a scale.

- Each scale is maintained on a set of germanium or platinum resistance standards. These standards are routinely checked by intercomparison with, and periodic calibration by, the U.S. National Institute of Standards and Technology or Great Britain's National Physical Laboratory.
- All sensors (two-lead or four-lead elements) are calibrated in a four-wire configuration. A comparison calibration is performed by measuring the resistance or forward voltage of both the sensor and the Standard. (the table below right shows the typical number of data points taken for selected temperature ranges)

The accuracy of Lake Shore calibrations is a function of temperature stability, instrumentation precision, temperature and sensor signal. Basic uncertainties in traceability of a scale must also be taken into account.

**Calibration Data Points and Printouts**

| Range (K) | Typical Number of Data Points | Interpolation Calibration Printout Interval |
|---|---|---|
| 0.050-0.100 | 6 | 0.005 |
| 0.100-0.300 | 9 | 0.010 |
| 0.300-0.500 | 5 | 0.020 |
| 0.500-1.00 | 7 | 0.050 |
| 1.00-2.00 | 18 | 0.10 |
| 2.00-5.00 | 18 | 0.20 |
| 5.00-10.0 | 40 | 0.50 |
| 10.0-30.0 | 40 | 1.0 |
| 30.0-40.0 | 40 | 2.0 |
| 40-100 | 40 | 5.0 |
| 100-300 | 28 | 5.0 |
| 300-380 | 28 | 5.0 |
| 340-480 (Silicon Diodes) | 10 | * |
| 340-480 Platinum and Rhodium-Iron Resistors (400K upper limit) | 15 | * |
| 480-800 Platinum sensors only | 2 | 5 |

* Above room temperature, three points resolved to a curve through interpolation.

Resultant calibration accuracy varies with both temperature range and sensor type. The above table profiles the accuracy of raw calibration data for selected sensor types.

**Accuracy of Lake Shore Calibrations (mk)**

| Temperature (kelvin) | Germanium 1000Ω | | Carbon-Glass 1000Ω | | Platinum 100Ω | | Silicon & GaAlAs Diodes | |
|---|---|---|---|---|---|---|---|---|
| | typ[1] | max | typ | max | typ | max | typ | max |
| < 10 | 4 | 5 | 4 | 5 | --- | --- | 12 | 20 |
| 10 | 4 | 5 | 4 | 5 | --- | --- | 12 | 20 |
| 20 | 8 | 15 | 10 | 20 | 15 | 25 | 15 | 25 |
| 30 | 12 | 25 | 20 | 35 | 10 | 20 | 25 | 45 |
| 50 | 20 | 35 | 30 | 55 | 10 | 20 | 30 | 55 |
| 100 | 45 | 90 | 65 | 125 | 10 | 20 | 25 | 50 |
| 300 | --- | --- | 250 | 450 | 20 | 35 | 25 | 50 |
| 340 - 480 | --- | --- | --- | --- | --- | 100 | --- | 100 |
| 800 | --- | --- | --- | --- | --- | 100 | --- | --- |

1 A summary of the calibration accuracy for selected Lake Shore sensors at specific temperatures. Errors in each case are expressed in millikelvin deviation from ITS-90. Shown are (1) the typical (typ) error of a given calibration, and (2) the maximum (max) allowable deviation, the value for which could occur only in the unlikely event that all standards and instrumentation fall simultaneously at the end of a recalibration cycle, and all error sources are linearly added.

## Sensor Calibrations
### *Ordering Information*

1. Calibration prices do not include sensor.

2. Calibrations for GR-200 series germanium resistors above 100K are not available.

3. DT-470 series silicon diodes coupled with mounting adaptors are calibrated to an upper limit of 325K with one exception. Diodes packaged with the -CO adaptor can be calibrated to 475K.

4. PT-100 series PRTs are calibrated to a lower limit of 14K.

5. Calibration documentation is maintained in an active data file *for a period of one year. It is accessed* by sensor model and serial number.

6. All precision measurement instrumentation requires periodic recalibration to assure continuing conformance to specification. Sensor calibrations are certified for six month periods. Depending upon the sensor type, and how it is used, it is recommended that sensors be processed through Lake Shore's Re-Calibration Service Department periodically.

All Lake Shore calibrations incorporate the following documentation:

*Certificate of Calibration*
Test data
Plot of test (raw) data versus temperature
*Polynomial Equation(s)*
Interpolation table
Low Temperature Calibration Service Data Sheet
Calibration Report Description

### Ordering Information

| | Type | Range (K) |
|---|---|---|
| DT-470 and DT-450 Silicon Diodes | 1.4DS | 1.4 to 100 |
| | 1.4LS | 1.4 to 325 |
| | 4DS | 4.0 to 100 |
| | 4LS | 4.0 to 325 |
| | 77LS | 75 to 325 |
| | -2S* | 2-point SoftCal™ |
| | -3S* | 3-point SoftCal™ |
| DT-470 Silicon Diodes only | 1.4HS | 1.4 to 475 |
| | 4HS | 4 to 475 |
| DT-471 Silicon Diodes | 10L | 10 to 325 |
| | 10M | 10 to 425 |
| | -2S* | 2-point SoftCal™ |
| TG-120 Gallium-Aluminum-Arsenide Diodes | 1.4B | 1.4 to 40 |
| | 1.4D | 1.4 to 100 |
| | 1.4L | 1.4 to 325 |
| | 4B | 4.0 to 40 |
| | 4D | 4.0 to 100 |
| | 4L | 4.0 to 325 |
| | 77L | 75 to 325 |
| GR-200 Germanium Sensors (Low Temperature) | | |
| 30 ohm only | 0.05A | 0.05 to 5.0 |
| 50 ohm only | 0.1A | 0.1 to 6.0 |
| 100 ohm only | 0.3A | 0.3 to 6.0 |
| 250 ohm only | 0.5A | 0.5 to 6.0 |
| For all Germanium Sensors (except 30 ohm, 50 ohm) | 1.4B | 1.4 to 40 |
| | 1.4D | 1.4 to 100 |
| | 4B | 4.0 to 40 |
| | 4D | 4.0 to 100 |
| CGR Carbon Glass Resistance Sensors | 1.4B | 1.4 to 40 |
| | 1.4D | 1.4 to 100 |
| | 1.4L | 1.4 to 325 |
| | 4B | 4 to 40 |
| | 4D | 4 to 100 |
| | 4L | 4 to 325 |
| PT-100 Platinum Resistance Thermometers | 14D | 14 to 100 |
| | 14L | 14 to 325 |
| | 14H | 14 to 475 |
| | 14J | 14 to 800 |
| | 77L | 75 to 325 |
| | 77H | 75 to 475 |
| | 77J | 75 to 800 |
| RF-800 Rhodium Iron Resistance Sensors | 1.4G | 1.4 to 400 |
| | 4G | 4.0 to 400 |

**Expanded Calibration Report Interpolation Tables**
Specify desired temperature intervals

**Printouts of old calibrations (1 year or less)**
*Calibration data is kept on file for one year only. Specify sensor* model and serial number.

* See SoftCal™ and the DT-470 application note on pages 24-25 for more information.

# Series PT-100 Platinum Resistance Thermometers

## An excellent, wide range, stable temperature sensor for use from 30K to 873K (-243°C to 600°C)

### Features

- *High reproducibility*
- *Low magnetic field dependence above 40K*
- *Conform to DIN 43760 and IEC 751 Standards*

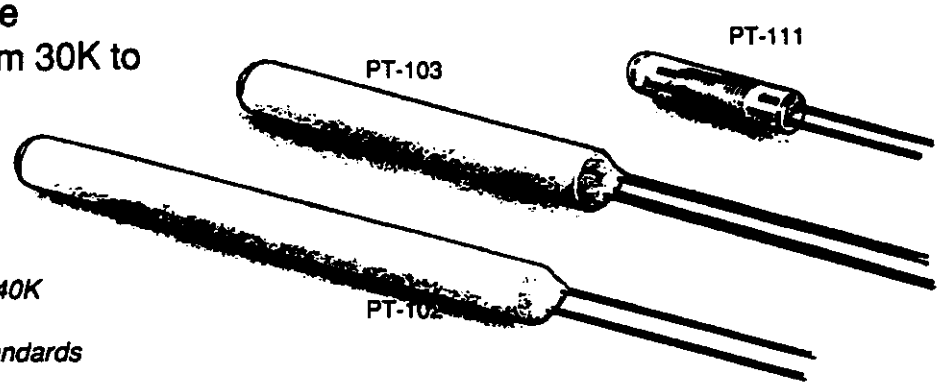


PT-100 series platinum resistance thermometers (PRTs) are an excellent choice for use as cryogenic temperature sensing and control elements in the range from 30K to 873K (-243°C to 600°C). Over this temperature span PRTs offer high reproducibility and nearly constant sensitivity, dR/dT (see table below). Platinum resistors are also of use as control elements in magnetic field environments where errors approaching a degree can be tolerated. PRTs are interchangeable. The use of controlled-purity platinum assures uniformity from device to device.
PRTs experience rapidly decreasing sensitivity below approximately 30K. Like many other cryogenic sensors, they should be calibrated in order to achieve desired accuracy in use below 100K. The table below illustrates platinum sensor conformance to the DIN curve.

| Characteristics | PT-102 | PT-103 | PT-111 |
|---|---|---|---|
| Resistance at 0°C (273.15K) | 100 ± 0.3 ohms | | |
| Type encapsulation | Ceramic | | Glass |
| Temperature range (°C) | -259 to +600 | | -259 to +400 |
| Self-heating Coefficient (K/mW, 1m/sec flowing air) | 0.25 | 0.4 | 0.4 |
| Dimensions: mm (inches) | | | |
| Body diameter | 2.0(0.08) | 1.8(0.07) | |
| Body length | 20.3(0.80) | 12.1(0.475) | 5(0.2) |
| Lead length | 15(0.60) | | 10(0.4) |
| Lead diameter | 0.25(0.010) | | |

**Characteristics of Lake Shore Platinum RTDs**
**Temperature in kelvin, Resistance in ohms and Slope in ohms/kelvin Temperature Coefficient (237.15 to 373.15): 0.00385 ohms/ohms•KConform to Din 43760:1980; IEC 751:1983; BS 1904:1984**

| T(K) | R(ohm)* | dR/dT (ohm/K) | Class B ±K | Class B ±ohm |
|---|---|---|---|---|
| 14.0 | 1.797 | +0.035 | | |
| 20.0 | 2.147 | +0.084 | | |
| 30.0 | 3.508 | +0.190 | | |
| 40.0 | 5.938 | +0.291 | | |
| 50.0 | 9.228 | +0.361 | | |
| 70.0 | 17.128 | +0.414 | 1.32 | 0.55 |
| 100.0 | 29.987 | +0.411 | 1.17 | 0.48 |
| 150.0 | 50.815 | +0.405 | 0.92 | 0.37 |
| 200.0 | 71.073 | +0.399 | 0.67 | 0.27 |
| 300.0 | 110.452 | +0.388 | 0.43 | 0.17 |
| 400.0 | 148.616 | +0.376 | 0.93 | 0.35 |
| 500.0 | 185.035 | +0.364 | 1.43 | 0.52 |
| 600.0 | 221.535 | +0.353 | 1.93 | 0.68 |
| 700.0 | 256.243 | +0.341 | 2.43 | 0.83 |
| 800.0 | 289.789 | +0.330 | 2.93 | 0.97 |
| 900.0 | 322.176 | +0.318 | 3.43 | 1.09 |
| 1000.0 | 353.402 | +0.306 | 3.93 | 1.20 |

* R (0°C) = 100 Standard 751 IEC 1983 from 70K to 1000K.

## Specifications

**Temperature reproducibility:** PT-100 series platinum series sensors are tested for use at low temperature (below -200°C). Under thermal cycling from room temperature to liquid nitrogen temperature the sensors are reproducible to better than ±10mK at 77K.

**Temperature range:** Model PT-102: 14K to 873K (-259°C to 600°C).PT-103: 14K to 873K (-259°C to 600°C). PT-111: 14K to 673K (-259°C to 400°C)

**Materials and construction**
High stability of the PT-100 series PRTs is achieved through production techniques that provide nearly strain-free, securely mounted elements rigidly encapsulated in ceramic or glass. Leads are platinum. All devices are carefully annealed after assembly.

**Use in magnetic field:** Because of their relatively low magnetic field dependence, platinum sensors are of use above 40K as control elements in magnetic field applications when errors as large as a degree or more can be tolerated. See table below.

**Calibrations:** PT-100 series PRTs conform to the DIN standard from 70K to 850K. When used at low temperatures, errors approaching a degree or more may be experienced. When greater precision is required, individual calibrations are available, with accuracy to ±0.01K above 77K (-196°C). For details of Lake Shore's Sensor Calibration Service, refer to pages 47-48.

**Installation:** Refer to the Installation Application Note on pages 8-13.

**Typical Magnetic Field-Dependent Temperature Error***
**ΔT/T (%)**
**at B (magnetic field)**

| T(K) | B (tesla units) 2.5 | 5 | 8 | 14 | 19 | Comments |
|---|---|---|---|---|---|---|
| 20 | 20 | --- | 100 | 250 | --- | Recommended |
| 40 | 0.5 | 1.5 | 3 | 6 | 8.8 | for use when |
| 87 | 0.04 | 0.14 | 0.4 | 1 | 1.7 | T ≥ 30K |
| 300 | <0.01 | 0.001 | 0.02 | 0.07 | 0.13 | |

* Long axis parallel to B; orientation effects exist. B.L. Brandt, L.G. Rubin and H.H. Sample, Low-temperature thermometry in high magnetic fields. VI. Industrial-grade Pt resistors above 66K; Rh-Fe and Au-Mn resistors above 40K, Rev. Sci. Instrum. 59, 642 (1988).

## Ordering Information

| Model | Nominal Resistance at 0°C | Temperature Range (K) |
|---|---|---|
| PT-102 | 100 ohms | 14 to 873K |
| PT-103 | 100 ohms | 14 to 873K |
| PT-111 | 100 ohms | 14 to 873K |

**Note:** PT-100 series sensors are not useful below 14K for metrology and are of limited use below 30K for temperature control because of the rapid decline in sensitivity below that point.

Up to five platinum resistors can be matched with one another to within ± 0.1K at liquid nitrogen temperature. For larger quantities, or for different requirements, consult Lake Shore.

Matching platinums at 77K: Add suffix -LN (Example: PT-103-LN)

**Platinum Calibration Options**

| Type | Range, K* | Range, °C |
|---|---|---|
| 14D | 14 to 100 | -259 to -173 |
| 14L | 14 to 325 | -259 to 52 |
| 14H | 14 to 475 | -259 to 202 |
| 14J | 14 to 800 | -259 to 527 |
| 77L | 75to 325 | -198 to 52 |
| 77 H | 75 to 475 | -198 to 202 |
| 77J | 75 to 800 | -198 to 527 |

* Sensitivity near 14K is very low

For detailed information on Calibration Services, see pages 47-48.

| DATE | LET | R N |
|---|---|---|
| 5-15-92 | A | NO TAB BLACK W/PINOUTS |
| | | |
| | | |

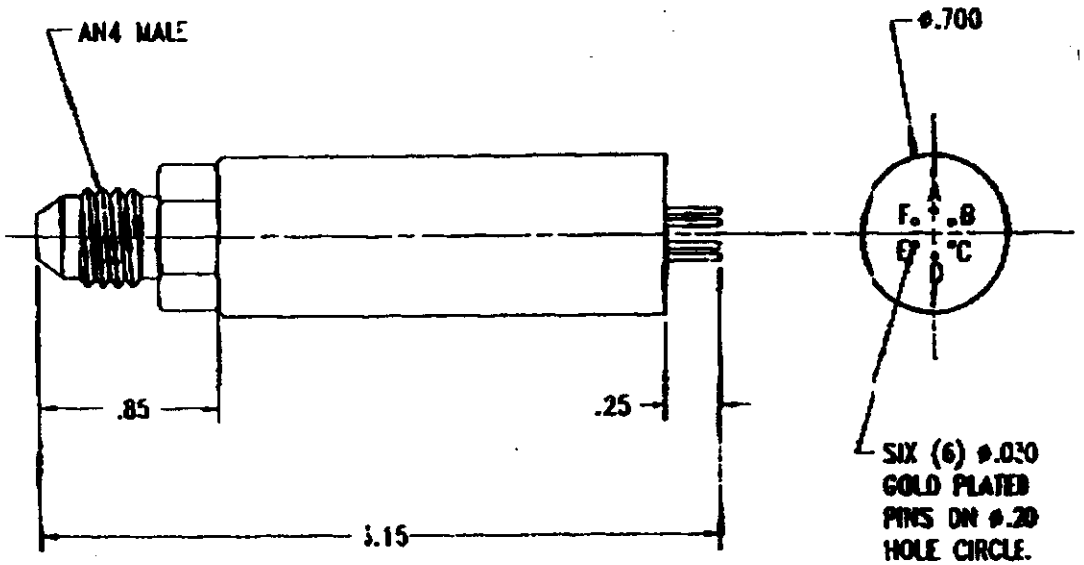


## SPECIFICATIONS

### PRESSURE SENSOR

PRESSURE RANGE: 0-1 THRU 0-500 PSIA, SEE NOTE 1.
EXCITATION: 1 mA CONSTANT CURRENT
OUTPUT: 4-9 mV/PSI
STATIC ACCURACY: ±0.25% F.S.O., BF.S.L.
PROOF PRESSURE: 2X RATED PRESSURE

### TEMPERATURE DIODE

TEMPERATURE RANGE: 1.5-450K
EXCITATION: 10μ AMP CONSTANT CURRENT
OUTPUT: VARIES FROM ~ 1.63 VDC @ 4K TO ~560mV @ 298K, SEE NOTE 2.
ACCURACY: BETTER THAN 1K

*NOTES:*

1. EXACT PRESSURE RANGE AND CALIBRATION TEMPERATURE(S) MUST BE SPECIFIED WHEN ORDERING.
2. TEMPERATURE VS. VOLTAGE DIODE CURVE SUPPLIED WITH UNIT.

| CONNECTOR PINOUTS: | | |
|---|---|---|
| | A | +EXCITATION |
| | B | +OUTPUT |
| | C | -EXCITATION |
| | D | -OUTPUT |
| | E | TEMP. DIODE- |
| | F | TEMP. DIODE+ |

| | | | PART NUMBER | ITEM | DESCRIPTION |
|---|---|---|---|---|---|
| DASH NO/ QTY REQD | | | | | LIST OF MATERIALS |

| DRAWN | CHECKED | ENGINEER | APPROVED |
|---|---|---|---|
| JW | MAM | MAM | MAM |
| 03-30-92 | 03-30-92 | 03-30-92 | 03-30-92 |

UNLESS OTHERWISE SPECIFIED, DIMENSIONS IN INCHES

| INCHES | MILLIMETERS | ANGLES +/- 3 |
|---|---|---|
| .XX ± 0.03<br>.XXX ± 0.005 | .X ± 0.8<br>.XX ± 0.13 | BREAK SHARP EDGE APPROX .005/.010 |
| ALL DIMENSIONS APPLICABLE AFTER SURFACE TREATMENT | | SURFACE FINISH 63 |
| HEAT TREATMENT | | CODE IDENT NO |
| MATERIAL SPEC | | DWG SCALE |

KELLER PSI

DRAWING TITLE
SPECIFICATION C
SERIES 425

DRAWING NO
600187

DO NOT SCALE DRAWING

# R. Churchill, D. Gaughen.

General dynamic.

# Review Relevant Portions of Master Test Plan.

# CRYOGENIC PERFORMANCE WORKSHOP # 2
## Relevant MTP Sections to Cryogenic Performance

- Section 2 - Component Testing
  - 2.2.2.1 - Thermal Straps
  - 2.2.2.2 - Thermal Shield Emissivity
  - 2.2.3 - Helium Adsorber Module
- Section 3 - System Performance Verification Plan
  - 3.2.1 - Standard Magnet Tests
  - 3.2.2.1 - Thermal Performance (Mapping)
  - 3.2.2.8 - String Test
- Section 4 - In-Process Test Development
  - 4.3.5 - Thermal Performance Verification

***Table 2.2.1-1 Support Post Test Requirements***

| Test Identification | Property | Test Level | Condition | Measured Element | Spec./ Dev. Plan |
|---|---|---|---|---|---|
| Structural Coupon Test | Stiffness, Ultimate Strength | Material | 80K, Incremental Compression to FailureCandidate Materials | Composite Cylinders of | M3A-100049 |
| Thermal Coupon Test | Thermal Conductivity | Material | 80K | Test Coupons – Thermal Conductivity Measurements | M3A-100049 |
| Structural Component Test | Stiffness, Ultimate Strength | Component | Ambient, – Lateral Loading (5 cycles) – Compression Proof Loading (5 cycles) – Compression to Failure | 3 Support Post Assemblies – Lateral Deflection – Deflection Under Compression | M3A-100049 |
| Thermal Component Test | Heat Leak | Component | 10K 20K 30K 40K | 2 Support Post Assemblies – Heat Leak Measurements | M3A-100049 |
| Slide Test | Sliding, Wear Characteristics | Component | Ambient, – 2/5 C. M. Weight Comp. – 1000 lbs Lateral Loading | 2 Support Post Assemblies | M3A-100049 |
| Long Term Creep | Viscoelastic Response (Creep) | Component | Ambient, – Compression (16 Month) | 1 Support Post Assembly | M3A-100049 |
| Material Property Testing | Stiffness, Ultimate Strength | Material | Ambient, Incremental Compression to FailureCylinders of | 30 Composite Tube Selected Material | M3A-100049 |
| Magnet Transportation Test | Vibration, Natural Frequency | Prototype Magnet No.4 | Transportation Environment | Prototype Magnet No. 4, Support Posts | M3A-100049 M3A-100056 |

The component test program with the exception of long term creep testing will be completed in support of manufacturing of the support posts for the No.4 prototype magnet (Transportation Test).

## 2.2.2 Thermal Shields

### 2.2.2.1 Thermal Straps

During assembly of the string test Collider Dipole Magnets at FNAL and BNL, considerable difficulties and time delays were encountered while installing the thermal shields. Significant distortions of the shields and insertion of the slide rings which provide slide surfaces between the thermal shields and the support posts complicated the assembly effort. The shield distortions were mostly due to the continuous longitudinal welds used to attach the cryogenic lines to the shields. To ensure lineup of all the cryogenic lines from one magnet to the next and prevent squirm of the connecting bellows, a spider arrangement was provided to force the cryogenic lines to be located within their locational tolerances. However, this

spider arrangement accounted for a large part of the total cryostat heat leak budget and had a rather high parts count.

Based on these lessons learned, the design was changed to make the cryogenic lines structurally independent from the thermal shields. This allows each shield segment to be firmly attached to a support post which eliminates the need for slide rings. It also eliminates the longitudinal welds which were the cause of shield distortion. In addition, the cryogenic lines can now be made of stainless steel, eliminating the use of aluminum-to-steel transition tubes and decreasing the axial deflections of the bellows. The lines are directly supported by the shields, and upward movement of the lines is prevented by springs which loosely hold the lines down. Thermal contact between the shields and the cryogenic lines is made by thermal straps. The spider assembly has been eliminated, and positioning of the different cryogenic lines in relation to the beam tube center is now performed with different means for the different lines.

All described design changes have been or can be established through analysis and vendor consultations. The construction of the thermal straps and their attachment to the aluminum shield at one end, and to a stainless cryogenic line at the other, requires special attention. Several methods of attachment have been evaluated and the method selected was local brush plating of copper to the aluminum shield at one end, and to the cryogenic line at the other, and soldering the thermal strap to the shield and the cryogenic line at the local copper pads. This method has been selected since it is well developed and commonly specified according to the requirements listed in Mil-Std-865 (Military Standard for Selective Brush Plating by Electrodeposition). The feasibility of magneforming a copper sleeve around the cryogenic line, and soldering the strap to the sleeve will be further investigated as a backup to the selected design.

The Thermal Shields Development Plan (M3A-100046) provides more detail about the development program and verification approach. To verify the brush plating process as well as successfully solder the thermal straps to the locally plated regions, a thermal strap test plan will be implemented. Table 2.2.2.1-1 provides a summary of the test program.

***Table 2.2.2.1-1 Thermal Straps Test Requirements***

| Test Identification | Property | Test Level | Condition | Measured Element | Spec./ Dev. Plan |
|---|---|---|---|---|---|
| Plating Cryoshock | Plating Quality | Material | 80K (LN2) | 50 Brush Plated Samples (304 SS)<br>10 Brush Plated Samples (6061-T6 AL) | M3A-100046 |
| Thermal Strap Attachment, Cryoshock | Adhesion | Material | 80K (LN2)<br>5 Cycles<br>(Ambient - 80K) | 50 Test Samples<br>(Thermal Strap Soldered to AL and SS Samples) | M3A-100046 |
| Thermal Strap Attachment, Structural | Adhesion | Material | 20K (LH)<br>200 Cycles<br>(Lateral Movement 1") | 10 Test Samples<br>(Thermal Strap Soldered to AL and SS Samples) | M3A-100046 |
| GDSS Prototype Magnets | Cryostat Thermal Performance | Prototype Magnets | 20K, 80K | Cryostat Shield Elements<br>– 80K Shield<br>– 20K Shield<br>– Cradle<br>– Support Post | M3A-100046 & GDSS Test Procedure |

The thermal strap component test program will be completed prior to fabrication of the first prototype magnet.

### 2.2.2.2 Thermal Shield Emissivity

Replacement of the MLI blankets baselined for the 20K and 4K thermal shields with a low emissivity surface treatment on aluminum offers several advantages: elimination of a potential source of heat leak due to the possible compaction of the MLI during installation, elimination of an outgassing source, material cost and installation time savings. Elimination of the MLI blankets requires the emissivity of the thermal shields to be less than or equal to 0.05. Limited data is available for 6061 aluminum which has been mechanically or chemically processed. Testing is required to determine a surface treatment that provides adequate thermal shield emissivity. Table 2.2.2.2-1 summarizes the four different surface treatments that will be tested at room temperature.

***Table 2.2.2.2-1 Surface Treatment Process Tests***

| Test Identification | Property | Test Level | Condition | Measured Element | Spec./ Dev. Plan |
|---|---|---|---|---|---|
| Alodine 1500 Coating | Emittance Absorbance | Material | Ambient | 6061-T6 AL Coated with Alodine 1500 | M3A-100046 |
| Polished Surface | Emittance Absorbance | Material | Ambient | 6061-T6 AL Polished Surface w/Plastic Sheet (bare) | M3A-100046 |
| Bare Material | Emittance Absorbance | Material | Ambient | 6061-T6 AL No Coating | M3A-100046 |
| Electropolished/ Anodized | Emittance Absorbance | Material | Ambient | 6061-T6 AL Electropolished, .0025mm Sulferic Acid Anodize | M3A-100046 |

Of the candidate surface treatments, the Alodine 1500 coating clearly represents the optimum process. Its emissivity value is .05 at room temperature with a substantial lower value expected at operating temperatures. A confirmatory test of the Alodine-coated aluminum still needs to be performed at cryogenic temperatures. This test, which will be done at liquid nitrogen temperature, shall confirm the fact that the emissivity value indeed declines sufficiently with declining temperatures. In the unlikely event that none of the surface treatments meet the emissivity criteria, the alternate approach would be the use of MLI blankets in the 20K and 4K regions.

### 2.2.3 Helium Adsorber Module

The GDSS cryostat design incorporates a Helium Adsorber Module (HAM) to control excessive helium leak rates. The baseline design consists of granular charcoal bonded to a stainless steel plate. The granular charcoal will be shrouded in a radiation shielded cover with access holes to allow the helium to come in contact with the charcoal. An alternative design would replace the granular charcoal with a charcoal cloth design. The cloth could be used if verification tests prove it performs better than granular charcoal. The backup alternative to the adsorbers is to mechanically pump out the magnets at half cell intervals. The Adsorber Development Plan (M3A-100046) provides more detail about adsorber development and verification.

Verification testing of the HAM will consist of two test series, component level testing performed by the vendors and magnet level testing performed by GDSS. The vendors will perform component level testing to verify the ability of the charcoal (granular or cloth) to absorb a calibrated amount of helium under the normal operating conditions (4.2K, $1 \times 10^{-6}$ torr) demonstrate the ability of the adsorbers to absorb helium after exposure to other gases and demonstrate the bond performance over long term exposure to radiation. The magnet level testing will demonstrate the ability of the adsorber in a functional cryostat. This test will demonstrate the ability of the HAM to absorb not only the calibrated helium leak but also any other gas constituents introduced due to outgassing from the MLI or other cryostat components. Several thermal cycles will need to be completed to demonstrate the ability of the adsorber to operate over repeated absorbing/desorbing cycles. These tests will define the maintenance procedure necessary to ensure continuous operation of the adsorber. The goal is to put enough of the charcoal into the cryostat to maintain the desired vacuum from one thermal cycle to the next. This would allow the maintenance of the adsorber to consist of warming up the module and pumping out the desorbed gas during the planned maintenance intervals. Table 2.2.3-1 summarizes the test requirements for adsorber development.

***Table 2.2.3-1 Adsorber Test Requirements***

| Test Identification | Property | Test Level | Condition | Measured Element | Spec./ Dev. Plan |
|---|---|---|---|---|---|
| Granular Charcoal | Absorption | Material | Nominal Operating (4.2K, 1x10^-6 torr) | Granular Charcoal, Helium Absorption | M3A-100072 |
| Granular Charcoal | Bond Performance | Material | Radiation Exposure | Granular Charcoal, Bond Performance | M3A-100072 |
| Charcoal Cloth | Absorption | Material | Nominal Operating (4.2K, 1x10^-6 torr) | Charcoal Cloth, Helium Absorption | M3A-100072 |
| Charcoal Cloth | Bond Performance | Material | Radiation Exposure | Charcoal Cloth, Bond Performance | M3A-100072 |
| Prototype Magnet Calibrated Leak Test | Absorption/ Desorption | Prototype Magnet | Thermal Cycling | Absorber, Helium & other Gas Absorption/desorption | M3A-100072 |

The vendor performed component verification testing will be completed by December 15, 1992. Upon successful component verification, the first articles will be tested in the Lot B prototype magnets. Modifications and design changes will follow the Lot B tests and the final concept will be tested on the Lot C magnets.

Failure of the adsorbers to perform to specification will initiate the fall back design using turbo pumps at half cell intervals.

## 2.3 INTERCONNECT

Performance verification on the bellows developed to date has been through bellows vendors and SSCL analysis and testing of the bellows used on the SSCL prototype magnets. Based on SSCL provided data and discussions with industry bellows designers and manufacturers, the following concerns have been identified:

- Bellows "squirm," a condition related to the length, diameter, and spring rate
- Leakage rates and paths
- Quick and catastrophic failure mode
- Life cycle requirements
- ASME codes
- Bellows producibility (high rate production, assembly, and installation)
- Displacement allowance
- Pressure drop

The GDSS Bellows Assembly Development Plan (M3A-100053) addresses these concerns and provides a mitigation approach for the associated risks. All bellows testing shall be completed before the on dock need date for prototype article 1 bellows.

### 2.3.1 Pipe Bellows

GDSS will receive assistance from the vendor in the design of the pipe bellows. GDSS will verify the vendor analysis and conduct bellows testing as outlined in Table 2.3.1.1-1. All test units will be tested with 1.8 MPa (260 psi) maximum internal helium pressure, with a vacuum surrounding the bellows and connected to a leak detector. All test units will be tested with a fixed 6 mm lateral offset. The first test of any given bellows (warm and cold) will be cycled until failure. If this failure occurs beyond 10,000 cycles subsequent tests shall be limited to 10,000 cycles (2.8 hrs at 1 Hz). For the thirty Single Phase bellows, ten shall be cycled until failure - 5 warm and 5 cold.

***Table 3.1.2-1 Model Magnet Test Objectives (Continued)***

| Test/Meas. Identification | Property | Condition | Measured Element | Specification/ Development Plan |
|---|---|---|---|---|
| Magnetic Measurements | Field Quality, transfer function, warm and cold correlation, ∫Bdl. | Warm and 4.22K | Cold Mass | SSCL Test Document |
| Quench Testing | Margin, ramp rate, quench velocity and location, MIITs, cold mass structural stability | 4.22K, 3.85K & 3.5K | Quench current, voltages, coil temperature, coil stress | SSCL Test Document |
| Quench Heater Studies | Quench Heater Performance | 4.22K | MIITs, Tfn | M3A-100068 and SSCL Test Document |

## 3.2 PROTOTYPE MAGNET TESTING

Testing during the Prototype phase of the CDM development program will evaluate the performance of the baseline CDM design and define any changes required to the design to meet magnet reliability, producibility and field quality requirements. Prototype magnets will also be used for developing and refining test procedures,and test equipment, and determining success criteria which will be used during acceptance and qualification testing in later program phases. The magnets will be instrumented to satisfy the test objectives of each magnet. Each of the prototype magnets will undergo a standard set of tests, with certain magnets used for specific design verification testing.

The 12 prototype magnets will be built in three lots, Lot A, Lot B, and Lot C, with different objectives for each lot. Lot A will consist of four magnets, Lot B will consist of three magnets and Lot C will consist of five magnets. Lot A magnets will be used for initial design and process validation and to identify adjustments which must be made in the design to optimize CDM magnetic, quench and margin performance. Lot B magnets will be used to validate process adjustments made as the result of Lot A magnet testing and further performance evaluation. The last five magnets, Lot C, will be used to validate CDM design changes identified as a result of Lot A model magnet and Lot A prototype magnet testing.

### 3.2.1 Standard Magnet Tests

Standard prototype magnet tests will verify CDM electrical integrity, magnetic field quality, strength and alignment, quench performance, mechanical stability and thermal performance. Cold mass design features which will be evaluated during

the prototype phase are similar to those discussed in model magnet testing Section 3.1.1. Cryostat design features that will be evaluated during standard prototype testing include vacuum integrity and thermal performance. Vacuum integrity will be performed prior to cool-down and once the magnet has reached operating temperature. Thermal performance will attempt to verify that there are no thermal shorts between the 20K and 80K thermal shields. The effect thermal cycling has on these performance parameters will also be studied. Table 3.2.1-1 lists the standard prototype tests.

***Table 3.2.1-1 Standard Prototype Magnet Tests***

| Test Identification | Property | Condition |
|---|---|---|
| **Electrical Integrity** | Insulation Integrity | Warm & 4.35K |
| **CDM/Test Stand Leak Check** | Vacuum Vessel Vacuum Integrity | 4.35K |
| **Quench Tests** | | |
| Manually Induced Quenches | Coil Protection System | 4.35K |
| Quench Heater Studies | Quench Heater Evaluation | 4.35K |
| Field Margin | CDM Field and Temperature Margin | 4.35K |
| Ramp Rate (di/dt) Studies | CDM Sensitivity to ± Ramp Rates | 4.35K |
| Quench Performance (Spot Heater) Studies | Quench Propagation Characteristics | 4.35K |
| Low Temp. Performance | Collar Structural Stability, Margin | 4.35K |
| **Magnetic Field Measurements** | | |
| Field Strength and Transfer Function | CDM Structure | Warm & 4.35K |
| Dipole Field Angle | CDM Structure | Warm & 4.35K |
| Field Quality and Stability | | Warm & 4.35K |
| **Coil Prestress Monitoring** | Coil Stress | Warm & 4.35K |
| **Thermal Performance (Mapping)** | 20 K and 80K Shield Performance | 4.35K |
| **Thermal Cycling** | Performance Sensitivity to Thermal Cycling | 4.35K |

Instrumentation required in the CDM for standard prototype tests is listed in Table 3.2.1-2. The Cold Test Stand contains additional instrumentation that will be used for testing; information on cold test stand instrumentation can be found in the Cold Test Facility Test Stand Critical Item Product Function Specification (M8A-100202).

***Table 3.2.1-2 Instrumentation Used During Standard Magnet Testing***

| Instrumentation Item | Purpose |
|---|---|
| **Voltage Taps** | |
| Coils | Locating Quench Initiation Point and Propagation Velocity. Coil Protection System |
| Expansion Loop | Coil Protection System |
| Quench Protection Heater | Four wire resistance checkout |
| Spot Heaters | Four wire resistance checkout |
| **Strain Gauges** | |
| Shell | Cold mass shell stresses resulting from welding, cool-down and warmup |
| Collar Pack Assy | Monitor Coil Stresses from Collaring through Cold Test |
| Bullet Gauge Assy | Monitor End Region Force on Coils |
| **Temperature Sensors** | |
| LHe Lead End | Measure LHe Temperature Leaving Cold Mass |
| LHe Non Lead End | Measure LHe Temperature Entering Cold Mass |
| **Pressure Transducers** | |
| LHe Lead End | Measure LHe Pressure Leaving Cold Mass |
| LHe Non Lead End | Measure LHe Pressure Entering Cold Mass |
| **Spot Heaters** | Induce Quenches in Inner Coil |

## 3.2.2 Specific Design Verification Testing

### 3.2.2.1 Thermal Performance (Mapping)

Thermal performance testing will be performed to determine transient and steady state temperature profiles for the CDM assembly consisting of the cold mass and the cryostat. Cold mass mapping will provide the temperature variations from the lead end to the return end. Cryostat mapping will investigate component interface thermal resistance interactions of the support posts, cold mass cradle, thermal shield, and cryogenic lines. Measurements will help validate analytical models and detect any thermal shorts between the thermal shields. Measurements will be made with instrumentation in the CDM and on the Cold Test Stand. Instrumentation located in the CDM is shown in Figure 3.2.2.1-1.

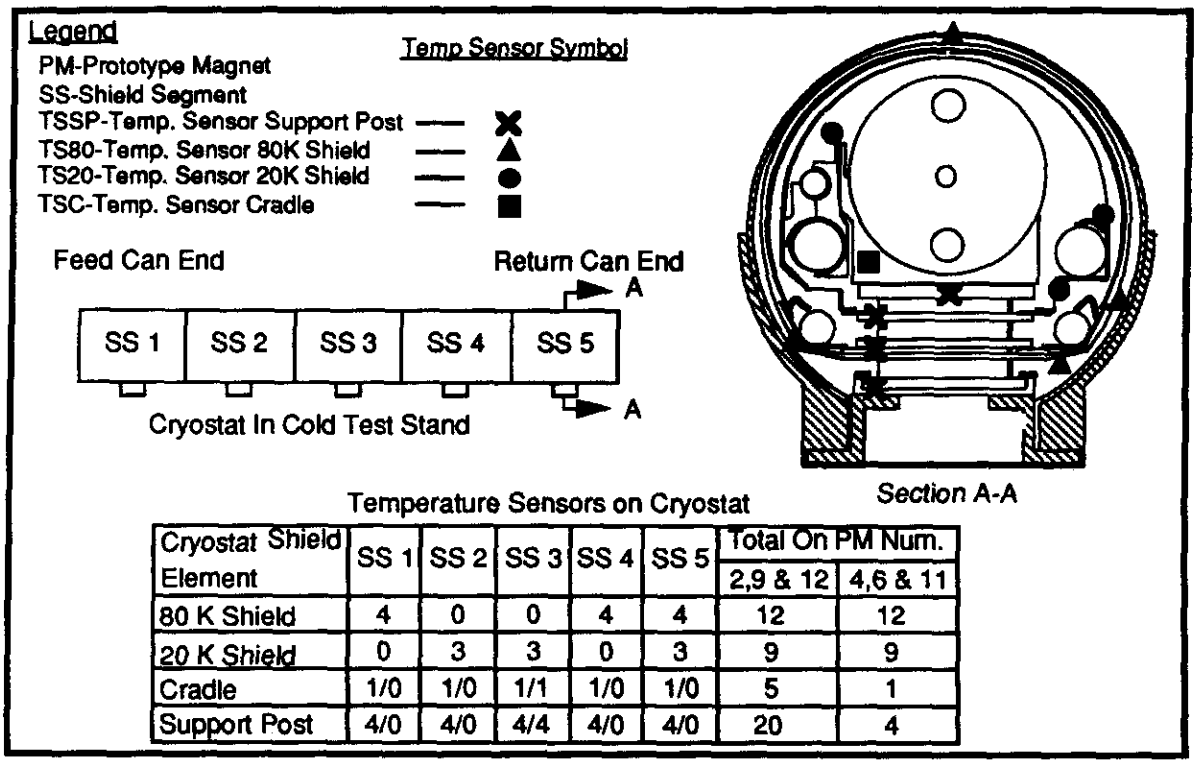


Temperature Sensors on Cryostat

| Cryostat Shield Element | SS 1 | SS 2 | SS 3 | SS 4 | SS 5 | Total On PM Num. | |
|---|---|---|---|---|---|---|---|
| | | | | | | 2,9 & 12 | 4,6 & 11 |
| 80 K Shield | 4 | 0 | 0 | 4 | 4 | 12 | 12 |
| 20 K Shield | 0 | 3 | 3 | 0 | 3 | 9 | 9 |
| Cradle | 1/0 | 1/0 | 1/1 | 1/0 | 1/0 | 5 | 1 |
| Support Post | 4/0 | 4/0 | 4/4 | 4/0 | 4/0 | 20 | 4 |

***Figure 3.2.2.1-1 Instrumentation Required for Thermal Performance Testing***

### 3.2.2.2 Structural Performance

Structural performance testing will be used to verify CDM structural integrity during tunnel operation. The cold mass support posts and cryostat vacuum vessel will be tested to verify adequate structural integrity. The ability of the support post to support the cold mass during cool-down, operation and warmup will be verified. During cool-down and warm up the four non fixed support posts must be free to slide at the 300K surface, during cold mass contraction and expansion. This will be monitored with extensiometers mounted to blocks. The stresses induced into the support post during cool-down and warmup will be monitored with strain gauges mounted on the support in the section between the 20K shield and the cold mass cradle. The ability of the support posts to handle transportation loading will be verified in the Transportation System Test discussed in Section 3.2.2.3. Structural stability of the vacuum vessel against deformation due to weld relaxation will be verified by Non Destructive Test (NDT) residual stress measurements. These

#### 3.2.2.8 String Testing

CDM prototype string testing will be required to verify PIDS requirements that cannot be validated in a single magnet test stand due to test configuration and end can thermal affects. All interconnect hardware performance requirements must be verified during the string test since they cannot be tested in single magnet cold tests. Verification of cryostat thermal performance parameters which cannot be tested in the cold test stand must also be performed. These include heat leak and pressure drops, verification of quench pressure relief, and verification of cool-down, warm-up and quench recovery times and vacuum integrity. String testing will be conducted at SSCL in an instrumented five prototype magnet string. Instrumentation will be similar to that used in single magnet prototype testing. Additional instrumentation will be installed by SSCL in the 20K and 80K cryogenic lines to monitor temperature along the length of the CDM string. Test planning for the string test will be performed by the TPWG. The TPWG will determine test sequence, instrumentation requirements and which magnets will be used for the String Test. GDSS support for string testing is presently not authorized by SSCL.

## 3.3 PREPRODUCTION MAGNET TESTING

### 3.3.1 Formal Qualification Testing (FQT)

FQT will be performed on a Preproduction magnet at both WMSD and GDSS in single magnet test stands. Qualification will be performed to limits specified in the PIDS with one thermal cycle. Requirements which cannot be verified in a single magnet test stand will be verified during the prototype phase in the string test or during the transportation test.

### 4.3.4 Leak Testing

Where appropriate, vacuum and pressure testing will be accomplished in accordance with ASME Boiler and Pressure Vessel Code, Section VIII, Division 1 including the winter 1991 addendum. A trade study during the prototype magnet test phase will determine the best test method, evaluating the options of using a vacuum seal around cryostat ports and introducing helium into the cryostat for leak detection; or performing a full cryostat pump down and injecting helium on the external surfaces of the cryostat seals. The advantages of not pumping down the entire system are the time and equipment cost savings achieved by reducing overall leak test time. However, the introduction of helium into the cryostat is considered a risk.

### 4.3.5 Thermal Performance Verification

Thermal performance testing will be evaluated during prototype testing. The cryogenic flow rate will be reduced, thereby increasing the detectable heat leak to the 20K and 80K cryogenic lines. The optimum test flow rate will be determined and the benefit of performing this testing will be evaluated during the prototype and possibly preproduction test phases. Additional in-process testing to determine that no thermal shield shorts exist between 20K and 80K shield is under evaluation by Quality Assurance.

**Bill Borosky.**

FNAL

# Thermal performance of 20 K MLI systems.

# HEAT LEAK TEST FACILITY LAYOUT FOR MLI MEASUREMENTS BELOW 80K

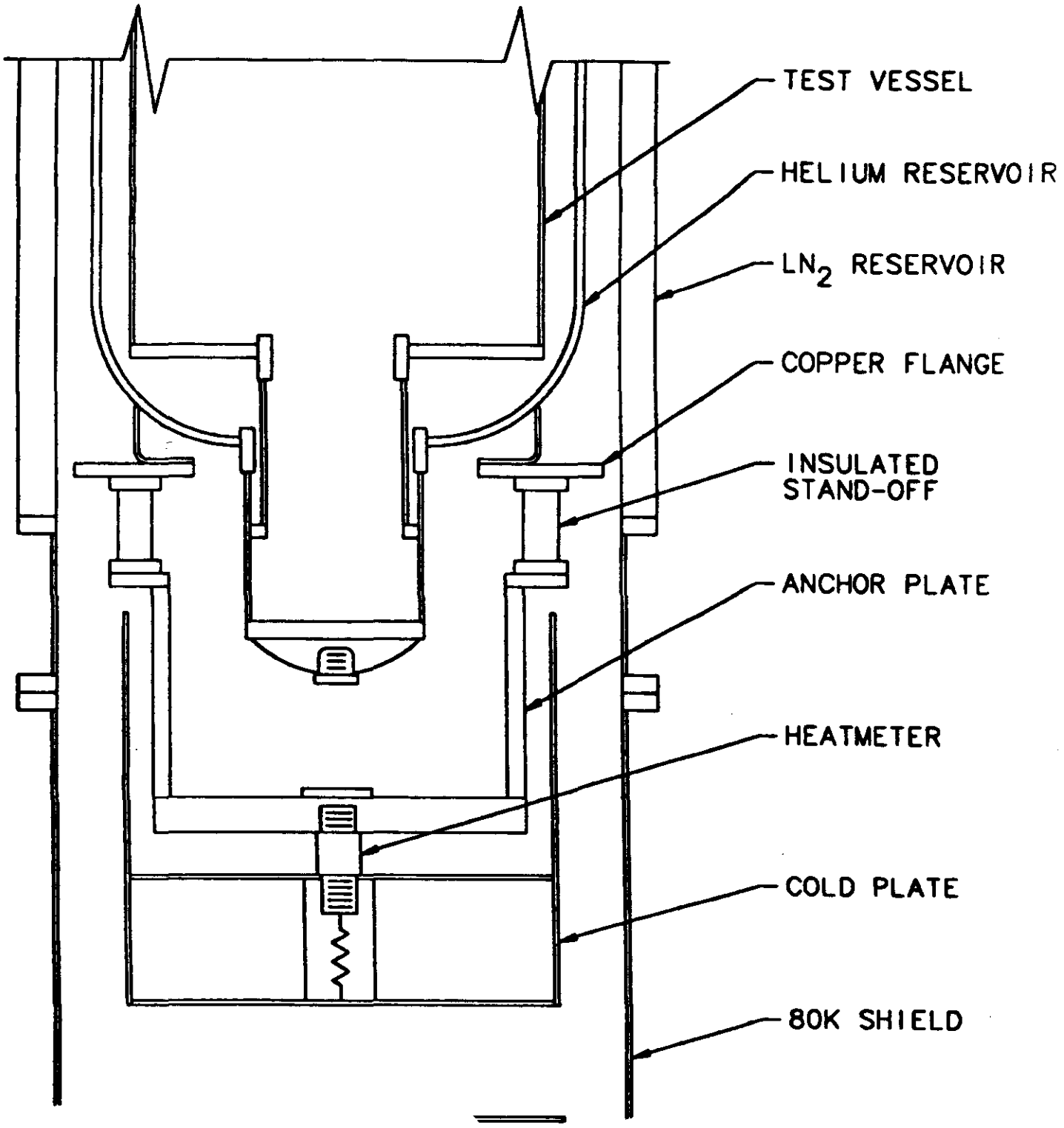

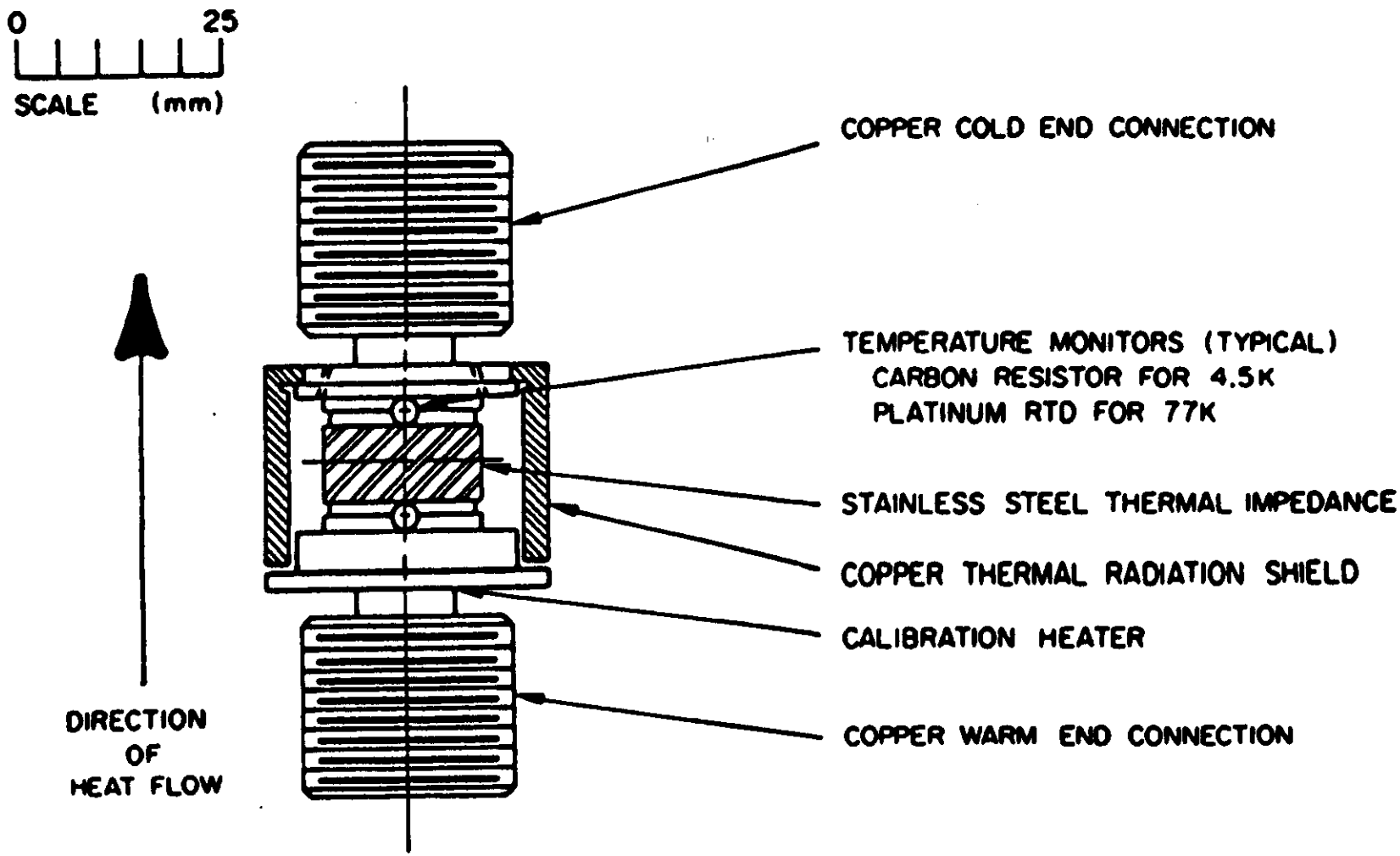
0
25
SCALE (mm)
COPPER COLD END CONNECTION
TEMPERATURE MONITORS (TYPICAL)
CARBON RESISTOR FOR 4.5K
PLATINUM RTD FOR 77K
STAINLESS STEEL THERMAL IMPEDANCE
COPPER THERMAL RADIATION SHIELD
CALIBRATION HEATER
COPPER WARM END CONNECTION
DIRECTION
OF
HEAT FLOW

HEATMETER

# Thermal Performance of Evaluated MLI Systems

| Test | System Description | Number of DAM Layers (N) | Layer Height (cm) | Layer Density (N/cm) | Heat Flux ($W/m^2$) | Apparent Thermal Conductivity (μW/cm-K) | Insulating Vacuum (torr) |
|---|---|---|---|---|---|---|---|
| T1 | No. 425 aluminum tape<br>o MLI installed | — | — | — | 0.057 | — | 3.57E-06 |
| | layers DAM, 600 Å/side<br>triple spunbonded polyester<br>spacer layers<br>stepped seam / stepped joint | 10 | 0.635 | 15.7 | 0.071 | [redacted] | 2.83E-06 |
| T3 | layers DAM, 600 Å/side<br>triple spunbonded polyester<br>spacer layers<br>straight seam / stepped joint | 5 | 0.318 | 15.7 | 0.093 | [redacted] | 2.76E-06 |
| | layers DAM, 600 Å/side<br>triple spunbonded polyester<br>spacer layers<br>straight seam / stepped joint | 10 | 0.635 | 15.7 | 0.112 | [redacted] | 3.34E-06 |
| T5 | layers DAM, 350 Å/side<br>triple spunbonded polyester<br>spacer layers<br>straight seam / stepped joint | 10 | 0.635 | 15.7 | 0.088 | [redacted] | 1.66E-06 |

Boundary Conditions: T = 80K; Surface Finish = 3M No. 425 aluminum tape

# *MLI Performance Below 80K*

- Using equations from Scott for radiant heat transfer and heat transfer by residual gas conduction, good agreement is achieved between predicted and measured values.

- Given system parameters:

  $T_h$ = 80.1K; $T_c$ = 21.6K; Pressure = 3.72E−07 torr

  and assuming:

  $e_h$ = 0.03; $e_c$ = 0.019; and residual gas = He

  then

  q(pred) = q(radiation) + q(gas conduction)

  q(pred) = 0.033 $W/m^2$ + 0.001 $W/m^2$ = 0.034 $W/m^2$

- In comparison:

  q(meas) = 0.033 $W/m^2$

- Concern is that these measured values are significantly higher than those found in the literature despite the good agreement between predicted and measured values.

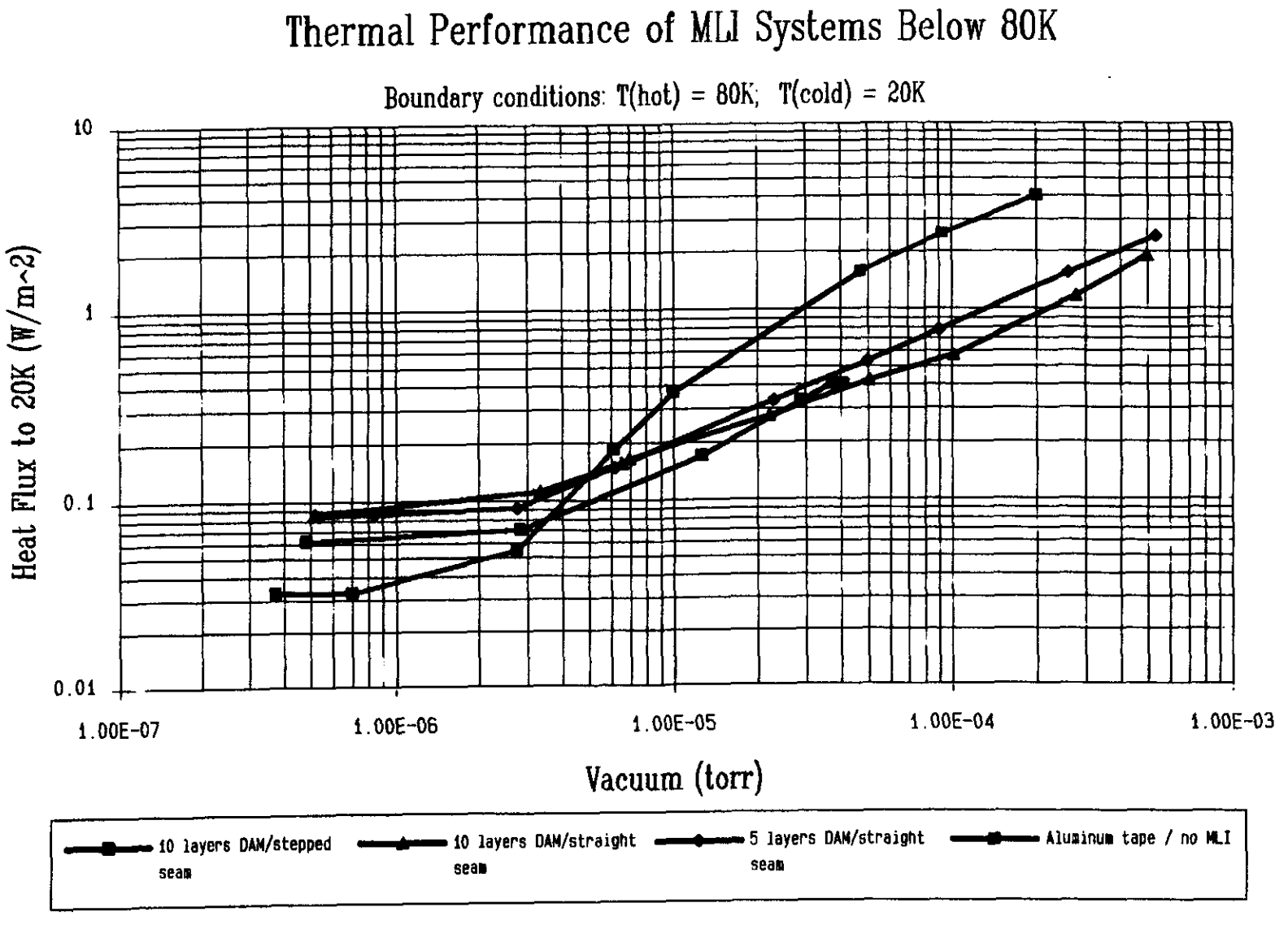
Thermal Performance of MLI Systems Below 80K
Boundary conditions: T(hot) = 80K; T(cold) = 20K
Heat Flux to 20K (W/m^2)
10
1
0.1
0.01
1.00E-07
1.00E-06
1.00E-05
1.00E-04
1.00E-03
Vacuum (torr)
10 layers DAM/stepped seam
10 layers DAM/straight seam
5 layers DAM/straight seam
Aluminum tape / no MLI

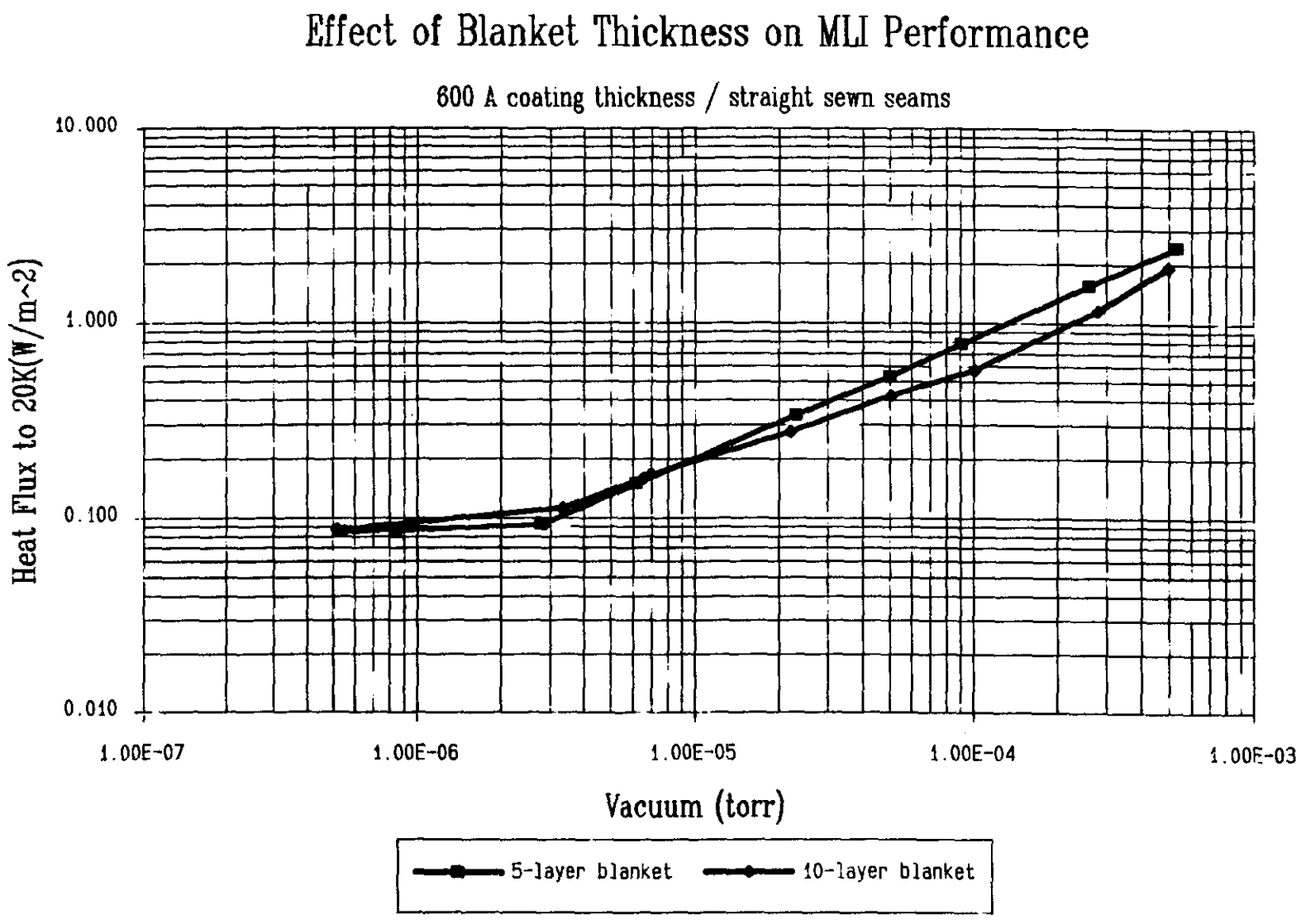
Effect of Blanket Thickness on MLI Performance
600 A coating thickness / straight sewn seams
10.000
1.000
0.100
0.010
Heat Flux to 20K(W/m^2)
1.00E-07
1.00E-06
1.00E-05
1.00E-04
1.00E-03
Vacuum (torr)
5-layer blanket
10-layer blanket

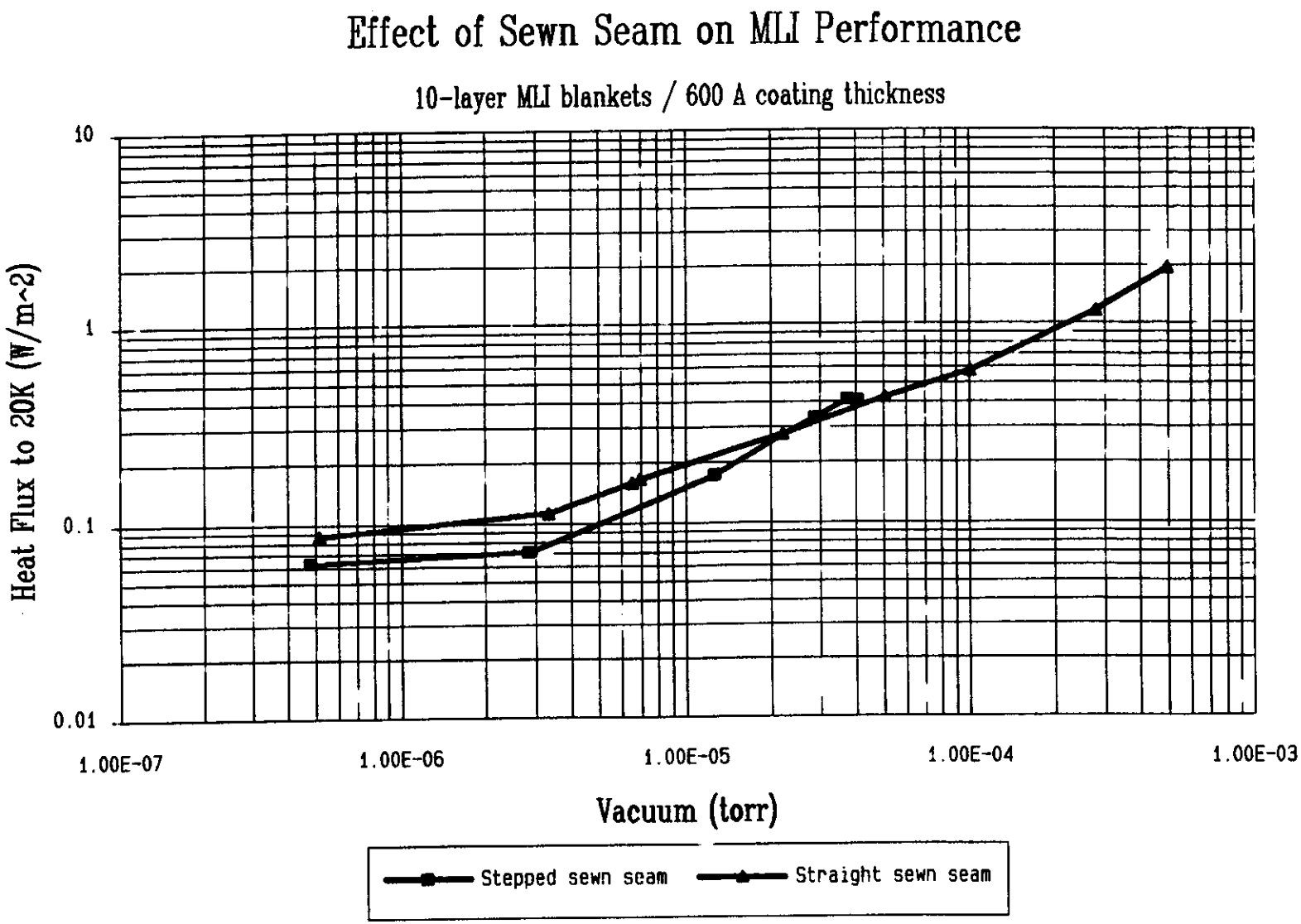
Effect of Sewn Seam on MLI Performance
10-layer MLI blankets / 600 A coating thickness
Heat Flux to 20K (W/m^2)
10
1
0.1
0.01
1.00E-07
1.00E-06
1.00E-05
1.00E-04
1.00E-03
Vacuum (torr)
Stepped sewn seam
Straight sewn seam

# TRANSMISSIVITY OF THIN ALUMINUM COATINGS

- Data show that heat transfer is lower between bare low emissivity surfaces than between surfaces with MLI on the cold boundary at very low temperatures.

- One explanation is that the emissivity of aluminized polyester films is much higher than that of clean aluminum surfaces near 4K.

- Since aluminum has electrical resistivity, an electro-magnetic wave will penetrate some distance into the aluminum before being absorbed or reflected. Theoretically, the thickness of an aluminum coating will have considerable effect on the emissivity of metallized films.

- Transmissivity is the percent of radiant energy striking an object that passes through without restriction. At low temperatures, the transmissivity of thin aluminum films increases as radiation tunneling depths become greater than the thickness of the coating.

- It then appears that increasing the aluminum coating thickness on metallized films should increase performance of the system by offering shields that remain reflective at low temperatures.

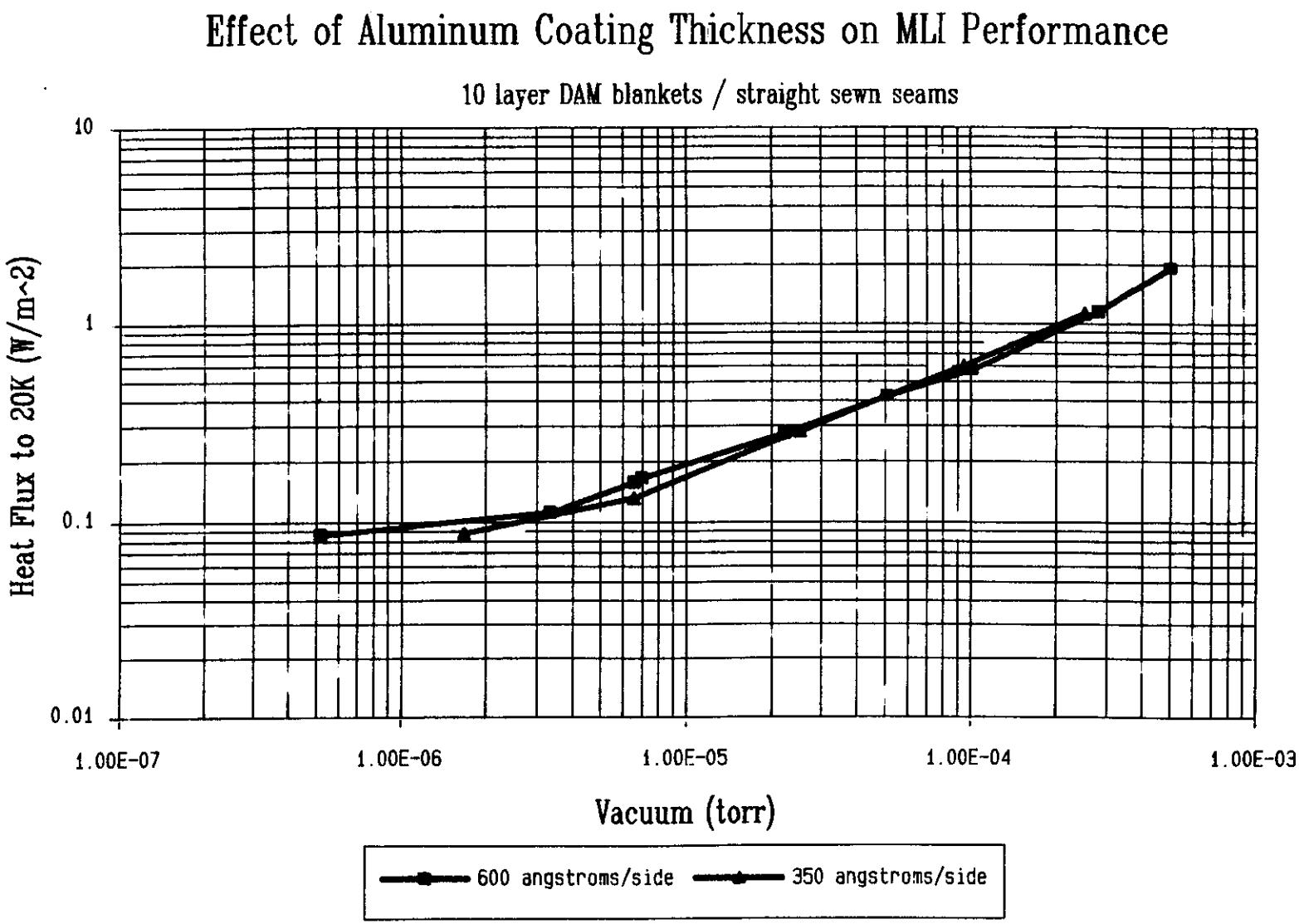
Effect of Aluminum Coating Thickness on MLI Performance
10 layer DAM blankets / straight sewn seams
Heat Flux to 20K (W/m^2)
10
1
0.1
0.01
1.00E-07
1.00E-06
1.00E-05
1.00E-04
1.00E-03
Vacuum (torr)
600 angstroms/side
350 angstroms/side

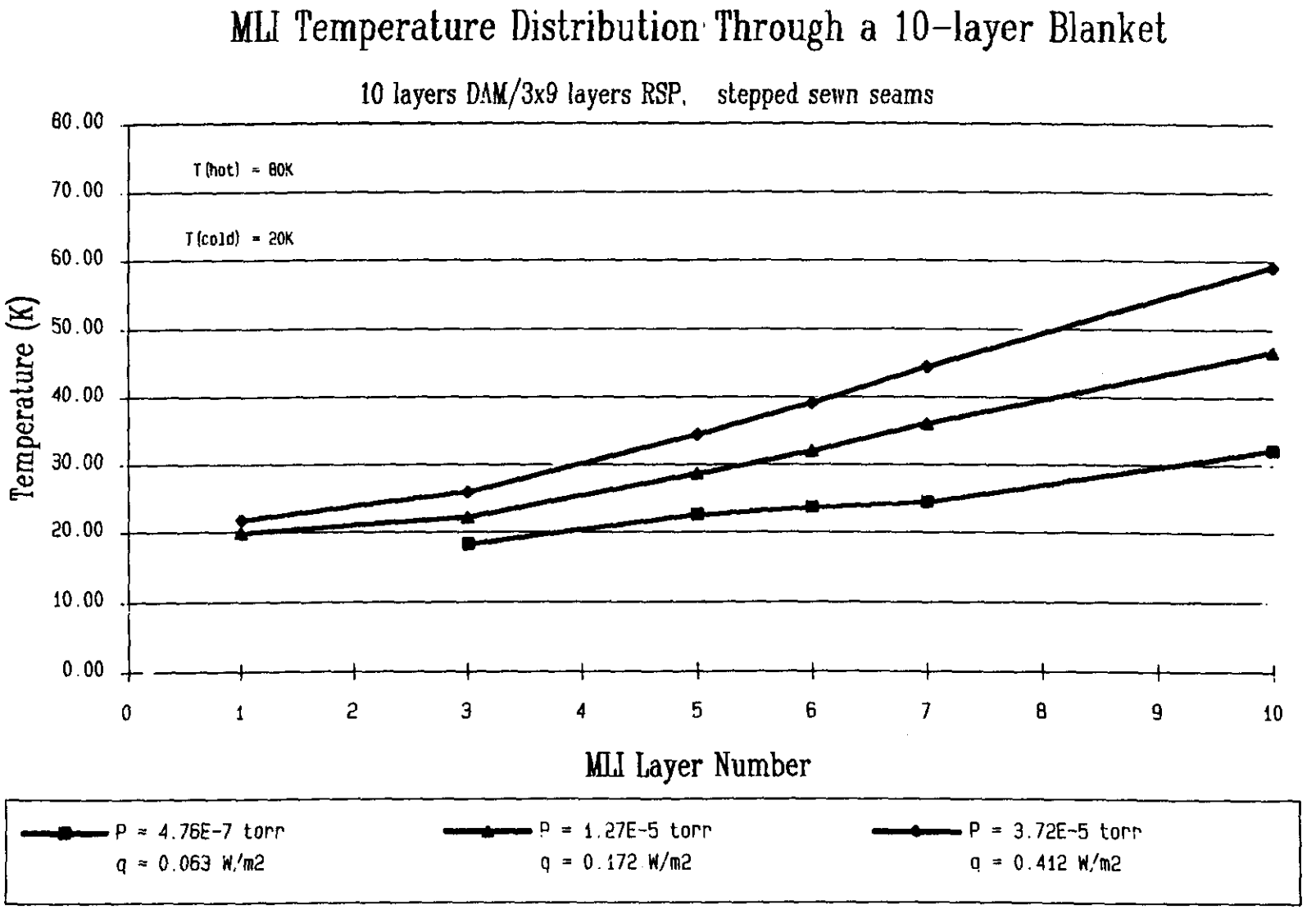
MLI Temperature Distribution Through a 10-layer Blanket
10 layers DAM/3x9 layers RSP, stepped sewn seams
T(hot) = 80K
T(cold) = 20K
Temperature (K)
80.00
70.00
60.00
50.00
40.00
30.00
20.00
10.00
0.00
0
1
2
3
4
5
6
7
8
9
10
MLI Layer Number
P = 4.76E-7 torr
q = 0.063 W/m2
P = 1.27E-5 torr
q = 0.172 W/m2
P = 3.72E-5 torr
q = 0.412 W/m2

# CONCLUSIONS

- Experimental results verify that the 10–layer MLI blanket specified for the SSC dipole cryostat 20K shield meets the design budget at an insulating vacuum of 1E–6 torr.

- The region near 20K is very sensitive to residual gas conduction. Insulating vacuum must be below 1E–7 torr before the contribution of gas conduction to insulation performance becomes negligible.

- At vacuum levels near 1E–6 torr, the number of reflective layers is not as important as how the blanket is configured. Blankets fabricated with similar layer densities and fastening methods had the same thermal performance even though one blanket had twice the number of reflective layers

# CONCLUSIONS

- The number of reflective layers becomes important when insulating vacuum increases above 1E−6 torr. Additional layers limit heat transfer by impeding residual gas conduction.
- Sewn seams impact the overall thermal performance of MLI blankets operating near 20K. The stepped sewn seam geometry specified for the SSC 20K MLI system allows the many layers to be handled as a single component while still meeting the thermal design requirements.
- The use of reflective films with 600 angstrom thick aluminum coatings offer no improvement in performance over similar systems comprised of films with 350 angstrom thick coatings. All MLI blankets in the SSC dipole cryostat can use films with 350 angstrom thick coatings.

# MTL Cold Test Stand Cryogenic Instrumentation

Q.S. Shu and I. Syromyatnikov

# MTL Cold Test Stand Cryogenic Instrumentation.

Q. S. Shu, I. Syromyatnikov.

*Superconducting Super Collider Laboratory.*
*Magnet System Division.*

# CONTENTS.

1. General overview of the MTL test stand cryogenic instrumentation.

2. Cryogenic instrumentation:
   a) Thermometry;
   b) Vapor Pressure Thermometry;
   c) Pressure;
   d) Flow;
   e) Power Leads Instrumentation;
   f) Electrical Heaters.

3. Instrumentation data acquisition system hardware schematic.

4. Instrumentation data acquisition system software structure.

| REVISIONS | | | |
|---|---|---|---|
| REV | DESCRIPTION | DATE | ECR NUMBER |

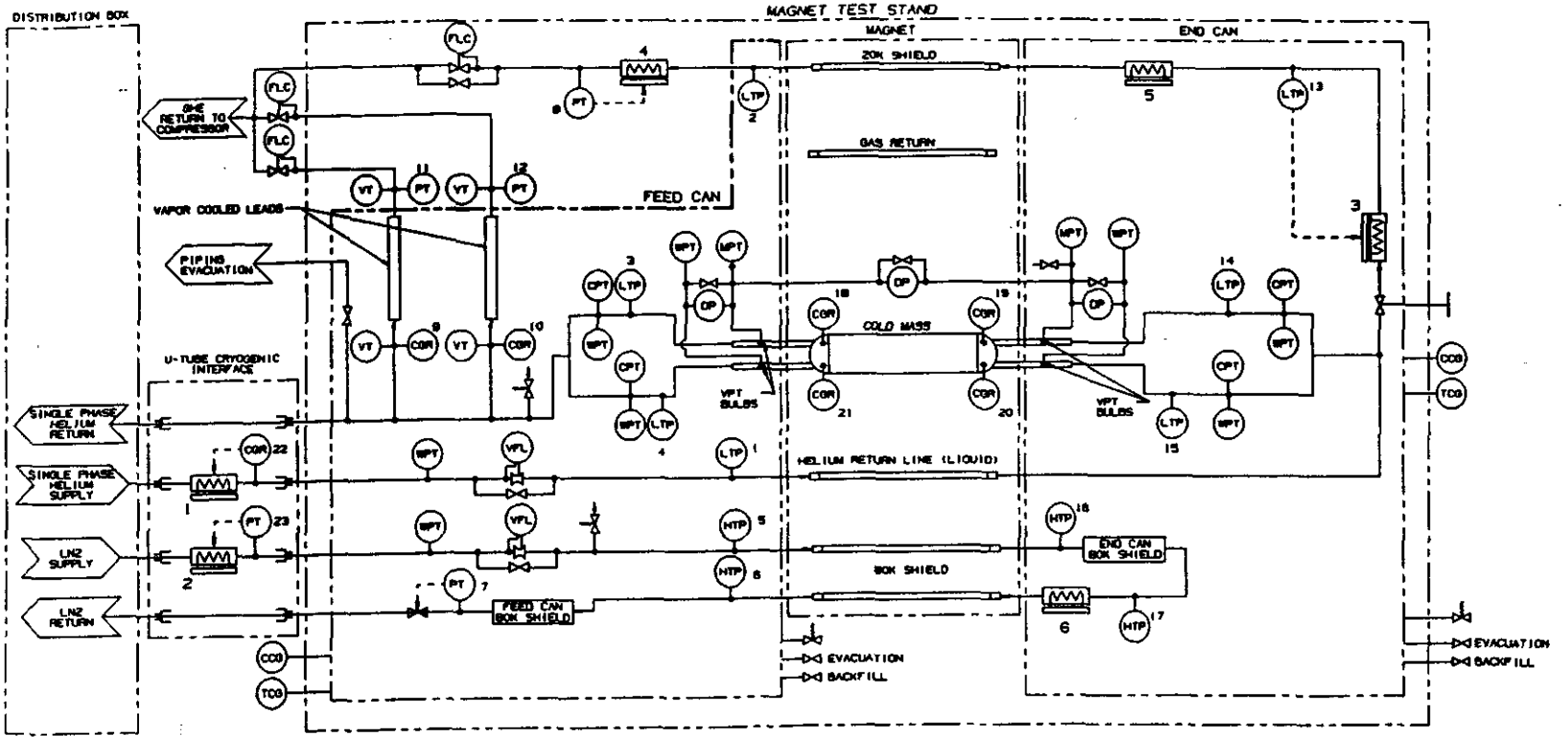


## LEGEND

- WPT — WARM PRESSURE TRANSDUCER
- CCG — COLD CATHODE GAUGE
- TCG — THERMOCOUPLE GAUGE
- PT — PLATINUM TEMPERATURE SENSOR
- VT — VOLTAGE TAP (SEE NOTE 2)
- ELECTRIC HEATER
- CPT — COLD PRESSURE TRANSDUCER
- HTP — HIGH TEMPERATURE SENSOR PACKAGE
- LTP — LOW TEMPERATURE SENSOR PACKAGE
- MPT — MECHANICAL PRESSURE TRANSDUCER
- PRESSURE TRANSDUCER
- DP — DIFFERENTIAL PRESSURE TRANSDUCER
- VPT — VAPOR PRESSURE THERMOMETER
- CGR — CARBON GLASS TEMPERATURE SENSOR
- VFL — VENTURI FLOWMETER
- FLC — FLOW CONTROLLER
- PROCESS
- ELECTRICAL OR CONTROL LEAD
- SAFETY VALVE (SEE NOTE 1)
- VALVE (SEE NOTE 1)
- BAYONET CONNECTION

NOTES:
1. ALL VALVES AND THEIR LOCATIONS SHOWN IN SIMPLIFIED FORM.
2. VOLTAGE TAPS ARE SHOWN ONLY FOR MAIN CURRENT LEADS. VOLTAGE TAPS SHALL BE PROVIDED AT SUPERCONDUCTING CABLE MECHANICAL JOINTS.

| | | |
|---|---|---|
| DRAWN | GONZALES | DATE 6-4-92 |
| CHKR | BOWERIDGE | 6-4-92 |
| APPD | SYROMYATNIKOV | 6-8-92 |
| APPD | SSHU | 6-8-92 |
| APPD | | |
| APPD | | |
| APPD | | |

CONTRACT NO. DE-ACD2-89ER40486

SSC — SUPERCONDUCTING SUPER COLLIDER LABORATORY, 2550 BECKLEYMEADE AVE., SUITE 125, DALLAS, TX. 75237-3946

# DIAGRAM, CRYOGENIC INSTRUMENTATION MAGNET TEST STAND

| SIZE | CAGEC | DRAWING NO. | REV |
|---|---|---|---|
| B | | M60-001500 | - |

/mad/design/tooling/mtl/m60-001500.prt — DRT # M81-000682

SCALE NONE — WEIGHT — SHEET 1 OF 1

# Thermometry.

## 1. Accuracy requirements.

| Cryogen | T Range | Accuracy |
|---|---|---|
| He | 2.5 - 10 K | ± 2 mK |
| | 10 - 20 K | ± 10 mK |
| | 20 - 40 K | ± 50 mK |
| | 40 - 80 K | ± 50 mK |
| | 80-300 K | ± 500 mK |
| $N_2$ | 80-300K | ± 50 mK |

## 2. Type of sensors.

a) Carbon-glass CGR-1-2000 2.5-40 K.
b) Platinum RTD PT - 103 30-300 K.

## 3. In-stream sensors mounting example:

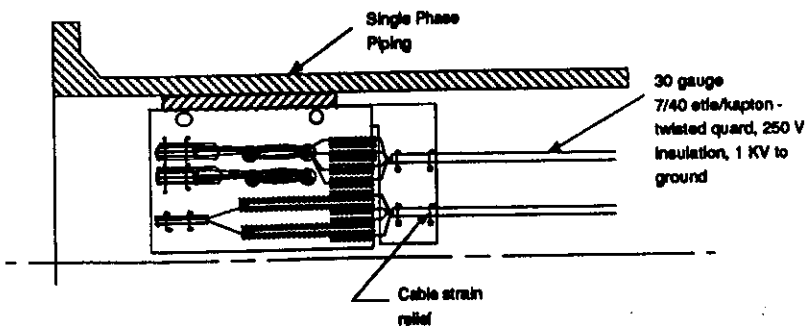


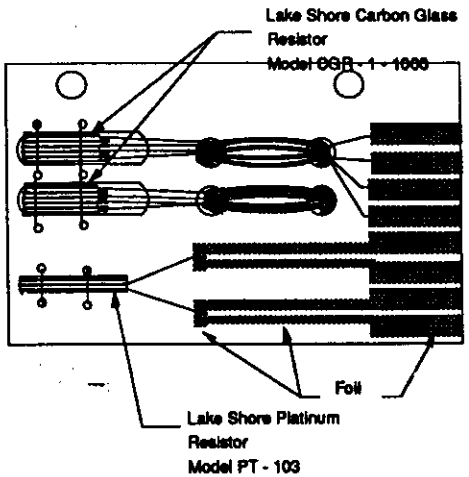

# Vapor pressure thermometry.

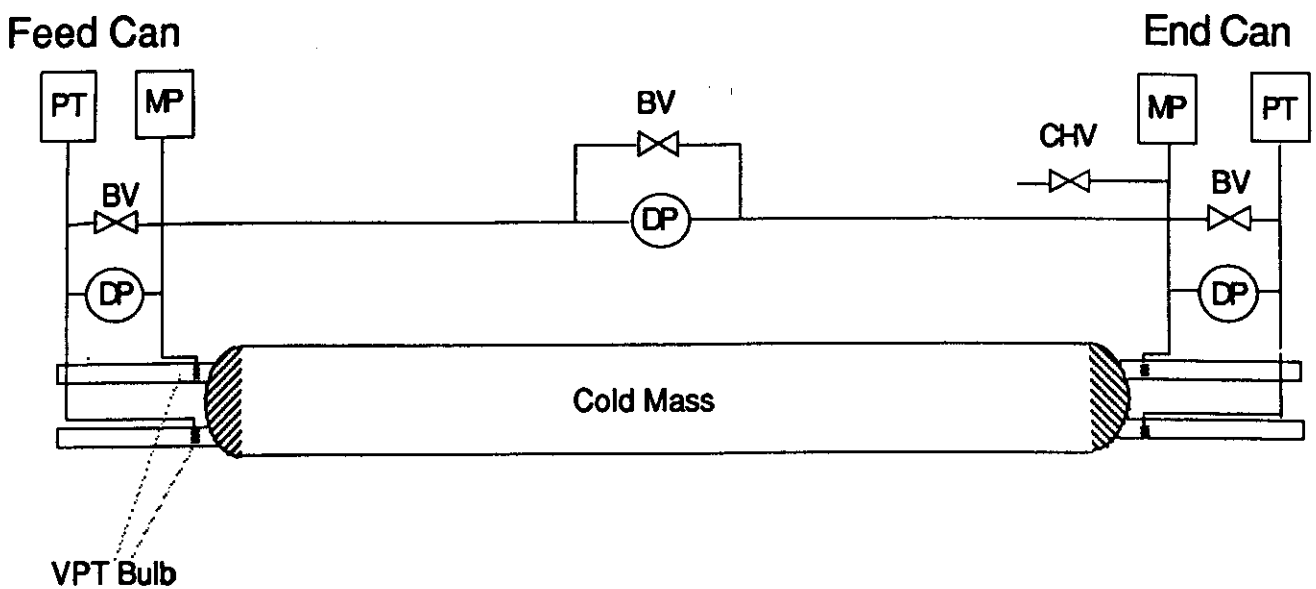


1. Pressure transducers. **Absolute: Sensotec Super TJE - 50 psia FS,**

**0.05 % FSO accuracy.**

**Differential: Sensotec Type Z - 5 psid FS,**
**0.25 % FSO accuracy.**

2. Temperature range and accuracy: **Absolute : 3.5 - 5.1 K ± 2 mK.**
**Gradient : 150 mK ± 0.5 mK**

# Pressure.

## 1. Cold pressure transducers.

Keller PSI 420 (250 psi FS, 0.25 % FSO accuracy) installed in-stream.
2900 PiezoCryometer (4 channels, 1 mA excitation current, RS-232) readout module.

## 2. Warm pressure transducers.

Sensotec TJE (200 psi FS, 0.1% FSO accuracy) installed outside the feed and end cans.

# Flow.

**1. Venturi flowmeters.** Shall be installed in He single phase and nitrogen piping.

| Line Function Description | Flowrate Range | Accuracy | Pressure drop at maximum flowrate | Operation pressure | Temperature Range |
|---|---|---|---|---|---|
| Single phase He supply | 5 - 20 g/s | 1 % | 3.6 PSID | 4 bar | 2.5 - 12 K |
| $N_2$ supply to 80 K shield | 1- 10 g/s | 1 % | 3.6 PSID | 2.5 bar | 77 - 110 K |

**2. Flow controllers.** Two MKS 1562A (480 SLPM, ± 1% FS accuracy) shall be installed in the power leads return lines (300 K).

One MKS 1559A (480 SLPM, ± 1% FS accuracy) shall be installed in 20 K shield return line (300 K).

# Power leads instrumentation.

**1. Thermometry:** One PT-103 at the top, two CGR-1-1000 at the bottom of each power lead.

**2. He flow:** Two MKS 1562A (480 SLPM, ± 1% FS accuracy) installed in the power leads return lines (300 K).

**2. Voltage taps.:** Shown on the picture.

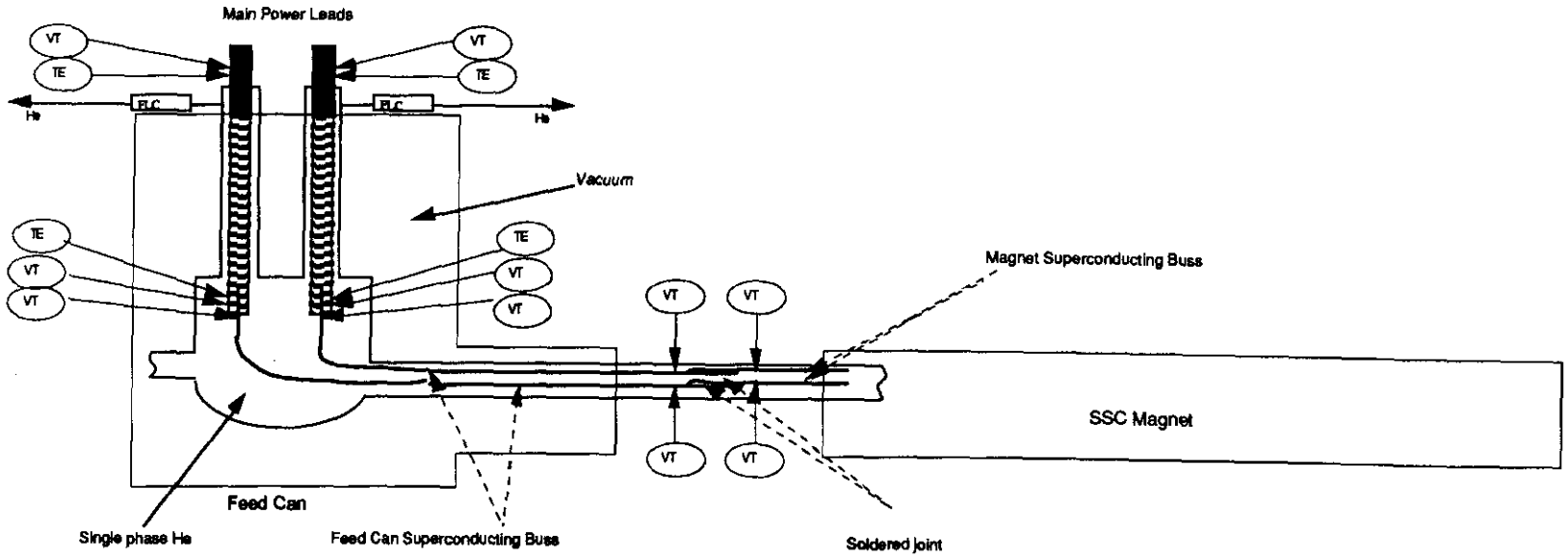


TE - temperature element;
VT - voltage taps;
FLC - flow controller.

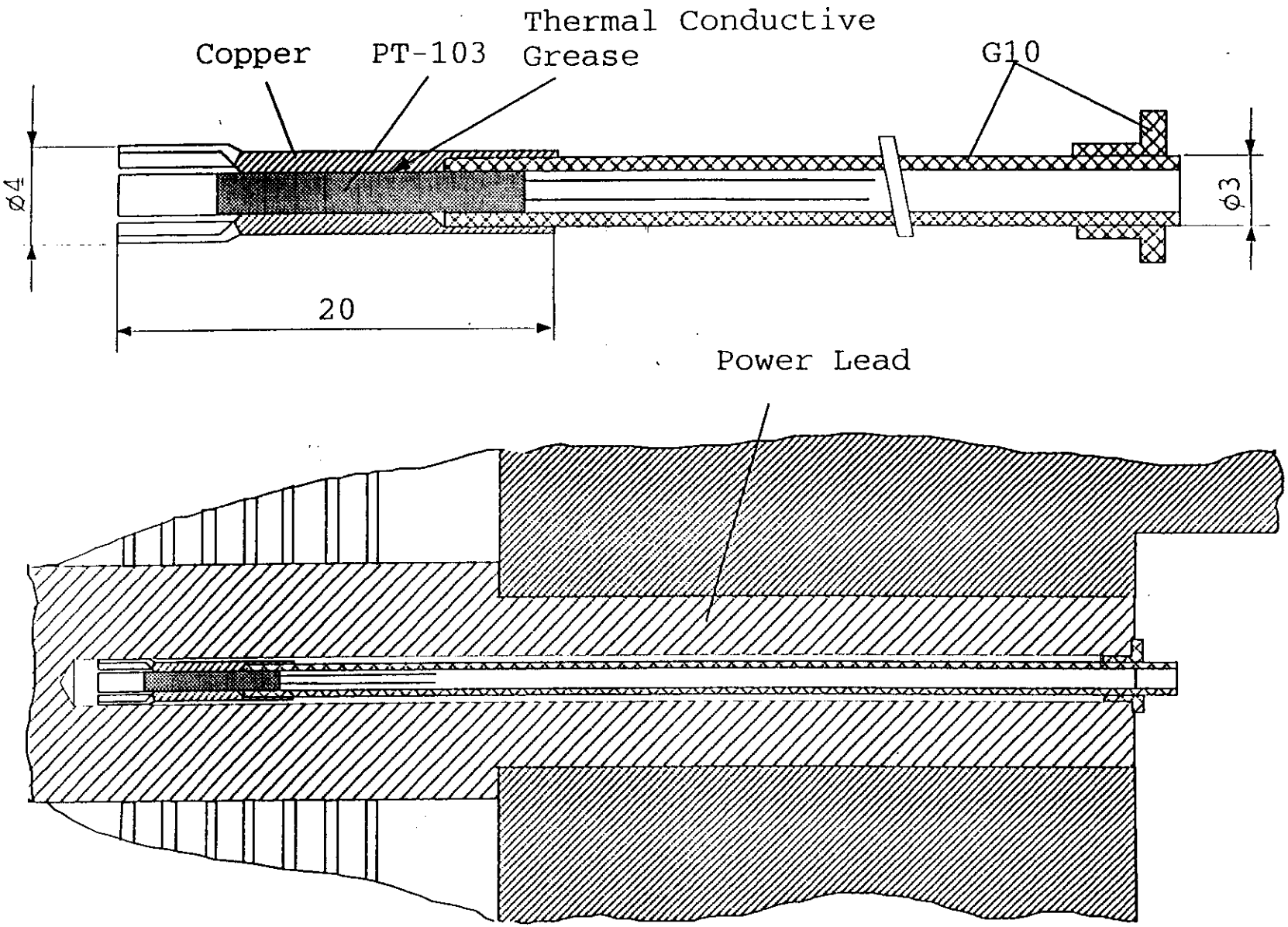


**Figure 4.1.** Temperature probe schematic.

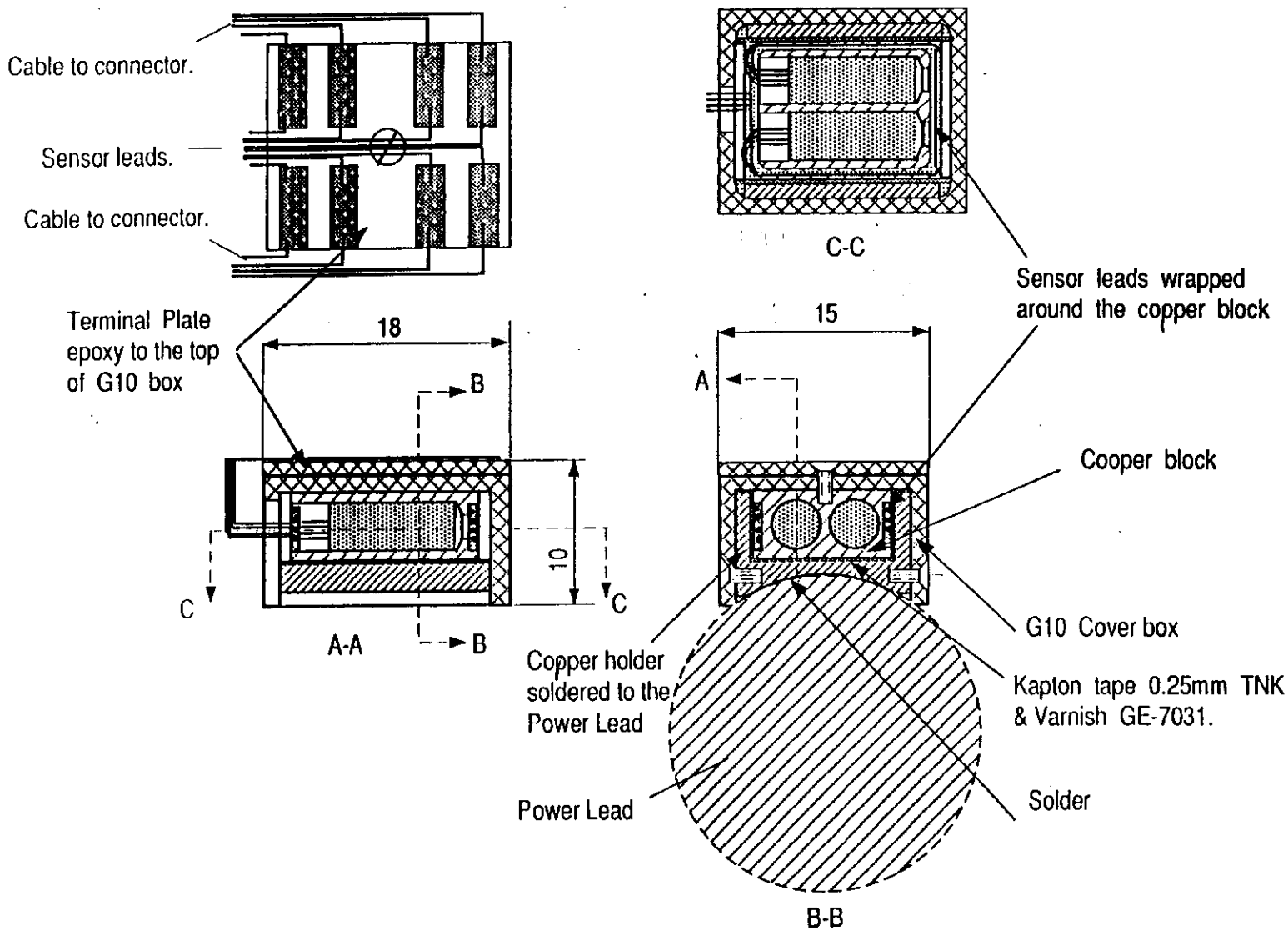


Fig.4.2. Power lead temperature sensors mounting details.

# Electrical heaters

| No | Service | Flowrate | Heater power | Temperature range | Controlled range | Accuracy |
|---|---|---|---|---|---|---|
| 1 | L He supply | 100 g/s | 50 W | 2.5 K - 5 K | 100 mK | ± 5 mK |
| 2 | L $N_2$ supply | 10 g/s | 1800 W | 77 K - 110 K | 35 K | ± 50 mK |
| 3 | 20K supply (EC) | 1 g/s | 250 W | 2.5 K- 40 K | 40 K | ± 10 mK |
| 4 | 20K return | 1 g/s | 1700 W | 2.5 K - 300 K | 300 K | ± 5K |
| 5 | 20K supply (EC) | 1 g/s | 10 W | Produces constant predefined heat load. | | |
| 6 | L $N_2$ supply | 10 g/s | 10 W | Produces constant predefined heat load. | | |

# MTL Cold Test Stand Instrumentation Hardware Schematic.

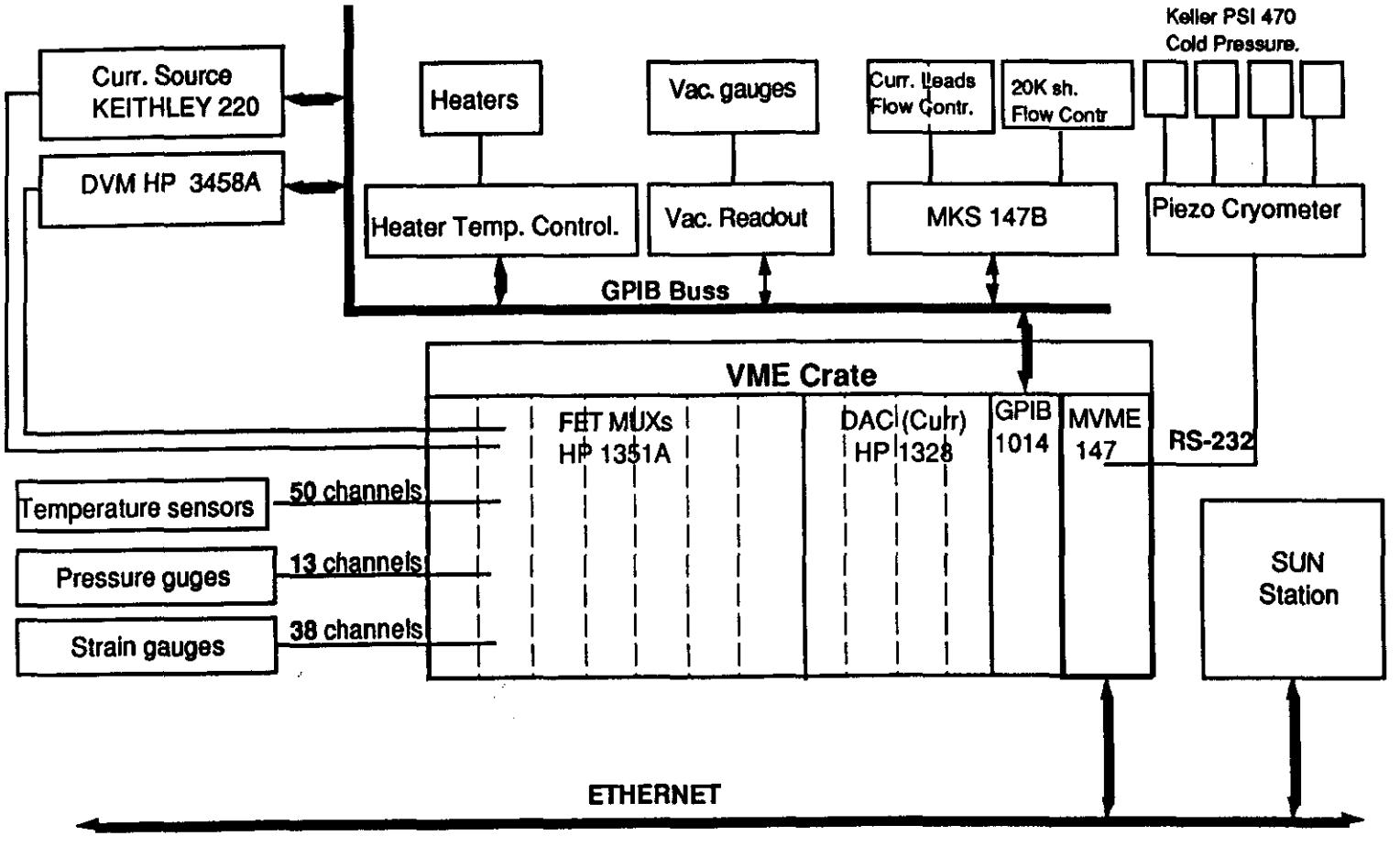

# MTL Dataflow

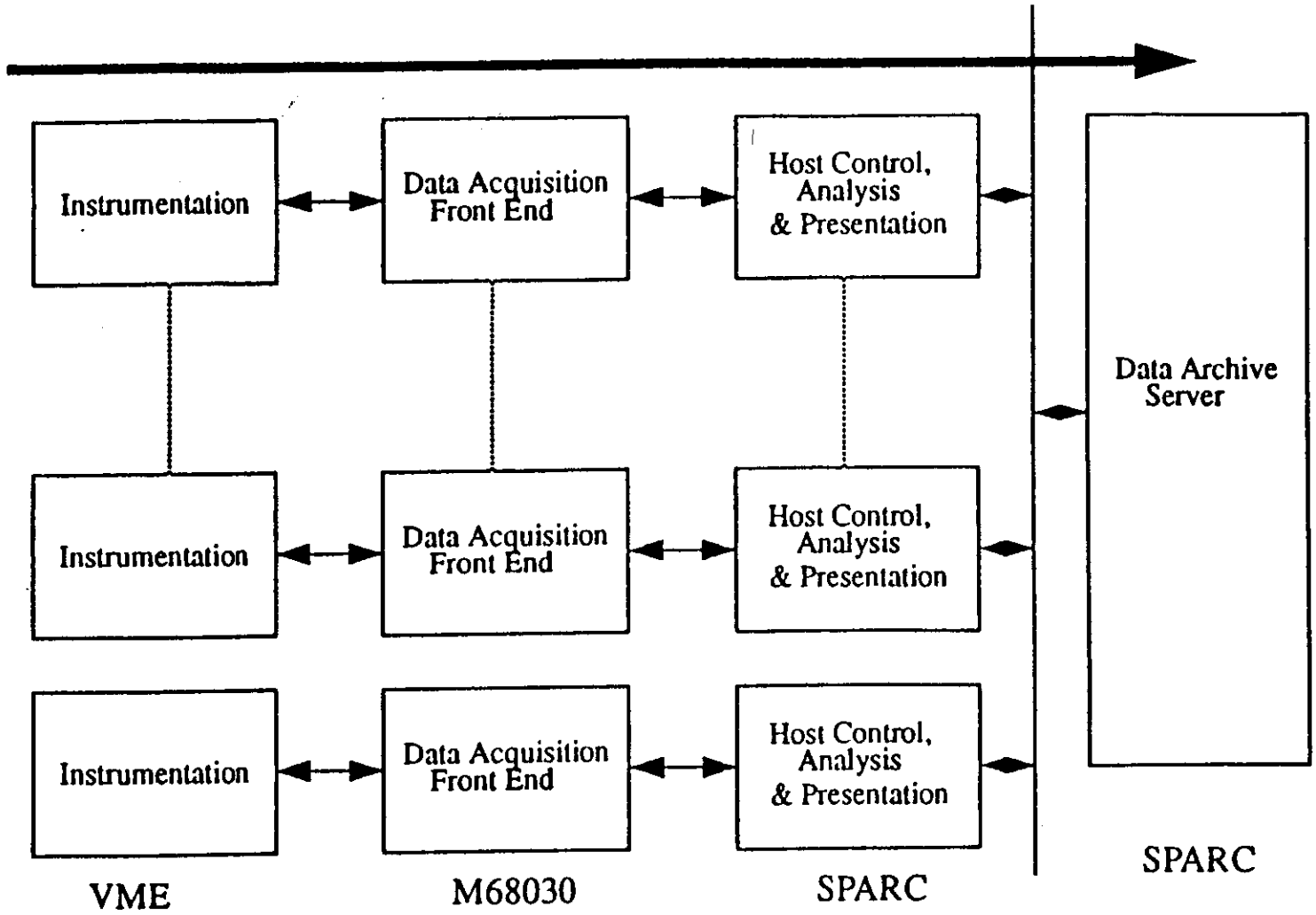

# Cryogenic Data Acquisition system software structure.

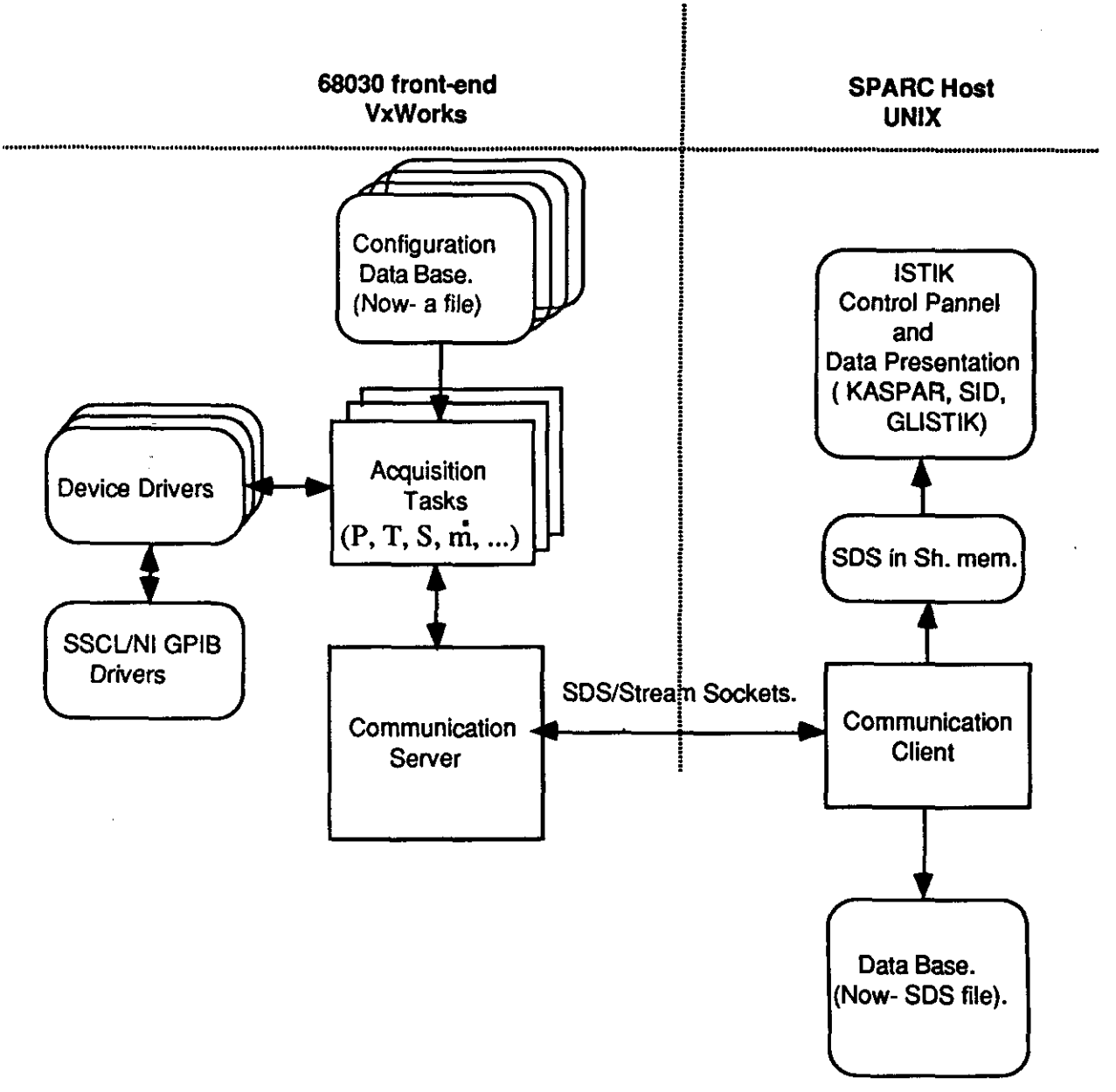

# Status of Cross Flow Cooling Calculations

S. Peck

# Status of Cross Flow Cooling Calculations

Scott Peck

2nd Workshop on Testing of SSC Magnet Cryogenic Performance
General Dynamics Space Systems Division, San Diego, Ca
June 29, 1992

# CROSS FLOW COOLING
## Design Recommendations / Implementation

- Needed to enable full field multipole measurements on test stand
  — maintains temperature margin in presence of mole heat leak

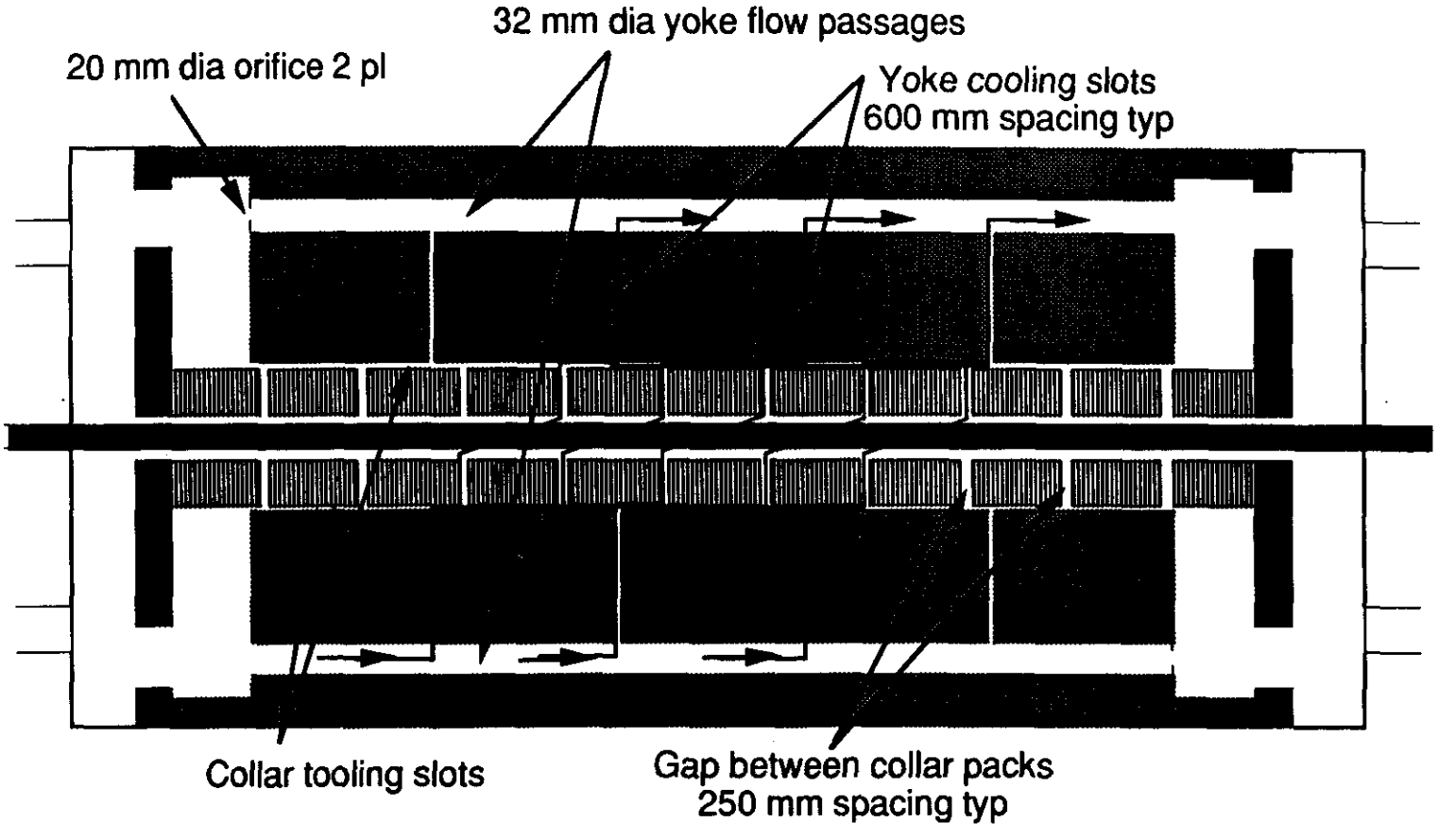


sdp310a-xflo imp

# CROSS FLOW COOLING
# Design Recommendations / Implementation

Cross flow cooling is implemented by placing orifices in the upper lead end and lower return end yoke flow passages. The orifices are created by altering the affected end yoke laminates to have 20 mm diameter holes instead of the nominal 32 mm diameter holes comprising the yoke flow passages.

The transverse flow starts from the lower yoke flow passages and runs through special cooling slots placed every 600 mm on the average in the lower yoke laminations. These slots run from the flow passages to the tooling slots in the collar packs. The flow then runs longitudinally along the tooling slots to the gaps between collar packs. It then makes a radial turn and runs to the opening at the pole and into the annulus where mixing occurs with the main annulus flow. The helium then flows out at the upper pole through collar pack gaps to the tooling slots to the yoke cooling slots and finally to the upper yoke flow passages

Primary leak paths exist running directly from lower to upper yoke cooling passages, and also in the collar pack gaps running azimuthally around the outside of the coils. The leakage in the collar pack gap is prevented with dams across the horizontal midplane, forcing all the transverse flow through the opening at the pole and into the annulus. The yoke leak path is minimized with a close fit of yoke laminations.

# CROSS-FLOW COOLING ANALYSIS

**Model:** Conservation of momentum in each longitudinal flow passage requires

$$\frac{dP_1}{dx} = -K_y \dot{m}_1^2 - \frac{1}{\rho A_y^2}\frac{d}{dx}(\dot{m}_1^2) \qquad (1)$$

$$\frac{dP_2}{dx} = -K_y \dot{m}_2^2 - \frac{1}{\rho A_y^2}\frac{d}{dx}(\dot{m}_2^2) \qquad (2)$$

$$\frac{dP_3}{dx} = -K_3 (\dot{m} - \dot{m}_1 - \dot{m}_2)^2 - \frac{1}{\rho A_3^2}\frac{d}{dx}((\dot{m} - \dot{m}_1 - \dot{m}_2)^2) \qquad (3)$$

while a mass balance accounting for the flow between channels requires

$$\frac{d\dot{m}_1}{dx} = C'_{3y}\sqrt{P_3 - P_1} + C'_{21}\sqrt{P_2 - P_1} \qquad (4)$$

$$\frac{d\dot{m}_2}{dx} = C'_{3y}\sqrt{P_3 - P_2} - C'_{21}\sqrt{P_2 - P_1} \qquad (5)$$

# CROSS-FLOW COOLING ANALYSIS

**Boundary Conditions:** At the ends,

$$P_{in} - P_1(0) = K_{1,in}\, \dot{m}_1^2(0) \qquad (6a)$$
$$P_1(l) - P_{out} = K_{1,out}\, \dot{m}_1^2(l) \qquad (6b)$$

$$P_{in} - P_2(0) = K_{2,in}\, \dot{m}_2^2(0) \qquad (6c)$$
$$P_2(l) - P_{out} = K_{2,out}\, \dot{m}_2^2(l) \qquad (6d)$$

$$P_{in} - P_3(0) = K_{3,in}\, [\, \dot{m} - \dot{m}_1(0) - \dot{m}_2(0)\, ]^2 \qquad (6e)$$
$$P_3(l) - P_{out} = K_{3,out}\, [\, \dot{m} - \dot{m}_1(l) - \dot{m}_2(l)\, ]^2 \qquad (6f)$$

# CROSS-FLOW COOLING ANALYSIS

Definition of variables:

$P_i$ = pressure distribution along channel i
$P_{in}$ = inlet pressure (presumed known)
$P_{out}$ = outlet pressure
$\dot{m}$ = combined mass flow rate in channels 1,2, and 3 (presumed known)
$\dot{m}_i$ = mass flow rate distribution along channel i
$C'_{3y}$ = flow conductance per unit length between channels 1 and 3; 2 and 3
$C'_{21}$ = flow conductance per unit length between channels 1 and 2 (leakage)
$K_y$ = flow impedance per unit length of channels 1 and 2
$K_3$ = flow impedance per unit length of channel 3
$K_{1,in}$ = inlet flow impedance of channel 1
$K_{1,out}$ = outlet flow impedance of channel 1
$K_{2,in}$ = inlet flow impedance of channel 2
$K_{2,out}$ = outlet flow impedance of channel 2
$K_{3,in}$ = inlet flow impedance of channel 3
$K_{3,out}$ = outlet flow impedance of channel 3
$\rho$ = density of flowing helium
$A_y$ = cross-sectional area of yoke channels
$A_3$ = cross-sectional area of channel 3

# CROSS-FLOW COOLING ANALYSIS
## If $K_3$ goes to infinity:

**Model:** Conservation of momentum in each longitudinal flow passage requires

$$\frac{dP_1}{dx} = - K_y \dot{m}_1^2 - \frac{1}{\rho A_y^2} \frac{d}{dx}(\dot{m}_1^2) \qquad (1)$$

$$\frac{dP_2}{dx} = - K_y (\dot{m} - \dot{m}_1)^2 - \frac{1}{\rho A_y^2} \frac{d}{dx}(\dot{m} - \dot{m}_1)^2 \qquad (2)$$

while a mass balance accounting for the flow between channels requires

$$\frac{d\dot{m}_1}{dx} = C'_{yy} \sqrt{P_2 - P_1} + C'_{21} \sqrt{P_2 - P_1} \qquad (3)$$

# CROSS-FLOW COOLING ANALYSIS
## If $K_3$ becomes infinite:

**Boundary Conditions:** At the ends,

$$P_{in} - P_1(0) = K_{1,in}\, \dot{m}_1^2(0) \quad (6a)$$
$$P_1(l) - P_{out} = K_{1,out}\, \dot{m}_1^2(l) \quad (6b)$$

$$P_{in} - P_2(0) = K_{2,in}\, [\, \dot{m} - \dot{m}_1(0)\, ]^2 \quad (6c)$$
$$P_2(l) - P_{out} = K_{2,out}\, [\, \dot{m} - \dot{m}_1(l)\, ]^2 \quad (6d)$$

# CROSS FLOW COOLING
## Cooling Model / Governing Equations

- Energy Balance on Helium in Annulus Leads to Description of Temperature Rise
  - Assume complete mixing of axial flow, transverse flow such that each flow has same temperature leaving control volume

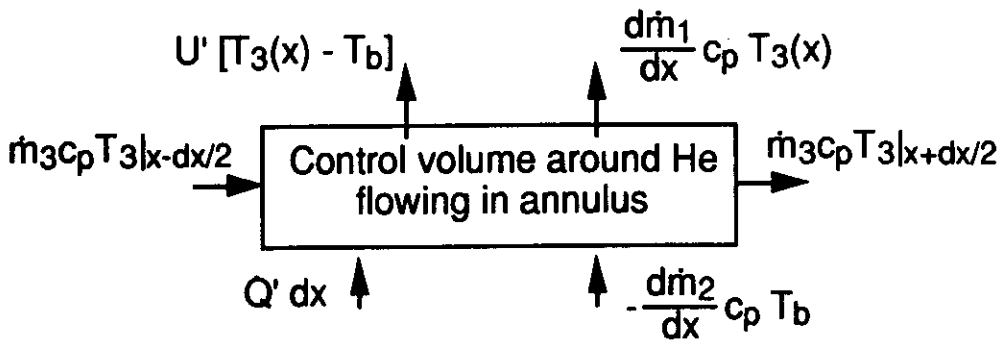


$$\dot{m}_3 C_p \frac{dT_3}{dx} = \dot{Q}' - \left[ U' - \frac{d\dot{m}_2}{dx} C_p \right] \left[ T_3(x) - T_b \right]$$

For the special case where $K_3$ goes to infinity (no axial annular flow):

$$\Delta T_3 = \frac{\dot{Q}'}{U' + \frac{d\,\dot{m}_1}{dx} C_p}$$

# CROSS FLOW COOLING
# Cooling Model / Governing Equations

Definition of Terms

| | | |
|---|---|---|
| $C_p$ | = | specific heat of helium |
| $l$ | = | length of flow passage through annulus |
| $\dot{m}_3$ | = | longitudinal flow rate in annulus |
| $\dot{m}_2$ | = | longitudinal flow rate in channel 2 |
| $\dot{m}_1$ | = | longitudinal flow rate in channel 1 |
| $Q'$ | = | heat leak per unit length imposed on beam tube |
| $T_3$ | = | temperature of helium in annulus |
| $T_b$ | = | bulk helium temperature in yoke flow passages (assumed constant) |
| $U'$ | = | thermal conductance between annulus and yoke flow passages due to heat diffusion |
| $x$ | = | distance measured from the inlet of the annulus |



sdp330a-mxngmodel

# CROSS FLOW COOLING
## 20 mm Orifice Diameter Meets ΔP Budget

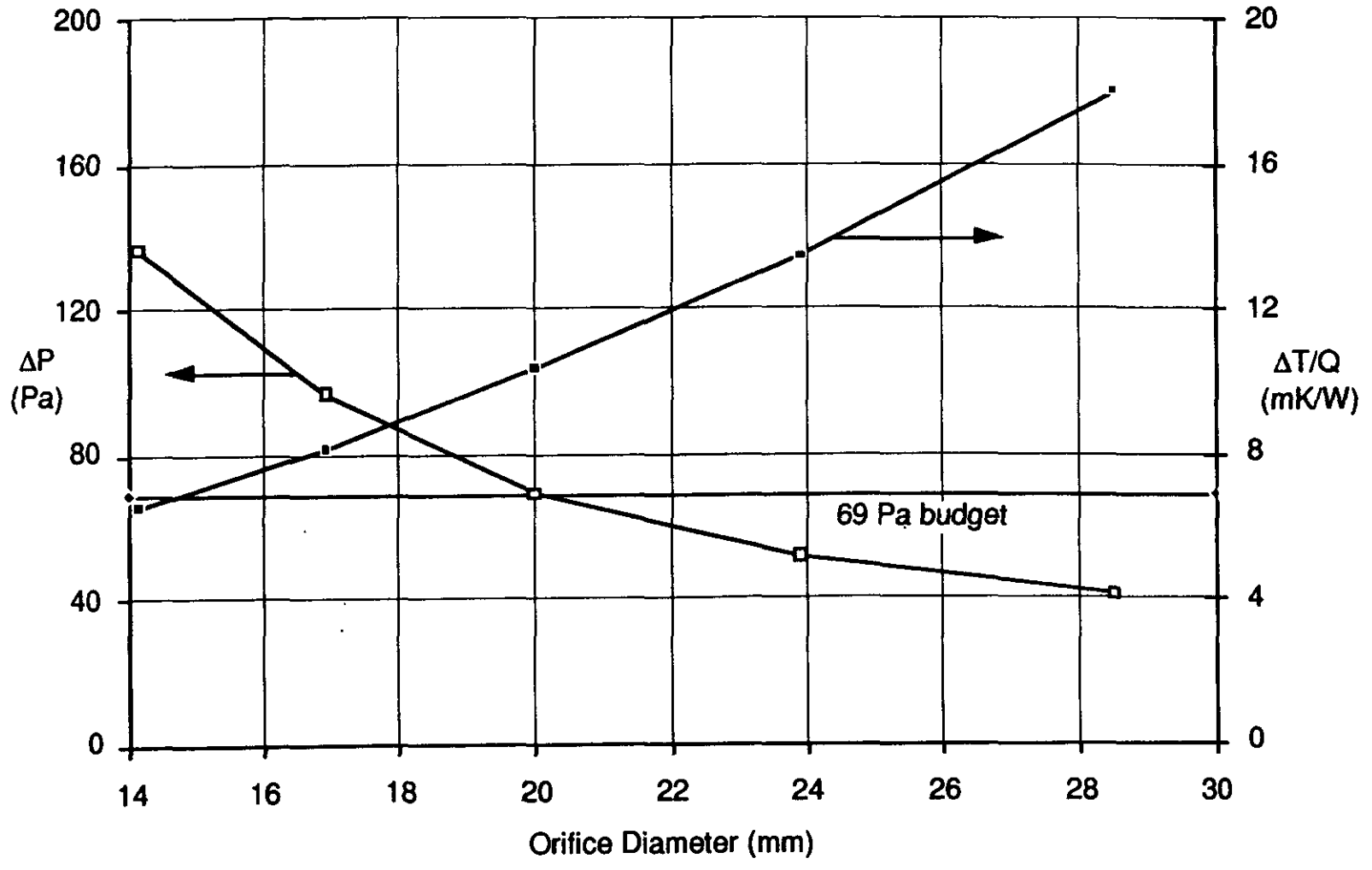

# Analysis of Crossflow Cooling for CDM with Orificed Channels

A. Yücel

ASD/Cryogenics Department
SSC Laboratory
Dallas, Texas

Second Workshop on Testing of SSC Magnet
Cryogenic Performance

General Dynamics Space Systems Division, San Diego, CA
June 29, 1992

# SSC CRYO NOTES

NOTE NO. 92-5

REQUESTER A. Yücel DATE 7/22/92

AUTHOR(S) Adnan Yücel

FULL TITLE Analysis of crossflow cooling in 50mm-CDM with orificed channels.

CROSS-FILE TO: (Incl. key words)
July 1992
General Dynamics, GD
Pressure drop

Distribution

| | |
|---|---|
| M. McAshan | R. Schermer |
| R. Carcagno | S. Abramovich |
| [redacted] | File |
| G. Snitchler | |
| B. Aksel | |
| D. Franks | |

# ANALYSIS OF CROSSFLOW COOLING IN 50mm-CDM WITH ORIFICED CHANNELS

Adnan Yücel
ASD Cryogenics Department
SSC Laboratory

## INTRODUCTION

The crossflow cooling scheme proposed by General Dynamics [1] employs yoke laminations with smaller holes (diameter < 0.03175 m) at the lead and return ends of the collider dipole magnet. A restricted yoke lamination is placed at the inlet for the upper two channels and another one is placed at the exit for the lower two channels. The smaller holes –orifices– limit the flows entering the upper channels and those exiting the lower channels, thus creating a pressure differential between the lower and upper channels. This pressure differential can divert flow from the lower half to the upper half via slotted yokes used periodically along the length of the magnet. The infusion of colder coolant from the lower channels into the annular channel and the discharge of warmer coolant out of the annular channel into the upper channels provide the crossflow cooling effect.

This note presents a parametric analysis of the above crossflow cooling scheme. There are two important parameters in assessing the effectiveness of crossflow cooling for a given design and operating conditions. These parameters are: a) the orifice loss coefficient which determines the pressure drop across the orifice plates and adds to the total pressure drop for the magnet, and b) the crossflow conductance which determines the transverse flow rate between the coolant channels and the annular channel.

## ANALYSIS

Figure 1 shows the incompressible flow network used in the analysis. The 15-m long dipole magnet is divided into 25 sections. The slotted yokes are assumed to be placed every 60 cm, accommodating transverse flow from the lower channels into the annular channel and from the annular channel into the upper channels. Since gaps between collar packs occur every 25 cm, there will be more than one crossflow path between the collar tooling slots and the annular channel for a given section. For simplicity, these branches are lumped together in the analysis. Hence, for each section, there is assumed to be a single but tortuous crossflow passage linking the lower two channels to the annular channel, and another one linking the annular channel to the upper channels. The conductance of the crossflow passages, Cx, is taken as a free parameter and varied

between 1.0 E-6 $m^2$ and 5.0 E-4 $m^2$. This wide range of crossflow conductance values covers the whole spectrum of crossflow regimes that will be discussed later. The geometry of the crossflow passages in a given magnet design will determine the actual crossflow conductance value for the passages. The results presented here for a wide range of crossflow conductance values can be used to determine the relative crossflow efficiency for a particular design and to determine the sensitivity of the predictions to the uncertainties in estimating the crossflow conductance for the given design.

The orifice loss coefficient, Ko, is varied primarily between 10 and 40 to represent different orifices; larger Ko values reaching up to fully blocked channels are also considered. The orifice size or diameter corresponding to a certain Ko value depends on the actual shape (contour) of the orifice and can be determined from experimental data [2]. Although the loss coefficient for inlet to a pipe through an orifice is somewhat lower than that for exit from a pipe through an orifice, the inlet and exit loss coefficients in this analysis are taken to be the same.

Unless otherwise noted, the values used for the remaining baseline parameters are as follows:

| | |
|---|---|
| Inlet and exit loss coefficients for a non-orificed channel | Ki = Ke = 1 |
| Friction factor, all channels | f = 0.02 |
| Cooling channel diameter | D = 0.03175 m |
| Beam tube diameter | $D_{bt}$ = 0.037 m |
| Helium density at 4.2 K, 0.4 MPa | $\rho$ = 138 kg/$m^3$ |
| Helium specific heat at 4.2 K, 0.4 MPa | Cp = 3.73E3 J/kg-K |
| Total mass flow rate | MT = 0.1 kg/s |
| Effective heat transfer conductance for the cold mass | U = 1.75 W/m-K |
| Linear heat input | Q = 1 W/m |

The linear heat input of 1 W/m used in the calculations is a nominal rate. The annular channel temperature rise values presented in this study can be regarded as being per W/m of linear heating and can be scaled to obtain the temperature rise for other linear heat rates.

*Flow analysis*

The equations governing pressure drops along the channels are

$$\Delta PL_i = \Delta PL_{i-1} + KL_i\, ML_i\, |ML_i|$$
$$\Delta PU_i = \Delta PU_{i-1} + KU_i\, MU_i\, |MU_i|$$
$$\Delta PA_i = \Delta PA_{i-1} + KA_i\, MA_i\, |MA_i|$$
$$= \Delta PA_{i-1} + KA_i\, (MT - ML_i - MU_i)\, |MT - ML_i - MU_i|$$

where

$$KL_i = (Ki\ \delta_{i1} + f\ \Delta x/D + Ko\ \delta_{iN})/(2\rho A^2)$$
$$KU_i = (Ko\ \delta_{i1} + f\ \Delta x/D + Ke\ \delta_{iN})/(2\rho A^2)$$
$$KA_i = (Ki\ \delta_{i1} + f\ \Delta x/D_a + Ke\ \delta_{iN})/(2\rho A_a^2)$$

for i = 1,2,...,N. The mass flow rates are governed by the mass balance equations for the mixing nodes

$$ML_{i+1} = ML_i - MXL_i = ML_i - Cx\ \mathrm{sign}(\Delta PA_i - \Delta PL_i)\ [\rho\ |\Delta PA_i - \Delta PL_i|]^{1/2}$$
$$MU_{i+1} = MU_i + MXU_i = MU_i - Cx\ \mathrm{sign}(\Delta PU_i - \Delta PA_i)\ [\rho\ |\Delta PU_i - \Delta PA_i|]^{1/2}$$

for i = 1,2,...,N-1. The boundary conditions on the system are:

$$\Delta PL_0 = \Delta PU_0 = \Delta PA_0 = 0$$
$$\Delta PL_N = \Delta PU_N = \Delta PA_N$$

A nonlinear equation system solver is used to obtain the solutions for the pressure drops at each node and the mass flow rates along each section.

*Temperature analysis*

The differential equations governing the helium temperature along a given section in the cooling channels and in the annular channel are given by

$$ML_i\ Cp\ d(TL_i)/dx = 1/2\ U\ (TA_i - TL_i)$$
$$MU_i\ Cp\ d(TU_i)/dx = 1/2\ U\ (TA_i - TU_i)$$
$$MA_i\ Cp\ d(TA_i)/dx = Q - 1/2\ U\ (TA_i - TL_i) - 1/2\ U\ (TA_i - TU_i)$$

for $x_{i-1} \le x \le x_i$, i = 1,2,...,N. Here, U represents the total heat transfer conductance for the cold mass between the annular channel and the cooling channels [3,4]. The static heat load on the cold mass and the back diffusion of heat from the upper half of the cold mass to the lower half are neglected. The initial conditions for each section are determined assuming perfect mixing at the nodes:

$$ML_i\ TL_i(x_i) = (ML_{i+1} + \langle MXL_i,0\rangle)\ TL_{i+1}(x_i) - \langle -MXL_i,0\rangle\ TA_{i+1}(x_i)$$
$$MU_i\ TU_i(x_i) = (MU_{i+1} + \langle -MXU_i,0\rangle)\ TU_{i+1}(x_i) - \langle MXU_i,0\rangle\ TA_{i+1}(x_i)$$
$$MA_i\ TA_i(x_i) = (MA_{i+1} + \langle -MXL_i,0\rangle + \langle MXU_i,0\rangle)\ TA_{i+1}(x_i)$$
$$- \langle MXL_i,0\rangle\ TL_{i+1}(x_i) - \langle -MXU_i,0\rangle)\ TU_{i+1}(x_i)$$

for i = 1,2,...,N-1. In the above equations, the brackets are used to denote the greater of the two variables inside the brackets, i.e. $\langle a,b\rangle = \max(a,b)$. The initial conditions for the first section are

$$TL_1(0) = TU_1(0) = TA_1(0) = T_0$$

Once the mass flow rates are determined, the above system of ordinary differential equations is solved using a suitable ODE integrator to obtain the temperature distributions in the channels.

## RESULTS

*Axial variations of pressure drop, mass flow rate and annular channel temperature*

In order to illustrate the effects of crossflow, we present in this section the pressure drops, mass flow rates and annular temperature profiles for an orificed magnet with Ko = 20.

Figure 2 shows the upper, lower and annular channel pressure drops along a dipole magnet; Figure 3 shows the corresponding mass flow rates. The upper channel which is orificed at the inlet has a large pressure drop across the orifice, while the lower channel experiences a large pressure drop across its orifice at the exit. The pressure and mass flow rate profiles are strongly influenced by the crossflow conductance between the channels:

- For low crossflow conductance values, there is little communication (i.e. crossflow) between the three channels. The channels serve merely as independent flow paths, with relatively small variations in the mass flow rates along the length of the magnet. Hence the pressure gradients remain fairly constant along the channels.
- For high crossflow conductance values, there is significant crossflow near the inlet from the annular channel to the upper channel due to the large pressure differential caused by the orifice. There is little crossflow, however, from the lower channel to the annular channel. As a result, the annular channel mass flow rate decreases near the inlet while the upper channel mass flow rate increases rapidly. The situation is reversed at the exit end of the magnet: crossflow is now driven by the large pressure difference between the lower and annular channels. The annular channel mass flow rate increases, while the lower channel flow rate decreases near the exit. Hence, for high conductance values, the lower channel pressure gradient decreases along the length of the magnet as its mass flow rate increases monotonically, while the converse is true for the upper channel. This leads towards equalization of channel pressures in the mid-section of the magnet, which in turn suppresses crossflows in this region.

The axial variations of crossflows from the lower channel to the annular channel and from the annular channel to the upper channel are shown in Figure 4 for three conductance values. For low conductance values, the upper and lower crossflow rates are low and comparable to each other. At intermediate Cx values, the crossflow rates rise but become skewed toward the ends. At higher conductance values, crossflow rates are quite large at the respective ends, but vanish in the center of the magnet. Figure 5 shows the corresponding annular mass flow rates. For low conductance values, the annular flow rate is higher than that for a non-orificed magnet (without crossflow), but this is primarily driven by the large pressure drop across magnet caused by the orificed channels. As the crossflow conductance increases, the annular mass flow rate increases near the ends, but decreases in the center of the magnet.

The variations in the annular channel mass flow rate discussed above have a strong influence on the temperature profiles and the maximum temperature attained in the annular channel (Figure 6). As expected, the temperature rise in the annular channel is lower everywhere compared to that for a magnet without crossflow. However, for higher conductance values, the location of the peak temperature in the annular channel shifts from the end of the magnet towards the middle. Furthermore, the peak temperature level rises rapidly with increasing crossflow conductance as the center of the magnet is deprived of crossflow.

*Total Pressure Drop and Maximum Annular Channel Temperature Rise*

This section presents a summary of the total pressure drops and the maximum annular channel temperatures for different orifice loss coefficients. For a magnet without crossflow cooling (i.e. with non-orificed cooling channels), the pressure drop is about 30 Pa with 15.9 g/s of flow in the annular channel; the increase in the annular channel helium temperature at the exit is 204 mK (per W/m of heating). The effectiveness of crossflow cooling in a magnet with a particular crossflow conductance and orifice area is judged based on comparisons with the above set of numbers. Additional constraints are the maximum allowable total pressure drop (60 Pa) and coil temperature (4.25 K).

Figure 7 shows the total pressure drop for a dipole magnet and the maximum temperature rise attained in the annular channel for four different orifice coefficients. As expected, the total pressure drop is higher for a magnet with orificed cooling channels; the smaller the orifice (higher Ko), the larger the pressure drop. The effect of crossflow is to reduce the total pressure drop: increased communication between the channels leads towards equalization of pressures, hence the pressure drop decreases as crossflow conductance increases. The reduction in the pressure drop is relatively small for lower Ko values but becomes significant for higher Ko values (greater blockage). A point of diminishing returns is reached around Cx = 10E-5 $m^2$; beyond this conductance, the decrease in the pressure drop is negligible for all Ko values.

For a given Ko value, the maximum temperature rise in the annular channel decreases initially with increasing crossflow conductance, but increases rapidly for higher conductance values. There is a narrow range of Cx values (4.0 E-5 to 10.0 E-5 $m^2$) for which the temperature rise in the annular channel is minimized (and significantly reduced compared to the no crossflow case). Within this range of Cx values, Ko values between 20 to 30 yield the highest reduction in the maximum temperature with "minimal" increase in the total pressure drop. Further reductions in the maximum temperature come at the expense of increasingly higher pressure drops for Ko > 30.

*Sensitivity to Coldmass Heat Transfer Conductance*

The above results are not very sensitive to the effective heat transfer conductance for the cold mass. Calculations using a value of U = 1.2 W/m-K yielded annular channel temperatures slightly higher than those presented above.

*System Behavior for large Ko*

As Ko is increased further (i.e. orifice diameter decreased), the total pressure drop increases rapidly, particularly at lower conductance values (Figure 8). However, the decrease in the maximum temperature rise in the annular channel with increasing crossflow conductance declines. Eventually, as Ko $\rightarrow \infty$ (cooling channel blocked fully at the inlet or exit), the maximum temperature increases monotonically with Cx (Figure 9). This is due to the fact that, as the orifice area is reduced, almost all of the flow is channeled into the annulus. Consequently, the temperature rise in the annular channel remains low at lower crossflow conductance values. As the conductance increases, crossflows reduce the annular channel mass flow rate, causing the annular channel temperature to rise.

*Effect of Increased Beam Tube Diameter*

The baseline beam tube outer diameter is 37 mm in this analysis. In order to quantify the effects of a reduced annular gap size, simulations were carried for beam tube outer diameters of

42 mm and 45 mm. The friction factor for the annular channel was increased from 0.020 to 0.025 in these simulations to account for the increased flow resistance in the annular channel. Without crossflow, the annular channel mass flow rate is 8.1 g/s for a beam tube diameter of 42 mm and 4.4 g/s for a beam tube diameter of 45 mm. The corresponding total pressure drops are 35 Pa and 38 Pa, and the maximum annular channel temperature rises (per W/m of linear heating) are 334 mK and 466 mK, respectively. The quantitative effects of crossflow on the total pressure drop and the maximum temperature rise in the annular channel for the three beam tube diameters can be compared in Figures 10 and 11. As expected the annular channel mass flow rate decreases and the total pressure drop increases as the beam tube diameter is increased. The increase in the pressure drop is more pronounced for larger Ko, i.e. for smaller orifices (Figure 10). For a given Ko, the maximum temperature rises in the annular channel can be considerably higher for the larger beam tube diameters as a result of the reduced flow rates in the annular channel (Figure 11). While the annular temperature rise can be reduced using smaller orifices (larger Ko), the accompanying total pressure drop may be prohibitive.

## SUMMARY

A network flow model for crossflow in a collider dipole magnet with orificed cooling channels is developed. A parametric study of the effects of transverse flow conductance and orifice loss coefficient is conducted. Crossflow cooling is found to be most effective for values within a narrow range of these parameters.

## NOMENCLATURE

| | |
|---|---|
| $A$, $A_a$ | Cross-sectional areas for the cooling channels and the annular channel, $m^2$ |
| Cp | Specific heat, J/kg-K |
| Cx | Crossflow conductance between the lower channels and the annular channel, and between the annular channel and the upper channels, $m^2$ |
| $D$, $D_a$ | Hydraulic diameters for the cooling channels, and for the annular channel, m |
| f | Friction factor |
| Ki, Ke | Inlet and exit loss coefficients |
| Ko | Orifice loss coefficient (inlet or exit) |
| MA | Annular mass flow rate, kg/s |
| MU, ML | Combined mass flow rate for the upper two channels, and for the lower two channels, kg/s |
| MT | Total mass flow rate, kg/s |
| MXU, MXL | Upper and lower crossflow rates, kg/s |
| N | Number of sections |
| $P_0$ | Pressure at inlet, Pa |
| PU, PL, PA | Upper, lower and annular channel pressures, Pa |
| Q | Linear heat input, W/m |
| $T_0$ | Temperature at inlet, K |
| TU, TL, TA | Upper, lower and annular channel temperatures, K |
| U | Effective heat transfer conductance for the cold mass, W/m-K |
| $x_i$ | Axial location for node i (= $i\Delta x$), m |

| | |
|---|---|
| $\Delta P_i$ | Cumulative pressure drop at node i ( $= P_0 - P(x_i)$ ), Pa |
| $\Delta x$ | Section length, m |
| $\delta_{ij}$ | Kronecker delta |
| $\rho$ | Density, $kg/m^3$ |
| i | quantity for section (or node) i |

## REFERENCES


1. General Dynamics Space Systems Division, Collider Dipole Magnets Preliminary Design Review, San Diego, CA, March 23-27, 1992.

2. Fried, E. and I. E. Idelchik, *Flow Resistance*, Hemisphere Publ. Co., New York, 1989.

3. Carcagno, R., *Temperature Rise in the SSC Dipole Coils under Synchrotron Radiation Heating, Preliminary Analysis*, SSC-N-514, May 27, 1988.

4. Aksel, B., "Parametric Study for Coil Temperatures in 50-mm CDM and 50-mm CQM," in *Study on Beam Tube Vacuum with Consideration of Synchrotron Light, Potential Liner Intercept, and Collider Quad/Spool Coil Diameter*, H. T. Edwards, ed., SSC-N-771, August 1991.

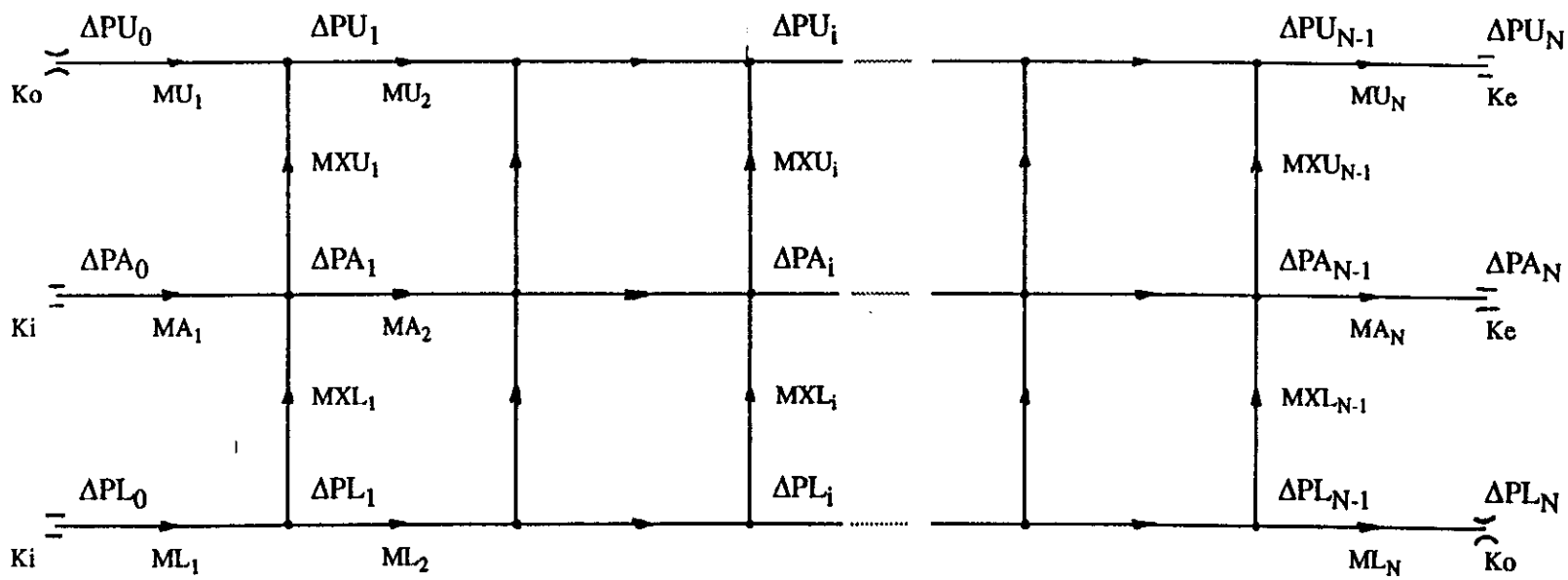


Figure 1. Flow network

Pressure Drop along a Dipole Magnet with Crossflow

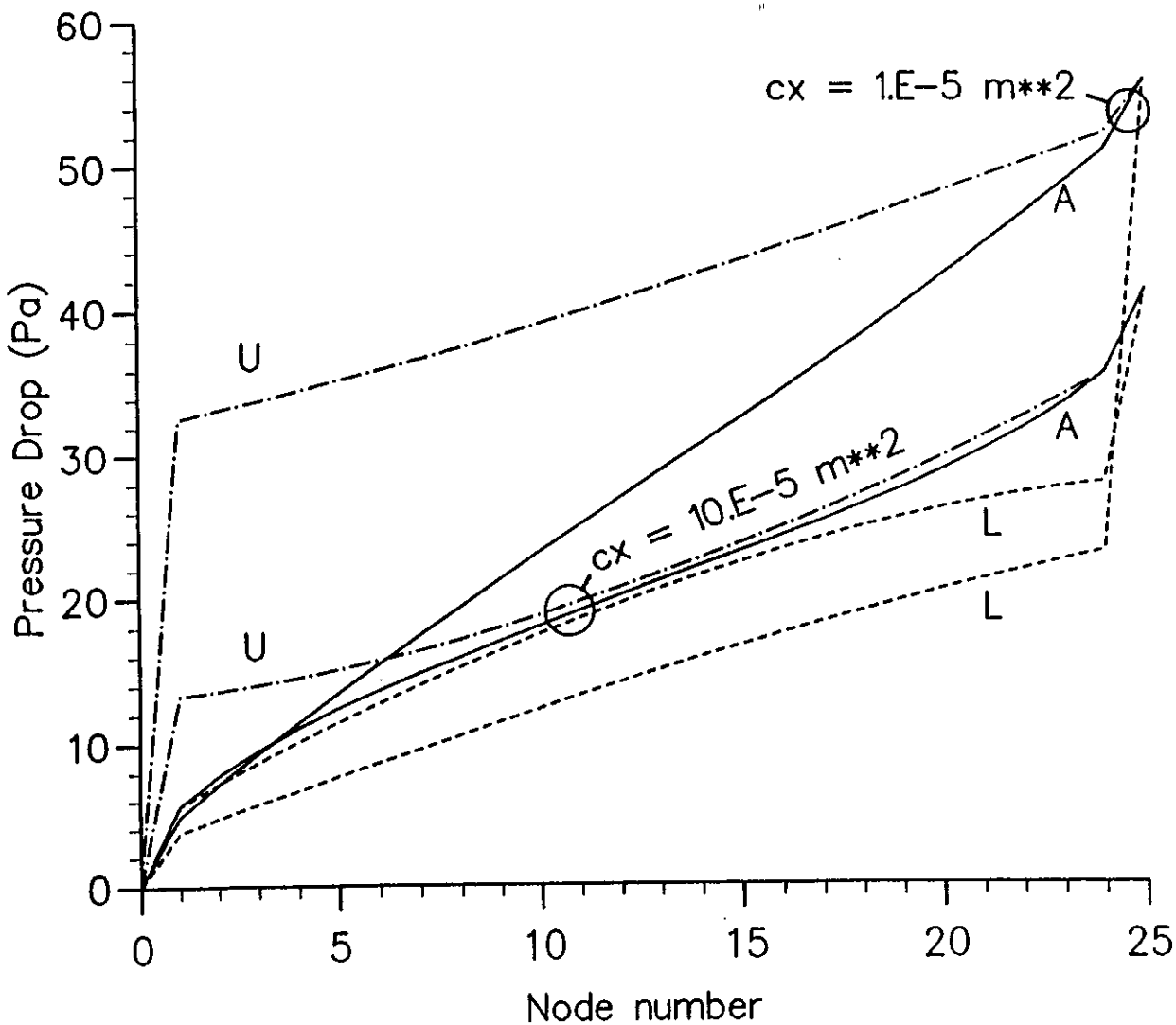

Mass Flow Rates along a Dipole Magnet with Crossflow

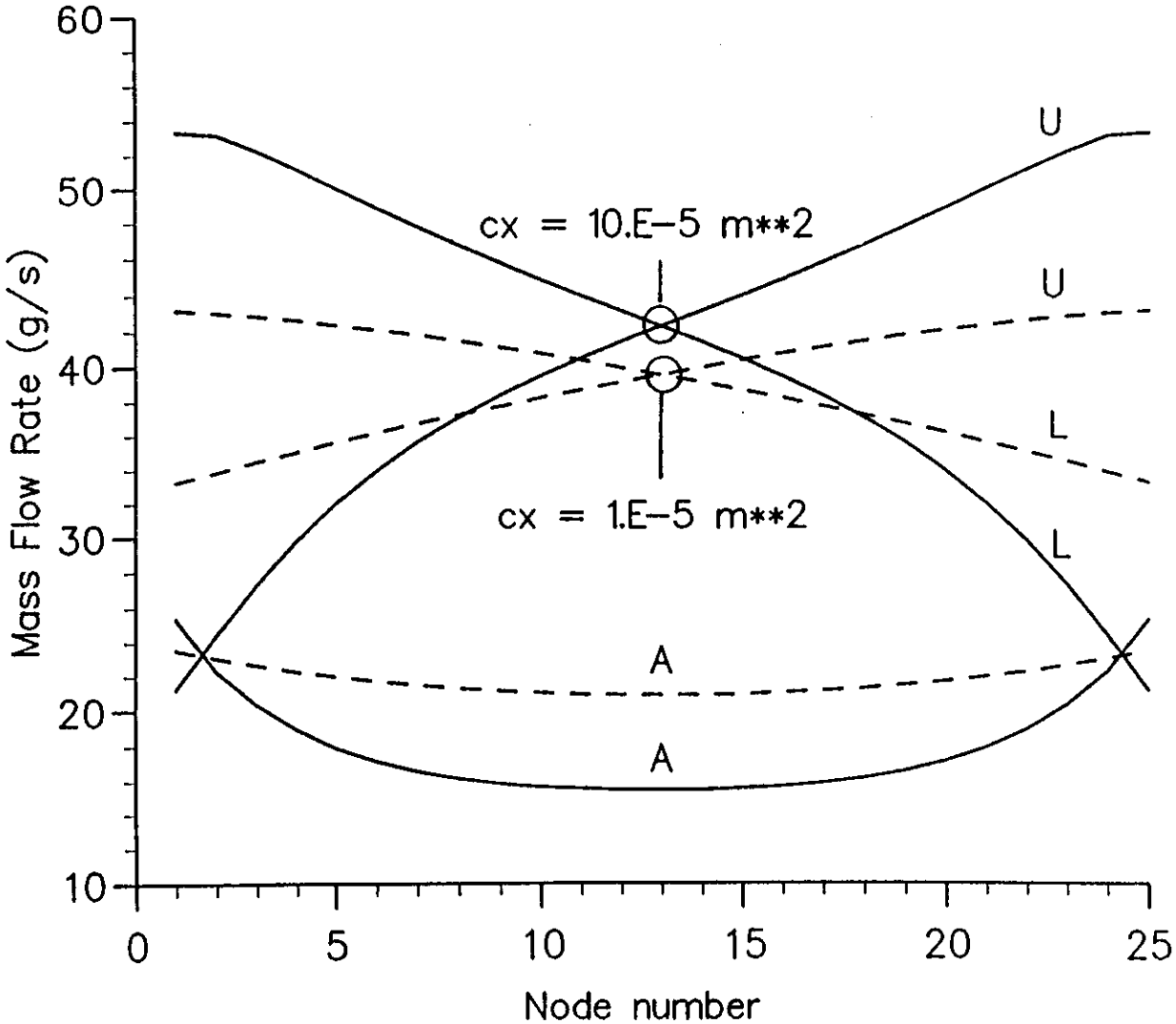

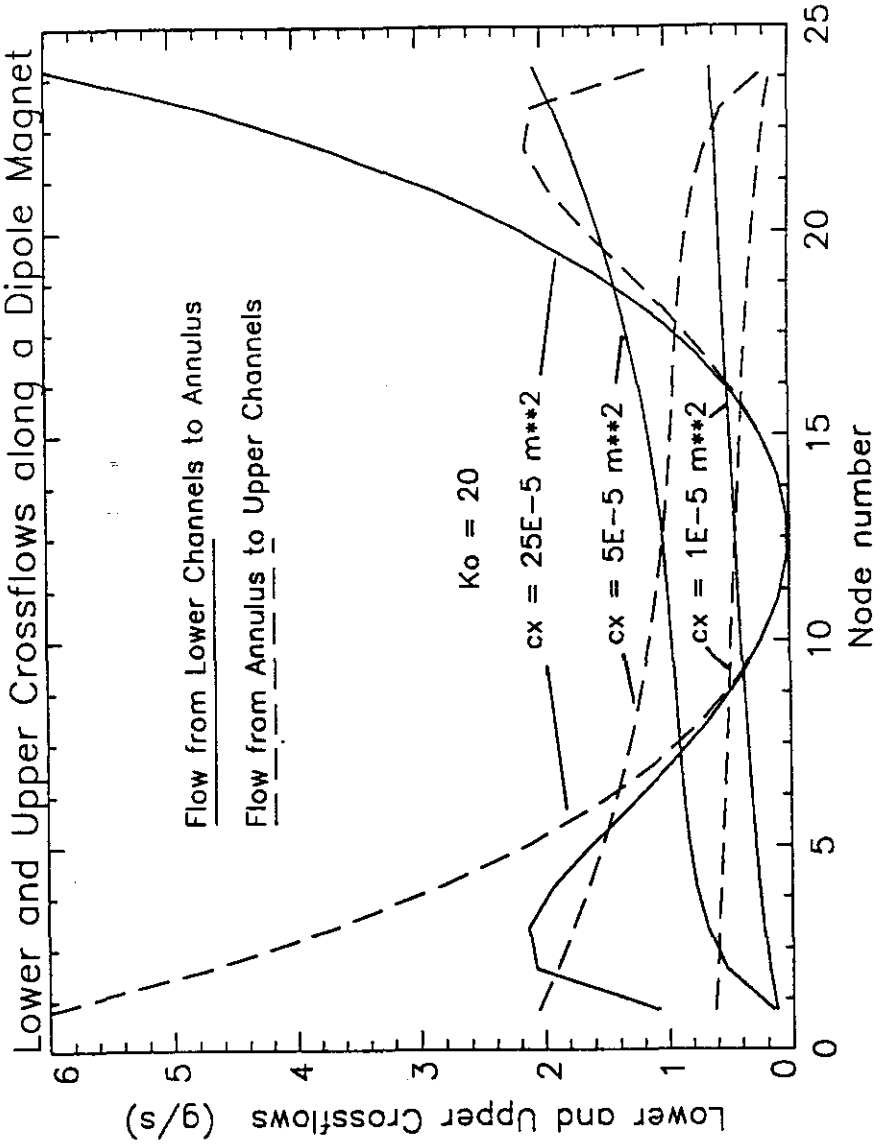
Lower and Upper Crossflows along a Dipole Magnet
Flow from Lower Channels to Annulus
Flow from Annulus to Upper Channels
Ko = 20
cx = 25E-5 m**2
cx = 5E-5 m**2
cx = 1E-5 m**2
Lower and Upper Crossflows (g/s)
Node number
0
1
2
3
4
5
6
0
5
10
15
20
25

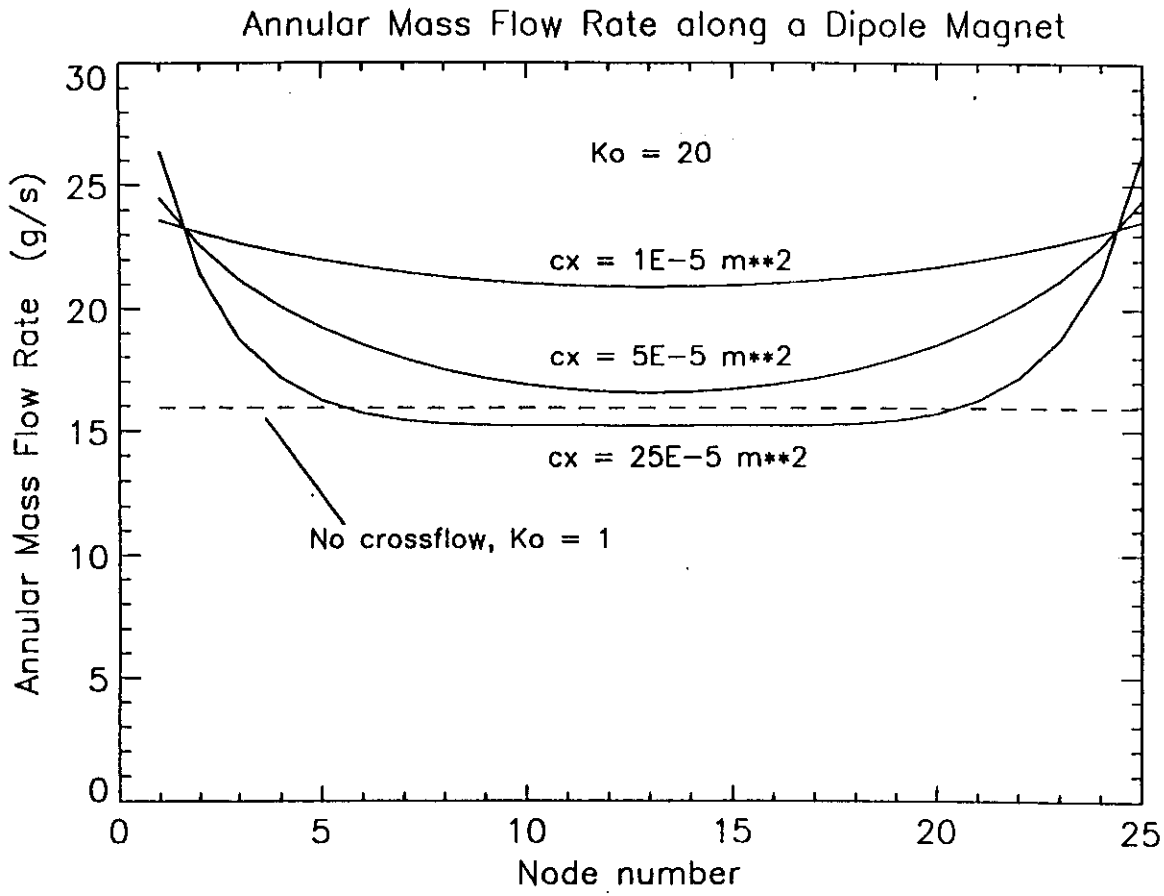
Annular Mass Flow Rate along a Dipole Magnet
Ko = 20
cx = 1E−5 m**2
cx = 5E−5 m**2
cx = 25E−5 m**2
No crossflow, Ko = 1
Annular Mass Flow Rate (g/s)
Node number
0
5
10
15
20
25
30

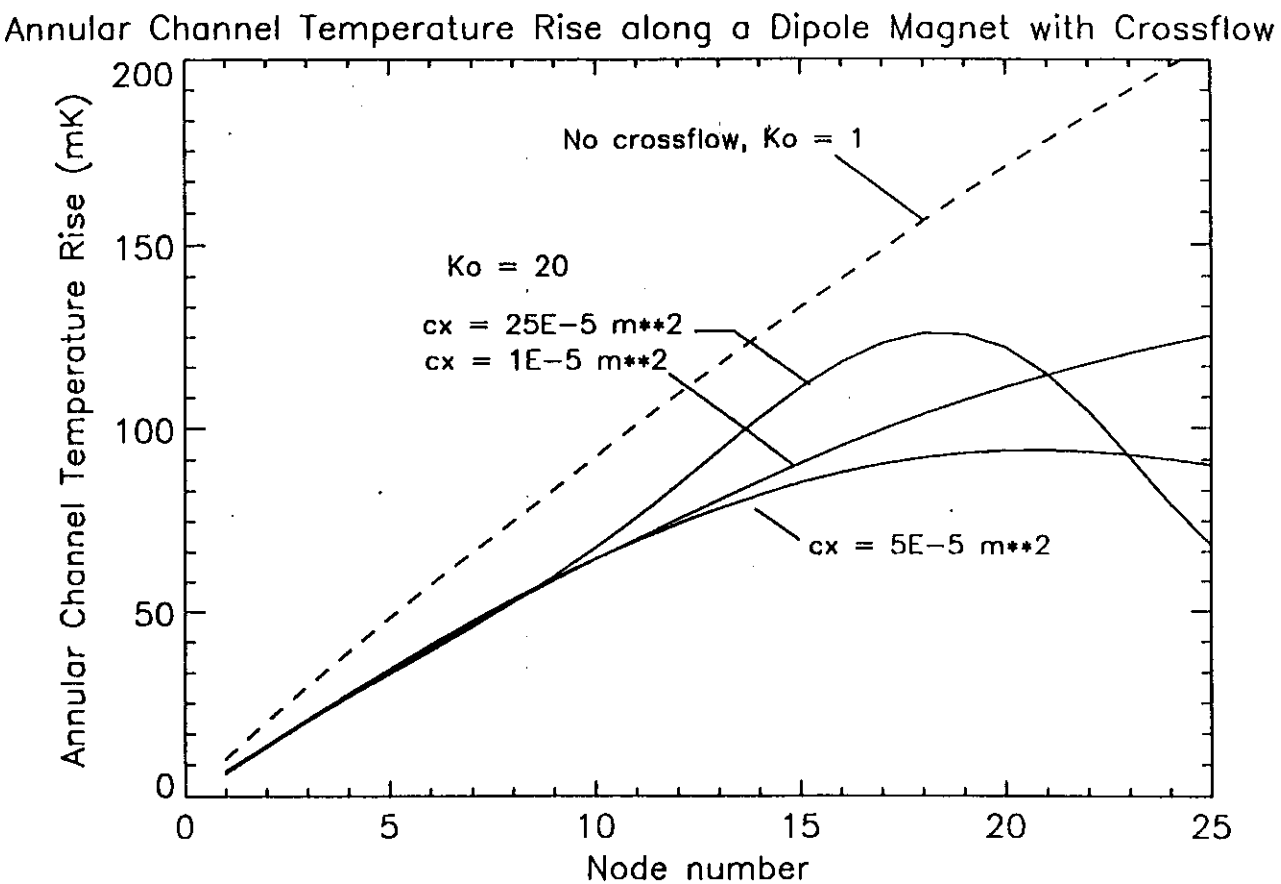
Annular Channel Temperature Rise along a Dipole Magnet with Crossflow
Annular Channel Temperature Rise (mK)
Node number
No crossflow, Ko = 1
Ko = 20
cx = 25E−5 m**2
cx = 1E−5 m**2
cx = 5E−5 m**2
0
50
100
150
200
0
5
10
15
20
25

## Annular Channel Maximum Temperature Rise and Total Pressure Drop for a Dipole Magnet with Crossflow

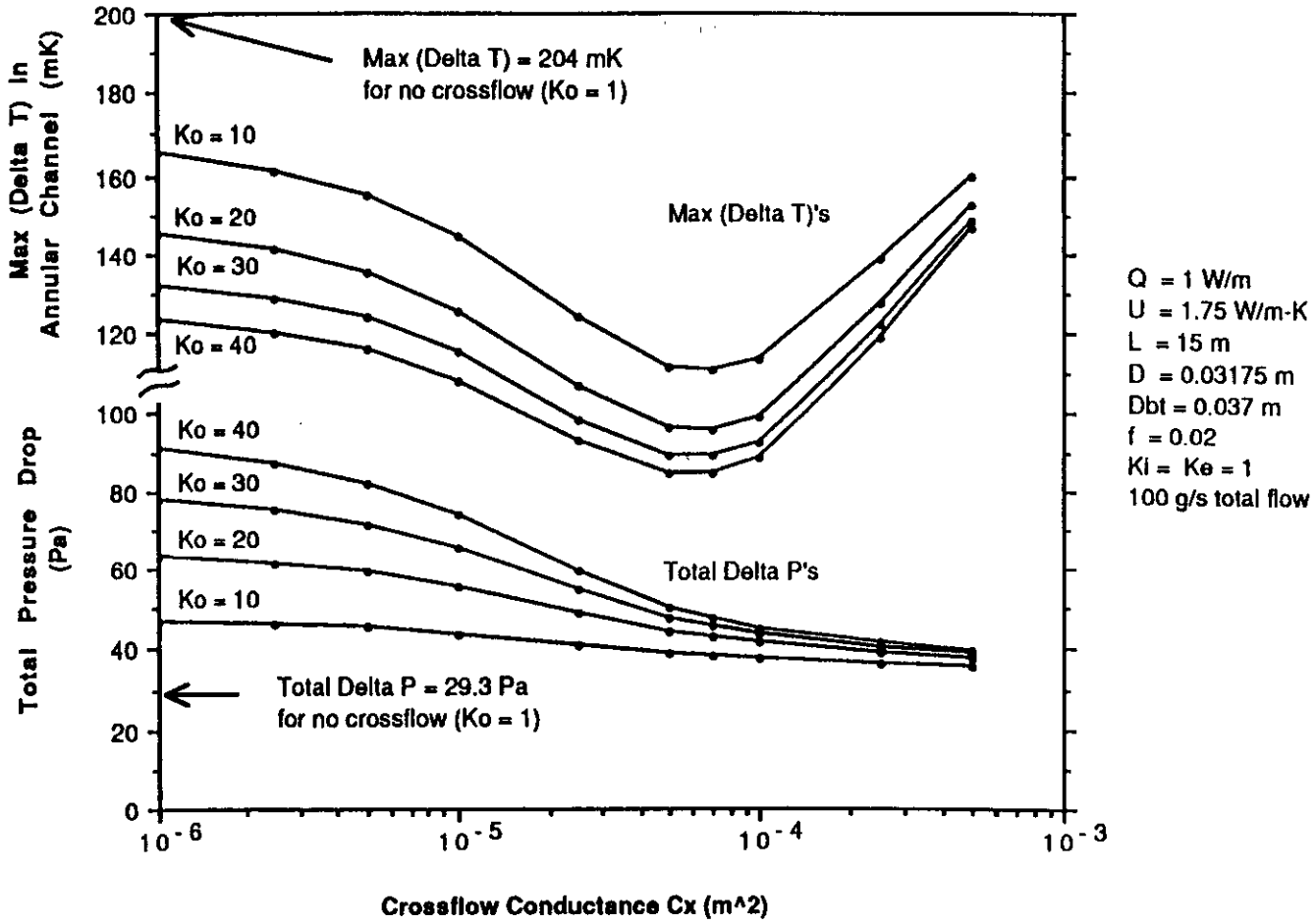


Figure 7

## Total Pressure Drop for a Dipole Magnet with Crossflow

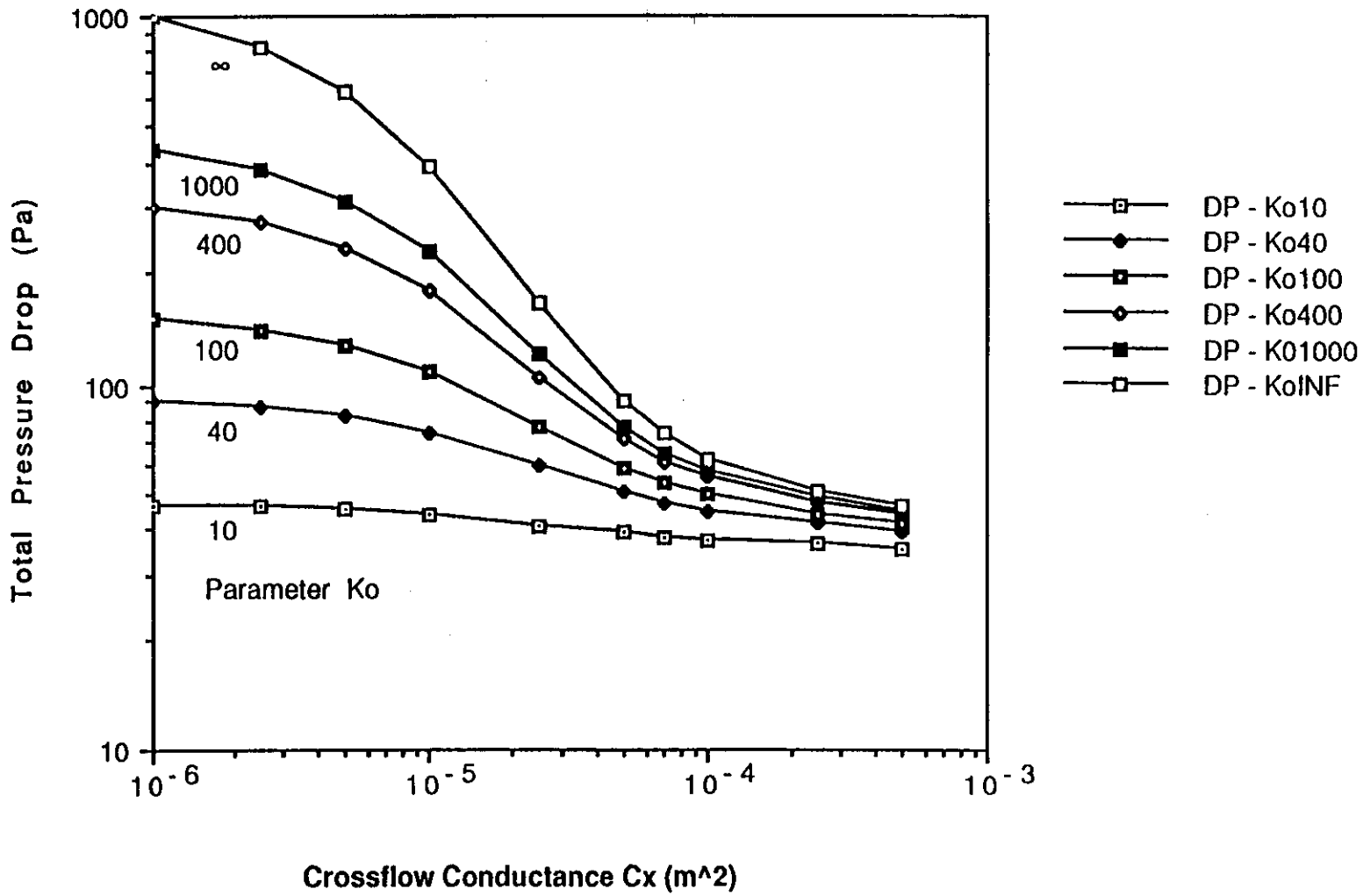

## Annular Channel Maximum Temperature Rise for a Dipole Magnet with Crossflow

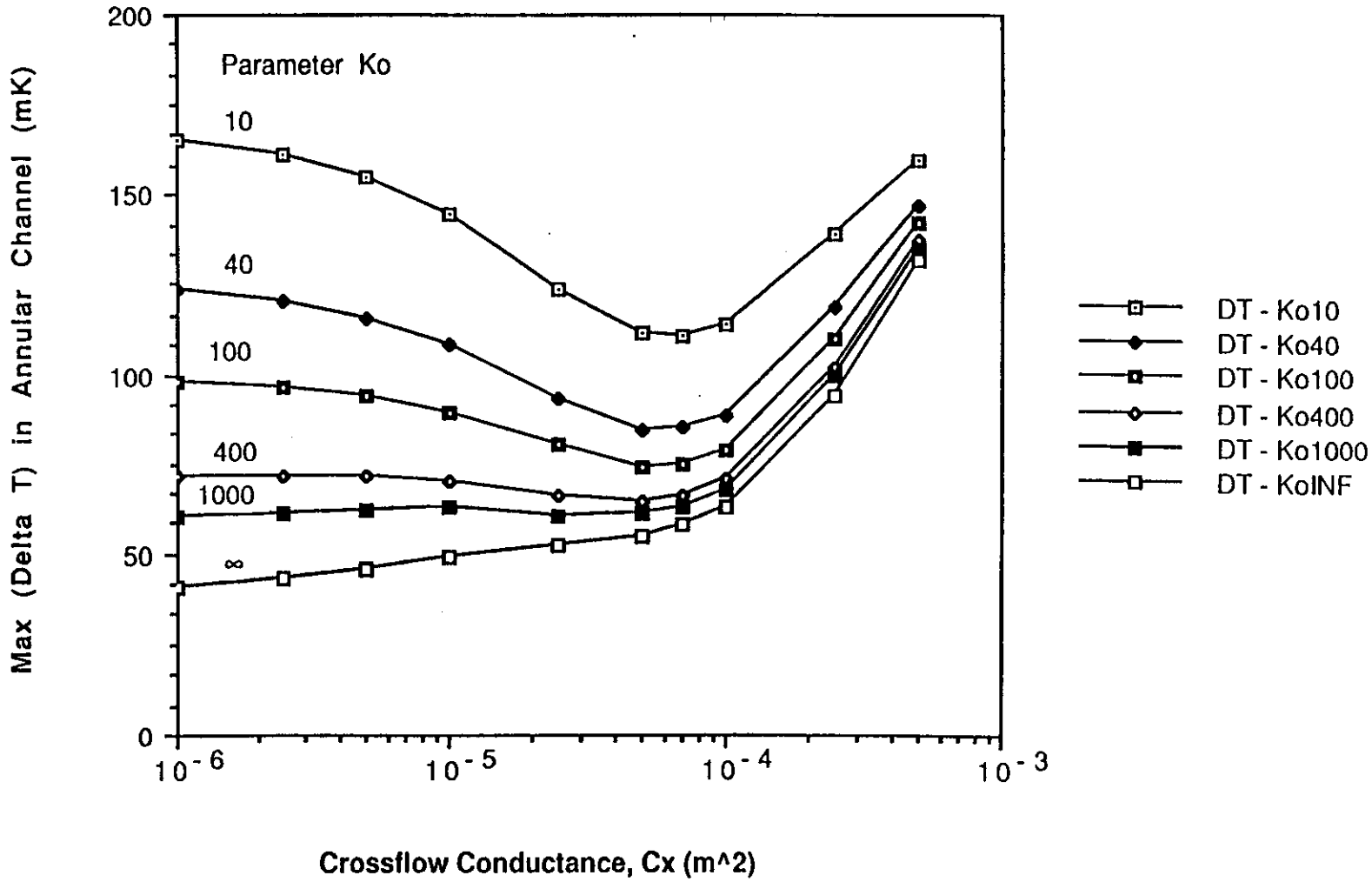

## Total Pressure Drop for a Dipole Magnet with Crossflow

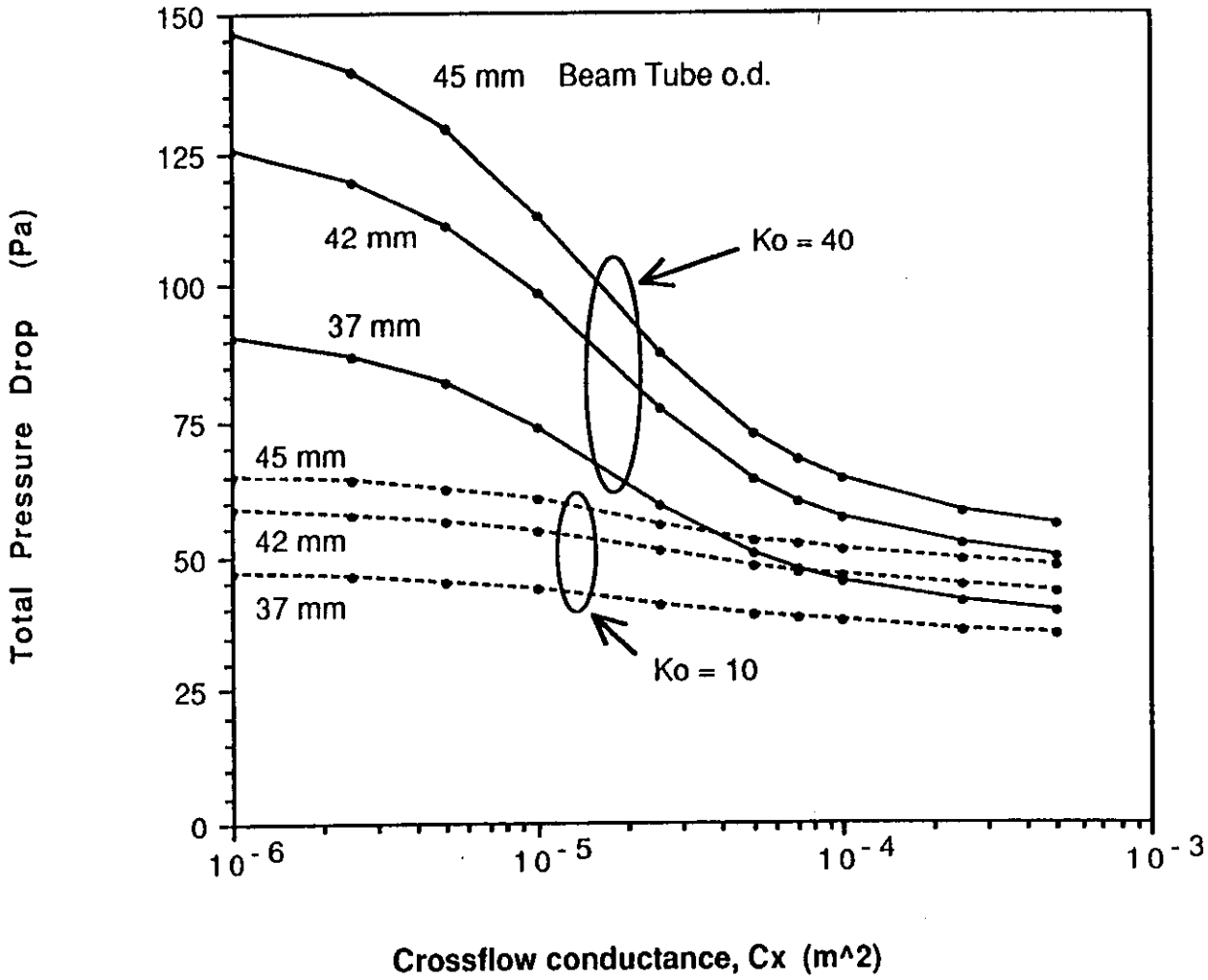


Figure 10

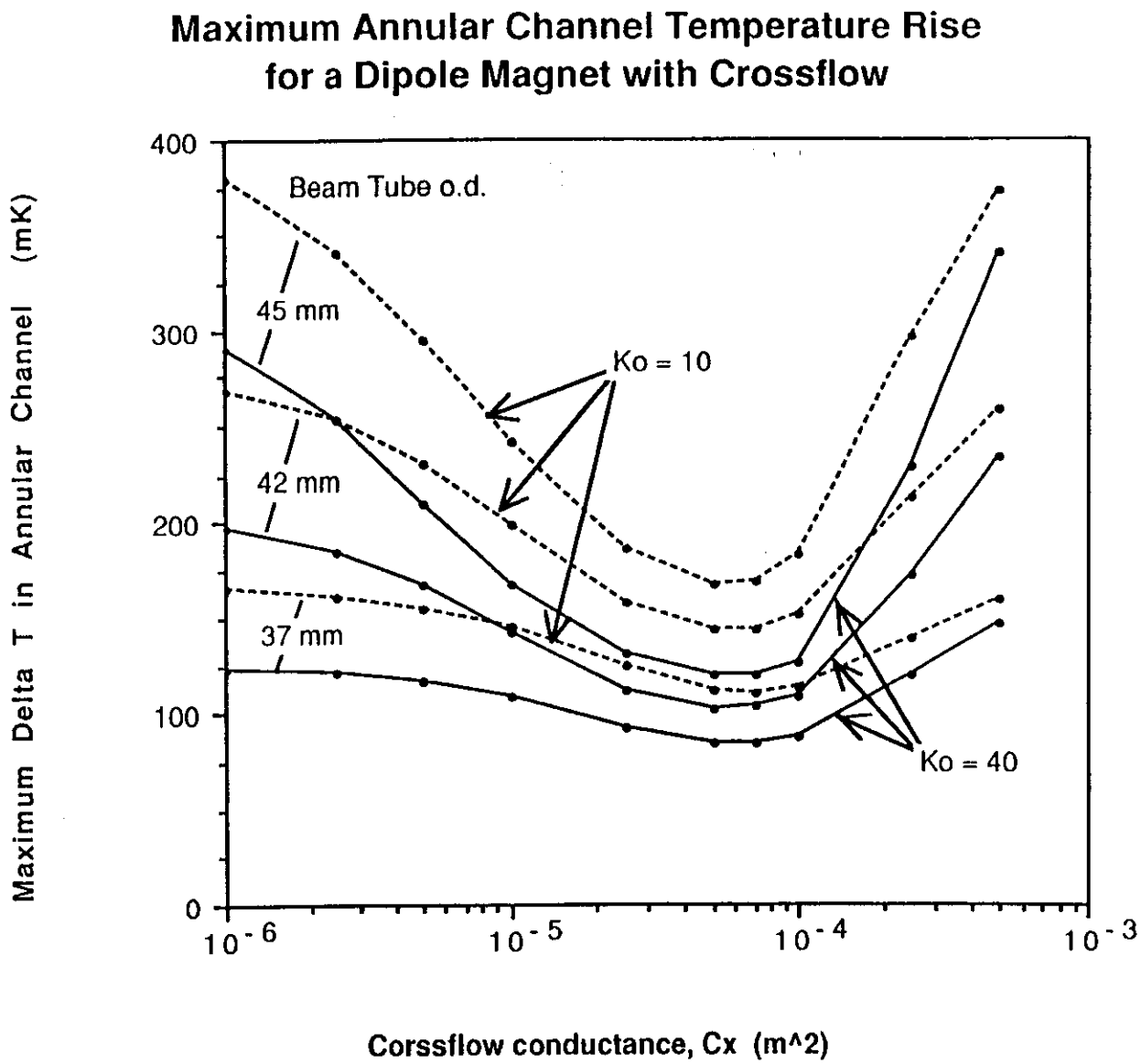
Maximum Annular Channel Temperature Rise
for a Dipole Magnet with Crossflow
Beam Tube o.d.
45 mm
42 mm
37 mm
Ko = 10
Ko = 40
400
300
200
100
0
10^-6
10^-5
10^-4
10^-3
Maximum Delta T in Annular Channel (mK)
Corssflow conductance, Cx (m^2)

Figure 11

# Cross-Flow Cooling

R.P. Shutt and M.L. Rehak

# CROSS–FLOW COOLING

**R.P.Shutt, M.L.Rehak**
Brookhaven National Laboratory

ABSTRACT

The cross–flow cooling scheme principle and implementation are presented. Comparison between the analytical model for the cross–flow cooling scheme and measurements on magnet DD0020 show excellent agreement. Presence of temperature peaks as well as their elimination is discussed. The effects of variations of coil cooling passage gap, orifice diameter and bypass diameter on coil temperature increase are addressed. Quench pressures are found to be comparable to those when there is no cross–flow cooling. Cross–flow cooling for HEB magnets where heat is generated in the main coil as opposed to the beam tube is addressed. Expressions to determine pressure drops across orifices are developed. More detailed discussions and the theory will appear in a final complete paper on cross–flow cooling.

**Contents**

1. CROSS–FLOW COOLING . . . . . 2
   1.1. NEED FOR CROSS–FLOW COOLING . . . . . 2
   1.2. CROSS–FLOW PRINCIPLE . . . . . 2
   1.3. CROSS–FLOW IMPLEMENTATION . . . . . 3
   1.4. RESULTS . . . . . 6
2. EXPERIMENTAL VERIFICATION . . . . . 9
   2.1. DESCRIPTION OF MEASUREMENTS . . . . . 9
   2.2. COMPARISON WITH DATA . . . . . 9
3. PARAMETER OPTIMIZATION . . . . . 20
   3.1. VARIATION OF COIL COOLING PASSAGE GAP . . . . . 20
   3.2. VARIATION OF ORIFICE SIZE . . . . . 33
   3.3. PRESSURE DROP VERSUS TEMPERATURE INCREASE . . . . 33
   3.4. VARIATION OF BYPASS DIAMETER . . . . . 33
4. PRESSURES DURING QUENCH WITH CROSS–FLOW . . . . . 38
   4.1. DYNAMICS OF QUENCH PRESSURE DEVELOPMENT . . . . . 38
   4.2. QUENCH PRESSURE RESULTS . . . . . 39
5. CROSS–FLOW COOLING IN HEB MAGNETS . . . . . 43
6. ORIFICES . . . . . 45

# 1. CROSS–FLOW COOLING

## 1.1 NEED FOR CROSS–FLOW COOLING

Originally cross–flow cooling was intended to provide the SSC with the capability of future upgrading. For magnets built without cross–flow cooling (through–flow) it was found that a coil cooling passage (CCP) gap of $d_c = 0.13\ cm$ is adequate for a synchrotron radiation heat load of $S_r = 2W$. For upgrading to 6 W, a CCP gap of $d_c = 0.50$ cm is needed to keep the magnet coil temperature sufficiently low. However in order to enable full field measurements, a "mole" generating 20 to 30 W is needed and cross–flow cooling is presently considered to accommodate this heat load.

Cross–flow cooling is also to be used in the High Energy Booster (HEB) magnets. In the HEB magnets there is no synchrotron radiation heat. However there is heat generated by eddy currents (in coil windings and bore tube copper plating) which are induced by rapid current ramping.

## 1.2 CROSS–FLOW PRINCIPLE

"Cross–flow" is obtained by installing orifices at the downstream ends of, say, the upper two bypass tubes through the yoke ( see Fig. 1.1) and at the upstream ends of the lower two tubes. Thus a pressure difference will result between top and bottom tubes which can force helium downward through vents provided between the yoke laminations. When arriving from the top at the collar laminations of the SSC, the helium is permitted to flow in an axial direction through passages along the outside of the collars (collar notches, see Fig. 1.2). Gaps are provided between collar packs for helium to reach the coil and pass into the CCP through gaps at the top and bottom poles of the coil. (The bottom pole gap is reached by helium passing downward around the coil, along the mentioned gaps between collar packs ). When helium reaches the next two pole gaps after flowing along the CCP, the given process is reversed. Helium exits from the CCP at the top and the bottom pole gaps in the coil. From the top gap it flows again around the coil along the mentioned gaps between collar packs. At the bottom it mixes with the helium exiting from the bottom gap, flows axially along the provided passages, reaches the bottom vent between the yoke laminations and finally enters the bottom bypass tubes.

Thus fresh cold helium enters the CCP every 30 cm instead at the CCP entrance only, which explains why the helium and coil temperature increases at the downstream end of the CCP can be considerably less than with "through–flow".

## 1.3 CROSS–FLOW IMPLEMENTATION

A magnet with cross–flow differs from a magnet with through–flow in the following.

- Orifices at bypass ends.
- Vents alternating top and bottom every 30 cm.

  Magnets with through–flow have vents in yoke laminations every 15 cm in order to provide pressure relief passages during a quench.
- Blocks in collar pickup notches.

  Indium plugs were used at Brookhaven National Laboratory where the collaring tool was pressing on the pickup notches. If the collaring tool is designed with a circular cross–section, several collars without pickup notches can be inserted in the middle of the collar packs instead of indium plugs.
- Blockage of leak paths:
- Leaks along the magnet length (see Fig. 1.3).

  There are leak paths through small holes along the magnet length which are blocked by welding patches on the yoke laminations at the magnet ends only. Other leak paths, such as holes in the collar laminations, need to be blocked for every collar packs.
- Radial leaks between yoke laminations.

  If yoke laminations are not sufficiently tightly packed, there will be leaks between upper and lower bypass and leaks between bypass and busbar passage. The magnet tested for cross–flow cooling at BNL was built with 1/16 in laminations and had a high packing factor (99.7 %). In addition, the busbar passages were completely filled up and required no special attention. It was estimated that leaks could lead to a maximum available axial mass flow loss of 25%. With 1/4 in laminations however the packing factor can drop to 98%. For laminar flow, the mass flow is proportional to the cube of the gap between laminations

**Figure 1.1:** Cross–flow cooling

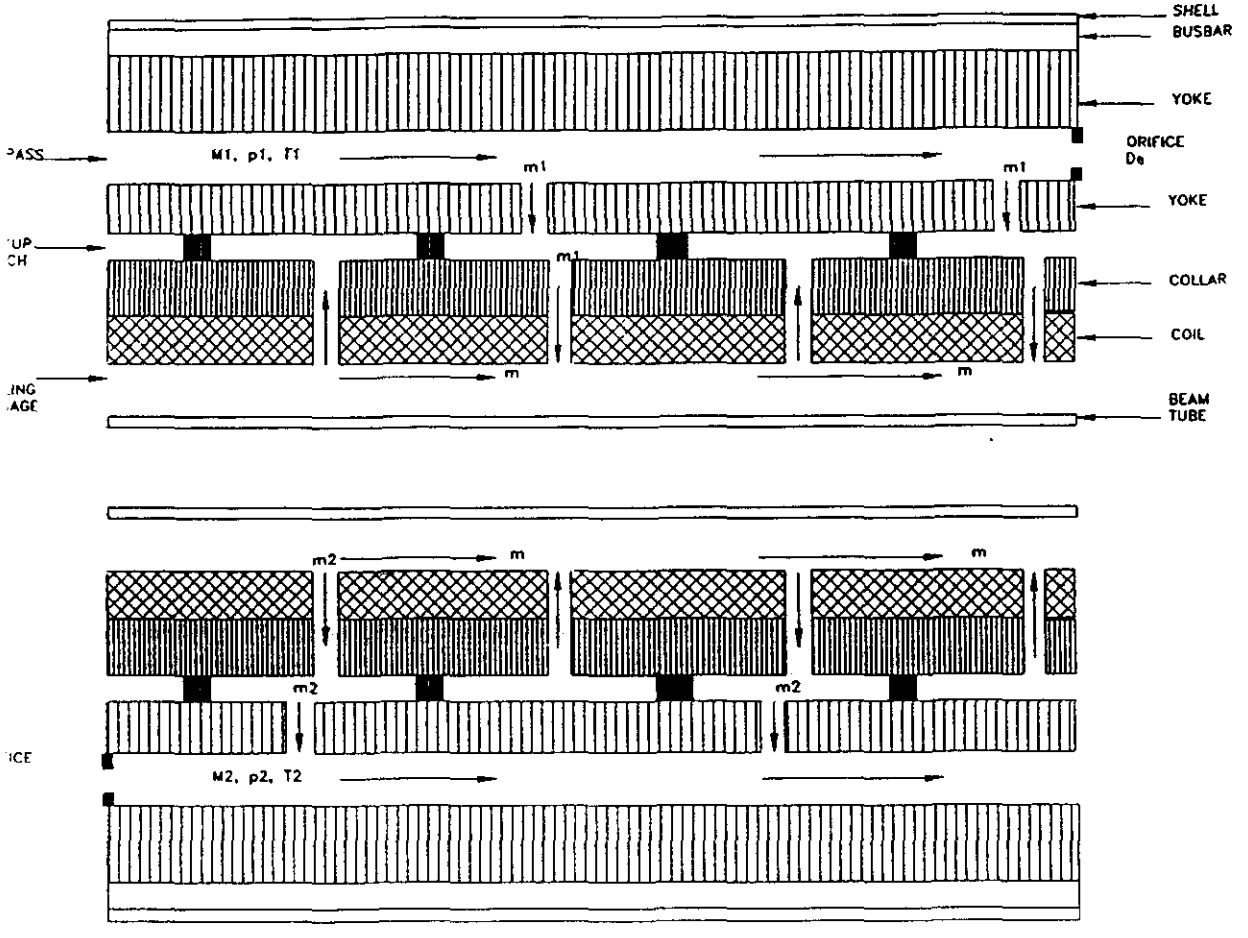

**Figure 1.2:** Cross-flow cooling

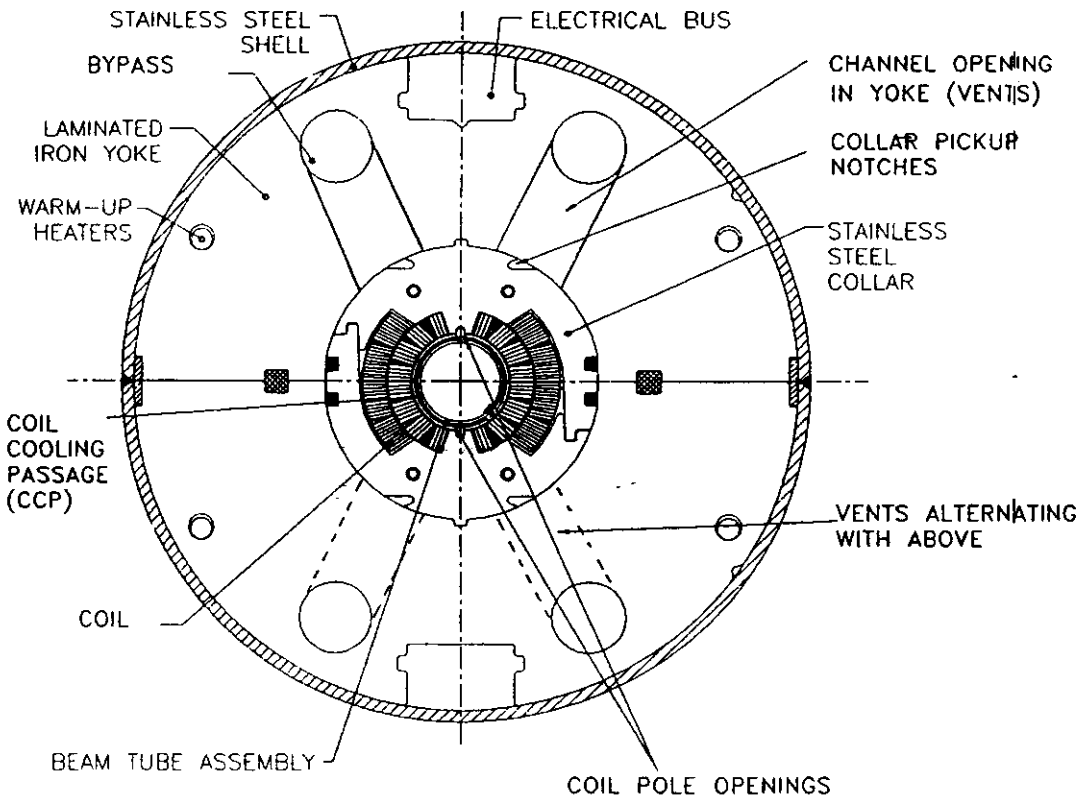

: $M_{1/4} = d^3_{1/4}c$, $M_{1/16} = d^3_{1/16}c$. With $d_{1/4} = 4d_{1/16}$ and one fourth the number of laminations, one finds $M_{1/4} = 16M_{1/16}$. Measurements have confirmed that $d_{1/4} = 4d_{1/16}$ is a reasonable assumption: thicker laminations come with larger out–of–flatness tolerances and are more difficult to compress than thin laminations.

These leaks can be entirely eliminated by lining the bypass tubes with stainless steel tube liners. Alternatively, leaks could be reduced by inserting a very thin stainless steel sheet in the midplane of the magnet. This doesn't block leaks from bypass to busbar unless busbar passages are completely filled up. Another option would be to revert to the use 1/16 in laminations.

- Collar pack laminations. Radial leaks between collar laminations are not a concern because blocks in the pickup notches redirect the flow to the CCP in addition to eliminating parallel axial flow passages.

## 1.4 RESULTS

The specifications and some parameters are listed below.

- coil temperature increase $\Delta T \leq 0.05\ K$ at $S_r = 2$W
- coil temperature increase $\Delta T \leq 0.15\ K$ at $S_r = 6$W
- pressure drop used to be $\Delta P \leq 250Pa$ per dipole, now changed to $\Delta P \leq 69Pa$ ( pressure drop for magnets without cross–flow)
- CCP gap used to be $d_c = 0.13$ cm , it is currently to be $d_c = 0.5$ cm.
- synchrotron radiation heat generates $S_r$=2 W, upgrade capability to 6 W was required. The mole generates 20 W to 30 W.

Table Table 1.1 shows that, for the original CCP gap of $d_c = 0.13$ cm, specifications at 6 W are not met. The next size which meets the 6W specification is $d_c = 0.50$ cm but this leads to unacceptably high coil temperature increases at 20 or 30 W during field measurements.

When the CCP gap quadruples (0.13 to 0.50 cm) coil temperatures decrease by a factor of 2 compared with through–flow. With cross–flow and $d_c = 0.13$ cm decreases are by a factor of 3.6 compared with through–flow and with $d_c = 0.50$ cm by 5.2. Table 1.1 also

**Figure 1.3:** Blockage of longitudinal leak paths

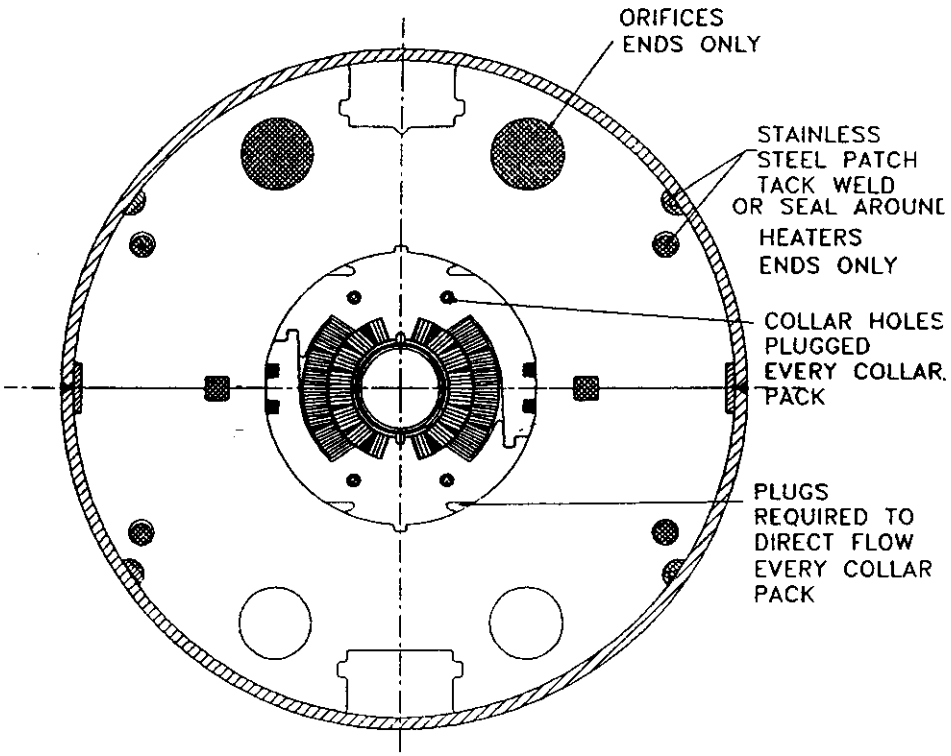

**Table 1.1:** Maximum coil temperature increase

| gap (cm) | heat (W) | through flow (K) | cross–flow (K) |
|---|---|---|---|
| $d_c$ | $S_r$ | $\Delta T$ | $\Delta T$ |
| 0.13 | 2 | 0.08 | 0.023 |
| 0.13 | 6 | **0.23** | 0.064 |
| 0.13 | 10 | 0.38 | 0.106 |
| 0.13 | 20 | 0.75 | 0.209 |
| 0.13 | 30 | 1.12 | 0.313 |
| 0.13 | 40 | 1.49 | 0.416 |
| 0.20 | 2 | 0.07 | 0.009 |
| 0.20 | 6 | **0.21** | 0.022 |
| 0.20 | 10 | 0.35 | 0.034 |
| 0.20 | 20 | 0.70 | 0.064 |
| 0.20 | 30 | 1.05 | 0.094 |
| 0.20 | 40 | 1.40 | 0.124 |
| 0.50 | 2 | 0.04 | 0.009 |
| 0.50 | 6 | 0.11 | 0.022 |
| 0.50 | 10 | 0.18 | 0.034 |
| 0.50 | 20 | **0.35** | 0.066 |
| 0.50 | 30 | 0.53 | 0.097 |
| 0.50 | 40 | 0.70 | 0.129 |

shows that a relatively small increase from $d_c = 0.13$ to $d_c = 0.20$ cm leads to a considerable decrease in cross–flow values, while through–flow values remain practically unchanged.

# 2. EXPERIMENTAL VERIFICATION

## 2.1 DESCRIPTION OF MEASUREMENTS

Measurements were performed by G.L.Ganetis at Brookhaven National Laboratory. Magnet DD0020 had a 1.3 mm cooling gap and was instrumented with temperature sensors glued on the outer surface of the beam tube which still had a trim coil. Tests were conducted for a total mass flow m=100 g/sec. The yoke lamination thickness was 1/16 in with a measured 99.7 % packing fraction. The orifices for cross–flow at the ends of the bypasses were completely closed. Two types of gages were used : carbon resistors and carbon–glass sensors. The first type of gages (numbers 1 to 4 in Fig. 2.1) reads values that are higher than those of the second type by 0.05 K with a spread of 0.025 K (numbers 5 and 6 in Fig. 2.1). The second type consists of high quality gages with readings within 0.005 K. Calibration curves in Fig. 2.1 indicate that, in the region of interest, both types of gages have the same slopes. Therefore while the absolute readings for the lower quality gages might be off, differences between readings on the same gage are as accurate as for the high quality gages. Errors on temperature difference readings are estimated at 0.005 K. Gages were positioned around the beam tube (see Fig. 2.2) at various azimuthal locations. Thus some gages will be closer to the heat source than others at the same distance along the magnet length. This will introduce a small amount of scatter in the data. Heat was provided by heating strips (see Fig. 2.3) placed inside the beam tube. Resistance wires were clamped inside the beam tube. Two wires were located on opposite sides which were alternately powered at 20, 30 and 40 W. Lower values were not tested since the increase in temperature is lower than could reliably be detected with the instrumentation. The magnet was kept at 4.35 K for two hours before turning one strip heater on, and measurements were taken at regular time intervals up to a total of two hours.

## 2.2 COMPARISON WITH DATA

The data which are measurements of helium temperatures in the coil cooling passage are compared to computed helium temperatures. The latter take into account heat diffusion along the magnet length and radial diffusion to the bypasses.

Fig. 2.4, Fig. 2.6, Fig. 2.8 show bore tube temperature differences between the time when the power was turned on and two hours later along the magnet length at 0, 30, and

**Figure 2.1:** Temperature sensor calibration

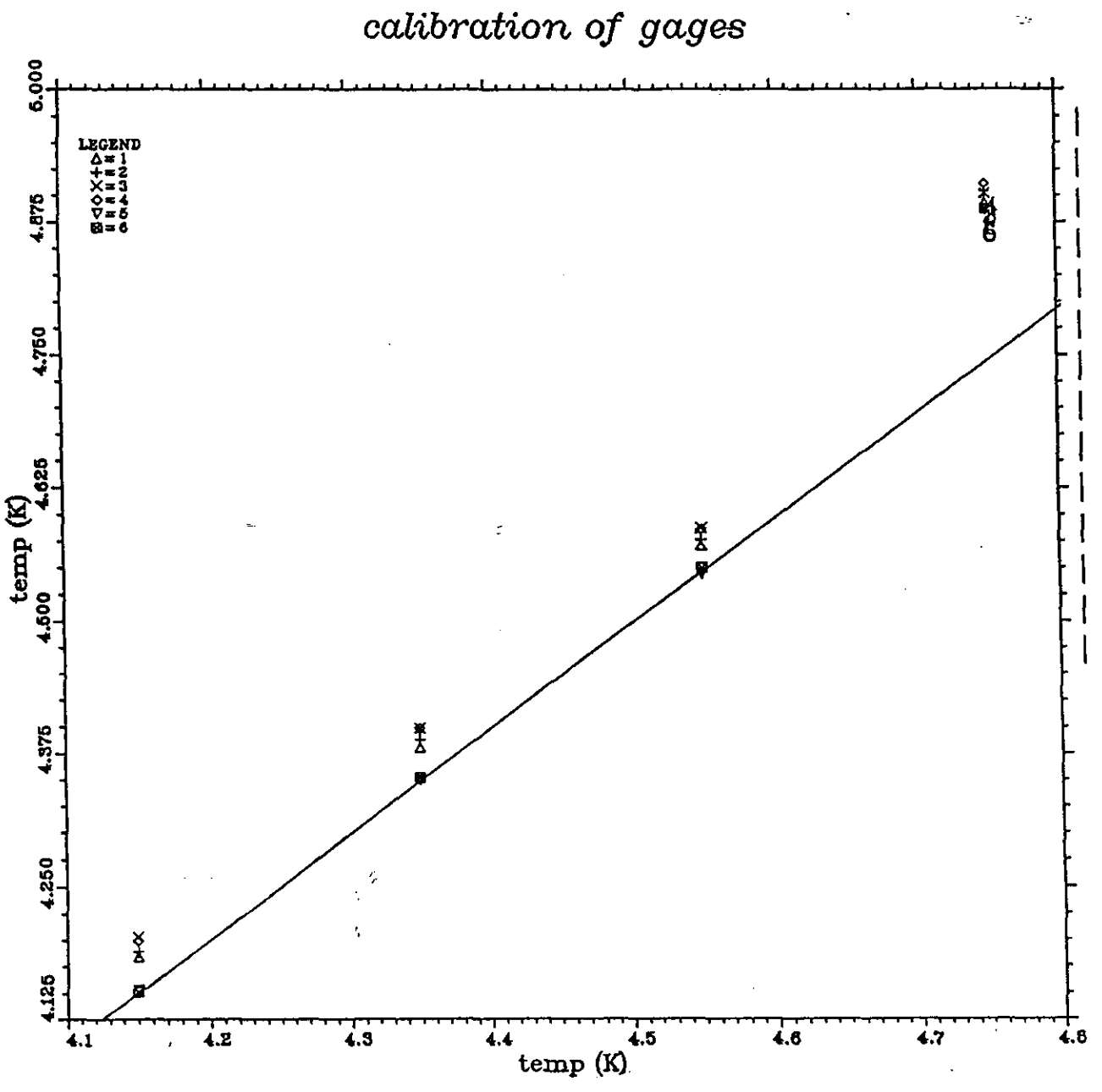

TS1 → TS10 are Carbon Resistors sticks
TS11 → TS13 are signal Cabon glass Sensors.

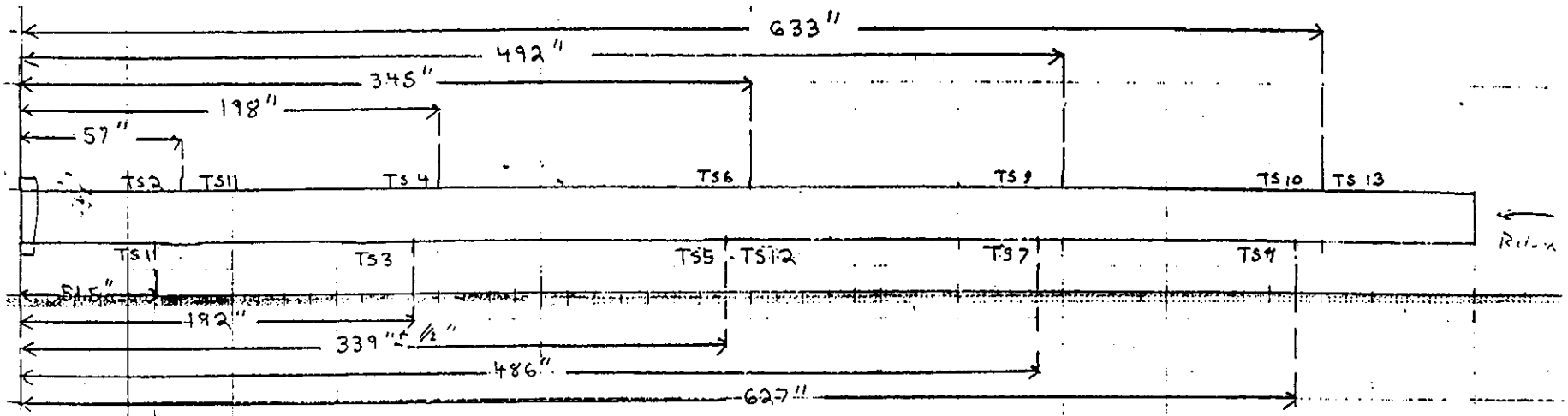


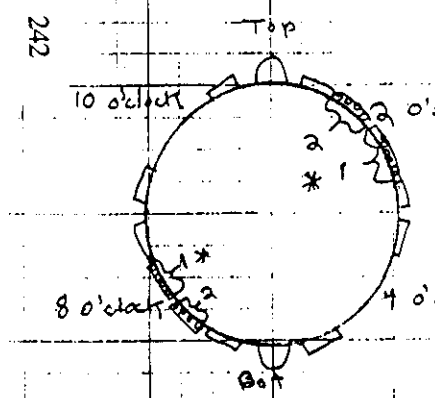


| | | | | | | | | | | | | |
|---|---|---|---|---|---|---|---|---|---|---|---|---|
| TS1A, TS1B | TS 1 | – | 4 | o'clock | pos. | – | Mid-plane* | 2 | – | Leads exiting | Lead End | TS4.001 | TS4.002 |
| TS2A | TS 2 | – | 2 | " | " | – | " | 2 | – | " | " | " | TS4.003 | |
| TS3A, TS3B | TS 3 | – | 4 | " | " | – | " | 1 | – | " | " | " | TS4.005 | TS4.006 |
| TS4B | TS 4 | – | 10 | " | " | – | " | 2 | – | " | " | " | | TS4.008 |
| TS5A, TS5B | TS 5 | – | 8 | " | " | – | " | 2 | – | " | " | " | TS4.009 | TS4.010 |
| TS6A | TS 6 | – | 10 | " | " | – | " | 1 | – | " | " | " | TS4.011 | |
| TS7A, TS7B | TS 7 | – | 4 | " | " | – | " | 1 | – | " | " | " | TS4.013 | TS4.014 |
| TS8A, TS8B | TS 8 | – | 10 | " | " | – | " | 1 | – | Leads exiting | Return | End | TS4.015 | TS4.016 |
| TS9A, TS9B | TS 9 | – | 4 | " | " | – | " | 2 | – | " | " | " | TS4.017 | TS4.018 |
| TS10A, TS10B | TS 10 | – | 10 | " | " | – | " | 1 | – | " | " | " | TS4.019 | TS4.020 |
| TS11 | TS 11 | – | 2 | " | " | – | " | 1 | – | Leads exiting | Lead | End | TS5.001 | |
| TS12 | TS 12 | – | 8 | " | " | – | " | 1 | " | " | " | | TS5.002 | |
| | TS 13 | | 10 | " | " | – | " | 2 | Leads exiting Return End. | | | | | |

New – Heat from Lead End Down bore tube

**Figure 2.2:** Temperature sensor locations

**Figure 2.3:** Heaters to simulate Synchrotron heat

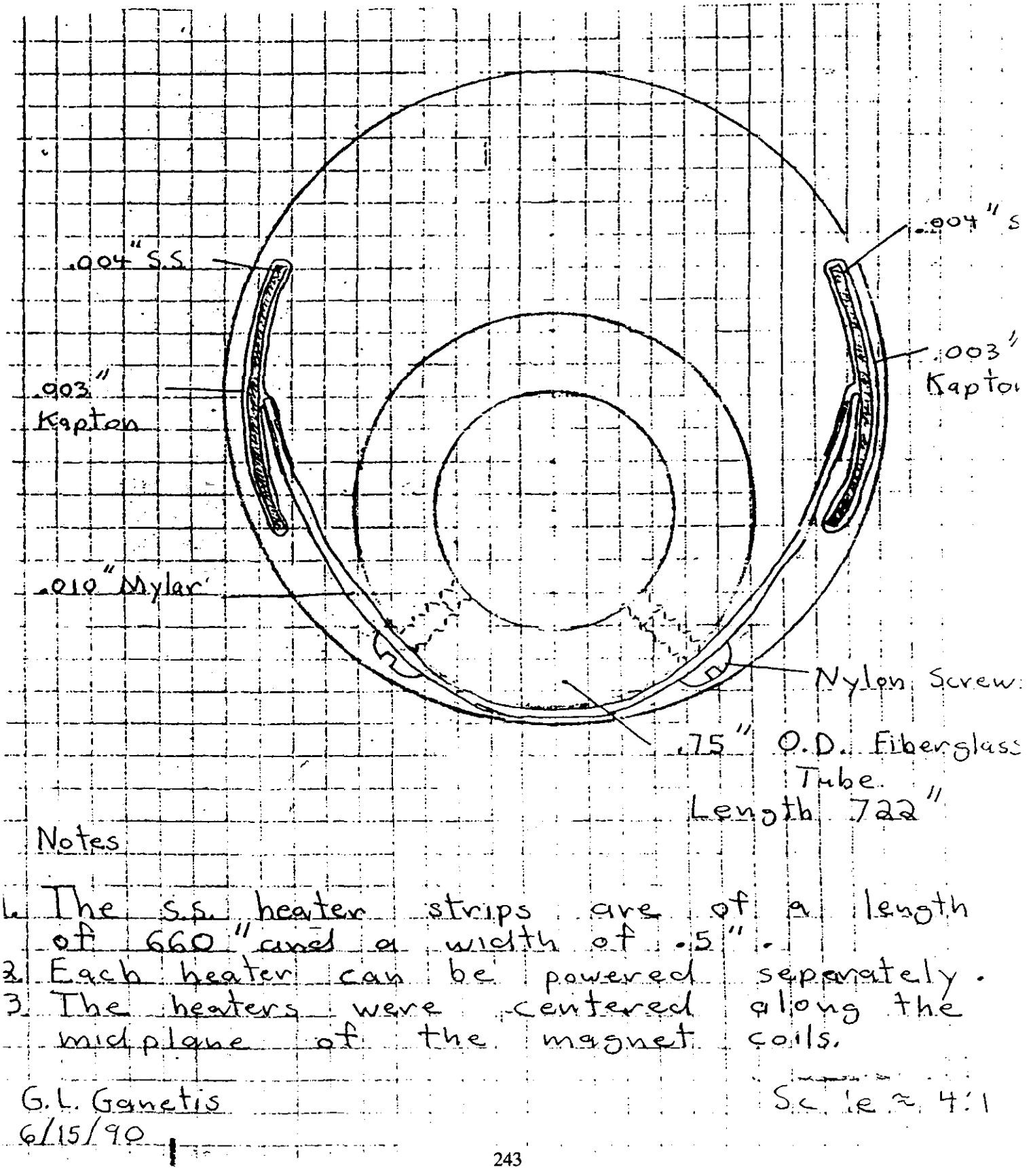

40 W. There are two sets of data points corresponding to the two strip heaters which were activated alternately to provide two sets of measurements. Fig. 2.5, Fig. 2.7, Fig. 2.9 show corresponding calculations performed with the computer model which includes formulation for end effects and recent measurements (at the National Bureau of Standards) of Kapton thermal conductivity.

Due to some amount of scatter in the data at each location along the magnet, a point by point comparison with the model is not as useful as comparing averaged values along the magnet length and maximum values.

**Table 2.1:** Coil temperature increase for a gap of 0.13 cm

| (W) | cross–flow (K) | measured (K) | cross–flow (K) | measured (K) |
|---|---|---|---|---|
| $S_r$ | $\Delta T_{av}$ | $\Delta T_{av}$ | $\Delta T_{peak}$ | $\Delta T_{peak}$ |
| 20 | 0.069 | 0.057 | 0.203 | 0.2 |
| 30 | 0.103 | 0.102 | 0.304 | 0.3 |
| 40 | 0.137 | 0.145 | 0.405 | 0.4 |

According to table Table 1.1 measured peak values could be substantially decreased if $d_c$ were slightly bigger, $d_c = 0.14$ cm for instance . Table 2.1 indicates an excellent agreement between the data and model for peak and averaged helium temperatures. Coil temperatures have not been measured but are always lower than the coil cooling passage helium temperature as long as there is no heat generated in the coil as would be the case with High Energy Booster magnets.

Temperature curves generated by the model exhibit two peaks (Fig. 2.5, Fig. 2.7, Fig. 2.9 ) but corresponding data show one (Fig. 2.4), two (Fig. 2.6) or even three peaks (Fig. 2.8). There are too few temperature sensors along the magnet length to attempt to fit the data to curves. While it cannot be said that the model describes the exact shape of temperature curves, it is in excellent agreement as far as maximum temperature values are concerned.

**Figure 2.4:** Data Temperature increase at 20 W

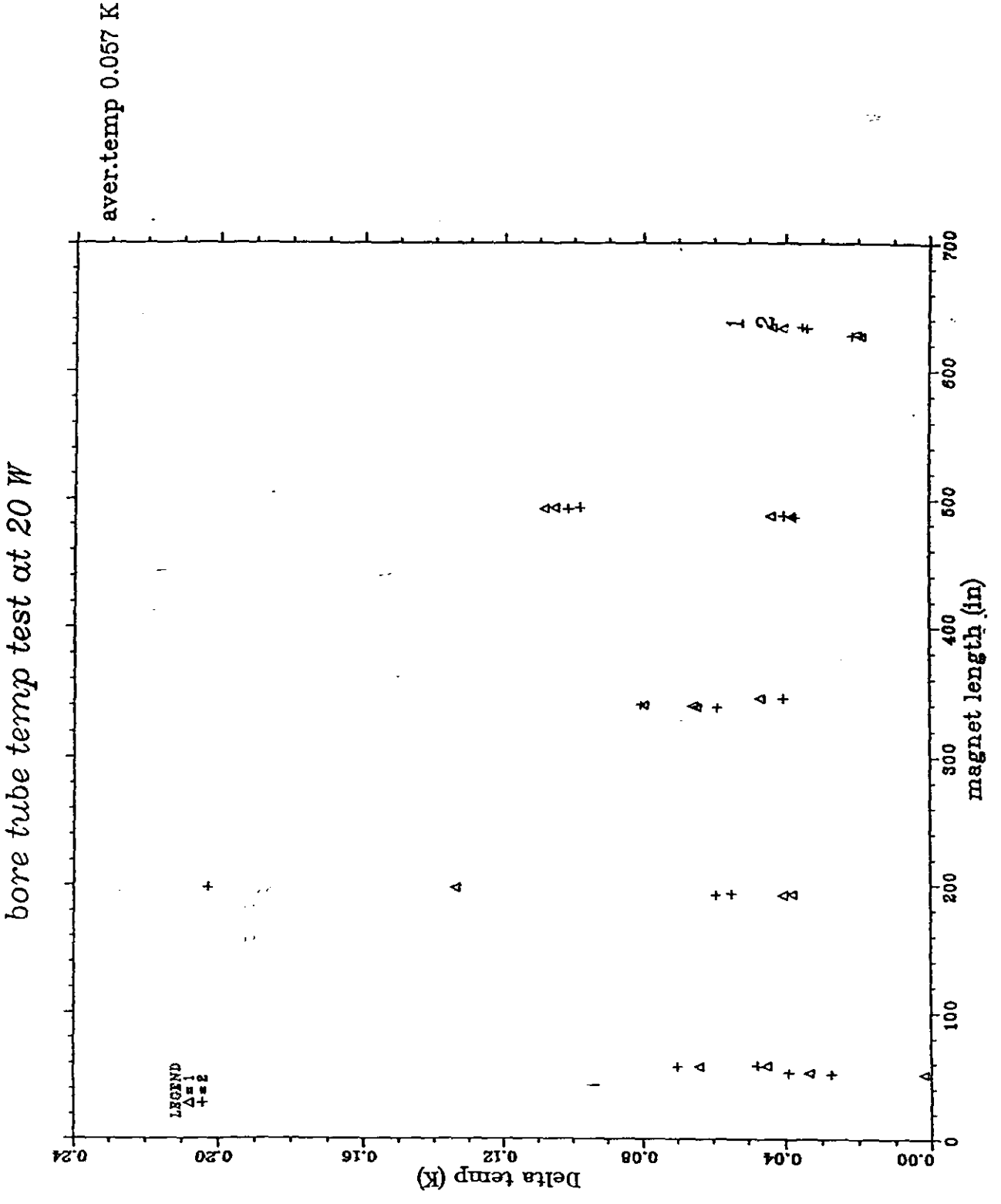


Test results of magnet DD0020 at 20 W

**Figure 2.5:** Computed Temperature increase at 20 W

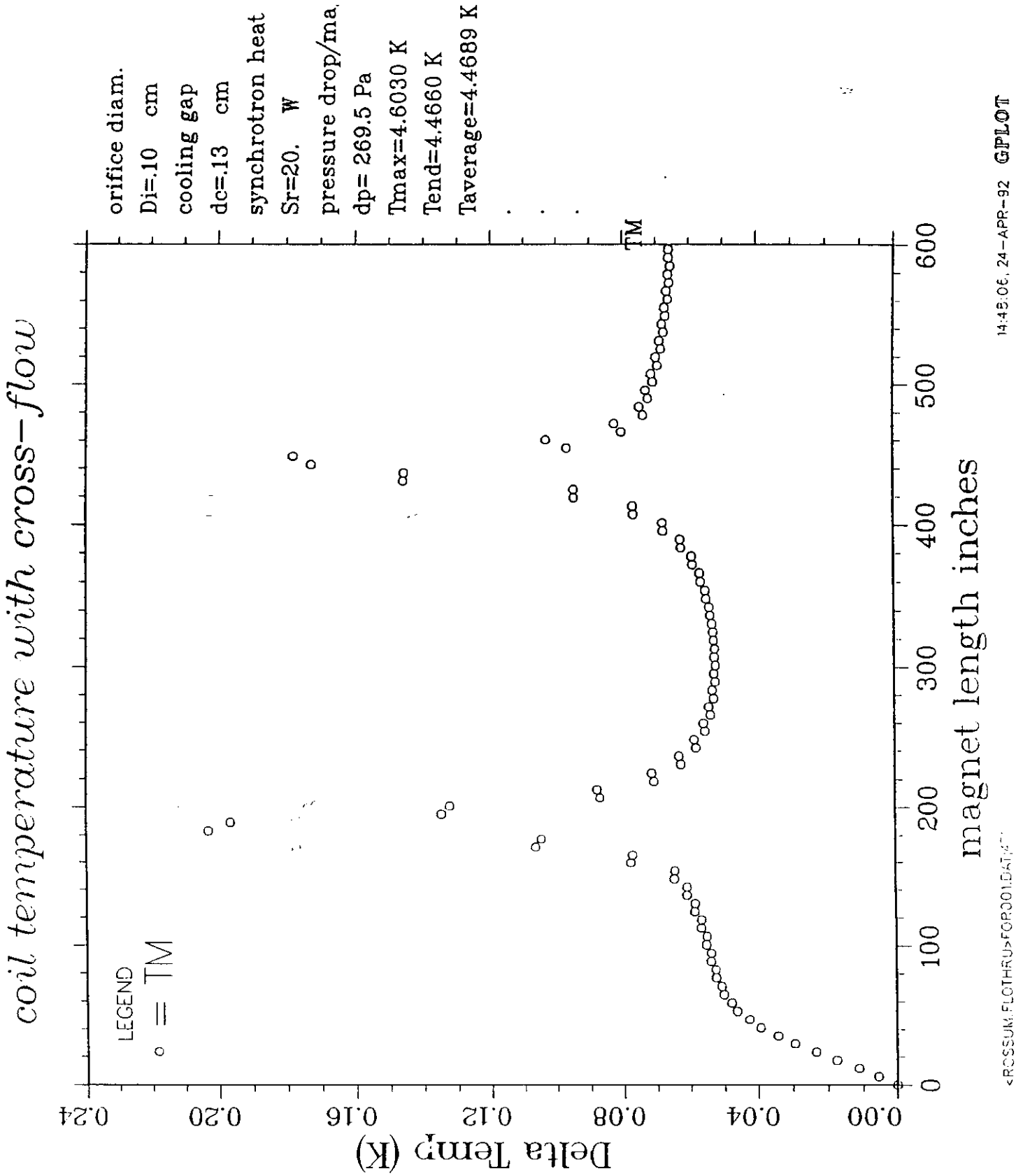

**Figure 2.6:** Data Temperature increase at 30 W

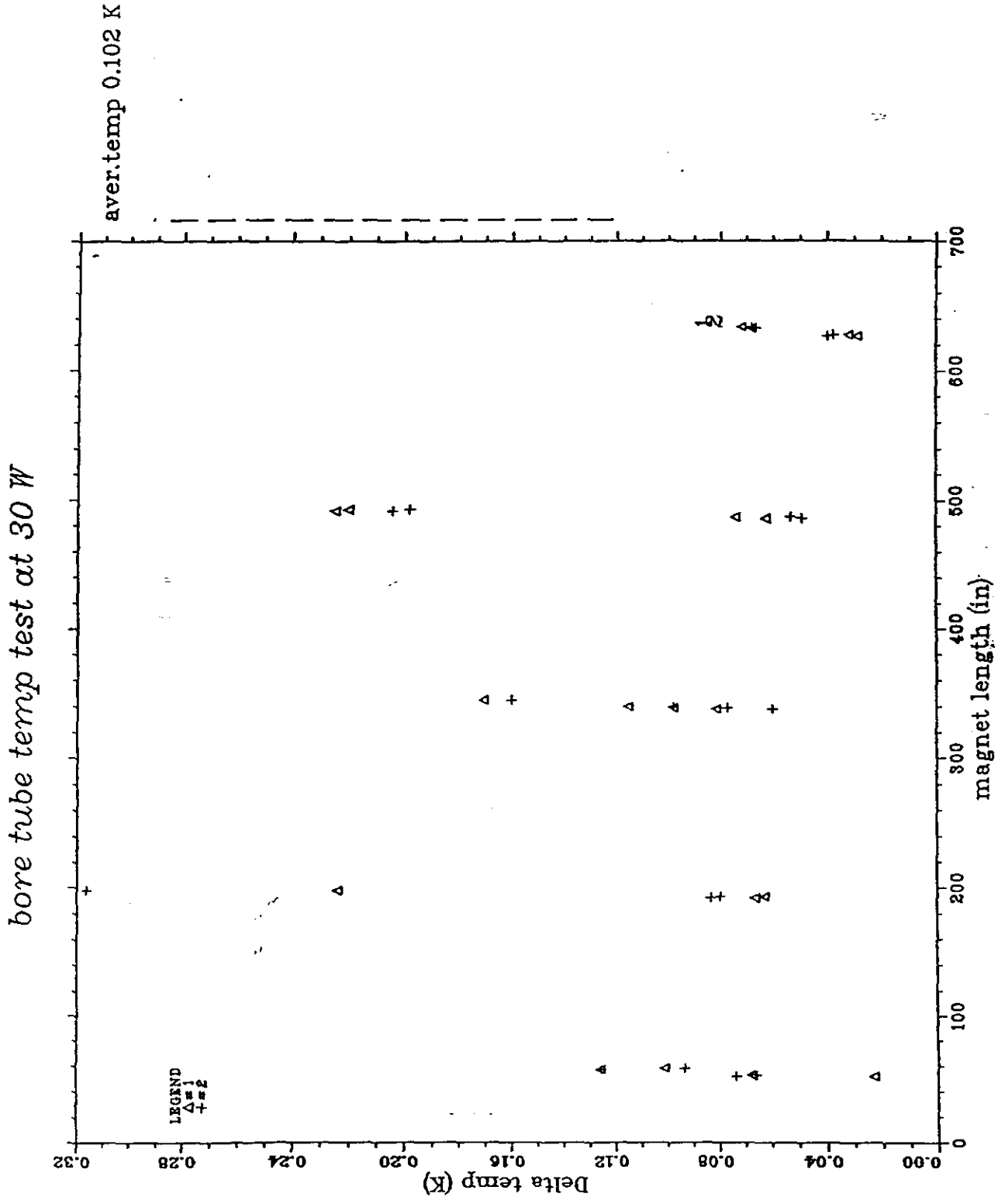


Test results of magnet DD0020 at 30 W

**Figure 2.7:** Computed Temperature increase at 30 W

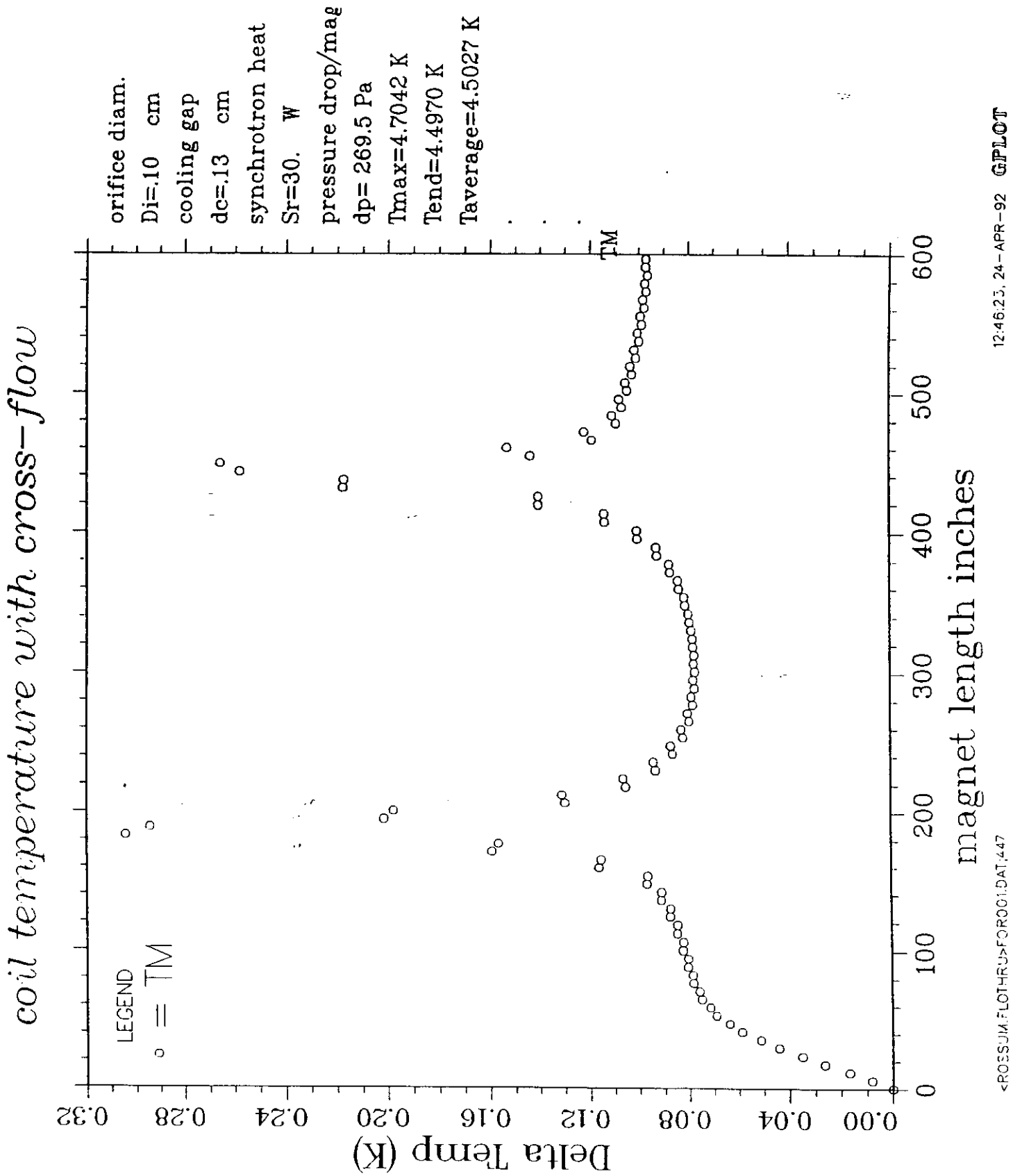

**Figure 2.8:** Data Temperature increase at 40 W

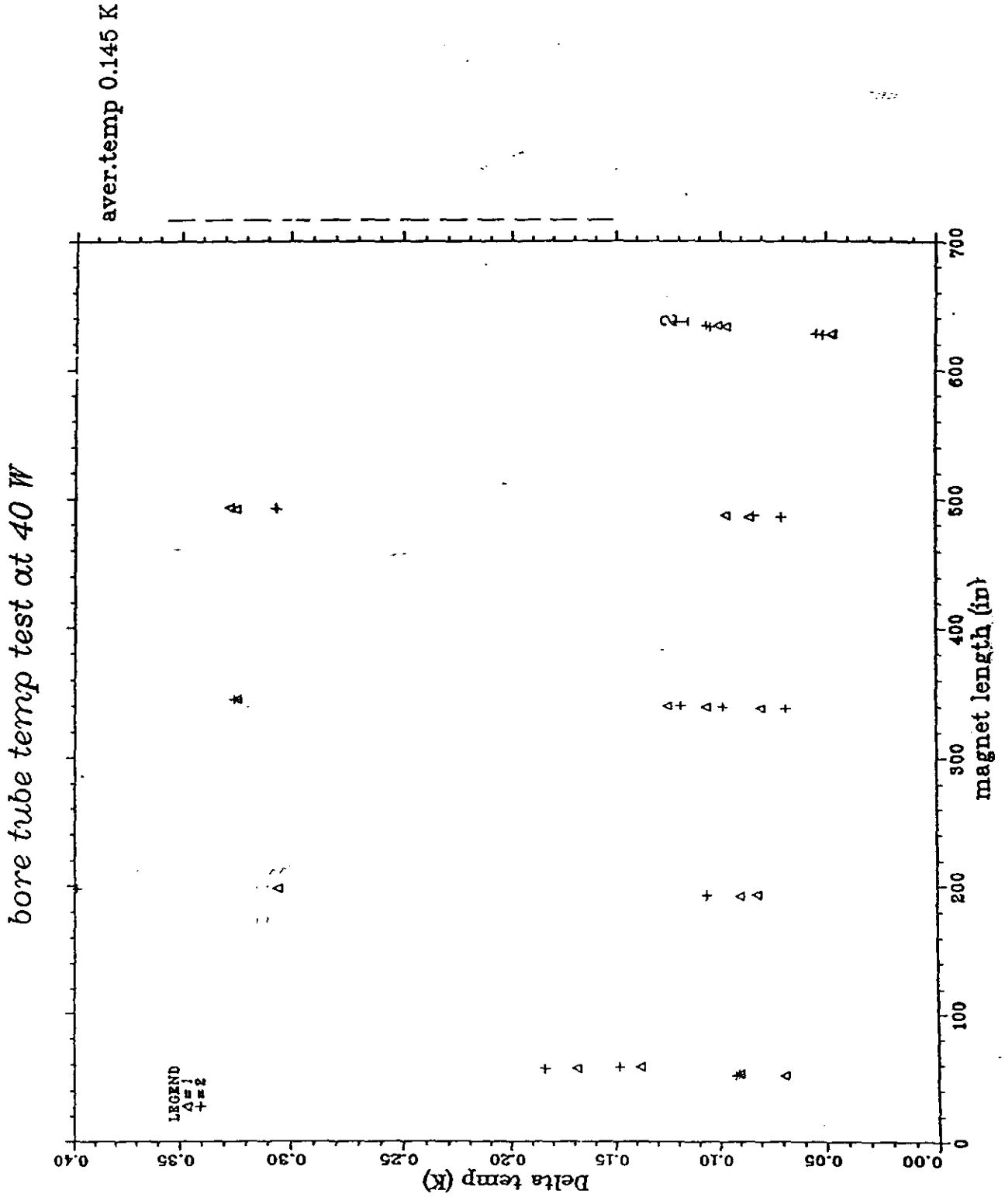


Test results of magnet DD0020 at 40 W

**Figure 2.9:** Computed Temperature increase at 40 W

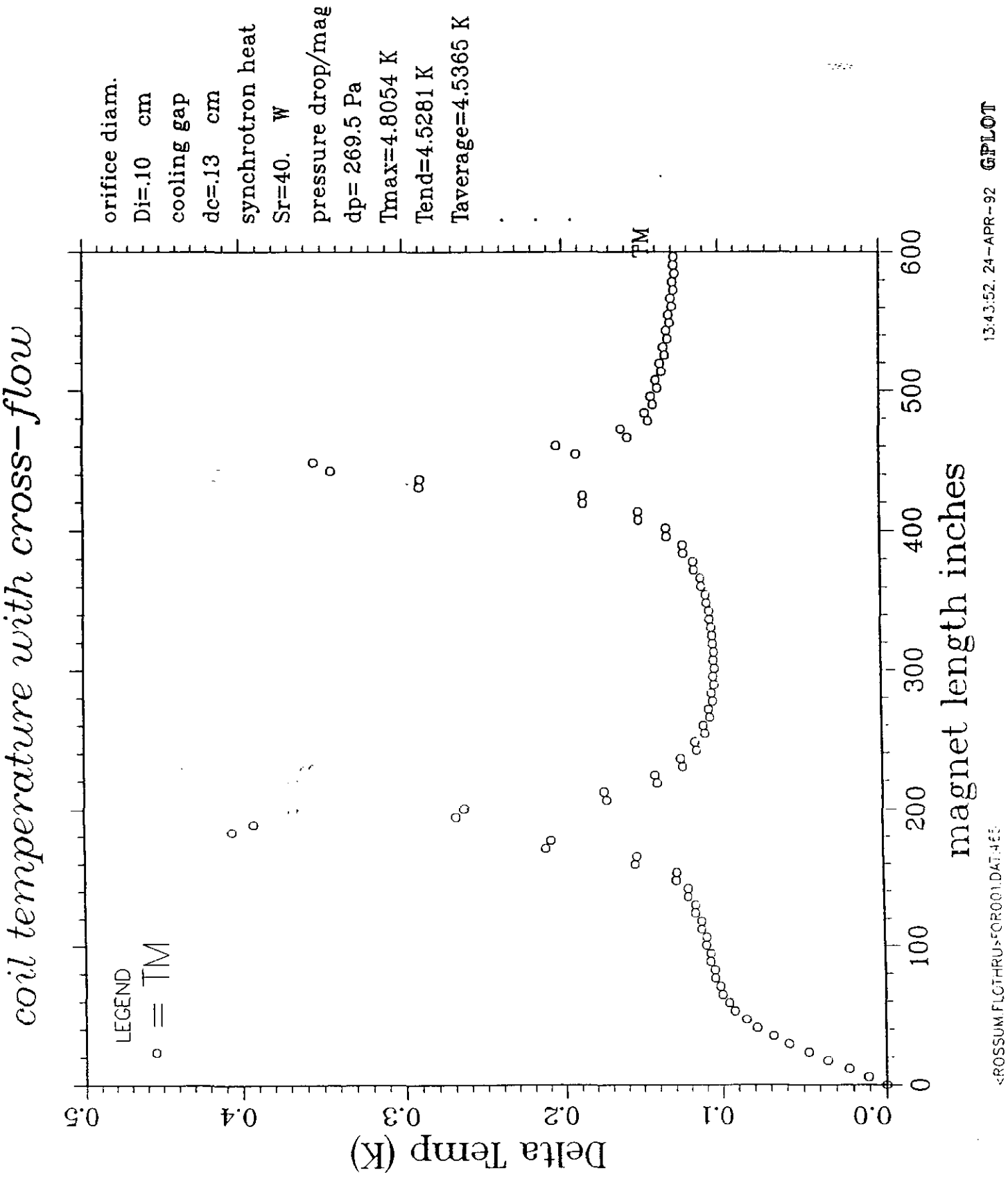

# 3. PARAMETER OPTIMIZATION

## 3.1 VARIATION OF COIL COOLING PASSAGE GAP

The presence of peaks in coil temperature curves (Fig. 2.5, Fig. 2.7, Fig. 2.9) generated by the model is now addressed. It is a consequence of the fact that for a coil cooling passage gap of $d_c = 0.13$ cm width the corresponding mass–flows in the CCP pass through zero (are reversing directions) at two locations in the magnet. The mass flow in the coil cooling passage corresponding to the temperature curve of Fig. 2.5 is shown in Fig. 3.1. It has the appearance of two curves which is explained by the fact that, for every inlet of mass flow from the upper bypass at any point $z$ along the magnet length, flow in the CCP will pass in two directions, one going in the $z$ direction, but the other either in the $z$ direction or opposite to it, depending on the situation upstream from point $z$. Sections next to those receiving little or no helium however receive an increased amount of helium and axial diffusion along the coil copper prevents temperatures from rising to unduly high values.

It should be noted that without cross–flow the maximum temperature increase at 20 W with $d_c = 0.13$ cm would be 0.75 K (see Table 1.1), or three and a half times higher than peak values with cross–flow.

**Figure 3.1:** Mass flow in cooling passage

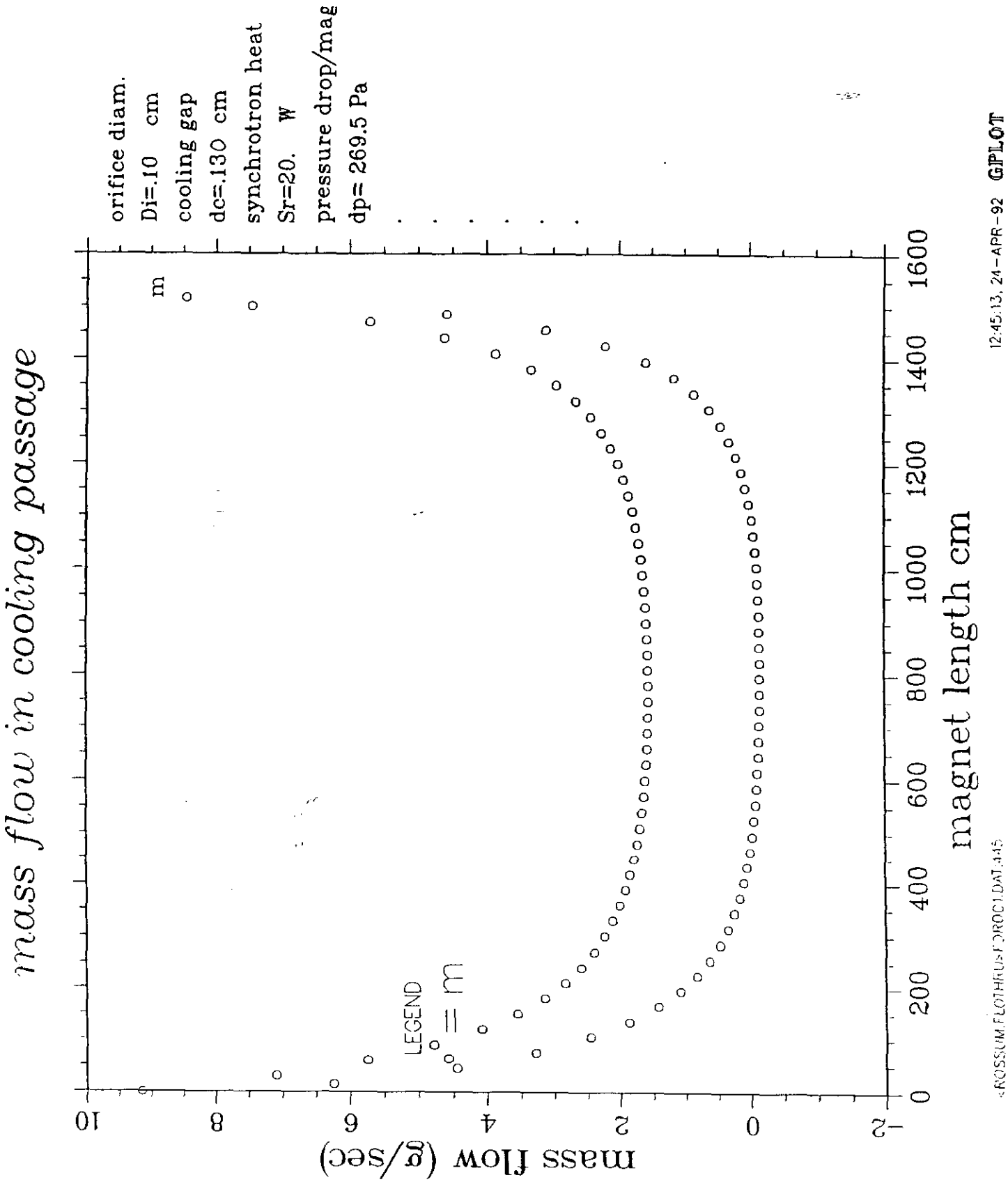

For comparison purposes Fig. 3.2 shows maximum temperature increases versus CCP gap for through–flow cooling. With cross–flow cooling and when the orifices are completely closed Fig. 3.3 shows that temperature increases drop sharply between 0.130 cm and 0.140 cm and then remain constant and equal to 0.066 K with increasing CCP gap. The transition to constant temperature occurs when the mass flow curves no longer pass through zero as will be shown in the following.

As the CCP gap is increased temperature peaks move closer to each other as can be seen by comparing Fig. 2.5 ($d_c$ = 0.130 cm) and Fig. 3.4 ($d_c$ = 0.135 cm) . They merge into one in Fig. 3.6 ($d_c$ = 0.138 cm) and finally disappear in Fig. 3.8 ($d_c$ = 0.150 cm). The presence and location of temperature peaks is related to the location where the mass flow curve crosses the zero line as can be verified from the corresponding mass flow curves (Fig. 3.1, Fig. 3.5, Fig. 3.7, Fig. 3.9).

Fig. 3.10 and Fig. 3.11 show mass flow and temperature curves for the case which is currently considered where the coil cooling gap is 0.5 cm.

Pressure drops however decrease as the CCP gaps increase : the pressure drop for $d_c$ = 0.500 cm is 173.5 Pa which is smaller than the drop of 263.6 Pa for $d_c$ = 0.150.

**Figure 3.2:** Temperature increase versus CCP gap with through-flow

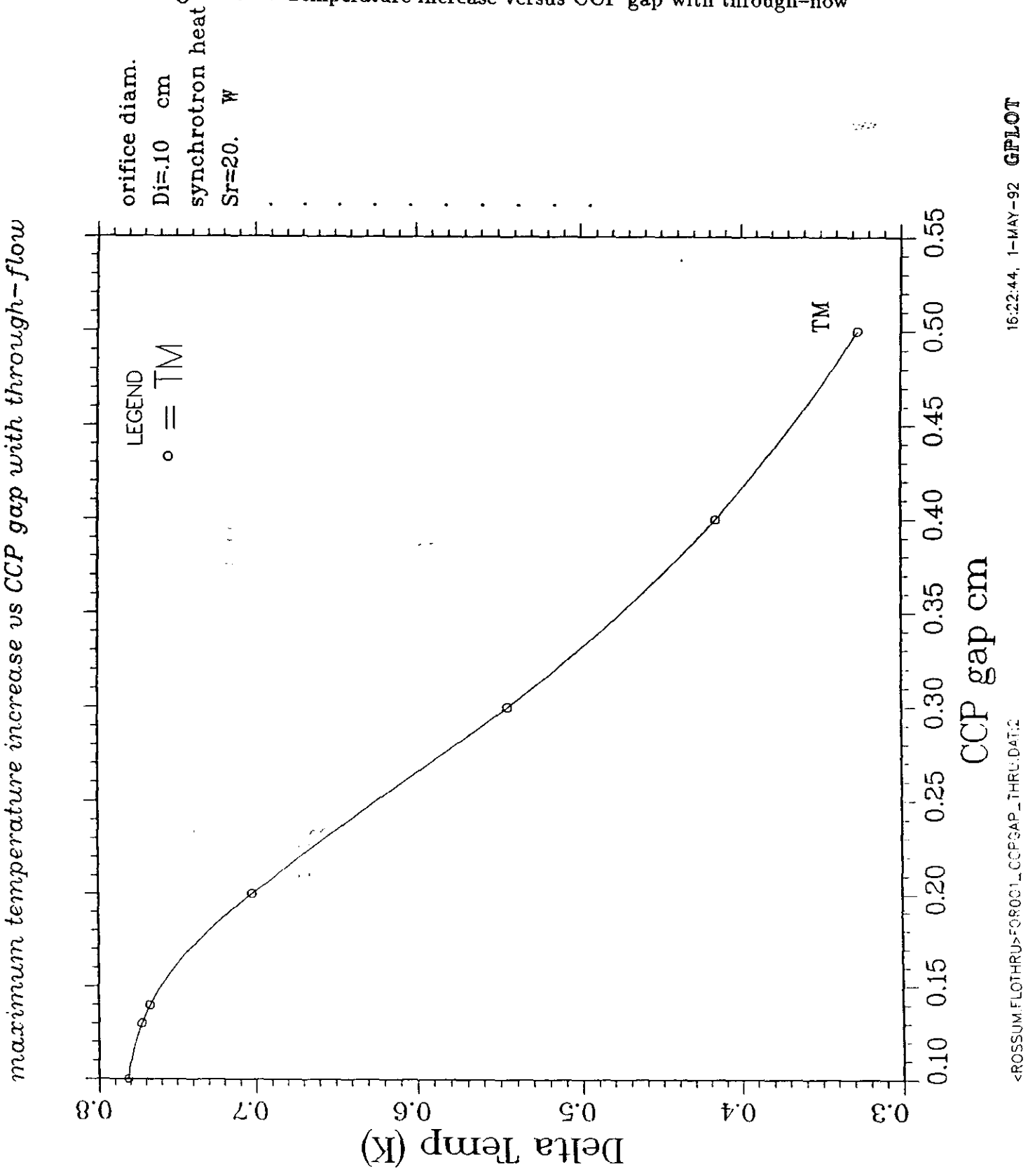

**Figure 3.3:** Temperature increase versus CCP gap with cross-flow orifices

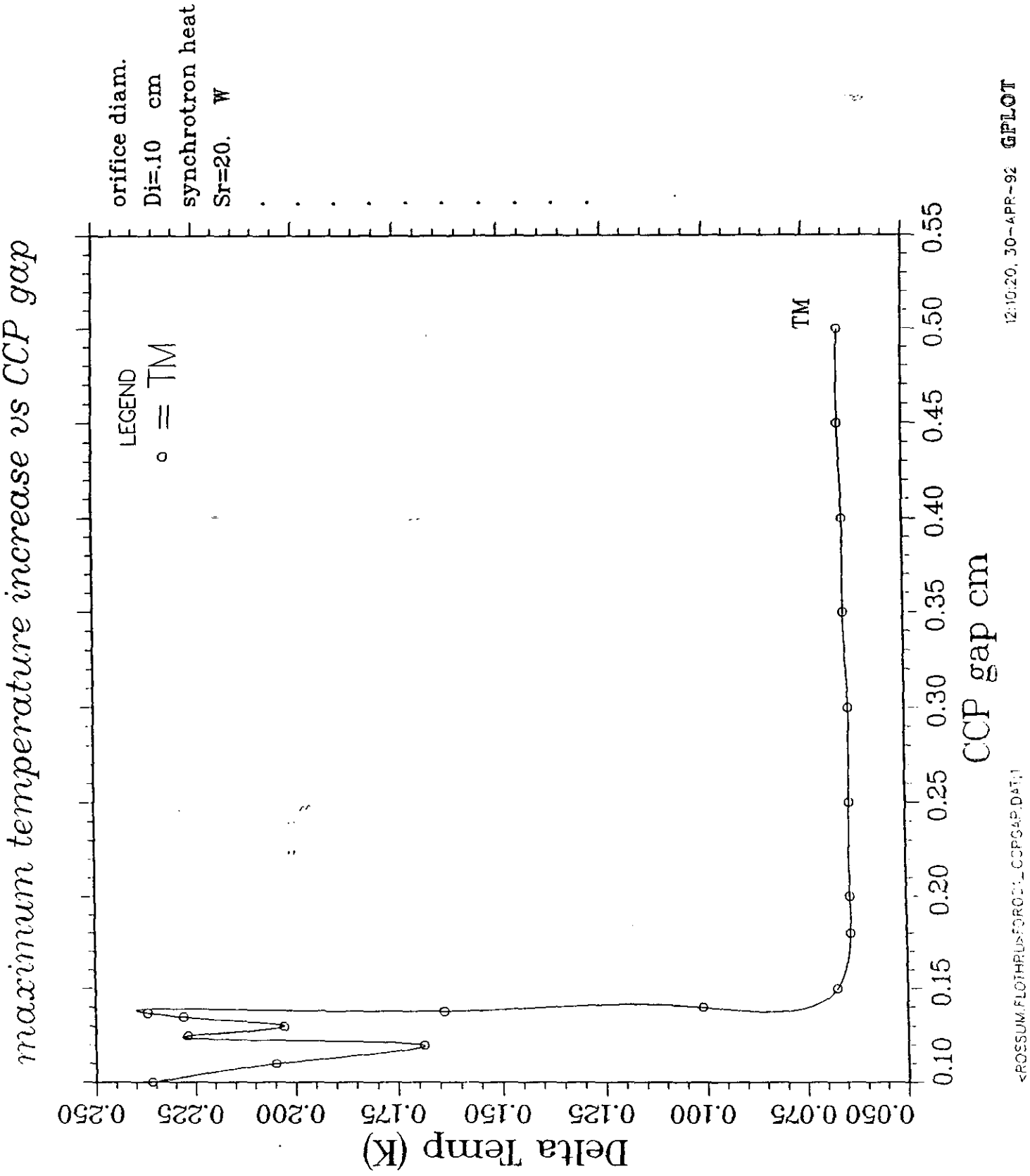

**Figure 3.4:** Temperature increase in cooling passage, $d_c$=0.135 cm

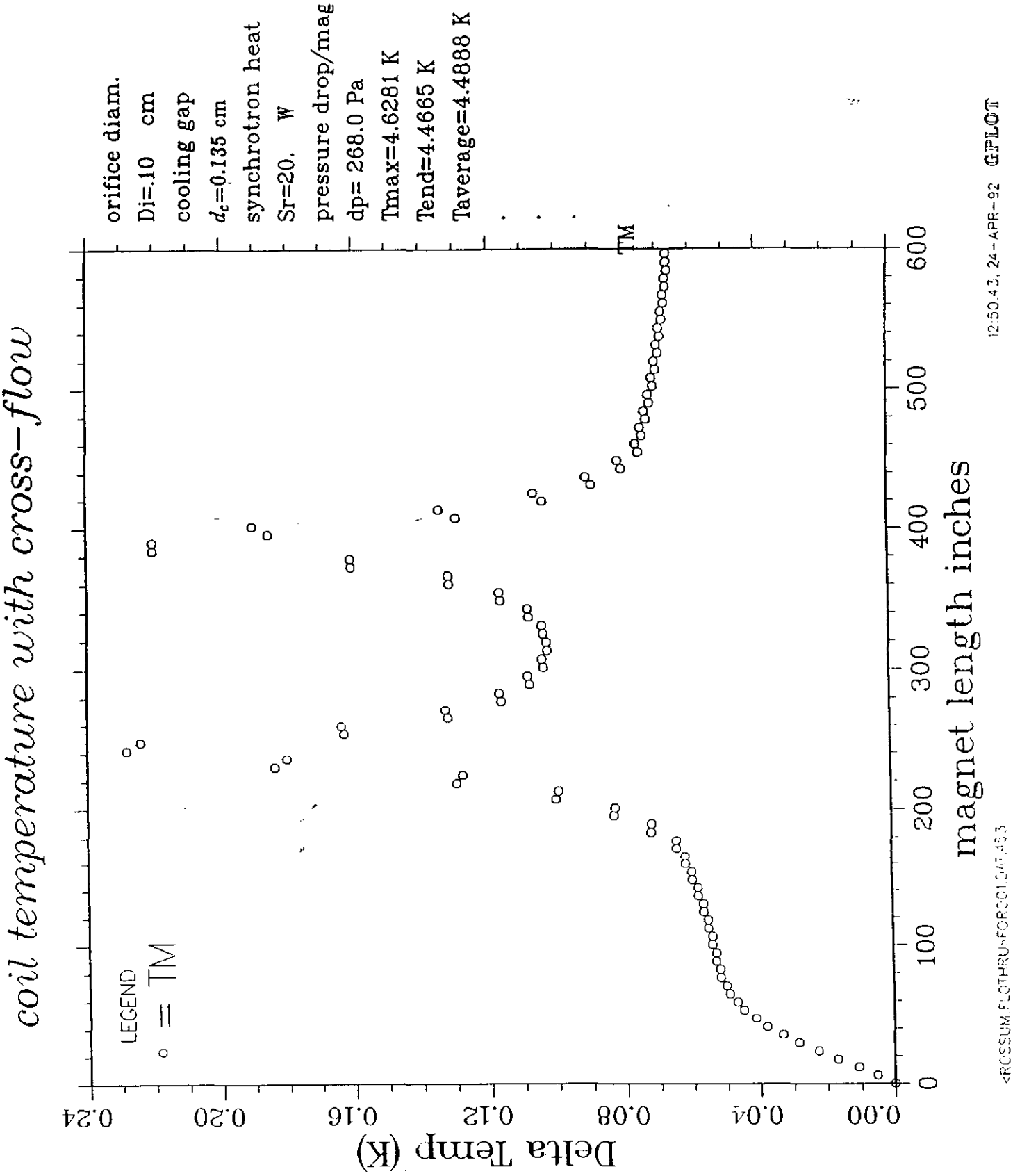

**Figure 3.5:** Mass flow in cooling passage, $d_c$ =0.135 cm

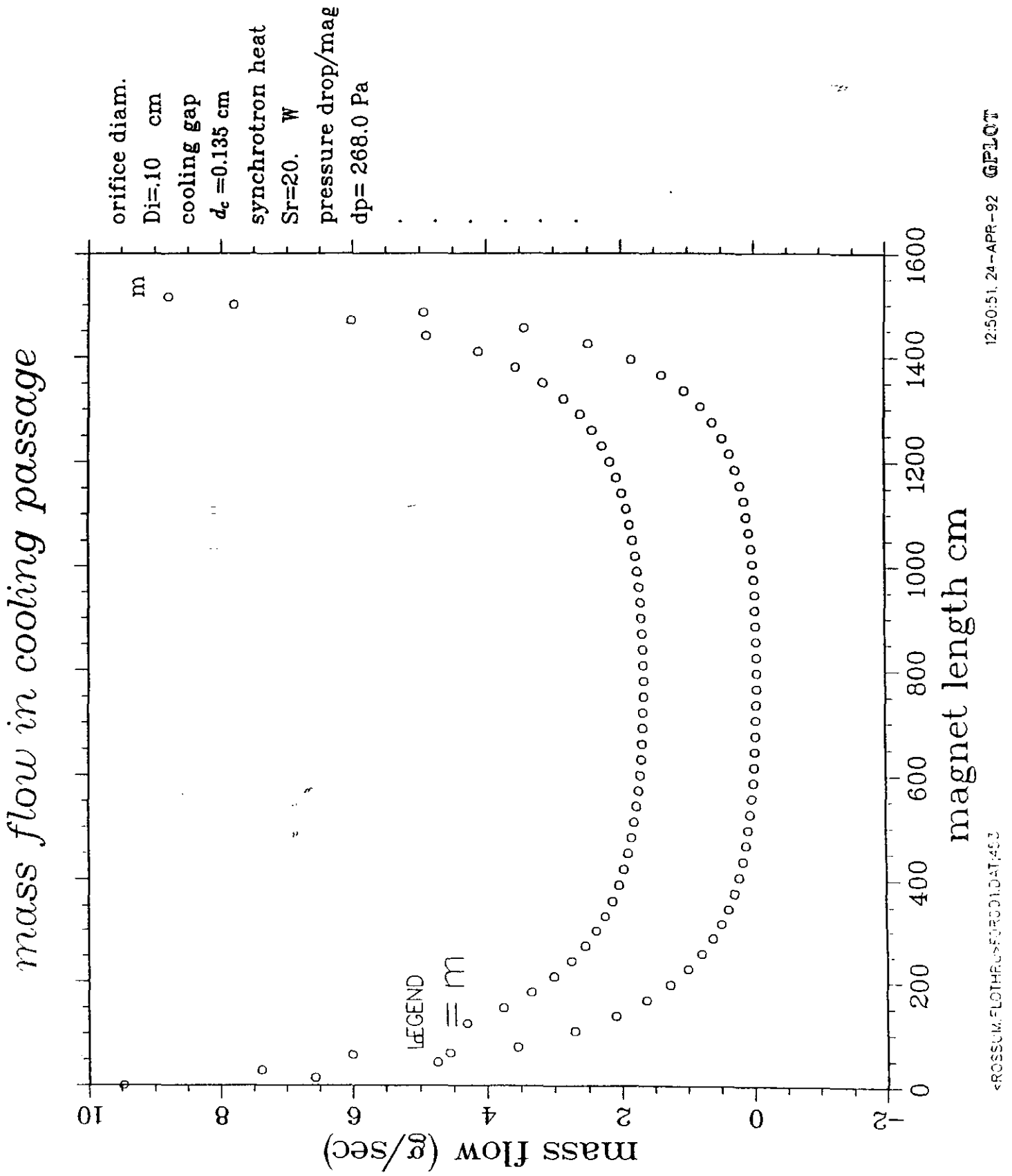

**Figure 3.6:** Temperature increase in cooling passage, $d_c$ =0.138 cm

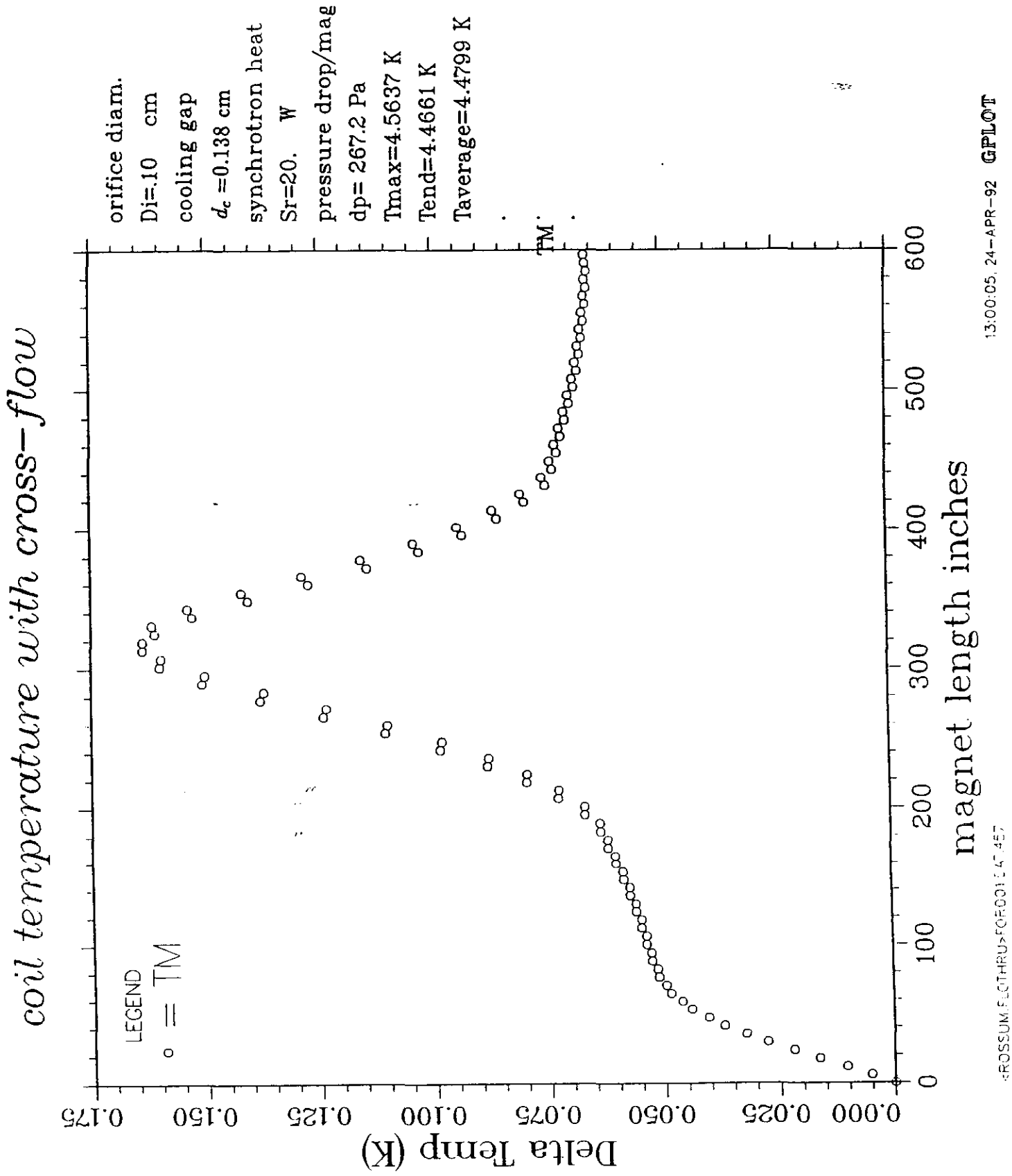

**Figure 3.7:** Mass flow in cooling passage, $d_c$ =0.138 cm

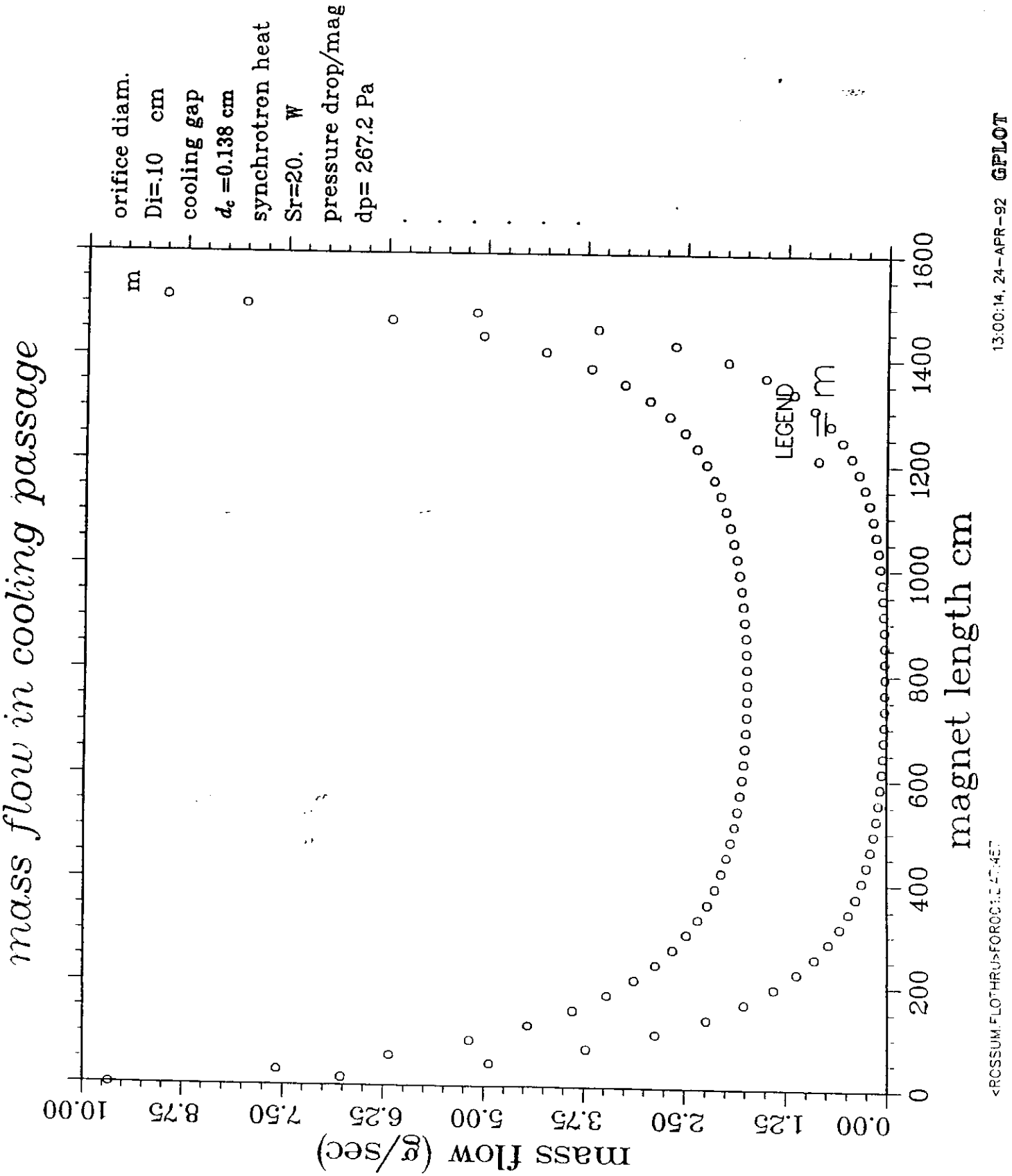

**Figure 3.8:** Temperature increase in cooling passage $d_c$ =0.150 cm

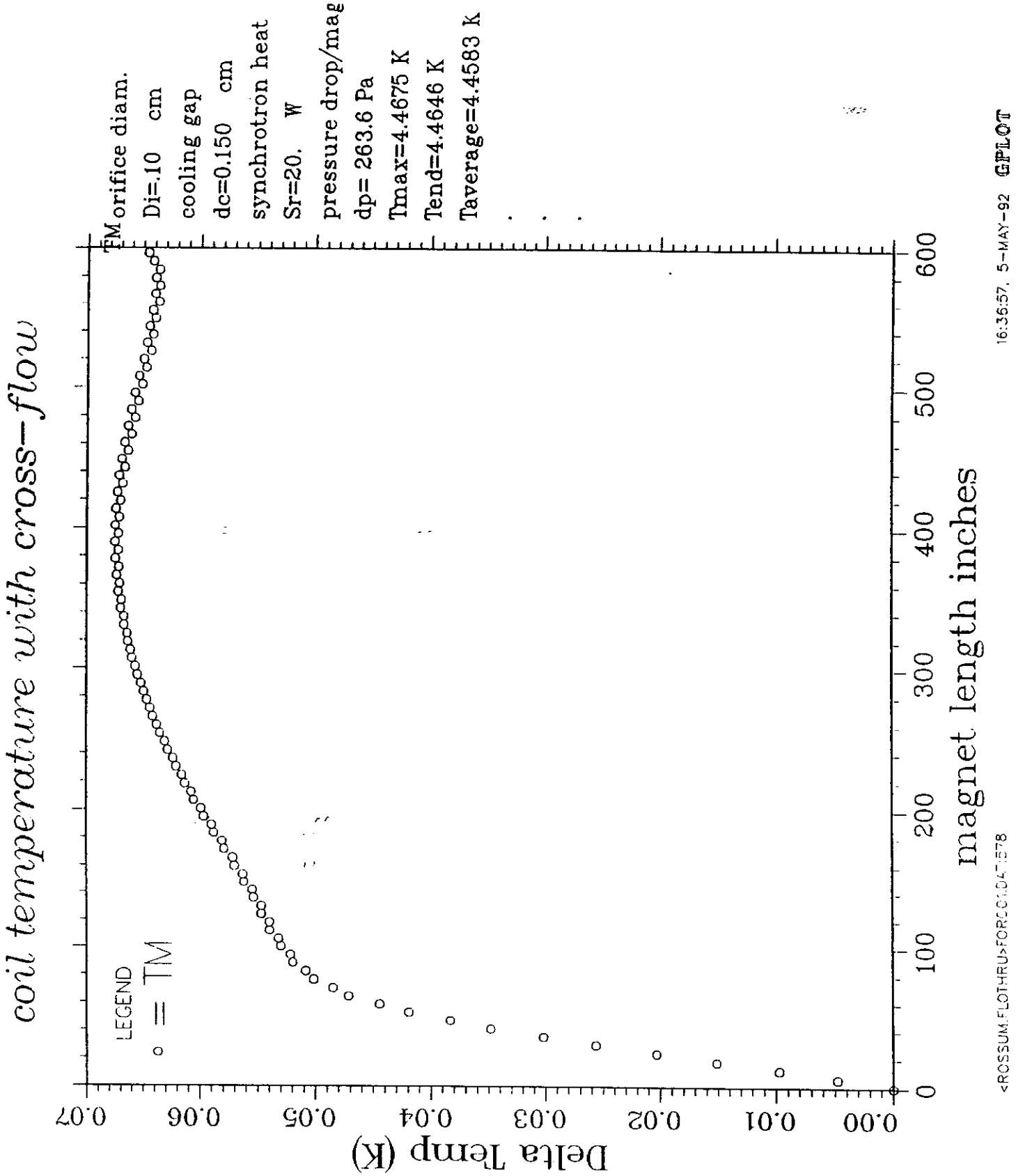

**Figure 3.9: Mass flow in cooling passage, $d_c$ =0.150 cm**

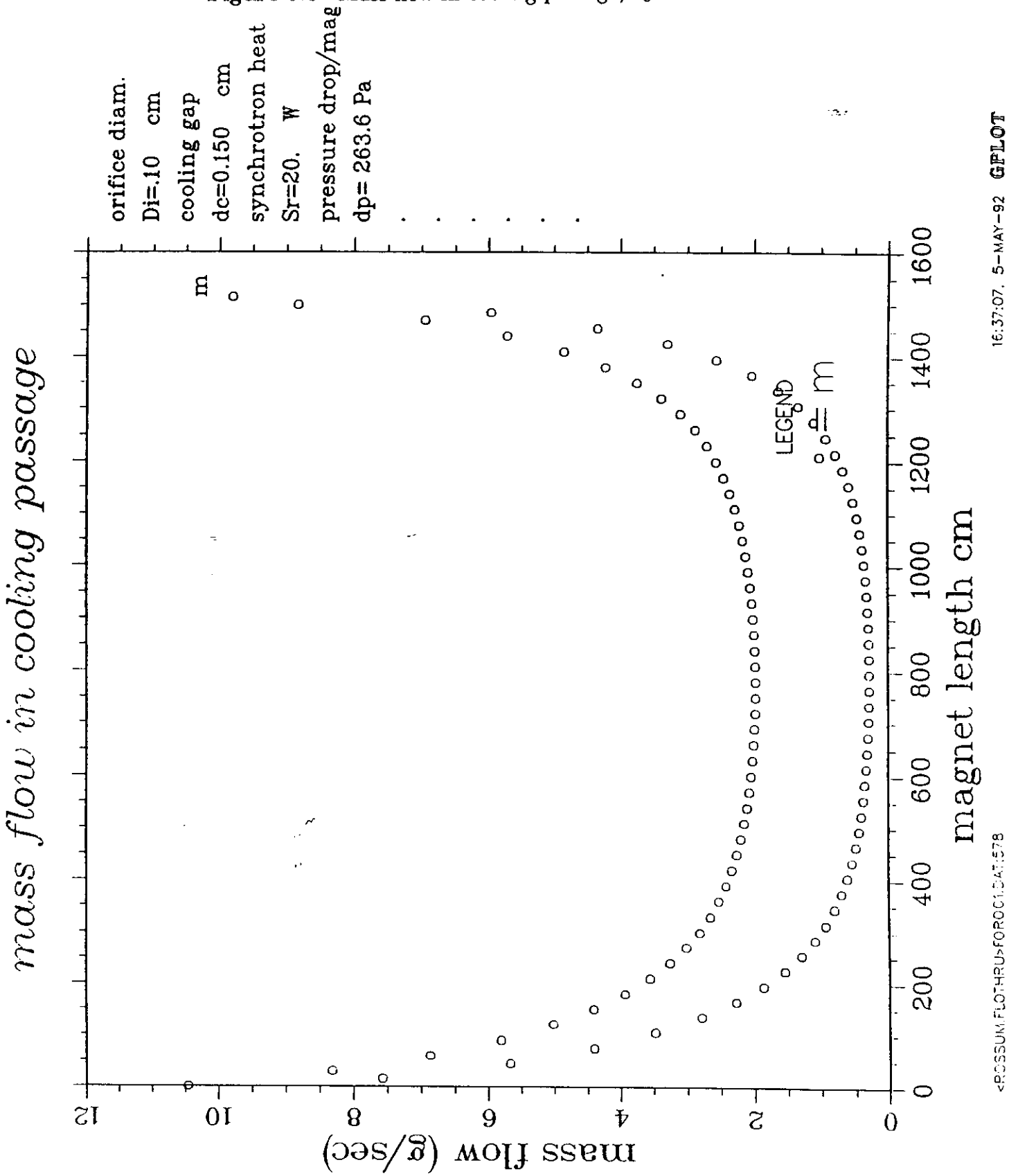

**Figure 3.10:** Temperature increase vs coil cooling gap, $d_c = 0.50$ cm

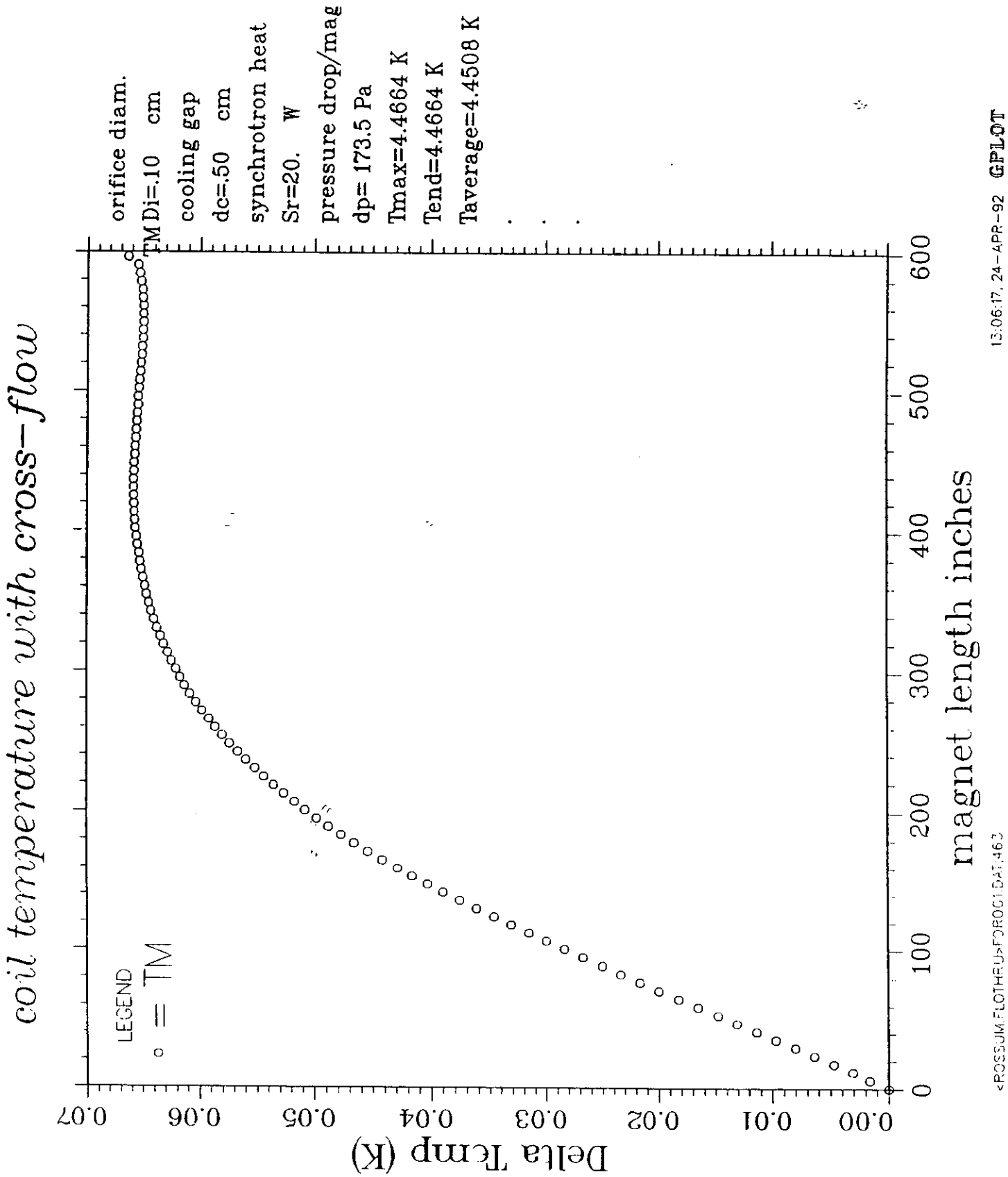

**Figure 3.11:** Mass flow in coil cooling passage $d_c = 0.50$ cm

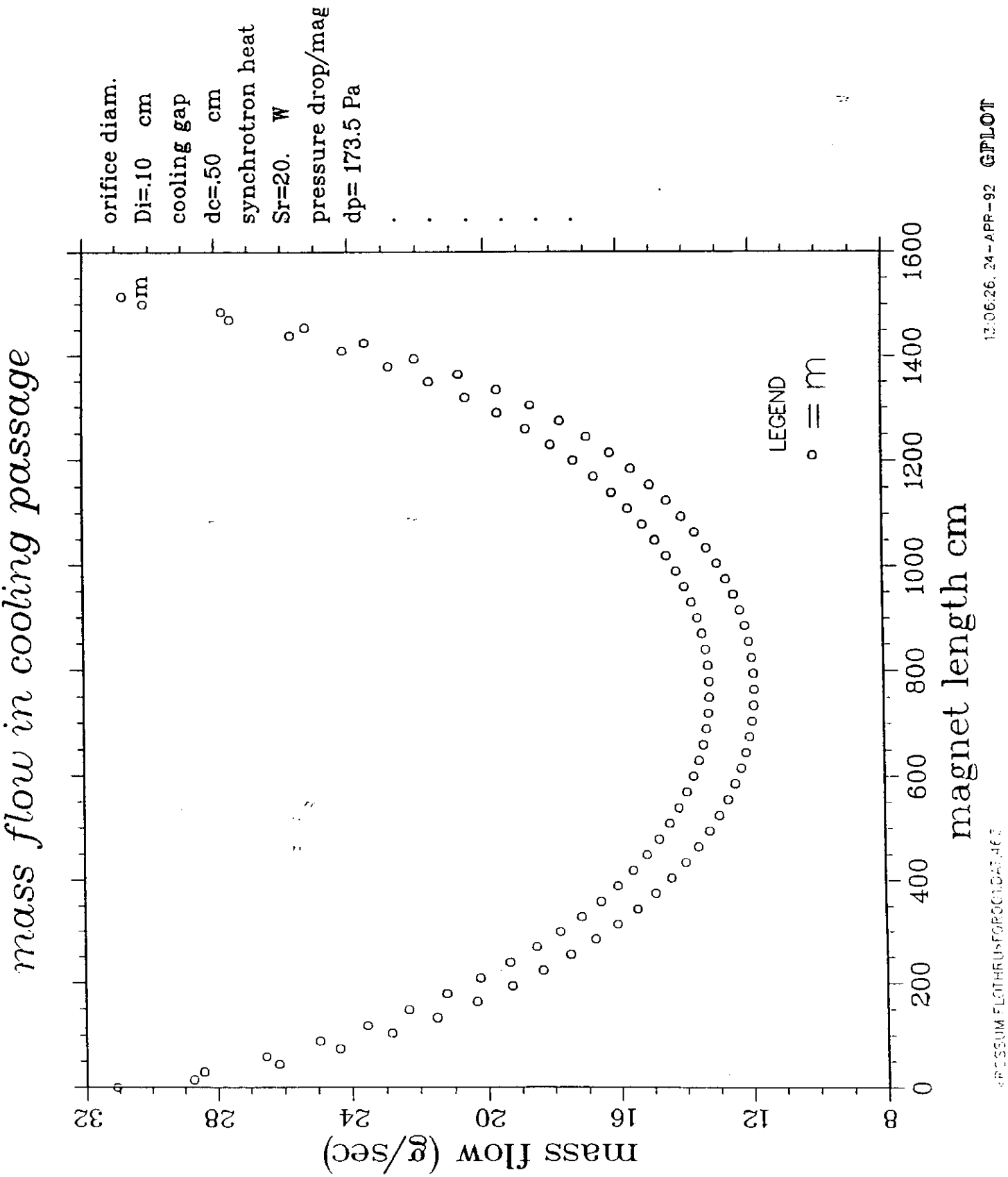

## 3.2 VARIATION OF ORIFICE SIZE

Maximum temperature increase versus orifice size is shown in Fig. 3.12 for a CCP gap of $d_c = 0.13$ cm and for $d_c = 0.50$ cm. Smallest temperature increases are expected to occur for closed orifices as is the case for $d_c = 0.50$ cm. With $d_c = 0.13$ cm this is not the case since temperature values decrease at first. Explanation for the irregularity in the data comes from the fact that these a peak values and a certain amount of error is introduced by the numerical procedure. Explanation for the decreasing trend in the initial part of the curve comes from the fact that there is more mass flow in the ccp for closed orifices and thus less input of cold helium from the upper bypass.

Table 1.1 and Fig. 3.12 show that the end orifices can be quite far open and still provide much improved cooling over the through–flow case. It can be noted that the two curves in Fig. 3.12 depart from each other as the orifice size approaches the bypass diameter in which case cross-flow cooling gives way to through–flow cooling and a large coil cooling passage becomes helpful in reducing temperatures.

## 3.3 PRESSURE DROP VERSUS TEMPERATURE INCREASE

The penalty incurred by a small temperature rise is an increased pressure drop. Although pressure drop specifications no not carry the same weight as temperature increase specifications, they are nevertheless a factor in choosing an orifice size. Fig. 3.13 shows pressure drops as functions of orifice size for the two ccp gaps considered in Fig. 3.12. Choosing an orifice size while giving consideration to temperature increases and pressure drops requirements can be done with the help of Fig. 3.14 and Fig. 3.15. Those figures are plots of temperature increases versus pressure drops (with $S_r = 30W$) for two ccp gaps presently considered.

## 3.4 VARIATION OF BYPASS DIAMETER

For a heat load of 20 W the maximum temperature increase is practically constant when the bypass diameter varies between 2.8 cm to 3.2 cm regardless of ccp gap. Since cross–flow relies on the mass flow (kept constant here) transfer of upper bypass to lower bypass, this is an expected result. For through flow however an increased bypass diameter would divert flow from the ccp where it is needed.

**Figure 3.12:** Temperature increase versus orifice with CCP gap $d_c = 0.13$ and $d_c = 0.5$ cm

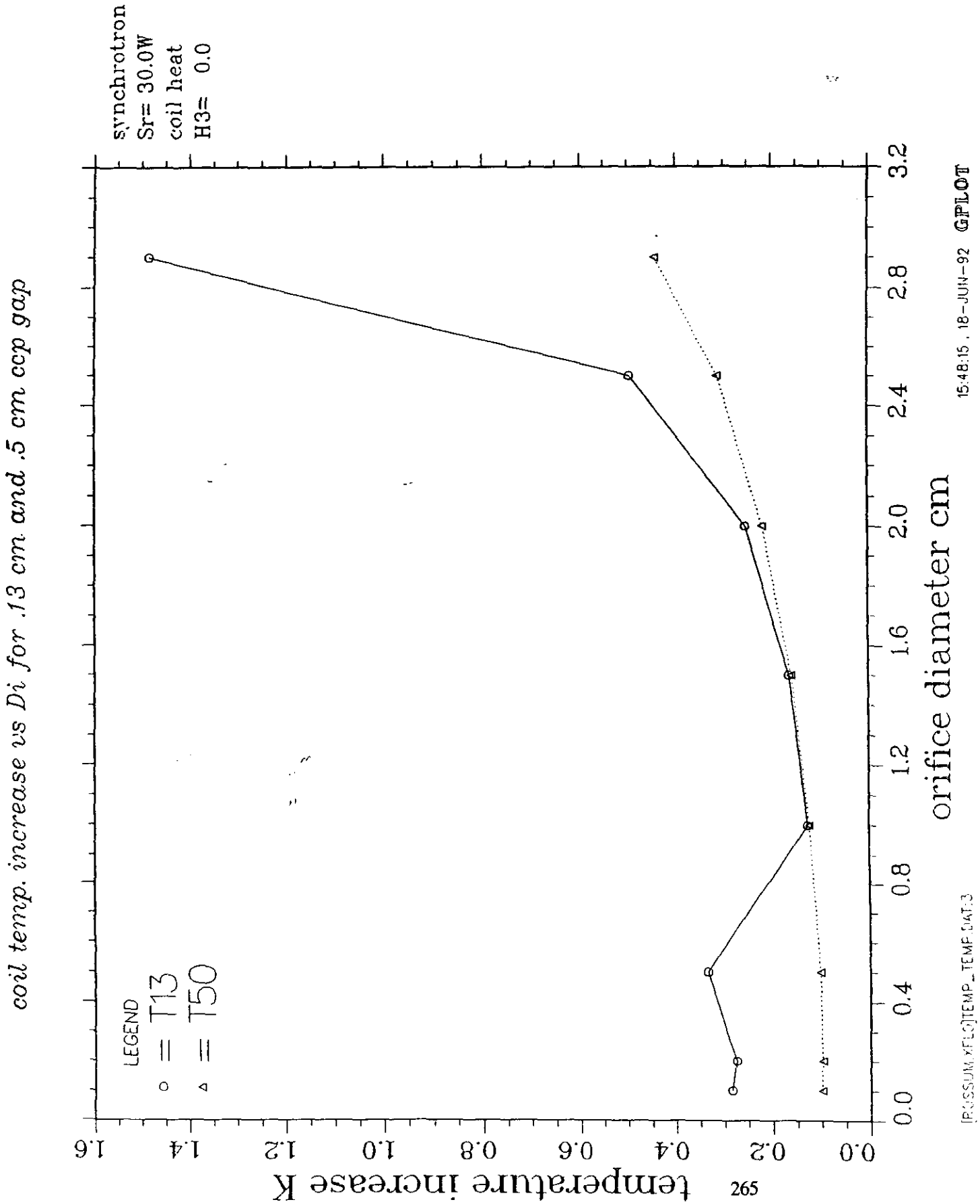

**Figure 3.13:** Pressure drop versus orifice with CCP gap $d_c = 0.13$ and $d_c = 0.5$ cm

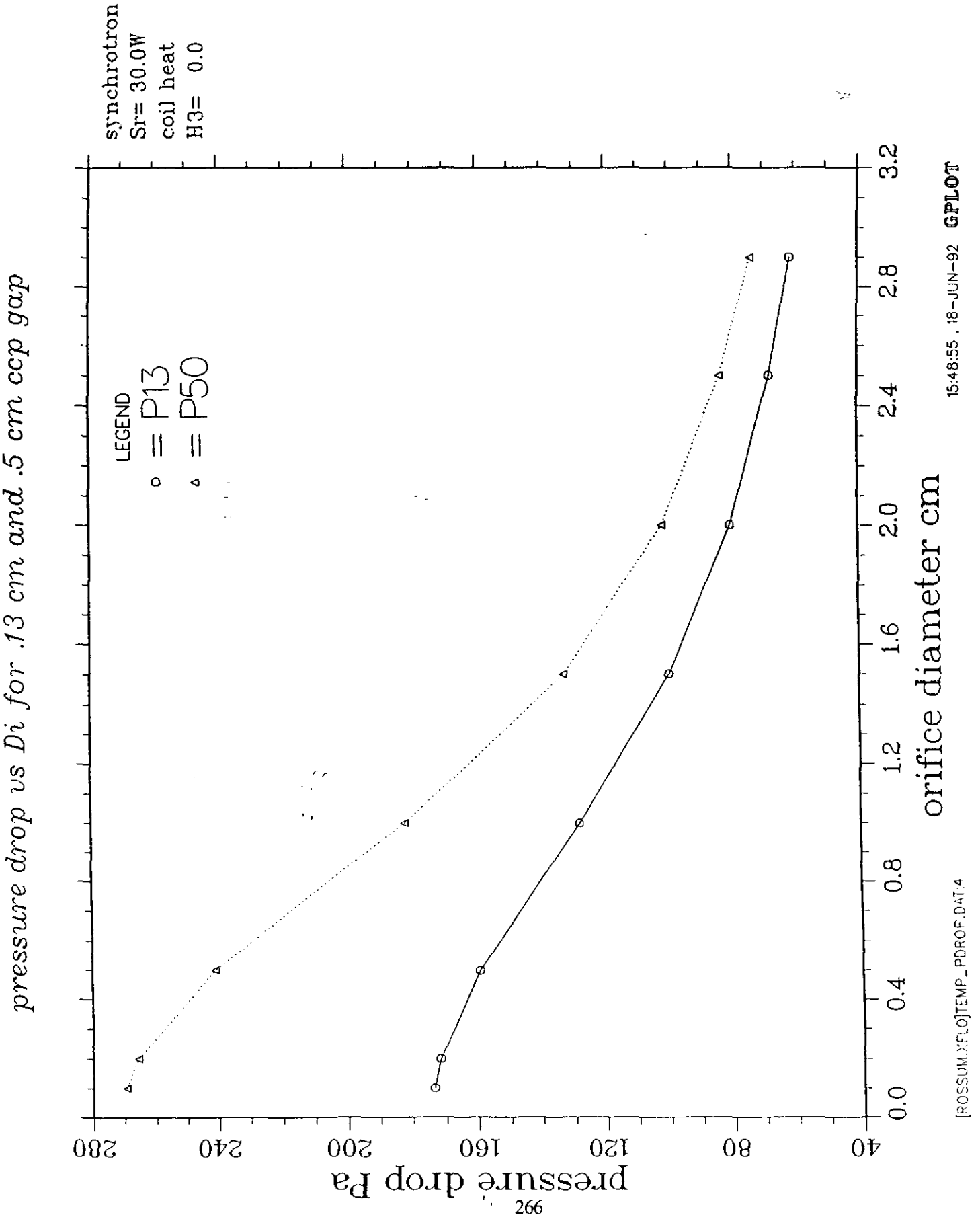

**Figure 3.14:** Temperature increase versus pressure drop with CCP gap $d_c = 0.13$

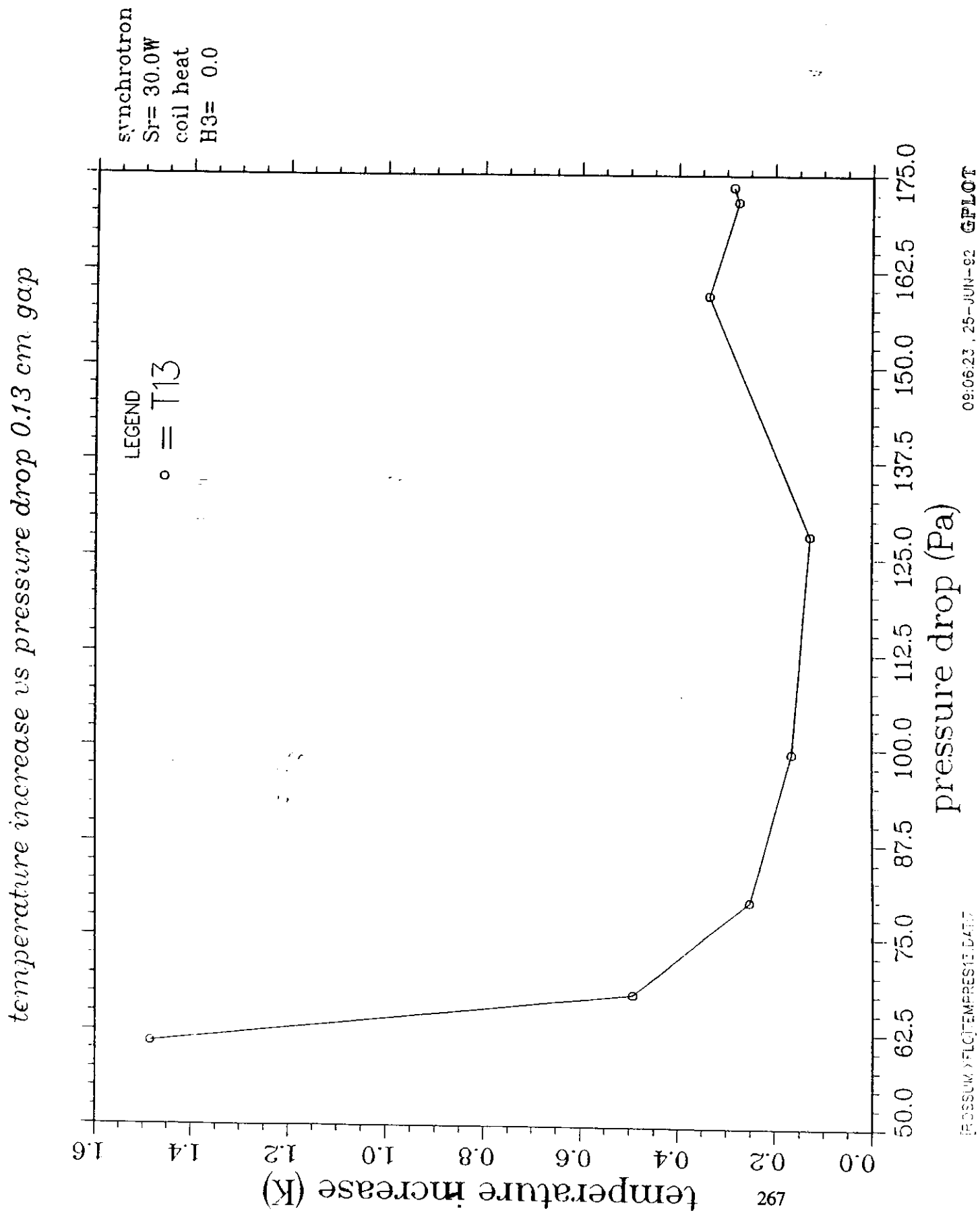

**Figure 3.15:** Temperature increase versus pressure drop with CCP gap $d_c = 0.50$ cm

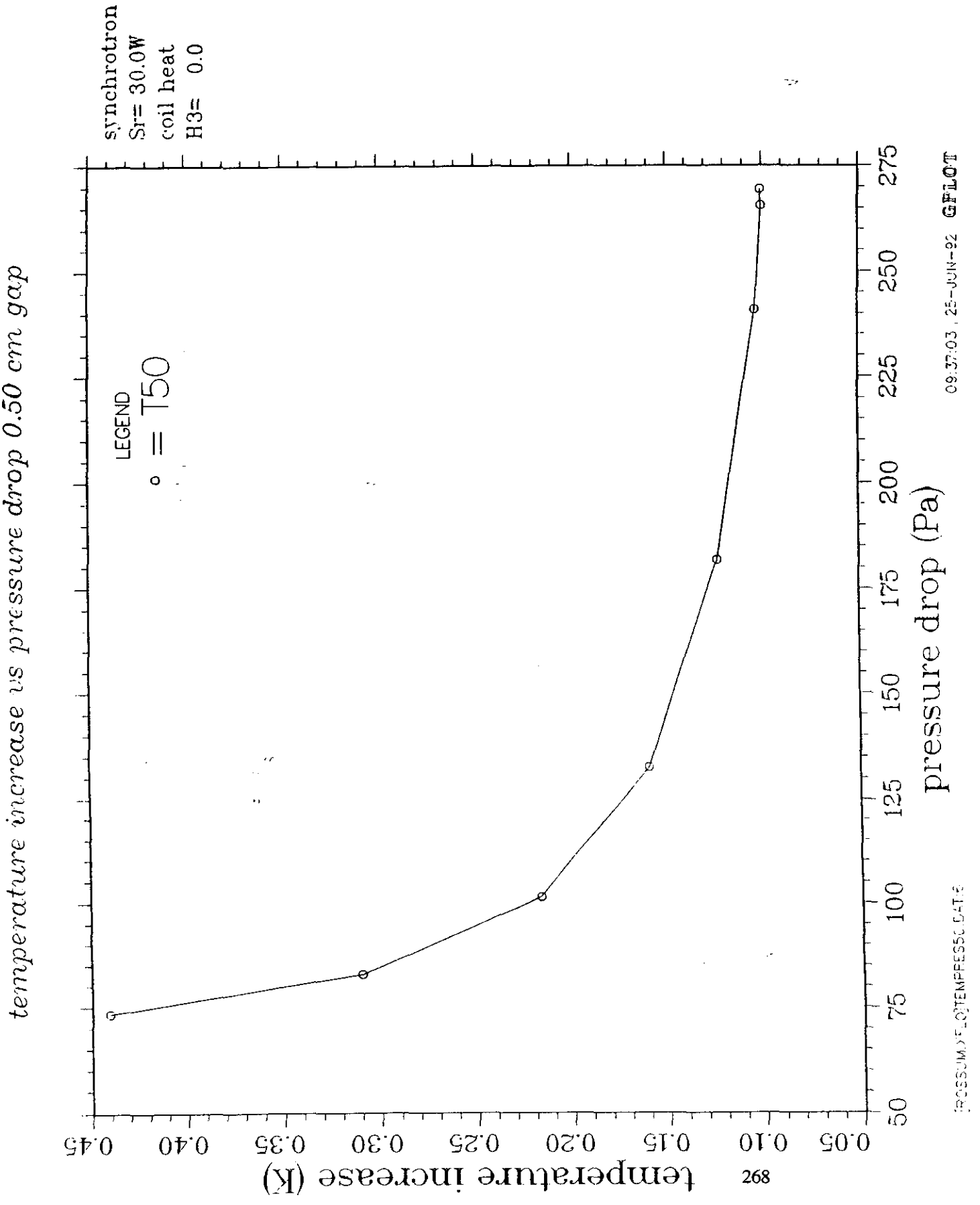

# 4. PRESSURES DURING QUENCH WITH CROSS–FLOW

## 4.1 DYNAMICS OF QUENCH PRESSURE DEVELOPMENT

The question as to how does the cross–flow arrangement affect pressures during a quench will now be discussed.

During a quench the stored magnetic field energy is dissipated by the coil which heats up. The heat is transferred to helium and yoke through insulation. The helium pressure rises in the cavities between coil conductor strands and is driven into the coil cooling passage through porosities in the insulation.

One might then ask at what helium pressure and temperature would equilibrium be reached at normal temperature without venting? Calculations show that

- the temperature of coil and helium in conductor cavities reaches 90 K (intermediate equilibrium until heat is exchanged), and the helium pressure in the cavities would reach $p_c = 370$ atm if the insulation had no porosities. It was estimated that above 100 atm the insulation may break.
- if the stored energy were distributed over coil and all helium in magnet: T=52 K, p=230 atm
- adding yoke mass: T=29 K , p=125 atm

These numbers show that venting must start regardless of the cooling method: sufficient venting is required to reduce these pressures below the design pressure of 20 atm. The quench duration is assumed to be between 0.15 to 0.3 sec (time for stored energy deposition in magnet coil). Calculations were performed under the following worst case assumptions. Many magnets quench simultaneously, such as with active quench protection. There is no venting during a quench for at least 0.15 sec (it takes time for vent valves to open). There is no mixing during a quench of helium from quenched magnets with the colder helium in interconnections. Modifications due to the presence of cross-flow cooling are introduced by reducing the total bypass cross–section by half.

The analytical model is described in "Derivations for calculation of helium pressure, Temperature, and mass flow distributions in superconducting magnets during quenches", R.P.Shutt, SSC Technical Note N0.59, SSC–N–266. The computer code developed for

CBA and RHIC models three partial differential equations for pressure, temperature and mass flow per passage. Here there are two passages : bypass and CCP. The model includes heat exchange functions, flow friction, flow acceleration, thermodynamic functions, helium properties, etc.

Some of the parameters used presently in the program for SSC magnets are listed below.

- Orifice size $D_i = 0$
- coil cooling passage area ar=7.07 $cm^2$
- total bypass equivalent cross–section a4=14.2 $cm^2$
- cross–section of cable insulation porosities ac=0.0008 $cm^2/cm$
- venting gap $\delta = 0.06$ $cm$ at coil poles (the actual value of 0.158 cm gives the same curves but with more oscillations).
- total interconnection length available at each end of a magnet $l_i$=20 cm
- average quench duration $\Delta q = 0.15$ $sec$
- average quench length in magnet $l_q$=magnet length; full length for active quench protection
- Kapton insulation thickness d=0.01 cm

## 4.2 QUENCH PRESSURE RESULTS

Values are shown at the center of the magnet where they are the highest, with the exception of the interconnect values where no mixing was assumed. Table 4.1 shows that there is little difference between magnets with and without cross–flow: CCP pressure is 16.3 versus 19 atm for instance. Orifices were almost completely closed in these computations. Since orifices could be larger the pressure difference could be decreased.

Pressure curves are almost constant with distance along the magnet by the time they have reached a plateau (this is not so at earlier times), Fig. 4.1 (through–flow) and Fig. 4.2 (cross–flow) show plots of CCP, bypass and interconnect pressures. The CCP pressure rises somewhat faster at first, then merges with the remaining two curves at 0.3 sec.

Pressures rise steeply after a quench, then the rise slows down as helium in the coil cooling passage is depleted

**Table 4.1:** Quench Pressures, Temperatures and Mass flows at time 0.87 sec

| variables | through–flow | cross–flow |
|---|---|---|
| coil temperature Ta (K) | 86.35 | 86.36 |
| bypass helium temperature Tb (K) | 12.75 | 12.06 |
| helium coil pressure pa (atm) | 16.32 | 19.05 |
| coil cooling pass. pr (atm) | 16.44 | 19.31 |
| bypass pressure p4 (atm) | 16.44 | 18.54 |
| CCP mass flow (g/sec) Mr | 85.65 | 115.63 |
| bypass mass flow (g/sec) M4 | 140.01 | -5.92 |
| interconnect press piu (atm) | 16.35 | 18.98 |
| interconnect temperature Tiu (K) | 5.025 | 5.152 |

Remembering that for the given calculations worse conditions were assumed, including no opening of vent valves for 0.9 sec, actual pressures will be considerably smaller when valves open at 0.3 sec. Quench pressures will be safe during and shortly after a quench after which venting must start regardless of cooling method used. After the quench helium temperature continues to rise and warm helium must flow through some adjacent magnets to reach vent valves. With cross–flow an additional vent valve may be necessary per half–cell because helium flow is impeded by orifices. Tests are needed to determine venting parameters. Calculations concerning needed number of valves are in progress.

**Figure 4.1:** Quench pressures with through-flow

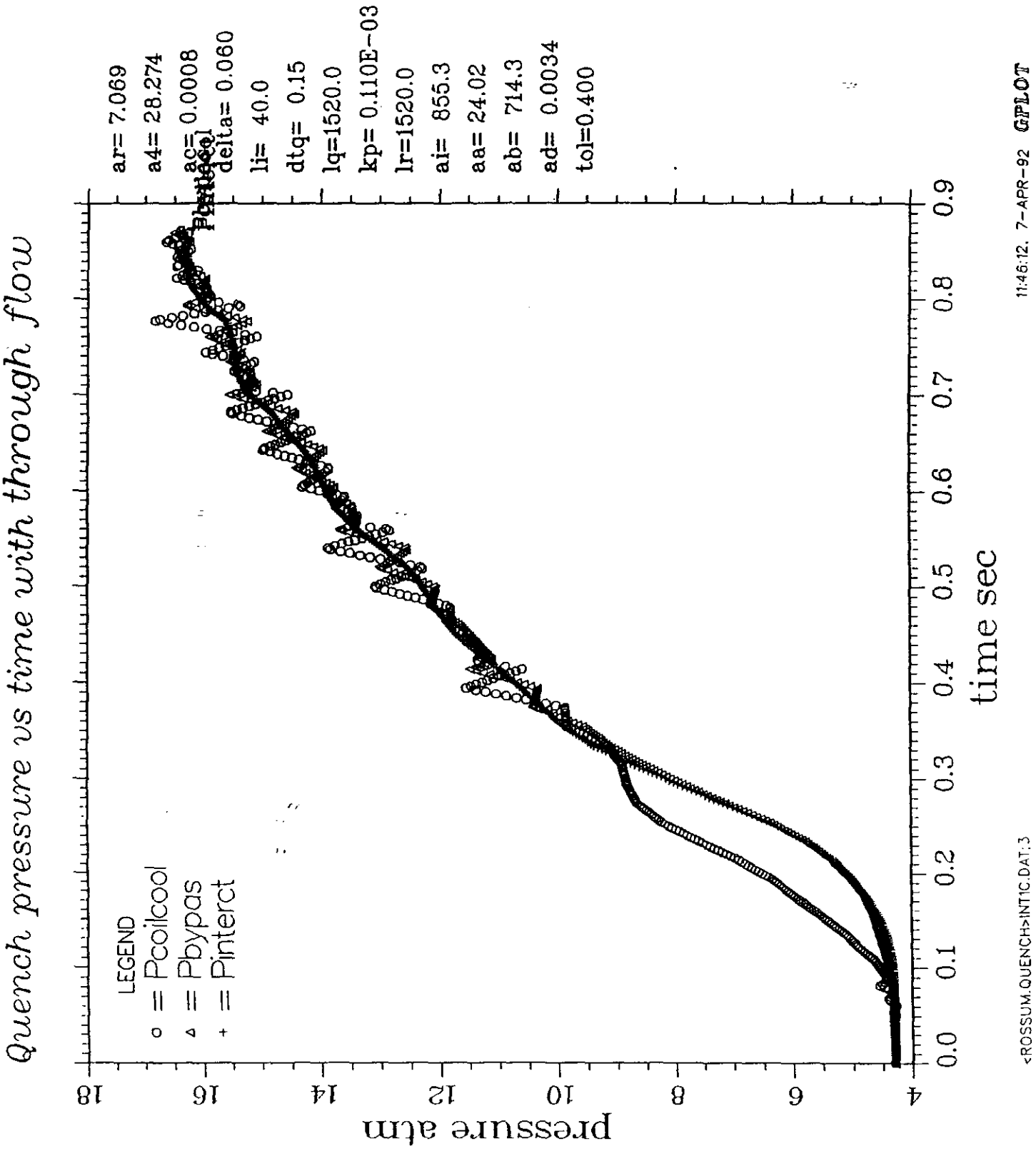

**Figure 4.2:** Quench pressures with cross–flow

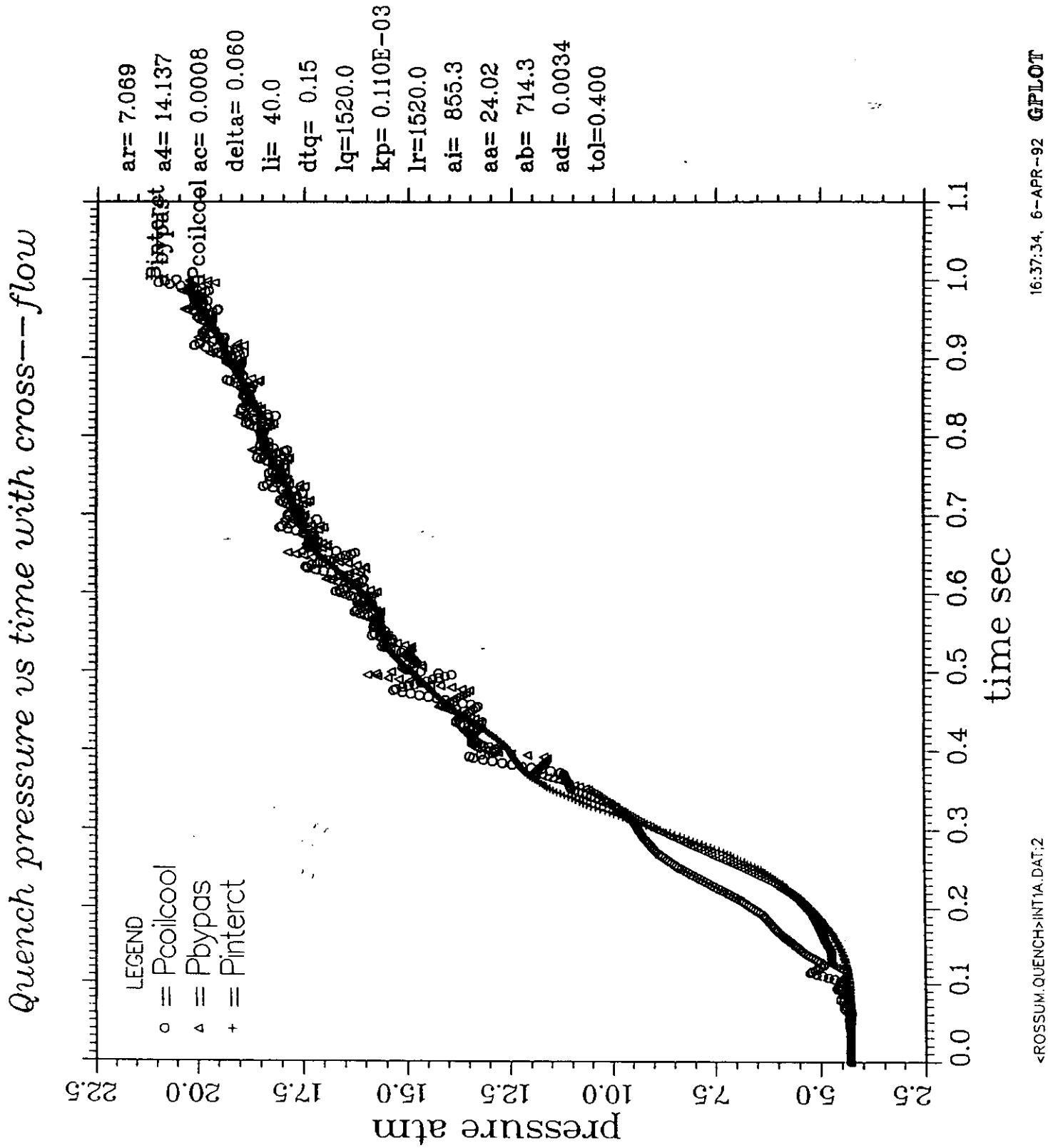

## 5. CROSS–FLOW COOLING IN HEB MAGNETS

Cross–flow cooling was implemented and successfully tested in SSC dipoles where the heat source is located inside the beam tube. The High Energy Booster magnets (HEB) are not subjected to heat load from synchrotron radiation but the heat source is located in the main coil as a result of eddy currents induced by rapid ramp rates. The question as to how efficient the cross–flow cooling is for this new case is addressed here. It can be anticipated that coil temperatures will be higher when heat is generated in the coil than when heat is generated in the beam tube. As the data pertaining to the details of the HEB cross–section were not made available to us at this time, the magnet analyzed here is an SSC dipole whose length is 13 m. The HEB magnet is currently thought to be 13 m long with a 0.30 cm coil cooling passage gap.

The effect of heat generated in the coil ($H_{coil}$) as opposed to heat on the beam tube ($S_r$) is shown in the table for three cases of coil cooling passage gap: $d_c = 0.13\ cm$, $d_c = 0.30\ cm$ and $d_c = 0.50\ cm$. Temperatures for the case where there is no cross–flow cooling (through–flow) are also included for comparison.

**Table 5.1:** Maximum coil temperature increases

| $d_c$ | $S_r$ | $H_{coil}$ | $\Delta T_{max}$ | $\Delta T_{max}$ |
|---|---|---|---|---|
| cm | W | W | cross–flow K | through–flow K |
| 0.13 | 20 | 0 | 0.207 | 0.818 |
| 0.13 | 0 | 20 | 0.294 | 0.822 |
| 0.30 | 20 | 0 | 0.065 | 0.552 |
| 0.30 | 0 | 20 | 0.164 | 0.591 |
| 0.50 | 20 | 0 | 0.069 | 0.327 |
| 0.50 | 0 | 20 | 0.159 | 0.394 |

The table shows that if the same amount of heat originates in the main coil instead of in the beam tube there is a noticeable temperature increase in the main coil. The

ratio of temperature increases is 1.4 for a narrow coil cooling passage gap of 0.13 cm, 2.5 for 0.30 cm and 2.3 for the large coil cooling passage gap of 0.50 cm. Cooling is greatly improved when the coil cooling passage gap increases from 0.13 cm to 0.3 cm and remains about the same for the larger value of 0.5 cm. This non–linear behavior is explained by the fact that there is a critical coil cooling passage gap around 0.14 cm below which some sections receive little or no mass flow leading to temperature peaks at those locations (see section 3.1). Above that critical value an increase in coil cooling gap does not reduce temperature for the cross–flow scheme. This is not the case for through–flow where temperatures decrease with increased coil cooling gap. In all cases cross–flow offers considerable improvement over through–flow since it lowers the temperature increase from 0.591 K to 0.164 K for the presently considered magnet. A more precise evaluation for the HEB magnets would require modeling the actual cross- -section and in particular the details of insulation between coil layers which are not present in the SSC dipole cross–section.

## 6. ORIFICES

Orifices are plates with circular holes placed at the two inlet bypass holes of the upper passage and at the two outlet bypass holes in the lower passage in order to induce a transverse pressure drop across the magnet. So far orifices were modeled using a modified form of simple head loss relations realizing that orifice theory would have to be used for later conversion of the simple head losses used so far. Simple head losses are insufficient if additional effects due to turbulence and radial flow velocity components at pipe transitions are to be considered. As such formulas were not found in the literature for the case of interest: a pipe terminated by an orifice and followed by a large interconnect volume, appropriate formulas were generated and are presented here.

For a pipe transition with an sudden contraction in diameter from $D_1$ to $D_2$ the pressure drop is (SSC Tech. Note # 91 SSC–N–753):

$$p_2 - p_1 = \frac{8\alpha M|M|}{\rho\pi^2 D_2^4}\left(1.5 - \frac{1}{2}\left(\frac{D_2}{D_1}\right)^2 - \left(\frac{D_2}{D_1}\right)^4\right), \alpha = 10^6$$

For a sudden pipe expansion from diameter $D_2$ to $D_3$ the pressure drop is:

$$p_3 - p_2 = \frac{8\alpha M|M|}{\rho\pi^2 D_2^4}\left(-\left(\frac{D_2}{D_3}\right)^2 + 2\left(\frac{D_2}{D_3}\right)^4\right)$$

It ensues that the total pressure drop for a pipe with a sudden contraction from $D_1$ to $D_2$ followed by a sudden expansion to $D_3$ is the sum of those two expressions:

$$\Delta P(M, D_1, D_2, D_3) = \frac{8\alpha M|M|}{\rho\pi^2 D_2^4}\left(1.5 - \frac{1}{2}\left(\frac{D_2}{D_1}\right)^2 - \left(\frac{D_2}{D_3}\right)^2 - \left(\frac{D_2}{D_1}\right)^4 + 2\left(\frac{D_2}{D_3}\right)^4\right)$$

The presence of an orifice in the bypass is treated here as a short pipe with a sudden contraction followed by a sudden expansion with the appropriate expressions for $D_1$, $D_2$, $D_3$. Values relevant to the upper bypass are identified by index k=1 while index k=2 is used to denote lower bypass values. Magnet ends are differentiated by the subscript i for inlet and e for exit of mass flow. Pressure drops at both ends of both passages for two cases of mass flow directions (positive an negative) can be inferred form the preceeding equation by using the appropriate values of $D_1$, $D_2$, $D_3$ as described in Table 5.1. $D$ is the bypass diameter, $D_{ik}$ is the inlet orifice diameter for passage k and $D_{ie}$ is the outlet orifice diameter.

**Table 6.1:** Pressure drop at bypass ends for upper passage (k=1) or lower passage (k=2)

| pressure drop | $M_k > 0$ | $M_k < 0$ |
|---|---|---|
| inlet | $\Delta P(M_k, \infty, D_{ik}, D)$ | $\Delta P(M_k, D, D_{ik}, \infty)$ |
| exit | $\Delta P(M_k, D, D_{ek}, \infty)$ | $\Delta P(M_k, \infty, D_{ek}, D)$ |

We will now compare the pressure drop at an orificed inlet to the pressure drop at an orificed outlet in order to determine by how much they differ. Let d denote the nondimensional orifice diameter $D_{i,e\ k}/D$ and $\Delta p$ denote the nondimensional pressure drop $\frac{\Delta P_{i,e\ k}}{\Delta P}$ where $\Delta P = \frac{1.5\times 8\alpha M|M|}{\rho\pi^2 D^4_{i,e\ k}}$ is the pressure drop form a large volume to a pipe of diameter $D_{i,e\ k}$. It follows from the above equations that comparing inlet to outlet pressure drops is achieved by comparing the following two nondimensional pressure drops: $\Delta p_i = 1 - \frac{4}{3}d^2 + \frac{4}{3}d^4$, $\Delta p_e = 1 - \frac{1}{3}d^2 - \frac{2}{3}d^4$. These formulas agree quite well with those found in the literature for related, but here not applicable, cases.) Fig. 6.1 which is a plot of $\Delta p_i, \Delta p_e$ versus d shows that

- Since the curves deviate considerably from the $\Delta p = 1$ line, there is an appreciable difference between orifice formulas and a simple head loss.
- Inlet and outlet pressure drops do not differ considerably for the range of values $0 \leq d \leq 0.7$.
- It appears that the simple average expression $(\Delta p_i + \Delta p_e)/2$ is adequate to treat both inlet and exit orifices. This would remove the complication of having to differentiate between inlet and outlet orifices. ( For instance if flow in magnets, as built, were to be reversed, orifices would also have to be exchanged.)
- Pressure drops diverge after d=0.7, thus the average pressure drop formula would not be applicable beyond d=0.7 or $D_{i,e\ k} = 2.03cm$ for the current bypass of D=2.9 cm.

**Figure 6.1:** Normalized pressure drop for inlet and exit orifices versus normalized orifice diameter

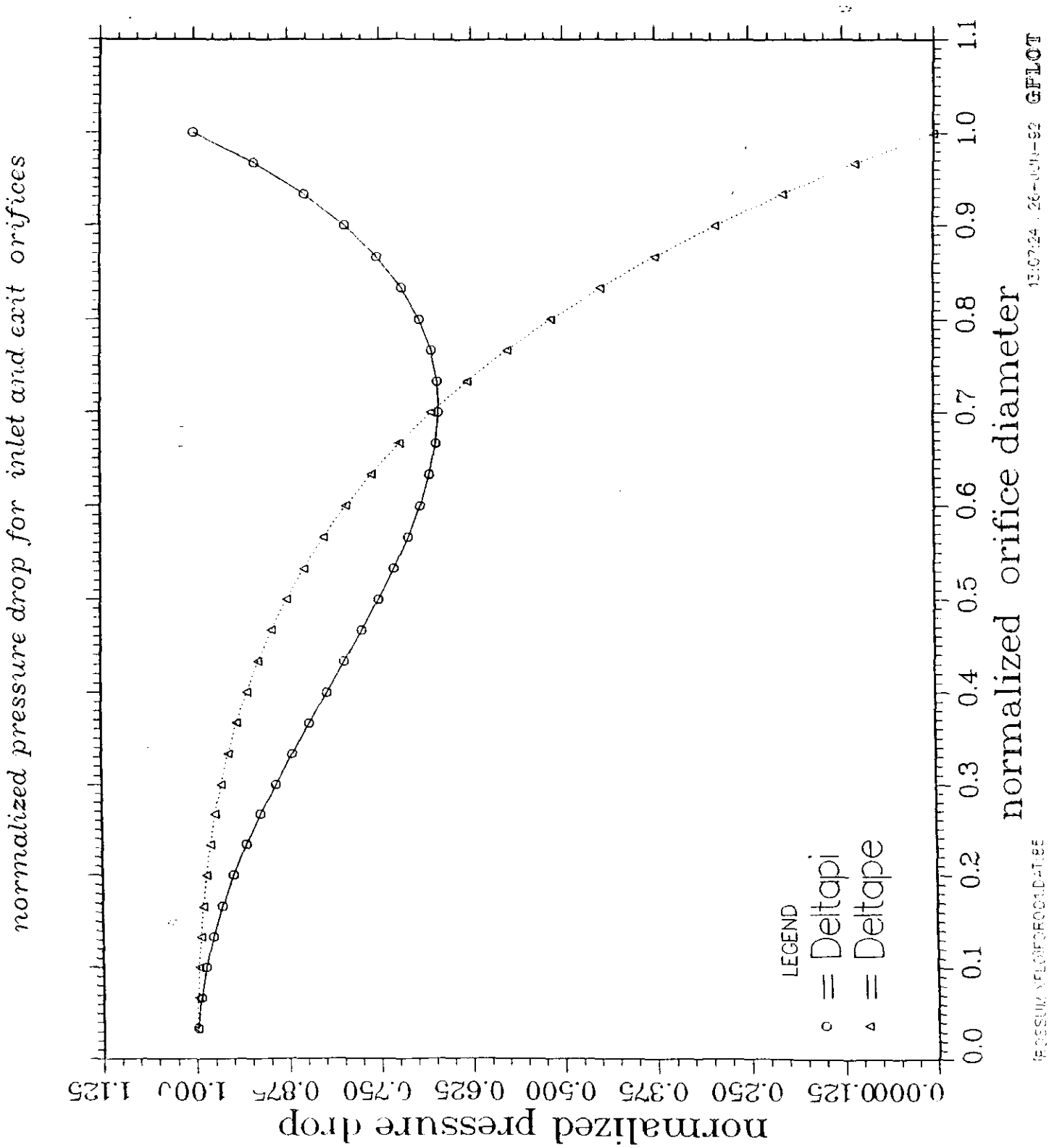

The preceeding discussion can be summarized as follows: pressure drops across inlet or exit orifices of diameter less than 2.03 cm (with D=2.9 cm) are given by:

$$\Delta p = \frac{1.5 \times 8\alpha M|M|}{\rho\pi^2 D^4_{i,e\ k}} \left(1 - \frac{2.5}{3}\frac{D^2_{i,e\ k}}{D^4} + \frac{1}{3}\frac{D^4_{i,e\ k}}{D^4}\right)$$

## Special attachments:

a) Beam tube support.
b) A.C. perfomance of SSC magnets.
c) Completion of thermal contraction measurements of some materials, used in magnet fabrication and assembly.

# CDM BEAM TUBE SUPPORT DESIGN & DEVELOPMENT STATUS

John Wohlwend

# CDM Beam Tube Support Issue History / Status

- SSCL evaluation of PDR baseline beam tube support design resulted in an action item to redesign the support.
  - PDR design was a coated metal spring that required additional Kapton ground plane insulation on the inside of the coil.
  - The additional ground plane insulation was unacceptable due to the possibility of blocking He flow in the annulus around the beam tube and due to possible restriction of He ventilation into the inner coil.
- GDSS re-visited the design criteria for the beam tube support
  - Stiffness criterial (required to support mole weight and provide sagitta)
  - Requirements to accomodate coil manufacturing tolerance and cooldown.
- GDSS evaluated a number of non-metallic support options and selected three options for further evaluation.
  - "Vespel" Clip
  - "Spiral Wrapped" Kapton ("Bullet Belt)
  - Corrugated Fiberglass Wrap
- Parts are being tested in a simulated coil test fixture that allows us to measure the stiffness of the support.

# SSC COIL CROSS SECTION
## Beam Tube/Coil-Collar Distance Variations

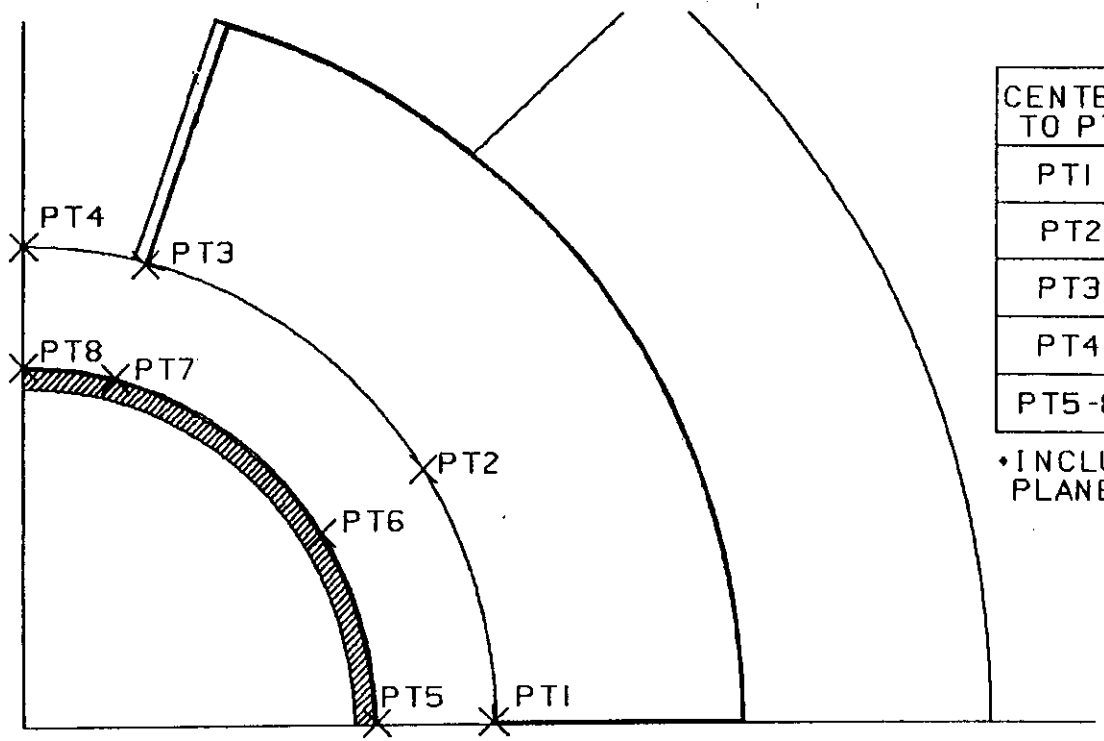


| CENTER TO PT | NOMINAL RADIUS |
|---|---|
| PT1 | 24.7452 * |
| PT2 | 24.8730 |
| PT3 | 24.7455 * |
| PT4 | 24.8700 |
| PT5-8 | 24.7452 |

*INCLUDES GROUND PLANE INSULATION

| PT TO PT | NOMINAL GAP | LARGEST GAP | SMALLEST GAP | DELTA DIFF |
|---|---|---|---|---|
| PT1 - PT5 | 6.0926 | 6.1474 | 5.9264 | 0.2210 |
| PT2 - PT6 | 6.2201 | 6.6452 | 6.2961 | 0.3491 |
| PT3 - PT7 | 6.0927 | 6.7789 | 6.3285 | 0.4504 |
| PT4 - PT8 | 6.2176 | 6.5077 | 6.1313 | 0.3764 |

ALL VALUES ARE IN MILLIMETERS

# CDM Beam Tube Support - Vespel SP-1 Clip Concept

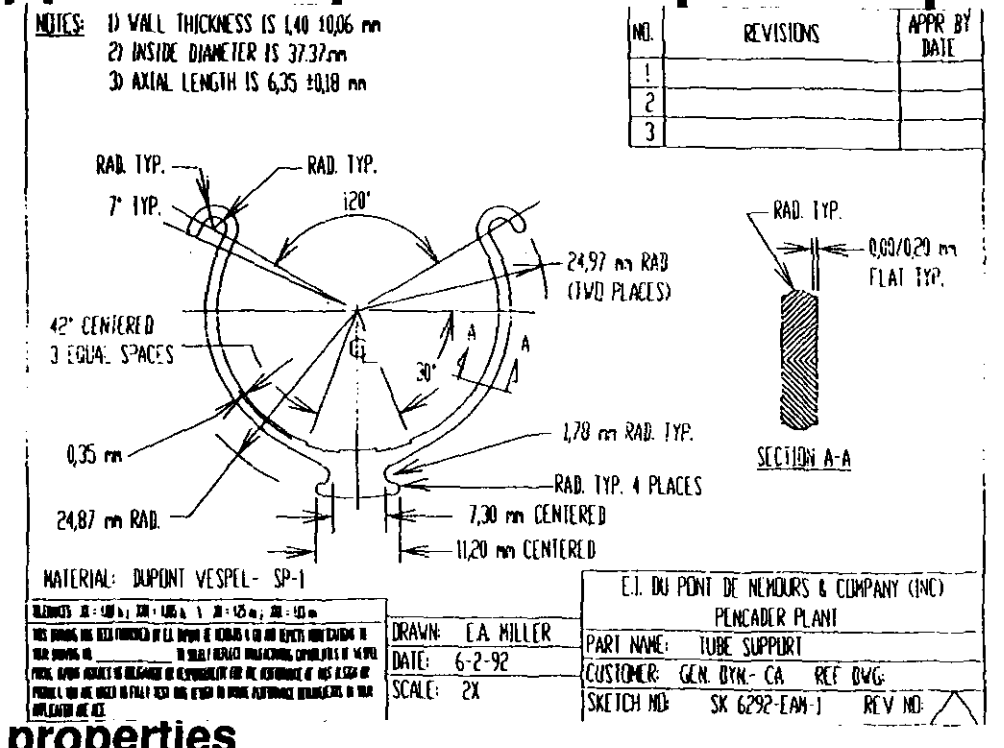


- Unfilled polyimide resin
- Low thermal expansion
- High creep resistance
- Demonstrated cryogenic properties
- High radiation resistance (1% wgt loss, 6.5% tensil srength loss)
- Easily formed or machined
- Low thermal conductivity (0.35 W/m Degrees K at 313 K)
- Bonded to beam tube insulation

# CDM Beam Tube Support - Glass Corrugation

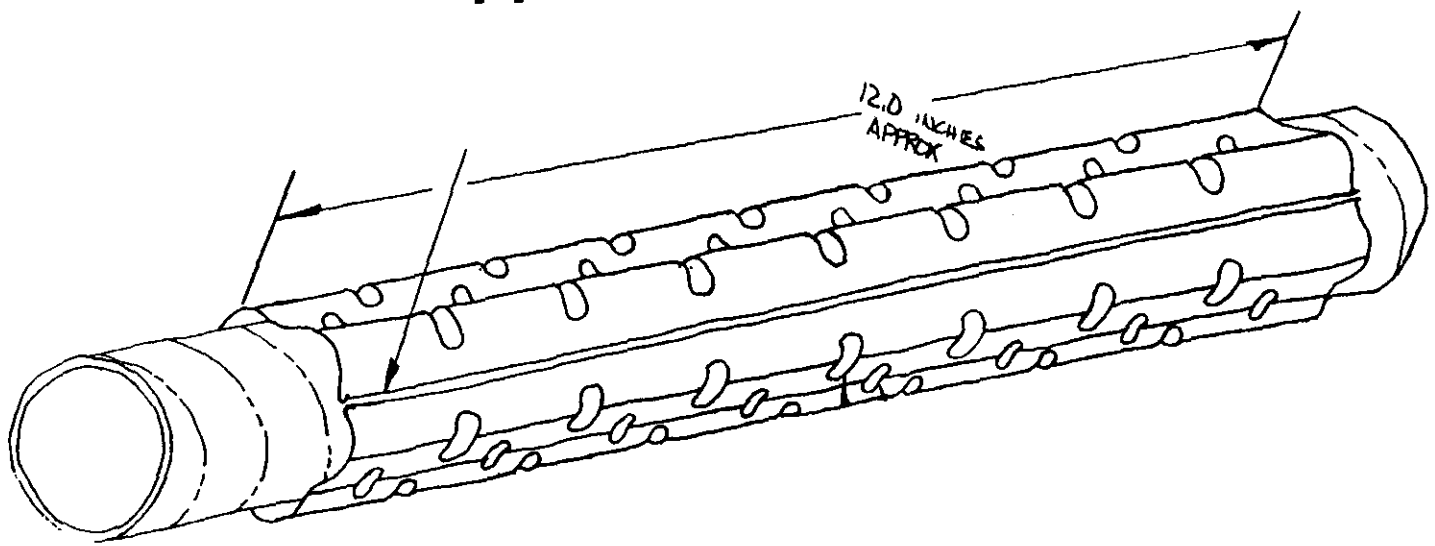


- Quadrax biaxial tape in polyetherimide / E-glass
- Properties need to be confirmed
- Easy to manufacture
- Easy to install
- Vendor: Quadrax

# CDM Beam Tube Support - Glass Corrugation

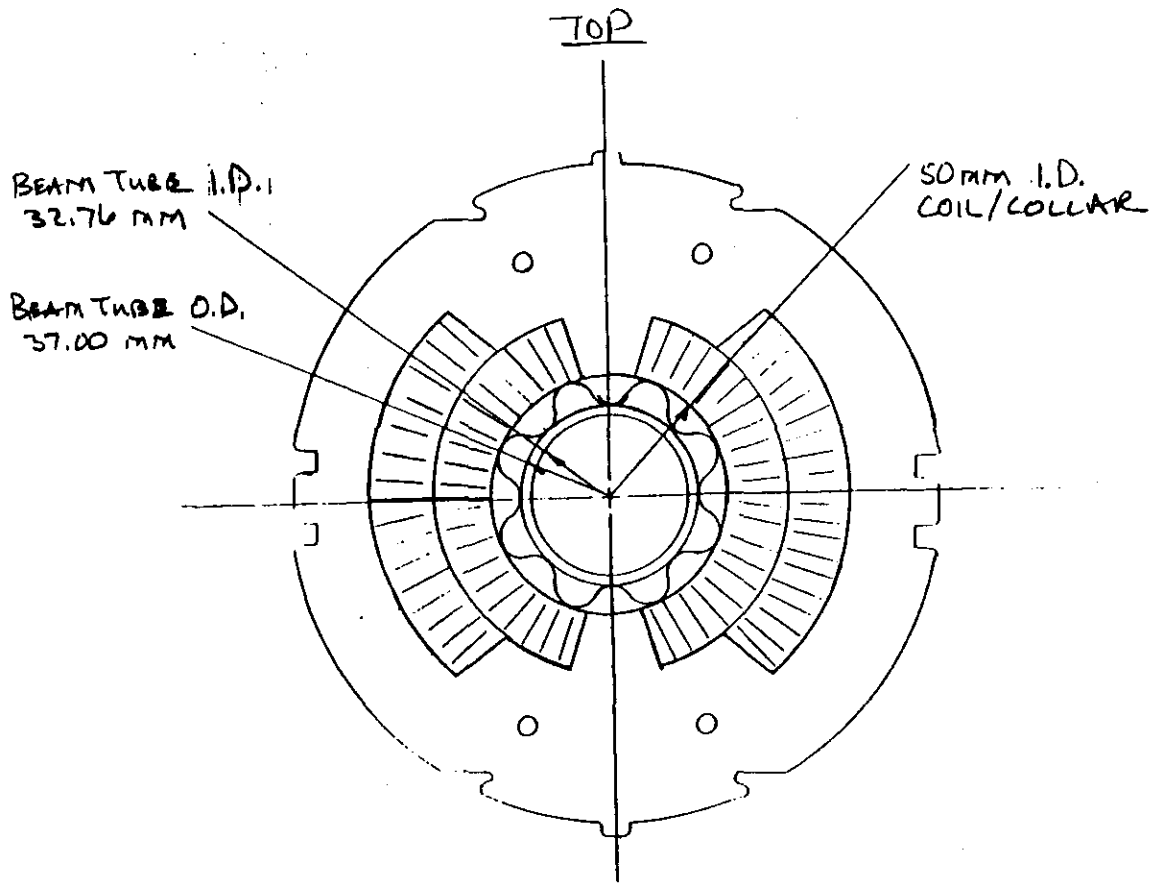

# CDM Beam Tube Support - Kapton Spiral Wrap

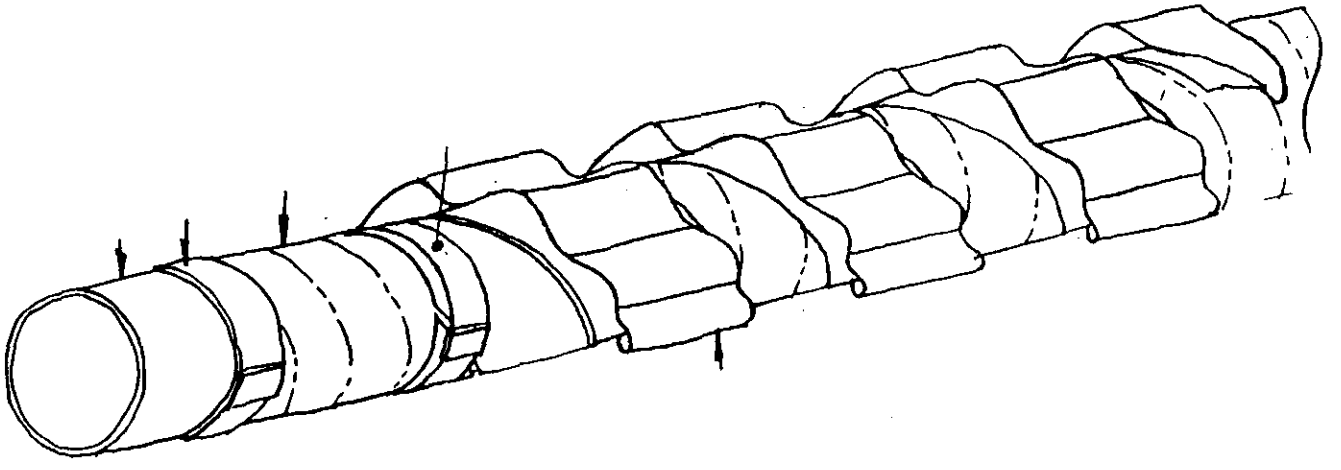

- 12 mil formed Kapton
- - Adhesively bonded to a 2 mil Kapton ribbon ("bullet belt")
- - "Button" strip bonded to beam tube Kapton
- Easily formed and assembled
- Demonstrated cryogenic / radiation resistance

Vendor: Astroseal

# CDM Beam Tube Support - Test Fixture

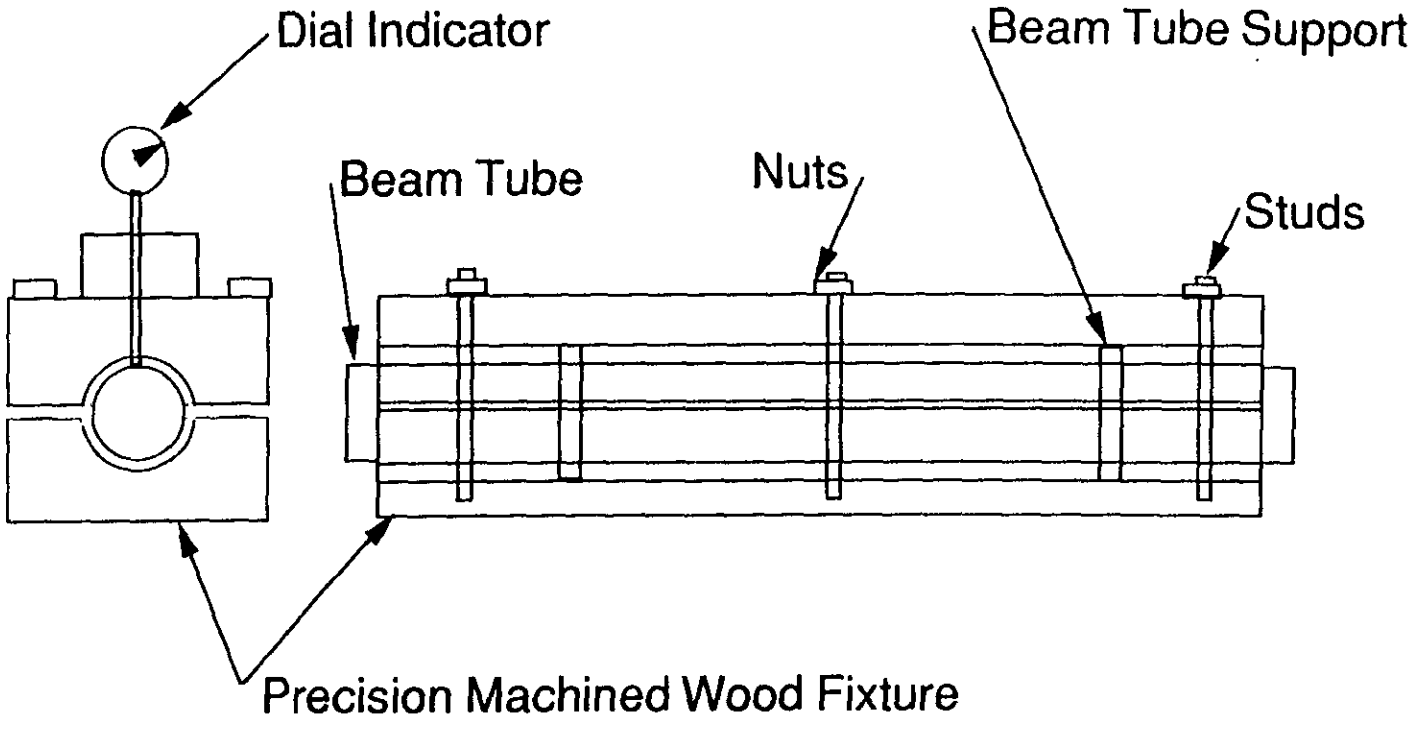

# AC Performance of SSC Magnets

R. Schermer, G. Snitchler, and B. Askel

# A. C. PERFORMANCE OF SSC MAGNETS

R. SCHERMER, G. SNITCHLER, B. AKSEL

- Introduction
- Experimental Results
- Analytic and Numerical Results
- Transverse Resistance in Cable
- Discussion: Is the problem serious?

  What can be done about it?



CEN Saclay 5/11/92

# THE SSC MAGNET COLLABORATION

- THERE ARE FIVE LABORATORIES INVOLVED IN THE MAGNET PROGRAM.

  FERMI NATIONAL ACCELERATOR LABORATORY (FNAL)

  BROOKHAVEN NATIONAL LABORATORY (BNL)

  SUPERCONDUCTING SUPERCOLLIDER LABORATORY (SSCL)

  LAWRENCE BERKELEY LABORATORY (LBL)

  C. E. N. SACLAY

- EACH LABORATORY USES A SLIGHTLY DIFFERENT MAGNET DESIGN; THE DIFFERENCES SHOULD NOT BE IMPORTANT FOR TODAY'S SUBJECT.

- EACH LABORATORY USES SLIGHTLY DIFFERENT MAGNET CONSTRUCTION TECHNIQUES; THE DIFFERENCES MAY BE IMPORTANT FOR TODAY'S SUBJECT.

- EACH LABORATORY USES SLIGHTLY DIFFERENT MAGNET TEST TECHNIQUES, TEST EQUIPMENT, AND CRYOGENIC CONDITIONS. DIFFERENCES IN CRYOGENICS ARE CERTAINLY IMPORTANT. DIFFERENCES IN TECHNIQUE JUST ADD TO THE CONFUSION; NOT ALL LABS CAN DO THE SAME KIND OF TESTS.

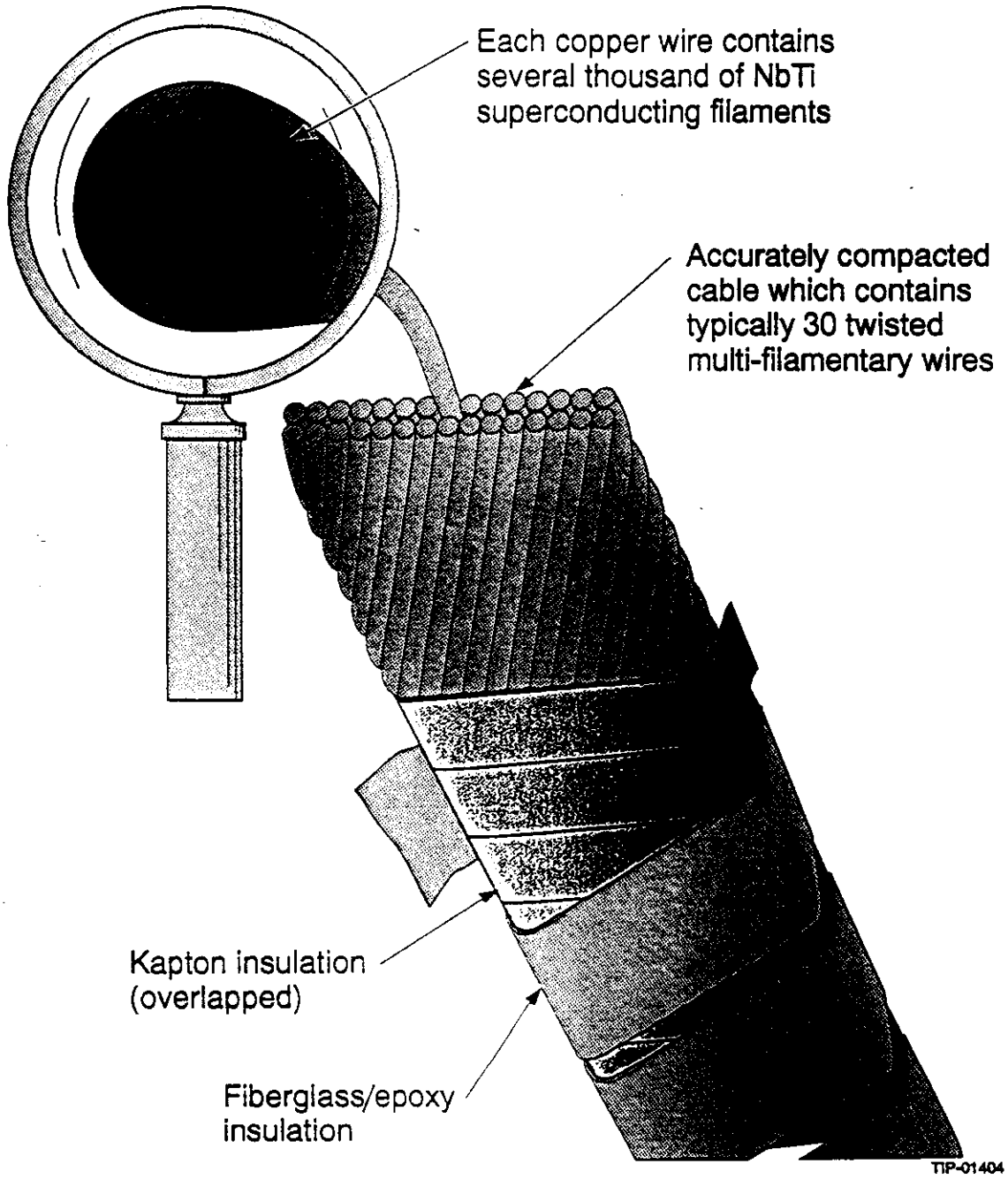
Each copper wire contains several thousand of NbTi superconducting filaments
Accurately compacted cable which contains typically 30 twisted multi-filamentary wires
Kapton insulation (overlapped)
Fiberglass/epoxy insulation
TIP-01404

## MAGNET CONSTRUCTION DIFFERENCES

- THERE ARE SEVERAL DIFFERENT VARIATIONS OF CONDUCTOR INSULATION:

  NUMBER OF KAPTON LAYERS

  WRAPPING PATTERN OF KAPTON

  TYPE OF ADHESIVE AND METHOD OF APPLICATION

  "ALL-KAPTON" VERSUS EPOXY/FIBERGLASS

- THERE ARE SEVERAL DIFFERENT VARIATIONS OF COIL CURING PARAMETERS (PRESSURE AND TEMPERATURE VERSUS TIME.) SOME OF THIS IS DUE TO THE DIFFERENT INSULATION AND ADHESIVE SCHEMES. SOME OF IT IS DUE TO PERSONAL PREFERENCES OF THE VARIOUS LABORATORIES.

- INSULATION AND COIL CURING DETAILS CAN EFFECT:

  HEAT TRANSFER TO THE HELIUM BATH

  AMOUNT OF HELIUM TRAPPED BETWEEN CONDUCTOR STRANDS

  RRR OF COPPER IN STRANDS

  TRANSVERSE RESISTANCE BETWEEN STRANDS

# CRYOGENIC CONDITIONS

- FOR TESTING SHORT MAGNETS (1-2 M LONG)

  FNAL, BNL. SSCL USES HELIUM BOILING AT 4.35 K IN A VERTICAL DEWAR.
  LBL USES HELIUM BOILING AT 4.35 K IN A HORIZONTAL DEWAR.

- FOR TESTING FULL LENGTH DIPOLES (15 M LONG) OR QUADRUPOLES (5 M LONG)

  BNL USES SUPERCRITICAL HELIUM AT 4 ATM. AND 4.35 K, FLOWING AT 150 G/S. ALL LONG MAGNETS BUILT BY BNL USE "CROSS-FLOW" COOLING.

  FNAL ALSO USES 4 ATM., 4.35 K HELIUM, BUT THE FLOW RATE IS ONLY 50 G/S.

  THE SSCL LONG MAGNET TEST FACILITY IS UNDER CONSTRUCTION; IT WILL FLOW 100 G/S OF SUPERCRITICAL HELIUM AT 4 ATM., 4.35 K.

LBL, WHICH ONLY TESTS LONG QUADRUPOLES, USES HELIUM BOILING AT 4.35 K IN A HORIZONTAL DEWAR

- WHEN WE PERFORM NUMERICAL COMPUTATIONS WE HAVE TO MODEL:

  POOL BOILING

  CROSS-FLOW COOLING

  STRAIGHT-THROUGH, OR "DIFFUSION" COOLING

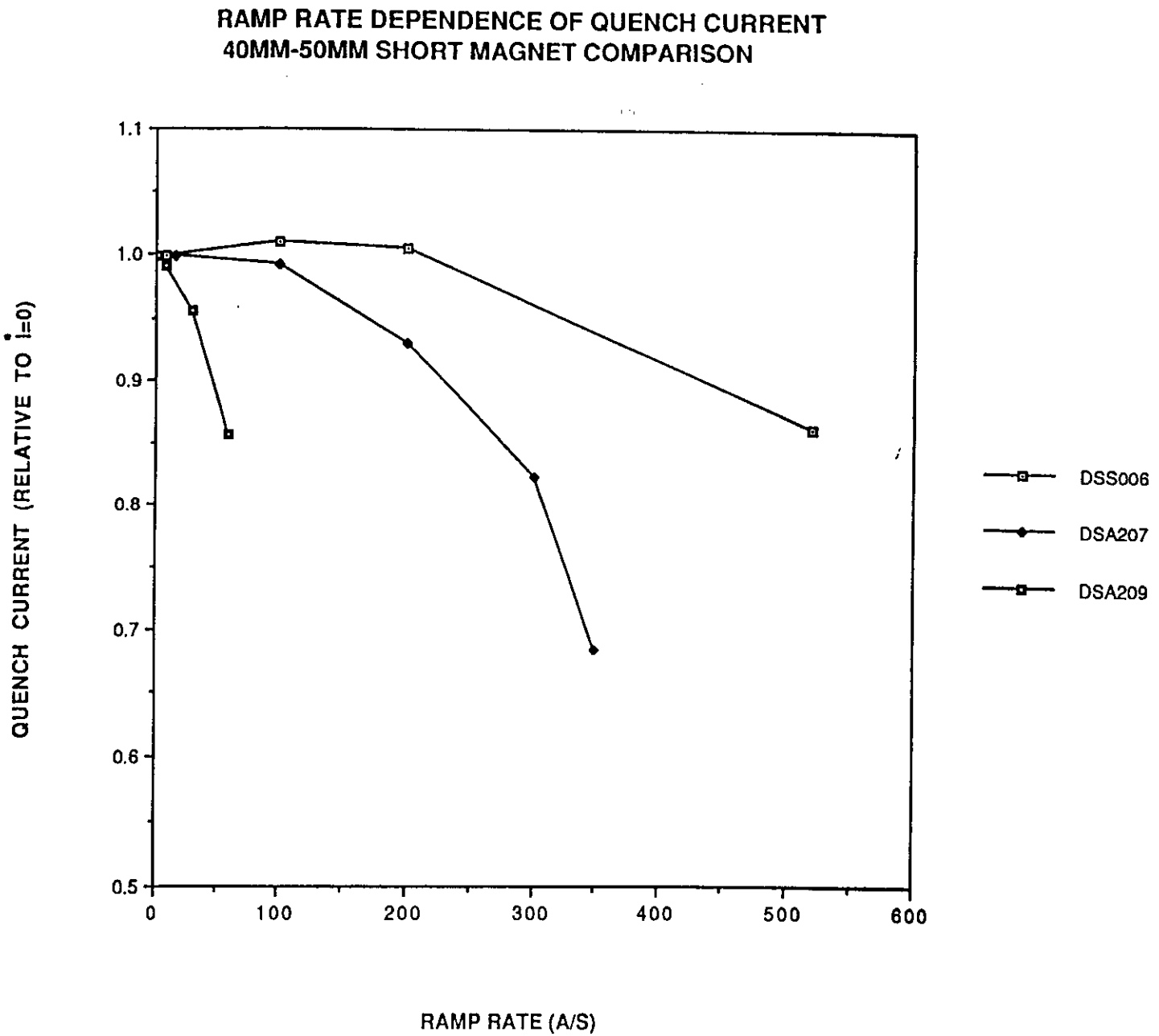
RAMP RATE DEPENDENCE OF QUENCH CURRENT
40MM-50MM SHORT MAGNET COMPARISON
QUENCH CURRENT (RELATIVE TO İ=0)
1.1
1.0
0.9
0.8
0.7
0.6
0.5
0
100
200
300
400
500
600
RAMP RATE (A/S)
DSS006
DSA207
DSA209

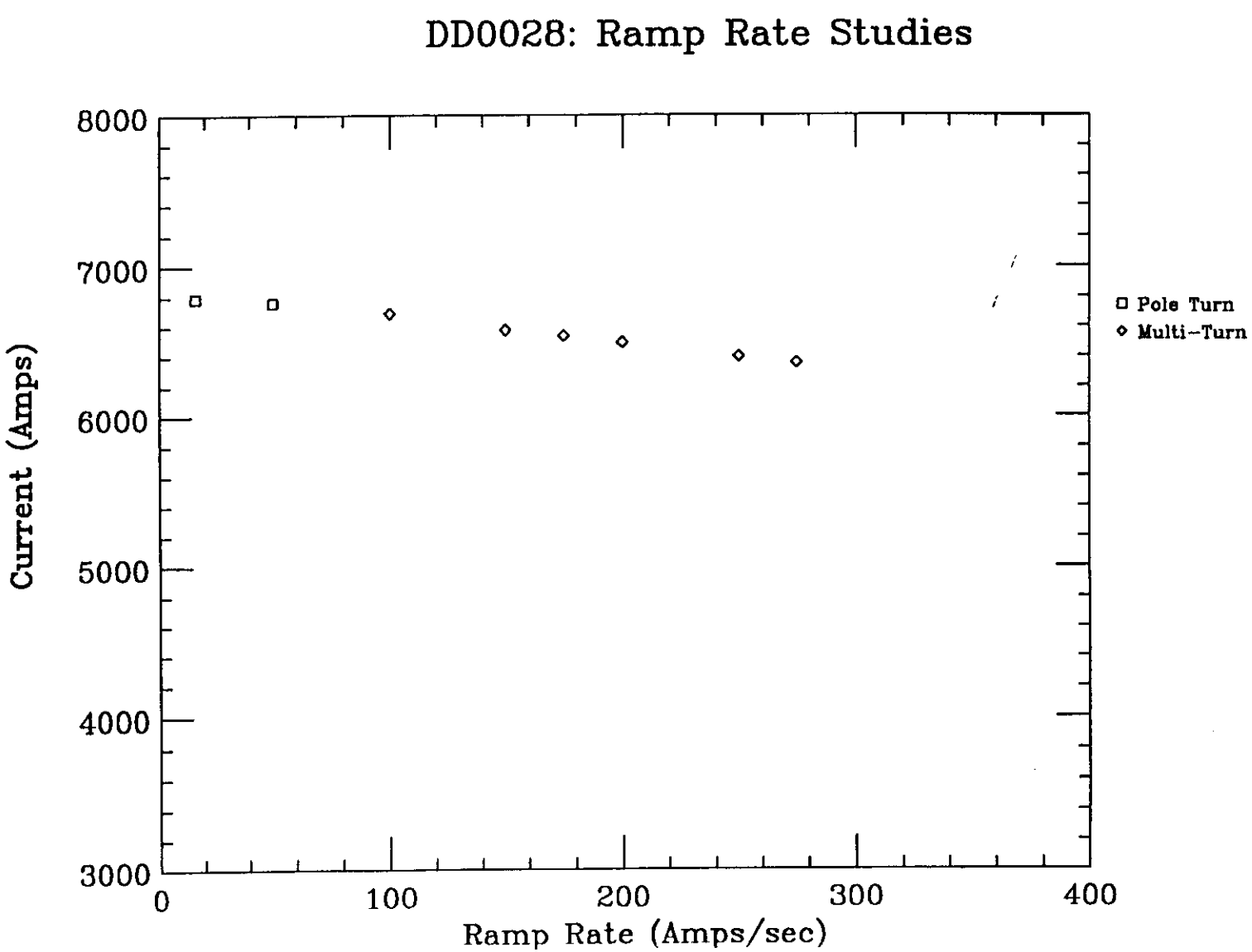
DD0028: Ramp Rate Studies
Current (Amps)
8000
7000
6000
5000
4000
3000
0
100
200
300
400
Ramp Rate (Amps/sec)
Pole Turn
Multi-Turn

# SHORT DIPOLE RAMP RATE DEPENDENCE

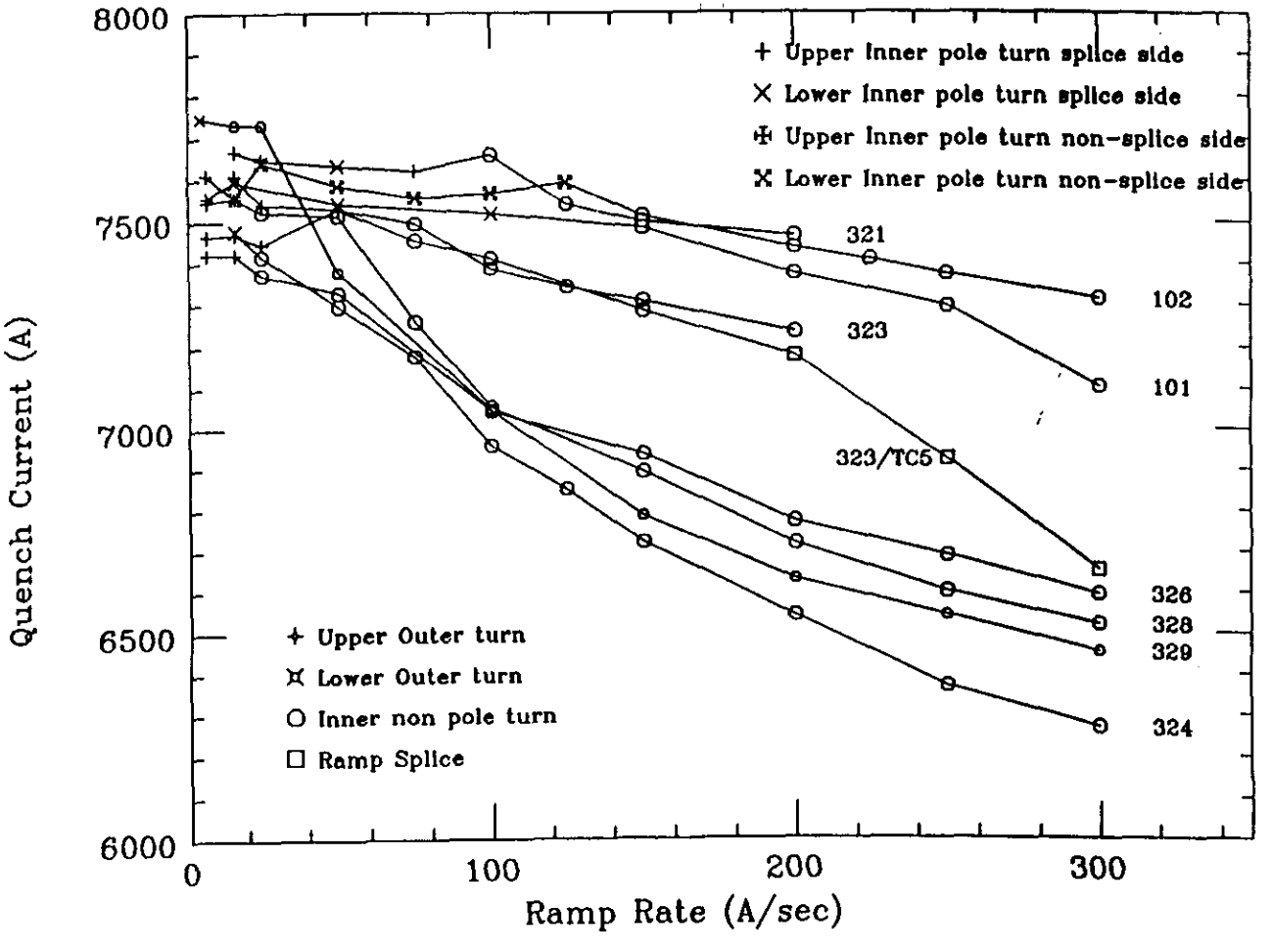

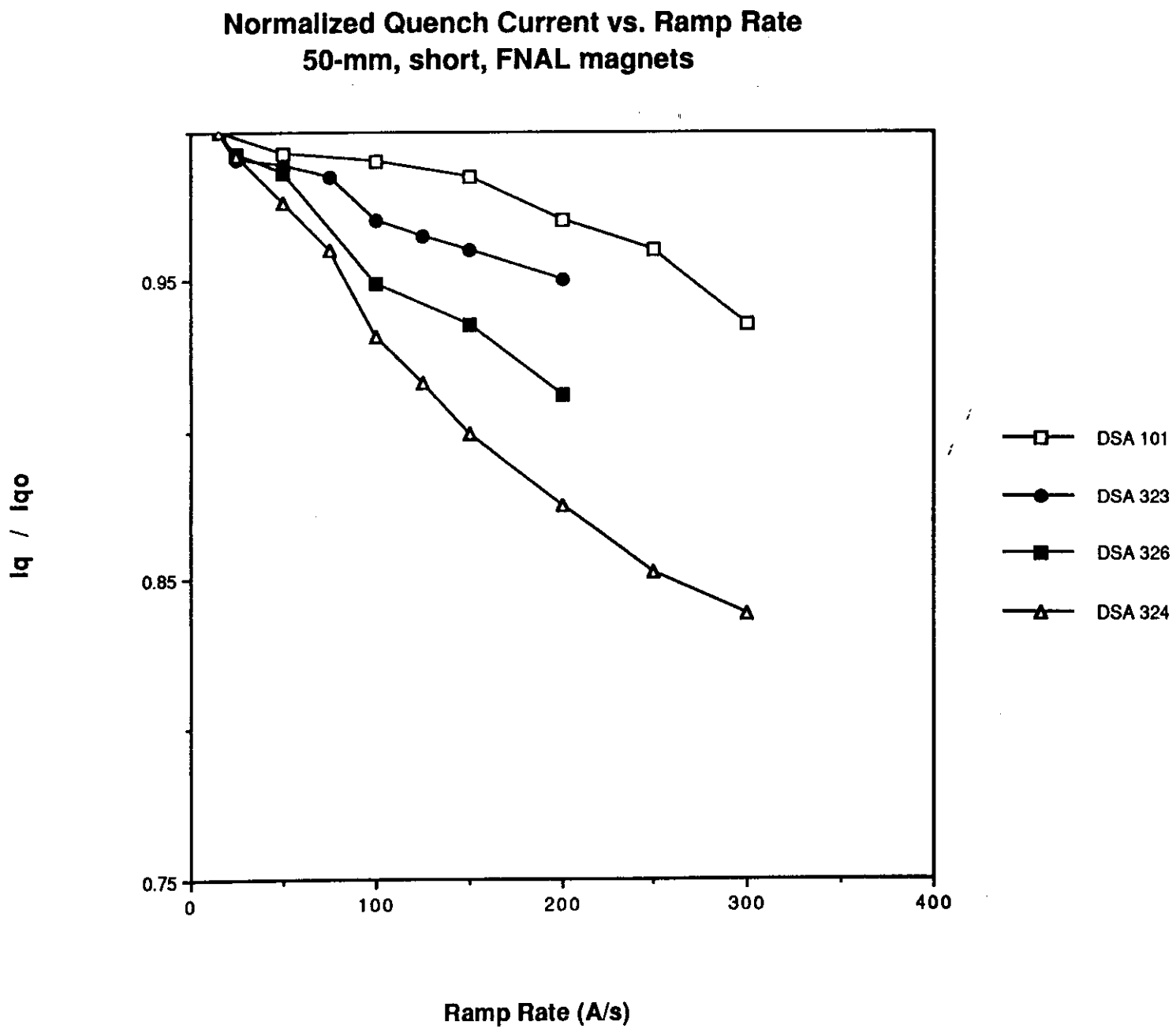
Normalized Quench Current vs. Ramp Rate
50-mm, short, FNAL magnets
Iq / Iqo
0.75
0.85
0.95
0
100
200
300
400
Ramp Rate (A/s)
DSA 101
DSA 323
DSA 326
DSA 324

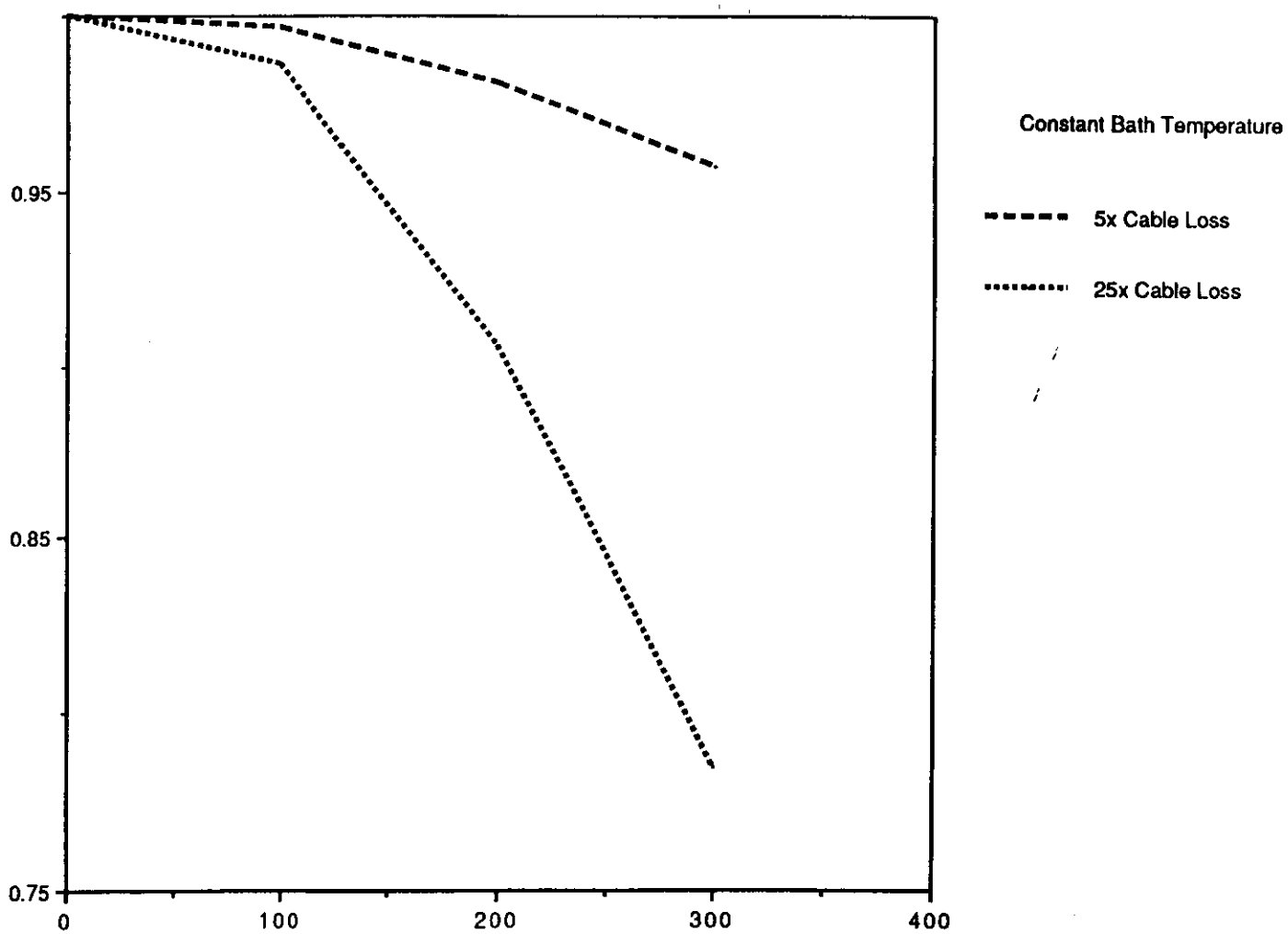
Constant Bath Temperature
5x Cable Loss
25x Cable Loss
0.95
0.85
0.75
0
100
200
300
400

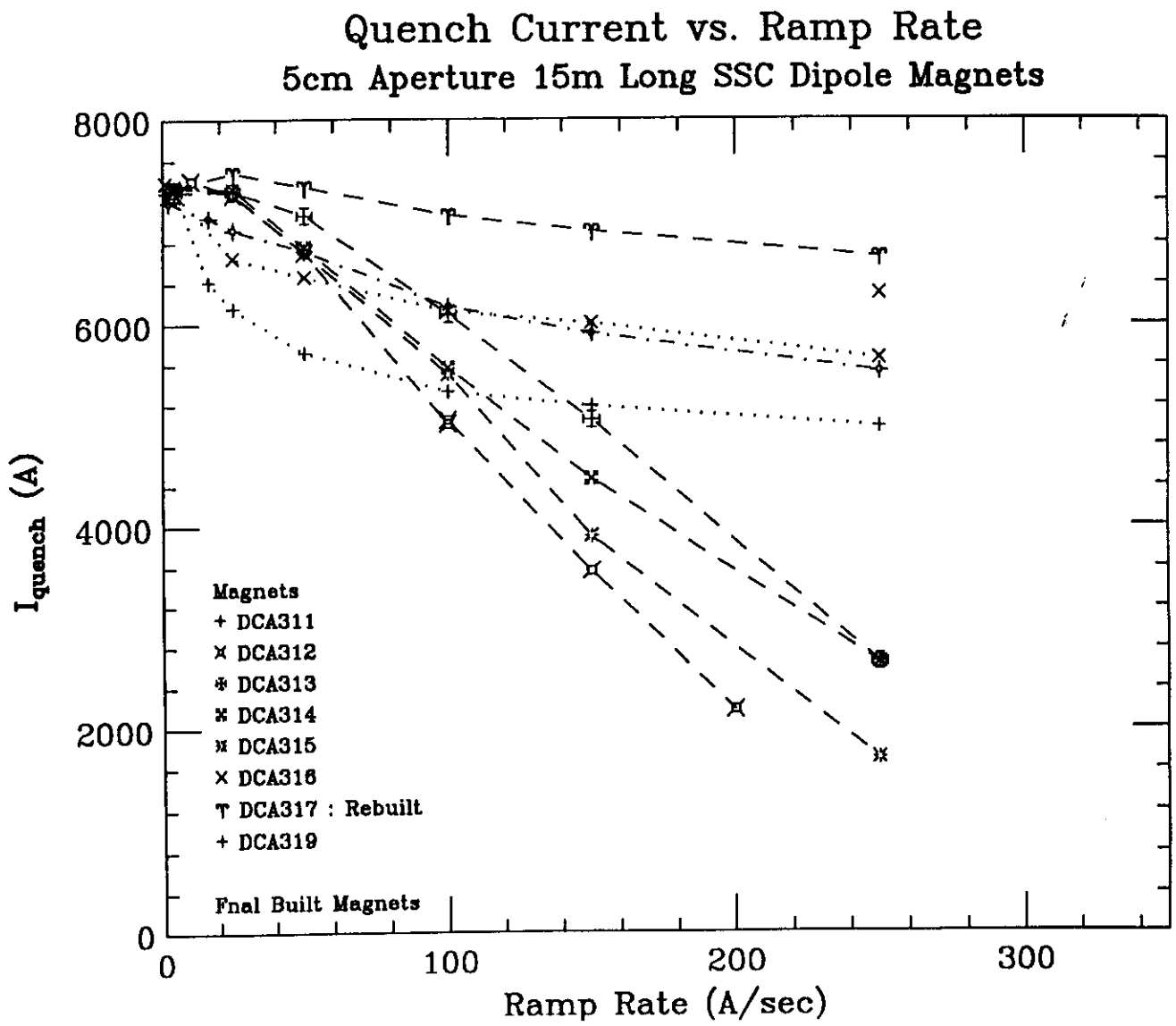
Quench Current vs. Ramp Rate
5cm Aperture 15m Long SSC Dipole Magnets
8000
6000
4000
2000
0
0
100
200
300
Ramp Rate (A/sec)
I_quench (A)
Magnets
+ DCA311
DCA312
DCA313
DCA314
DCA315
DCA316
DCA317 : Rebuilt
+ DCA319
Fnal Built Magnets

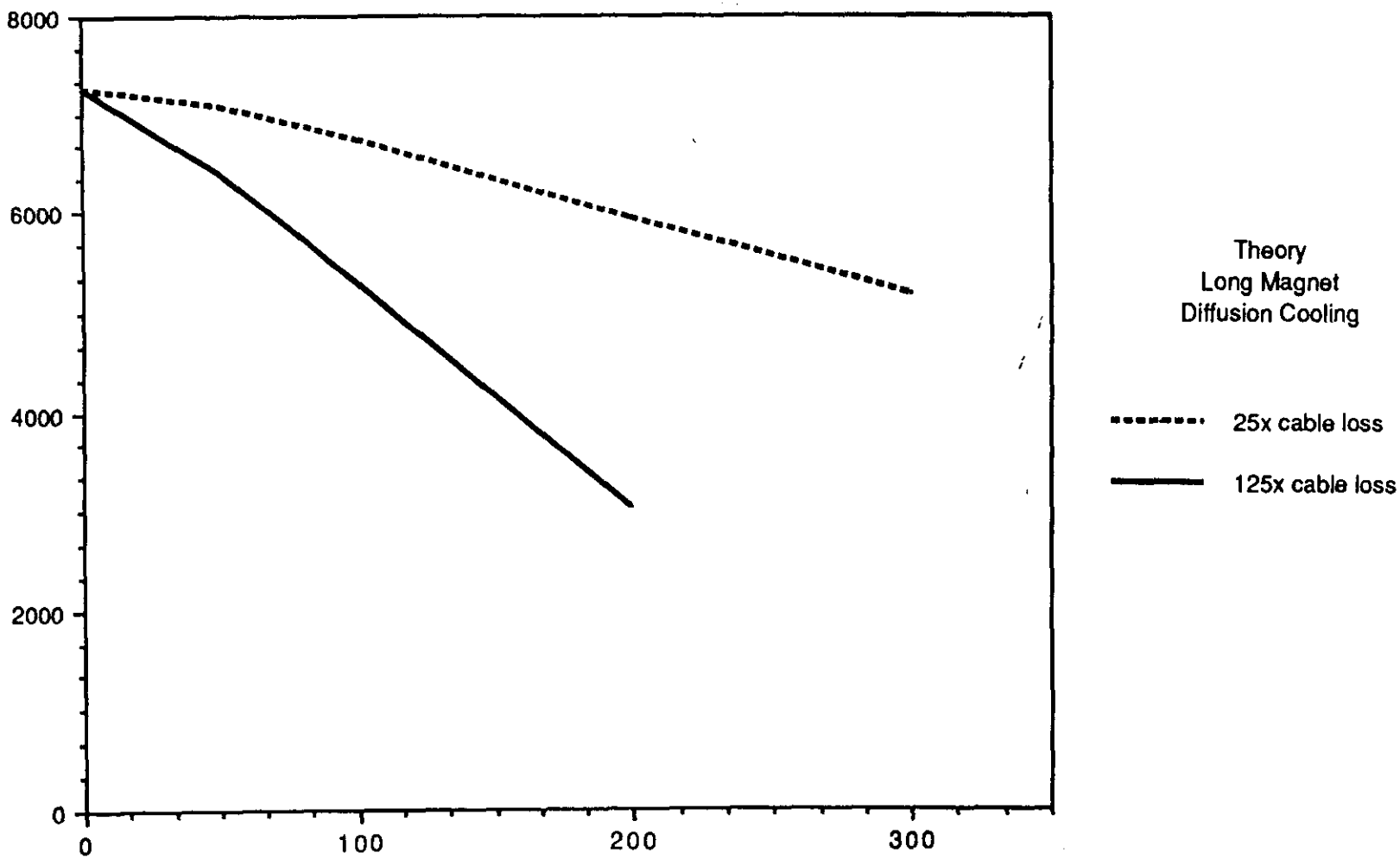
8000
6000
4000
2000
0
0
100
200
300
Theory
Long Magnet
Diffusion Cooling
25x cable loss
125x cable loss

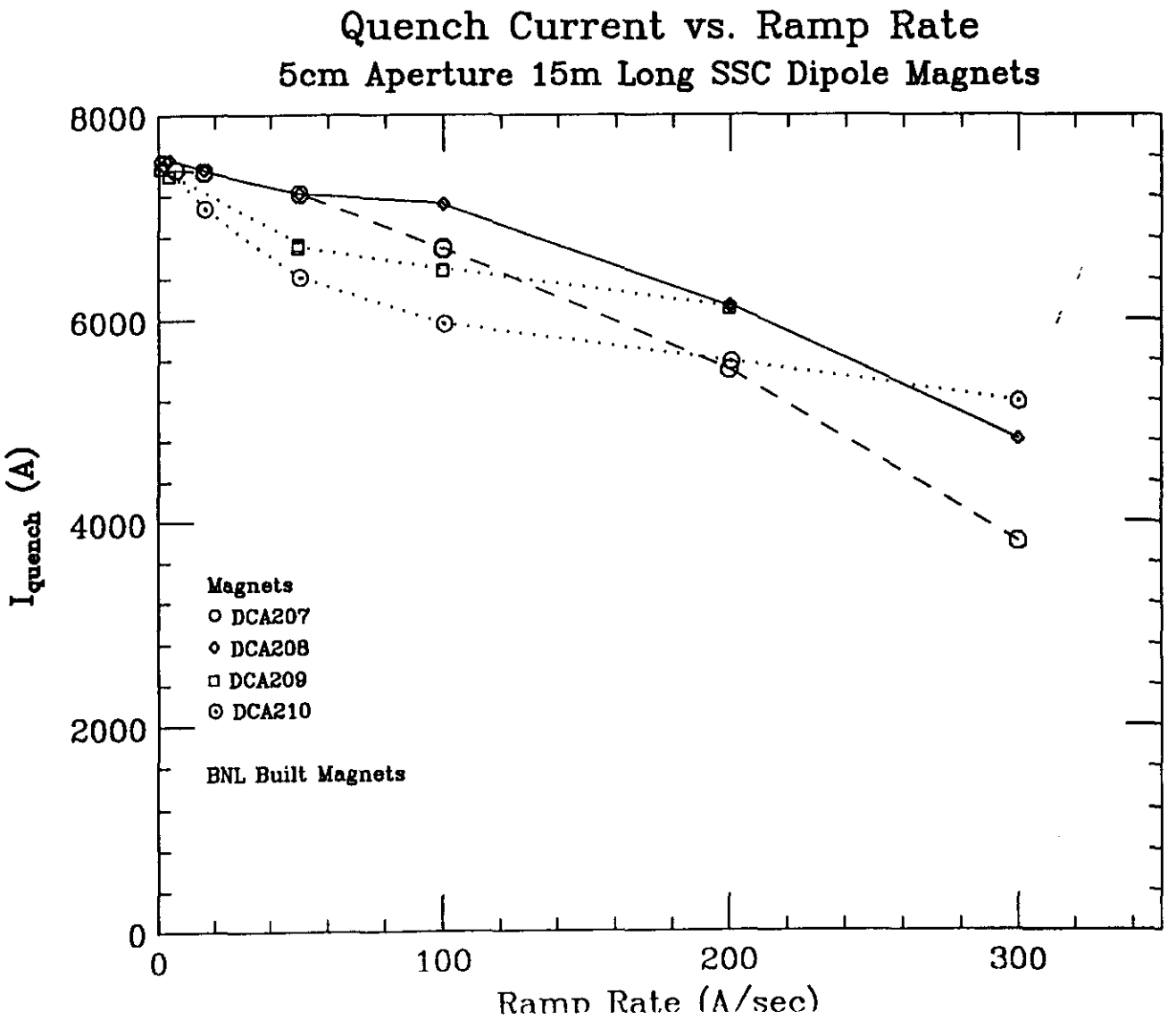
Quench Current vs. Ramp Rate
5cm Aperture 15m Long SSC Dipole Magnets
8000
6000
4000
2000
0
$I_{quench}$ (A)
0
100
200
300
Ramp Rate (A/sec)
Magnets
DCA207
DCA208
DCA209
DCA210
BNL Built Magnets

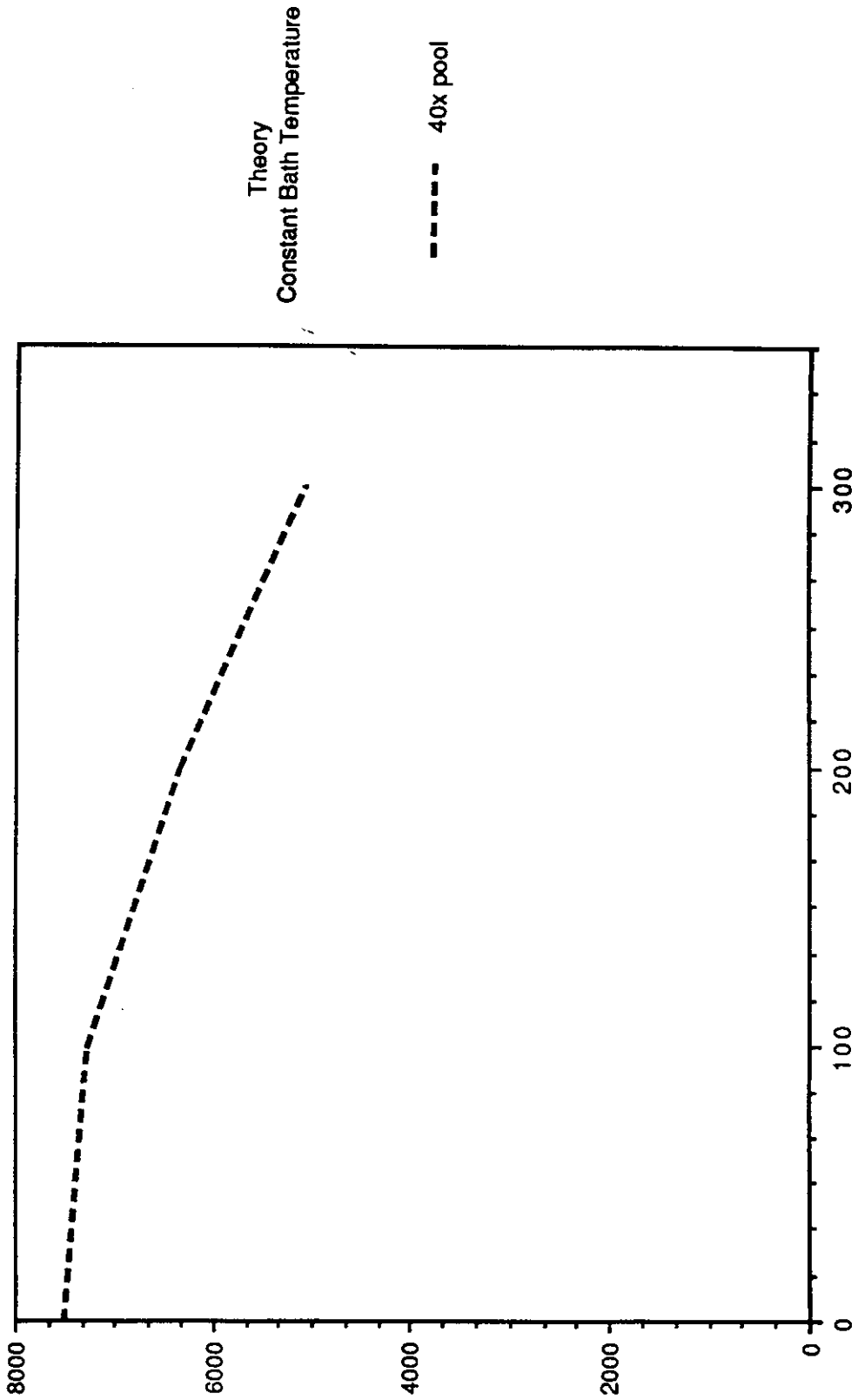
Theory
Constant Bath Temperature
40x pool
8000
6000
4000
2000
0
0
100
200
300

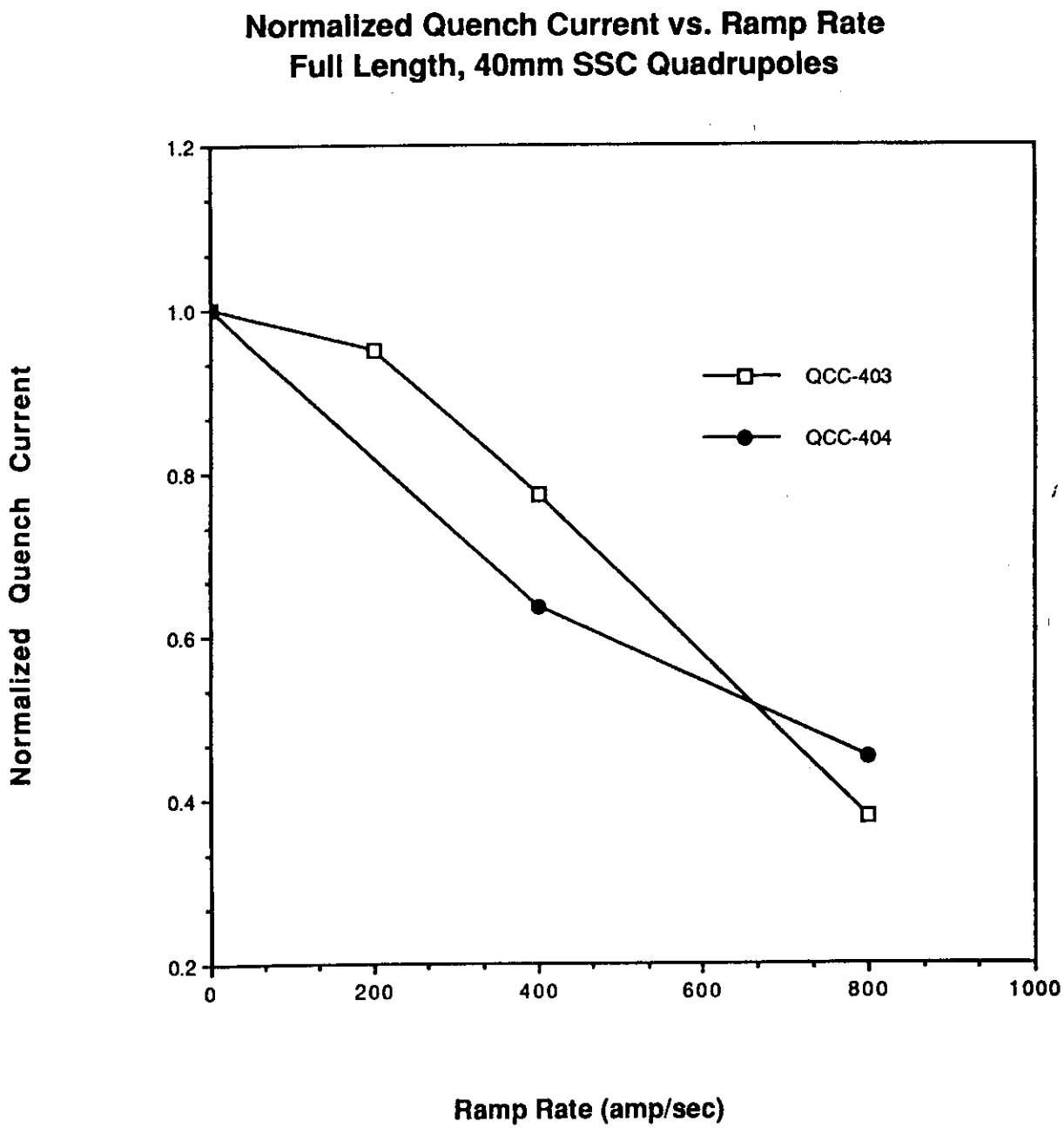
Normalized Quench Current vs. Ramp Rate
Full Length, 40mm SSC Quadrupoles
Normalized Quench Current
1.2
1.0
0.8
0.6
0.4
0.2
0
200
400
600
800
1000
Ramp Rate (amp/sec)
QCC-403
QCC-404

# MAGNET COOLING GEOMETRIES

## I. SHORT MAGNETS TESTED IN A HELIUM BATH

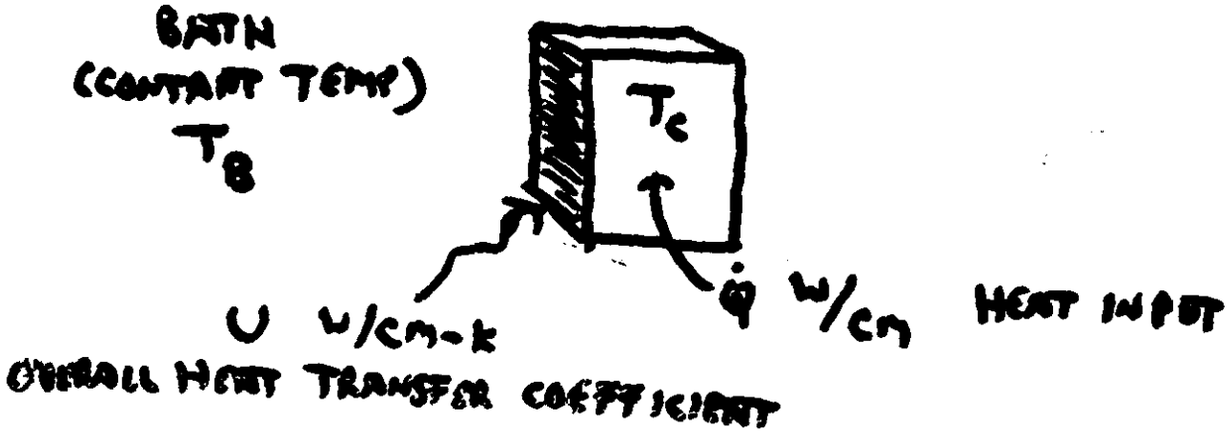


$$\frac{1}{U} = \left(\frac{T}{k}\right)_{KAPTON} + \cancel{\frac{1}{h}}$$

$\dot{Q}$ = INSTANTANEOUS POWER DEPOSITION

$$\simeq \int \frac{2\dot{B}^2}{\mu_0} \tau \, dA$$ IN A RAMP-RATE EXPERIMENT

$$U(T_c - T_B) = \dot{Q}$$

# MAGNET COOLING GEOMETRIES

## II. LONG MAGNETS IN FLOWING HELIUM

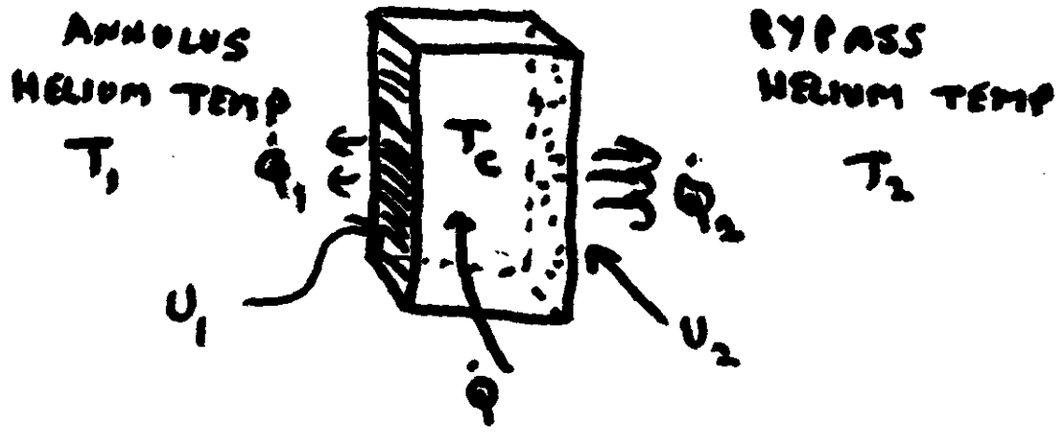


$$\dot{Q}_i = U_i (T_c - T_i)$$

$$\dot{Q}_1 + \dot{Q}_2 = \dot{Q}$$

$$T_i(z) = \int_0^z \frac{\dot{Q}_i}{\dot{m}_i c} \, dz$$

SOLVE TWO COUPLED, FIRST ORDER, O.D.E.

## III. LONG MAGNETS IN SUPERFLUID

$$T_i(z) = T_i(z, \text{GEOMETRY}, \text{HEAT FLUX})$$

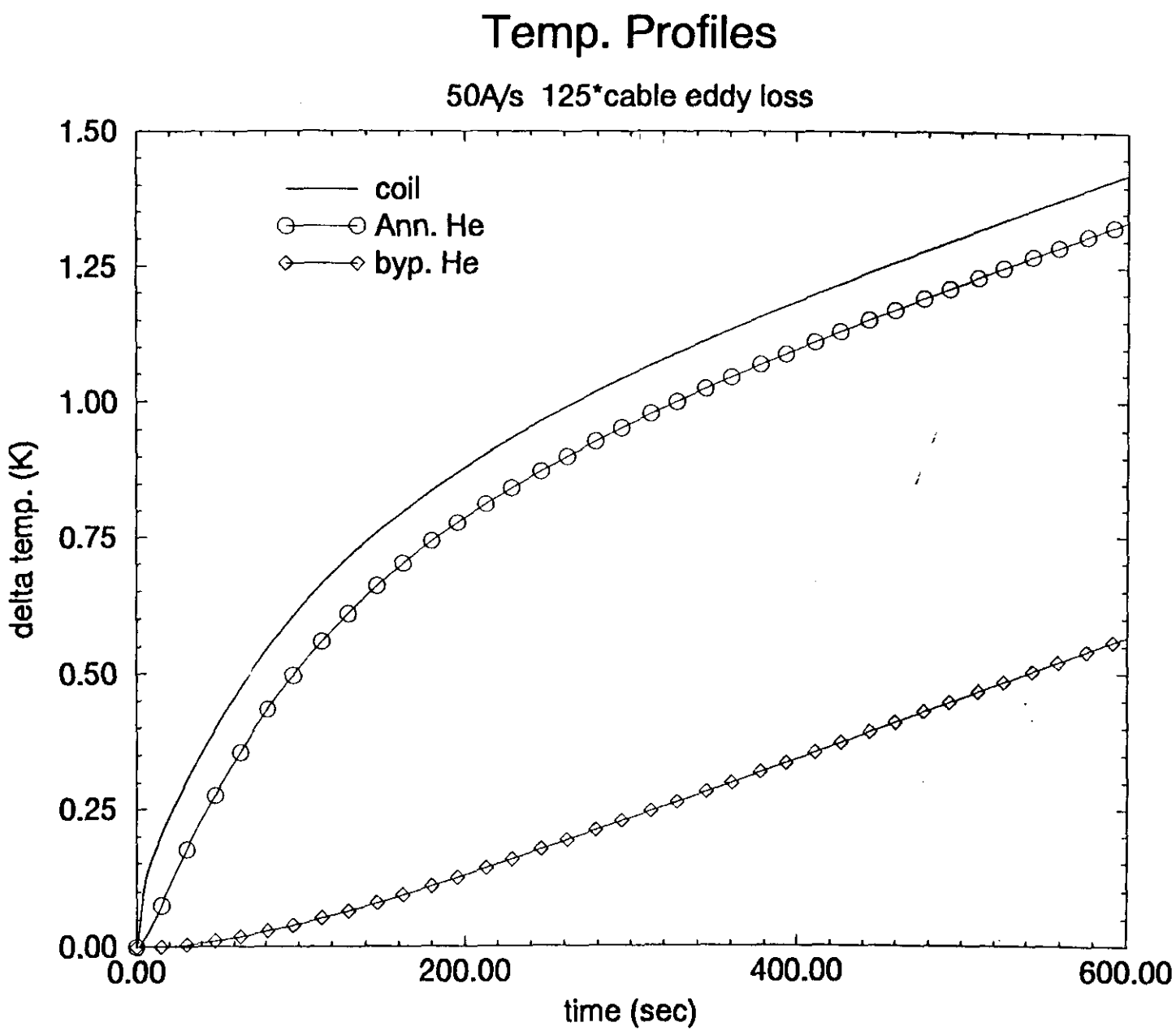
Temp. Profiles
50A/s 125*cable eddy loss
coil
Ann. He
byp. He
delta temp. (K)
1.50
1.25
1.00
0.75
0.50
0.25
0.00
0.00
200.00
400.00
600.00
time (sec)

# Transient Thermal Model

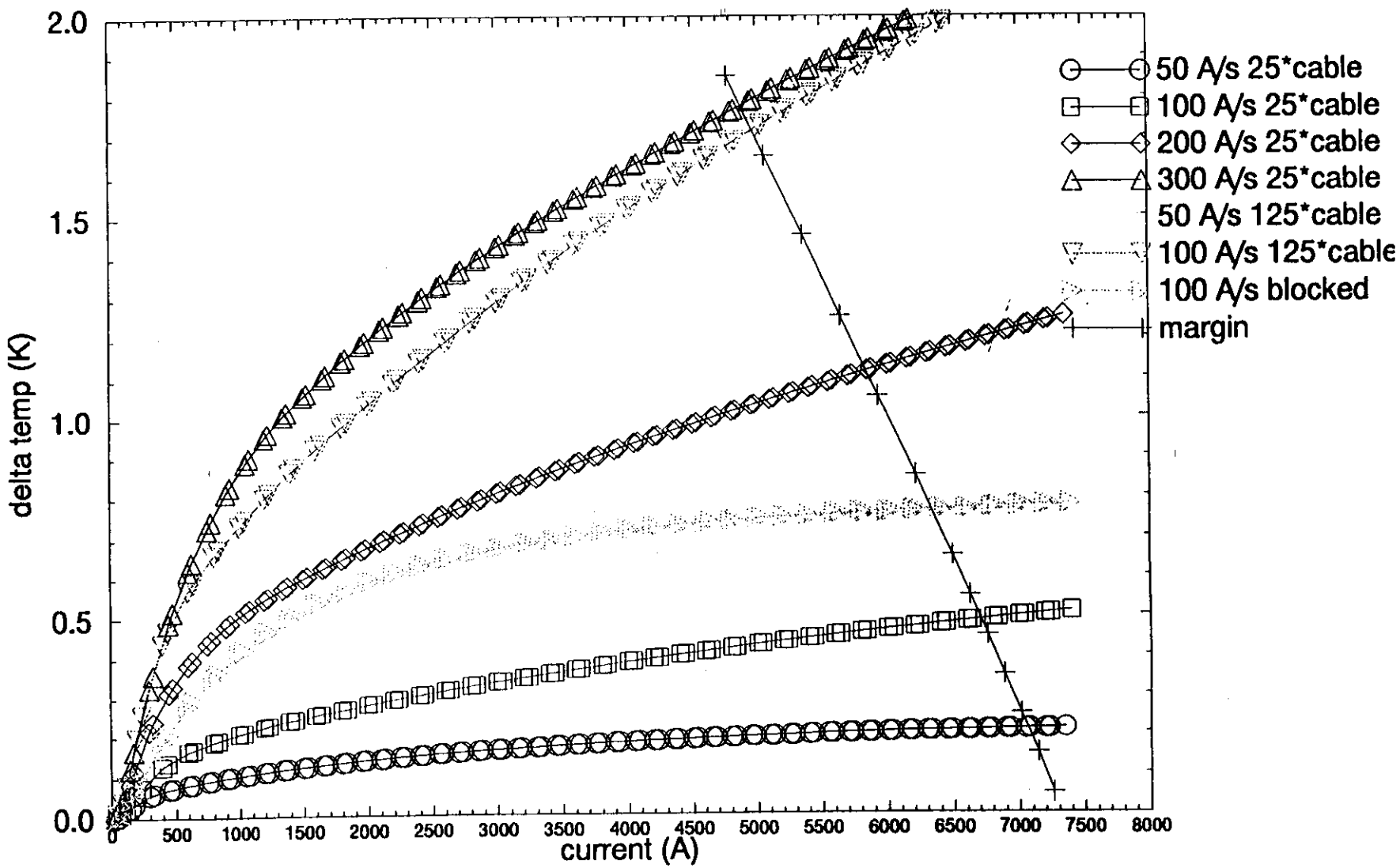

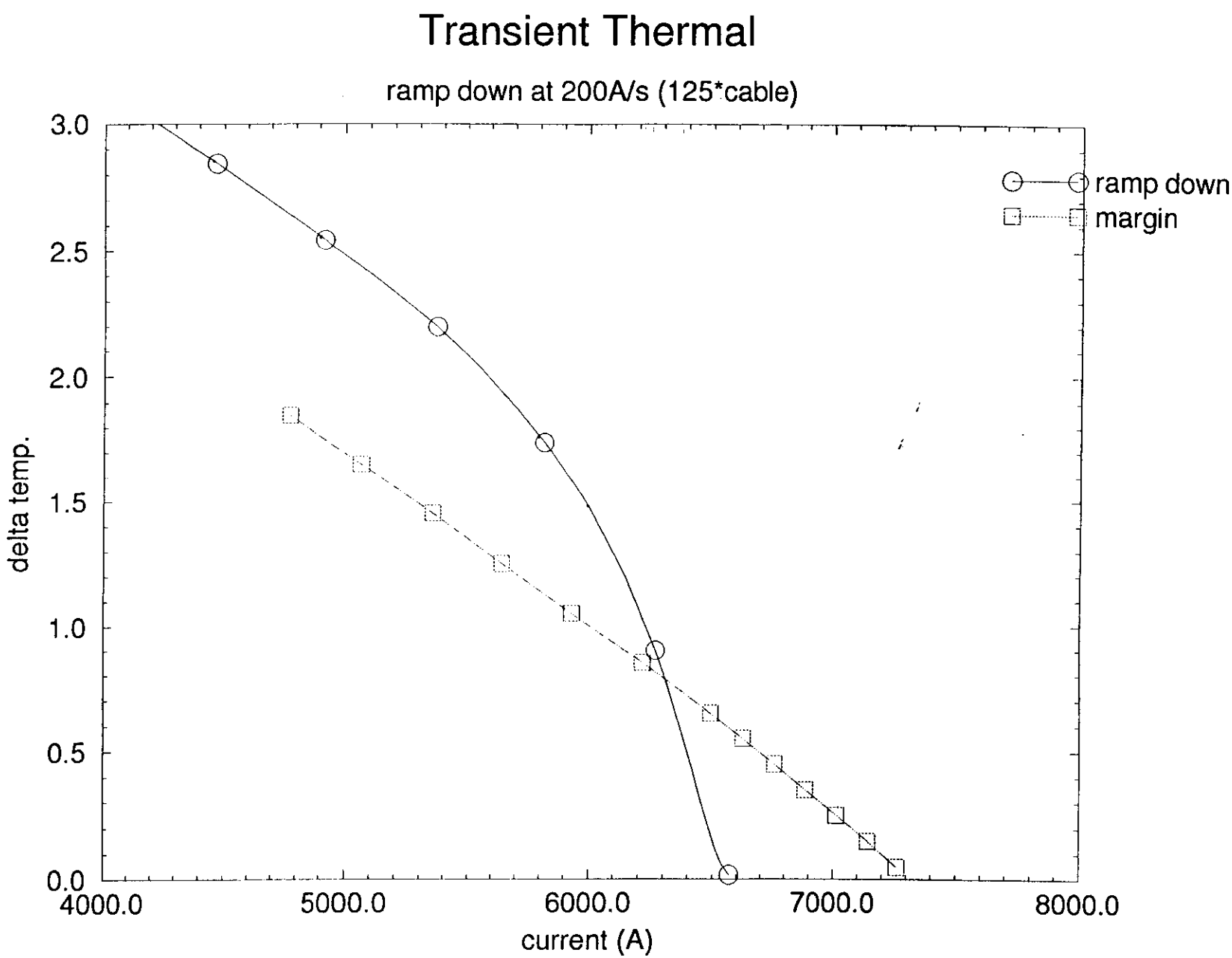
Transient Thermal
ramp down at 200A/s (125*cable)
3.0
2.5
2.0
1.5
1.0
0.5
0.0
delta temp.
4000.0
5000.0
6000.0
7000.0
8000.0
current (A)
ramp down
margin

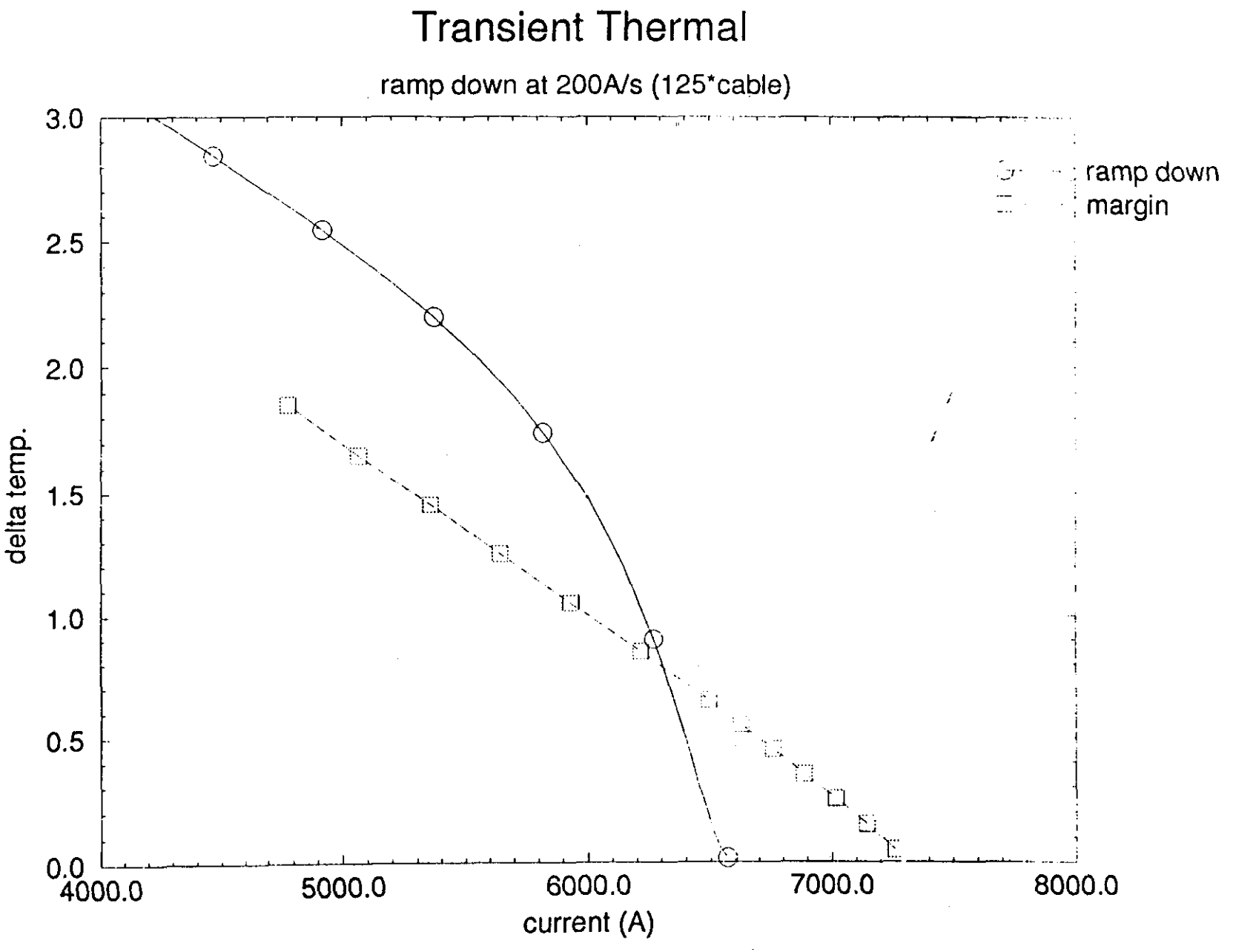
Transient Thermal
ramp down at 200A/s (125*cable)
3.0
2.5
2.0
1.5
1.0
0.5
0.0
delta temp.
4000.0
5000.0
6000.0
7000.0
8000.0
current (A)
ramp down
margin

911206 J. Ozelis, FNAL

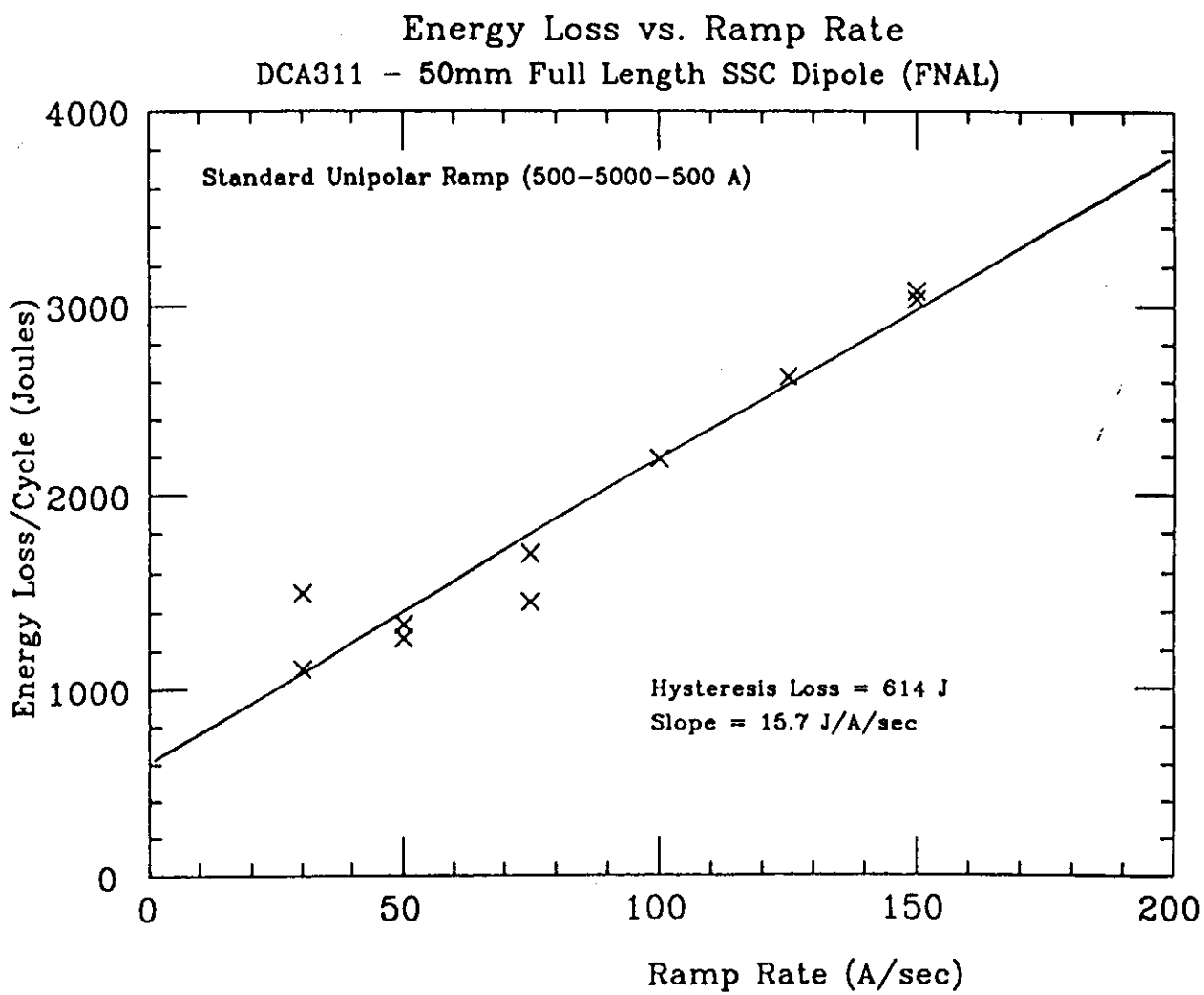

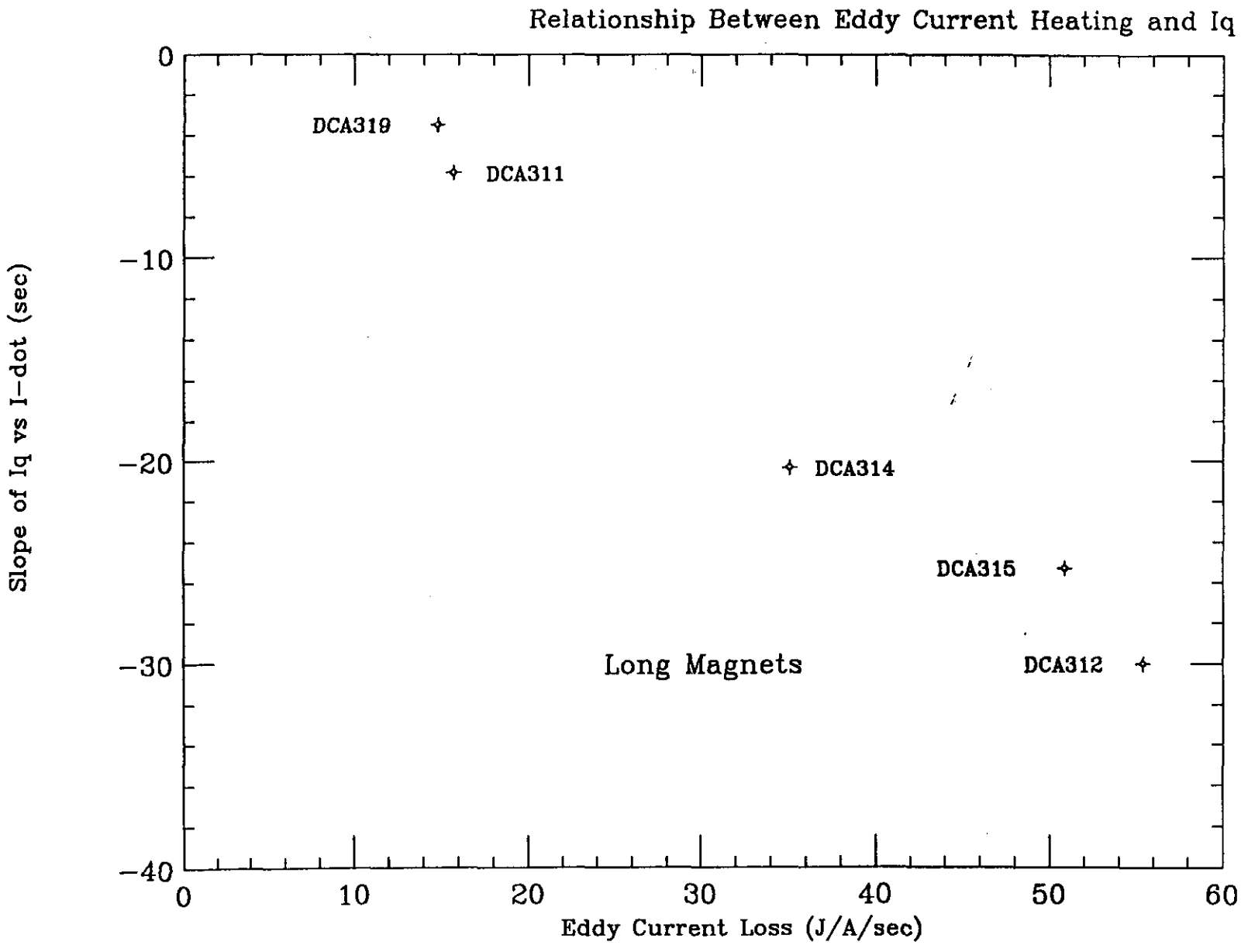
Relationship Between Eddy Current Heating and Iq
Slope of Iq vs I-dot (sec)
Eddy Current Loss (J/A/sec)
0
-10
-20
-30
-40
0
10
20
30
40
50
60
DCA319
DCA311
DCA314
DCA315
DCA312
Long Magnets

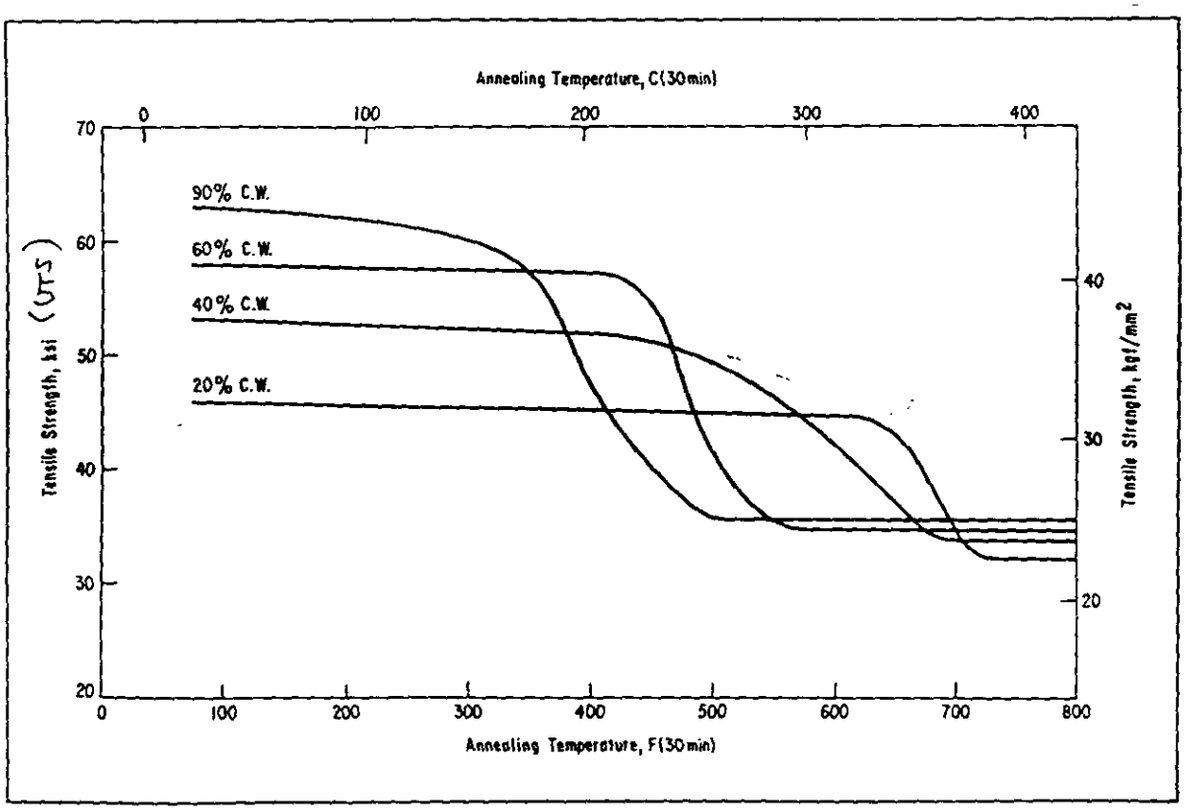


Figure 3-8. Softening curves for cold worked OFHC copper (AMAX data).

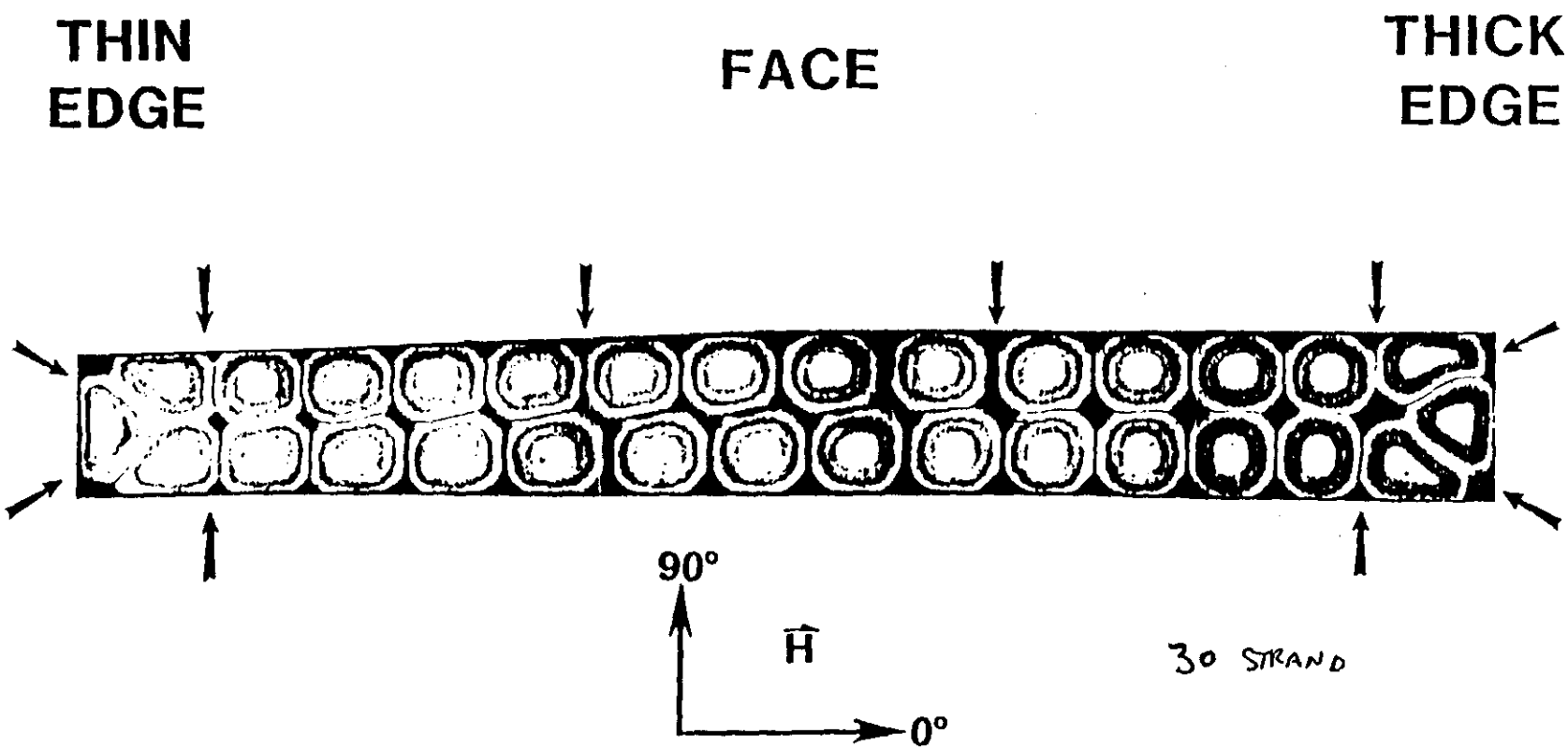


Figure 1. Cross section of cable W showing the orientation of the applied magnetic field and the approximate locations of the voltage taps, indicated by arrows in the figure (full cable pitch tap positions omitted for clarity).

# CONCLUSIONS

- HOW SERIOUS IS THE PROBLEM? IT DEPENDS ON WHICH ACCELERATOR WE ARE DISCUSSING.

FOR THE COLLIDER, THE PROBLEM IS ANNOYING, BUT NOT SERIOUS:

MULTIPOLES DUE TO EDDY CURRENTS SEEM TO BE RANDOM IN SIGN AND MAGNITUDE, AND MUCH SMALLER THAN THE ALLOWED MAGNET-TO-MAGNET VARIATION.

THE EXTRA HEAT LOAD IS QUITE SMALL, BECAUSE THE RAMP RATE IS ONLY 4 A/S.

ONLY THE VERY WORST MAGNETS WOULD QUENCH DURING RAMP DOWN.

FOR THE HIGH ENERGY BOOSTER THE PROBLEM IS SERIOUS. THE RAMP RATE IS 65 A/S, AND THE EXTRA HEAT LOAD IS FAR TOO MUCH FOR THE CRYOGENIC SYSTEM.

- WE DO NOT UNDERSTAND WHY, FOR SOME MAGNETS, THE QUENCH CURRENT FALLS VERY RAPIDLY AT LOW RAMP RATES.

- WE HAVE AN EXPERIMENTAL PROGRAM IN PLACE TO UNDERSTAND, AND CONTROL, THE CAUSE OF LOW TRANSVERSE RESISTANCE.

- WE NEED AN EXPERIMENTAL PROGRAM TO VALIDATE OUR FINITE ELEMENT THERMAL MODEL.

# RAMP RATE EFFECT ON QUENCH: THERMAL ANALYSIS

$$\frac{\Delta I_q}{I_q} = -0.195\,\Delta T$$

HISTORY:

I. ANALYTIC CALCULATIONS FOR LIMITING CASES

"D.C." <u>POWER</u> COMPUTED BY KOVACHEV, SNITCHLER

THERMAL CONDUCTANCES COMPUTED BY AKSEL

"FAST RAMP" <u>ENERGY</u> FROM KOVACHEV, SNITCHLER

ENTHALPY FROM PUGLISI.

CABLE $R_\perp$ IS A FREE PARAMETER

COMPARE TO A.C. LOSS MEASUREMENTS

COMPARE TO $R_\perp$ MEASUREMENTS (GHOSH)

<u>BUT</u>: INTERESTING EXPERIMENTS ARE NEITHER FAST NOR SLOW. NEED TRANSIENT COMPUTATIONS (AKSEL, SNITCHLER)

(2)

1. THERE IS A LARGE MAGNET-TO-MAGNET VARIATION IN $R_\perp$ EVEN WHEN THE SAME CABLE IS USED

2. IT APPEARS THAT QUENCH IS DETERMINED BY A "LOCAL" $R_\perp$, WHEREAS A LOSS EXPERIMENT MEASURES AN INTEGRAL PROPERTY

3. IF WE STOP A RAMP ON A LONG MAGNET FOR 10 MINUTES WE RECOVER ALMOST 1K IN TEMPERATURE RISE. WE SHOULD LOOK FOR THE PREDICTED NEGATIVE RESULT ON A SHORT MAGNET

4. EXTEND COMPUTATIONS:
   CROSS-FLOW
   SHORT MAGNETS
   EMERGENCY SHUT DOWN

# Completion Of Thermal Contraction Measurements of some Materials used in Magnet Fabrication & Assembly

**Sample Preparation: Rick Jackimowicz, BNL**
**Measurements: Bill Kuhnle, BNL**

**C. Goodzeit, June 30, 1992**

**Gives results of materials added since the last report:**

1. **16 gauge yoke iron**
2. **1/4 inch yoke iron**
3. **Two formulations of Epoxy (un reinforced)**
4. **Kapton film (.005 inch)**
5. **A286 Strain Gauge Beam**
6. **Invar**
7. **316 stainless steel**
8. **304 stainless steel**

**Measurements were taken relative to Titanium Silicate from 273K to 4.2 K. The measured values for the materials added since the last report are shown in Figures 1 and 2. Figure 1 replaces the Plastics 2 figure in the previous report. In order to check these results a comparison was made with the value for copper presented in NIST Monograph 177. This is shown on the revised Metals (1) chart, Figure 3.**

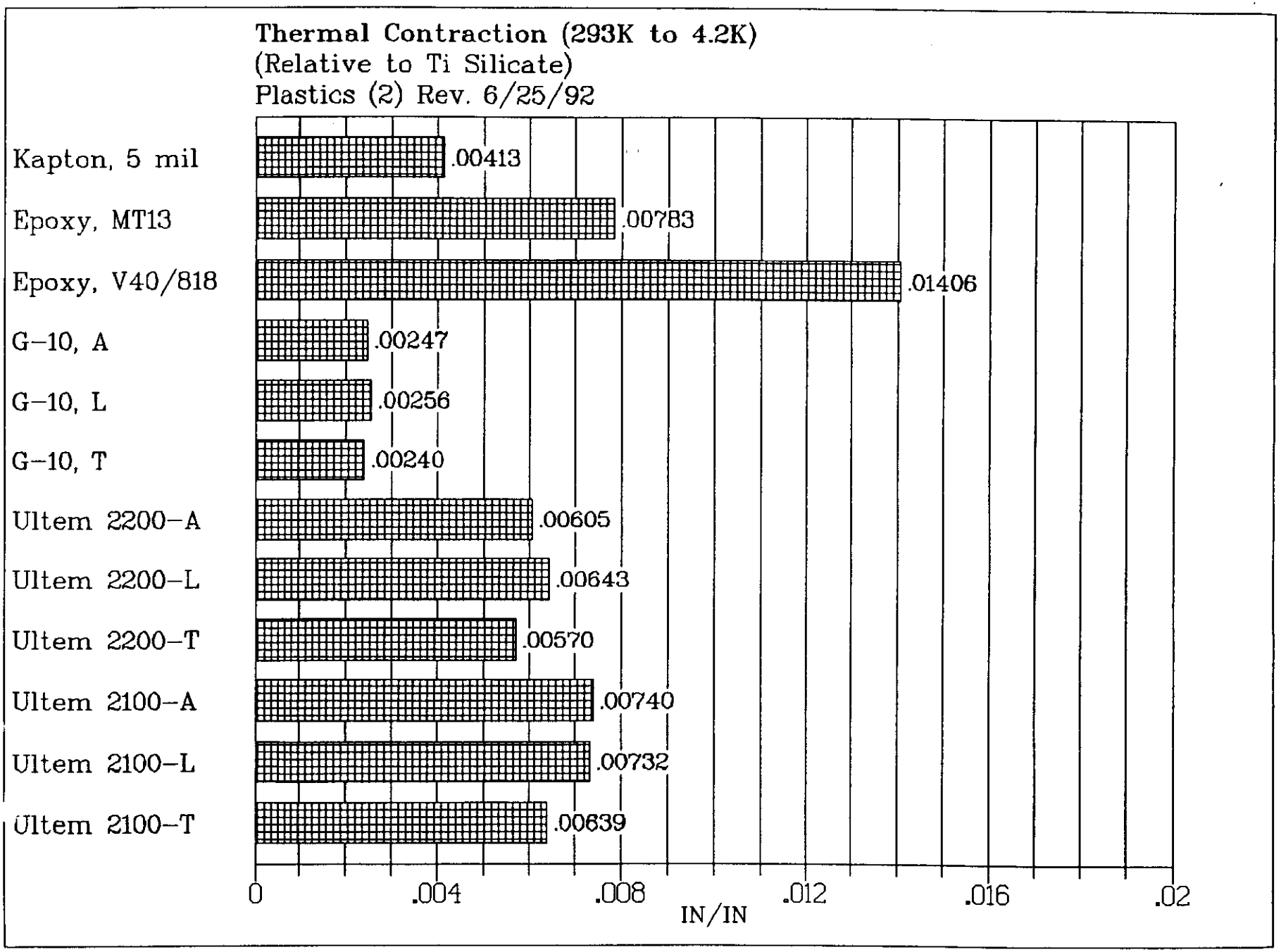
Thermal Contraction (293K to 4.2K)
(Relative to Ti Silicate)
Plastics (2) Rev. 6/25/92
Kapton, 5 mil
Epoxy, MT13
Epoxy, V40/818
G-10, A
G-10, L
G-10, T
Ultem 2200-A
Ultem 2200-L
Ultem 2200-T
Ultem 2100-A
Ultem 2100-L
Ultem 2100-T
.00413
.00783
.01406
.00247
.00256
.00240
.00605
.00643
.00570
.00740
.00732
.00639
0
.004
.008
.012
.016
.02
IN/IN

FIGURE 1

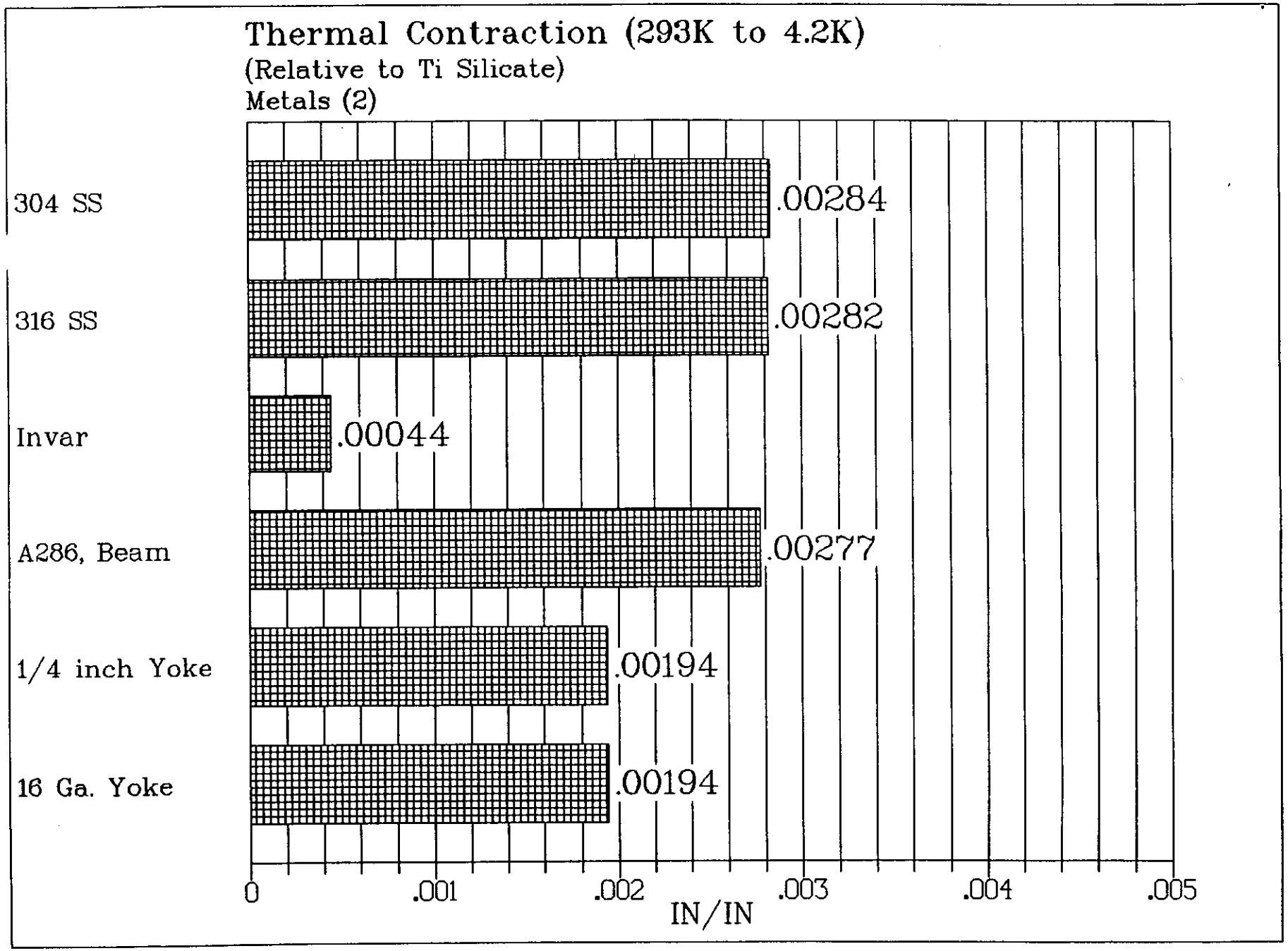
Thermal Contraction (293K to 4.2K)
(Relative to Ti Silicate)
Metals (2)
304 SS
316 SS
Invar
A286, Beam
1/4 inch Yoke
16 Ga. Yoke
.00284
.00282
.00044
.00277
.00194
.00194
0
.001
.002
.003
.004
.005
IN/IN

FIGURE 2

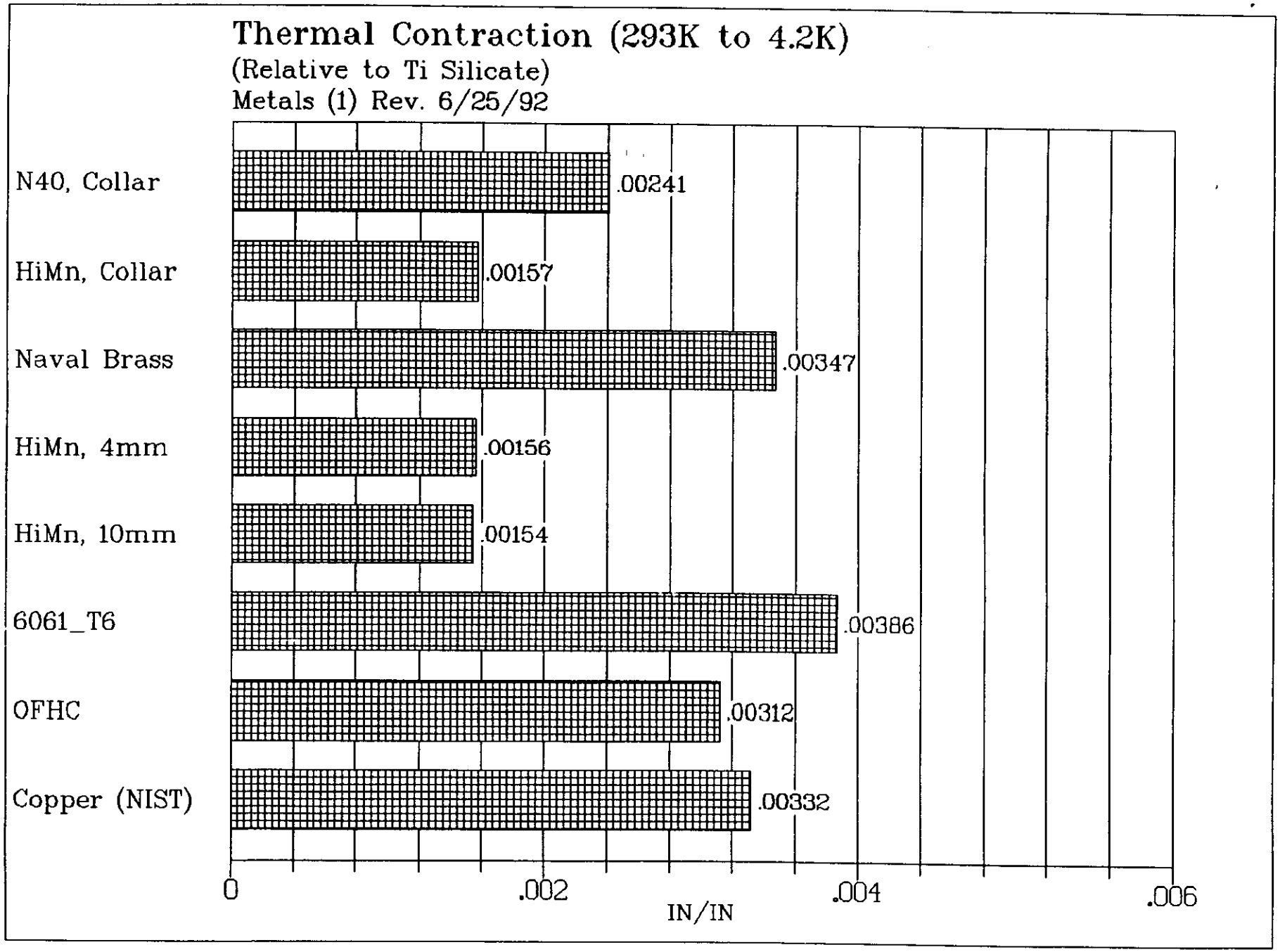
Thermal Contraction (293K to 4.2K)
(Relative to Ti Silicate)
Metals (1) Rev. 6/25/92
N40, Collar
HiMn, Collar
Naval Brass
HiMn, 4mm
HiMn, 10mm
6061_T6
OFHC
Copper (NIST)
.00241
.00157
.00347
.00156
.00154
.00386
.00312
.00332
0
.002
.004
.006
IN/IN

FIGURE 3

# List of Attendees

**Attendants:**

| | |
|---|---|
| Boroski Bill | FNAL |
| Christianson Owen | WSTC |
| Franks Don | SSCL |
| Hardy Ted | GD |
| Isaacs Bill | GD |
| Kraushaan Philip | SSCL |
| Mazur Peter | FNAL |
| Peck Scot | GD |
| Rekah Margarita | BNL |
| Simmons Jon | SSCL |
| Smellie Robert | SSCL |
| Syromyatnikov Igor | SSCL |
| Shu Quang Seng | SSCL |
| Weisend Jon | SSCL |
| Yucel Adan | SSCL |
| Moyses Kuchmir | FNAL |